HYDRODYNAMICS, HEAT AND MASS TRANSFER PHENOMENA IN REVERBERATORY FURNACES — MATHEMATICAL MODELLING AND EXPERIMENTATION

by

Denis Frayce

A dissertation submitted to the Faculty of Graduate Studies
in partial fulfilment of the requirements for the degree of
Doctor of Philosophy
Department of Mining and Metallurgical Engineering
McGill University
Montreal, Quebec, H3A 2A7 Canada
August 1990

(c) Denis Frayce, 1990

NOTE. *Figures 50-54, 55-59 and 60-69 which are printed in color (pages 100-102) are also reproduced in black and white for microfilming purposes. They are situated just after the color prints (pages 100a-100e, 101a-101e and 102a-102j)*

ABSTRACT

Following melt alloying and chlorine fluxing in reverbatory-like aluminum holding furnaces, it is common practice to allow the melt to settle for about an hour prior to casting operations. The purpose of this procedure is to allow inclusions to settle to the surface bottom or to float out to an overlying layer of dross. Mathematical modelling of this process reveals that significant natural convection currents are generated, particularly during the early part of this holding period, and that as these currents gradually diminish, so does the rate of precipitation of inclusions. A 6.25 ton pilot scale holding furnace was used to test the model's predictions of changes in metal quality with holding time. Satisfactory agreement was observed between predicted and "LiMCA"* measured changes in inclusion density levels of $(Ti\text{-}V)B_2$. Both approaches revealed exponential-like decays in inclusion density levels, with time constants in order of 10 to 60 minutes.

KEYWORDS: Aluminum holding/reverbatory furnaces, mathematical/physical modelling, natural convection, turbulence, inclusions, LiMCA/PoDFA measurements, liquid metal quality.

---

* LiMCA--Liquid Metal Cleanliness Analyzer

ABSTRACT - RESUME

Bien que l' importance des phénomènes de sédimentation des inclusions rencontrées dans les fours de coulée d' aluminium soit déjà connue depuis longtemps, le comportement hydrodynamique de ces particules n' avait jamais été étudié sur des bases scientifiques solides. Cette étude est cependant déterminante pour comprendre les facteurs clés de la qualité (ou "propreté") du métal à la sortie du four (coulée et solidification).

Les études entreprises à McGill pour ce projet conjointement avec ALCAN INTERNATIONAL LTEE ont permis d' élucider des phénomènes complexes mis en jeu: en particulier, la convection naturelle tridimensionnelle, due aux gradients thermiques en présence a un effet particulièrement important. De nature hautement turbulente, ce problème a été traité par la résolution des équations de Navier-Stokes en régime turbulent. La modélisation mathématique complexe a pu ensuite être validée par des mesures fiables effectuées sur un four à échelle réduite (6 tonnes de métal en fusion) lors d'une campagne d'expériences effectuée au Centre de Recherche ALCAN à Jonquière, Québec. En particulier, les variables Enthalpie et Concentrations ont ainsi pu être vérifiées; l' adéquation modèle mathématique/physique s'est avérée satisfaisante.

Ce projet, grâce à l' utilisation de moyens de calcul importants (VAX, CRAY) alliée à des facilités industrielles de premier plan permet de montrer sur un problème concret le bien fondé de la modélisation mathématique de procédés et aura un aspect déterminant sur la conception de nouveaux fours.

ACKNOWLEDGMENTS

I wish to express my sincere appreciation to Professor R.I.L. Guthrie, Dr M. Hasan, Dr J.P. Martin and Dr V. Potocnik for their guidance, encouragement and support throughout my years as a research assistant at McGill University

Furthermore, I wish to thank my friends and colleagues from the McGill Metals Processing Centre, whose presence and company made these work and studies more enjoyable.

Last but not least, I would like to express my appreciation to ALCAN INTERNATIONAL for providing excellent experimental facilities at their Jonquière Research Laboratories, and financial support during the course of these studies

TABLE OF CONTENTS

English abstract

French abstract

Acknowledgments

Table of contents

CHAPTER I

General content of the proposed modelling ; Introduction

The presence of non metallic inclusions in molten aluminium has a direct bearing on the final product quality. More and more, a high level of metal cleanliness is required by the customer in order to avoid detrimental effects during the transformation. flange cracks in beverage containers or microscopic holes in thin aluminium foils have disastrous consequences from the economic and marketing points of view. Therefore, strenuous efforts have been made for the last ten years to improve (and create) inclusion removal from the molten metal. For example, settling mechanisms in reverbatory furnaces are combined with gas fluxing practices (Argon or Chlorine) and filtration at the exit of the furnace to add the best value possible to the final product.

As in other traditional industries, the sequence of these operations were developped in an empirical way to a great extent. The results of the furnace practices were until recently very dependent on operator behaviour and habits Process optimization was thus far from being achieved

Many factors are responsible for this state of affairs; these are:

1) The complexity and the level of interlinkage of the processes involved; for example, if chlorine fluxing is currently used to remove non metallic inclusions from molten aluminium by flotation, it can have the inconvenience to resuspend other inclusions that had already settled In spite of noteworthy progress in the knowledge of physico-chemical aspects of each process (for example filtration), uncertainties remain about the overall dependence of the operating parameters and variables on the final product quality

2) Until recently, the lack of online methods able to provide information of the metal quality within a short delay was a major

drawback in helping the operator take appropriate action Even measuring the concentration of inclusions versus time as well as their size distribution versus time was not an easy task The usual methods presently available to assess the metal cleanliness are of three types These methods are well described by Doutre, Gariepy, Martin and Dubé (ref 1) They are based on chemical analysis, metallographic evaluations or techniques issued from physical principles Because of very low concentrations to be measured, chemical methods are rarely applicable to quantify the metal cleanliness, metallographic methods, after preconcentration of the sample may be a great help to find the relative proportions of different inclusions that can be indentified They are widely used at ALCAN for both research purposes and quality control (PODFA or Porous disk filtration appartus, ref 1) The disadvantages of using metallographic methods are mainly of two kinds first, it is not an online method; as a result sampling a whole cast can become tedious and secondly, analysis of the sample takes significant time for sample preparation, polishing, observation under microscopes etc; hence a delay up to one or two days is needed before obtaining the results Methods based on physical principles seem to be quite promising as a tool to assess metal cleanliness on line or so In particular, methods based on the electrical properties of aluminum have lead to a major breakthrough in online sensing of inclusions This was achieved through a joint project between ALCAN INT and McGILL University researchers From the measurements of the electrical properties of an inclusion containing thin metal stream crossing an orifice, a rapid method able of providing continuous concentrations numbers of particles and the size distribution larger than 15 to 20 microns was developed and termed: LiMCA (Liquid Metal Cleanliness Analyser) A more detailed description of this device is reported in the experimental part of this thesis

3) Some variables of the processes seem to have been neglected in the design of some equipments; sometimes, the difficulty of measuring these variables is the main problem, but in other cases, the

importance of the role of these variables has not been understood yet. For example, furnaces design for molten aluminum appears to have been dictated more by thermal considerations than by the requirements for an efficient reaction vessel. Bath depths are typically 1m and the free surface is typically 20m^2, the furnaces are difficult to stir and residence times for gases in the melt are short. Because of measurement difficulties, the actual hydrodynamic behaviour of the fluid has been only partly studied, most of the time by reference to physical modelling with water models. Particularly, the flow field distribution and magnitude is not known with precision within a holding furnace. This induces a lack of knowledge about the concentration field of inclusions since they are generally driven by the flow field. In the early attempts to model transport phenomena in such systems, some factors have been arbitrarily neglected: among these factors the natural convection currents which, as we will see later, can have significant influence on the flow field and hence on inclusion behaviour and have not been properly studied.

4) In other cases, some physical parameters are just not known: because inclusions are formed of exogenous solid or liquid phases present within the aluminum, their shape, aspect, density, surface tension are highly non uniform and thereby difficult to evaluate.

OBJECTIVES

The purpose of this research was to give a better understanding of the behaviour of holding / reverbatory furnaces encountered in the aluminum industry. Specific objectives are:

1) To study the flow patterns of the molten metal, heat transfer and turbulence;

2) To study the mass transfer and concentration fields of inclusions subject to these flow fields and to Stokes settling velocities.

In order to achieve these goals, the intention was to provide a powerful and economic tool to study these phenomena in the form of a validated mathematical model Thus, mathematical modelling can find the response of the furnace to a given set of perturbations without increasing the considerable costs of full scale experimental tests or the design and constuction of new equipment

To insure that the model is reliable and robust it needs to be verified through comparing its predictions with data from a matching set of experiments designed on a reduced scale furnace (6 25 ton) In particular, measurements of temperatures and concentrations *inside* the furnace were carried out for two purposes: firstly, to set up precisely some of the boundary conditions such as enthalpy of the fluid at the free surface, secondly, to validate the results obtained from this mathematical model based on the resolution of the Navier Stokes Equations

CHAPTER II

Preliminary work and statistical background

1 Measurements achieved in casting centres

As mentioned above, the wide use of PODFA and LiMCA techniques by ALCAN have generated a large number of data sets during their many casts at the industrial scale (several locations in Canada, US and Europe) as well as at the laboratory level for specific studies.

It should be noted that industrial metal cleanliness measurements during casts were taken at the exit of the holding furnace, in the trough, not in the furnace itself The cleanliness levels measured there integrate in some way all phenomena such as settling, stirring or fluxing effects which take place both before and during casting From these integrated results, it is almost impossible to deduce the exact behaviour of the fluid and inclusions in front of this monitoring point

Also it is be noted that the molten aluminum arrives at the trough either by tapping the furnace at its bottom level (case of stationary furnaces) or is poured from the top level of the furnace after skimming (case of tilting furnaces) The question is why not take measurements in the furnace itself at several locations? The lack of measurement in the furnace is due to the fact that it is virtually impossible to manipulate sensitive equipment from the top side of a reverbatory furnace while it is sequentially heated by a flat flame gas burner at high temperatures.

Nevertheless, measurements of metal cleanliness levels in the trough have been revealed to be quite reliable by two different and complementary methods LiMCA and PODFA. As an example, Fig 1 shows the correlation of these two methods during settling of inclusions within a cast. The LiMCA method has the advantage of providing a large number of data points for a typical settling curve since approximately a minute only is needed to sample and record a point on the curve. However, the PODFA technique, while not an in-line technique, is very useful for providing qualitative information about

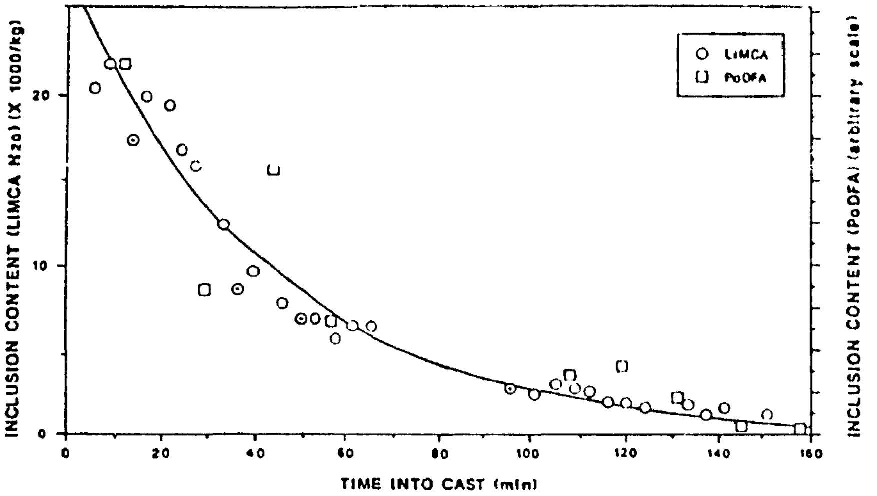

Figure 1 - Effect of settling on inclusion concentration as measured by PoDFA and LiMCA.

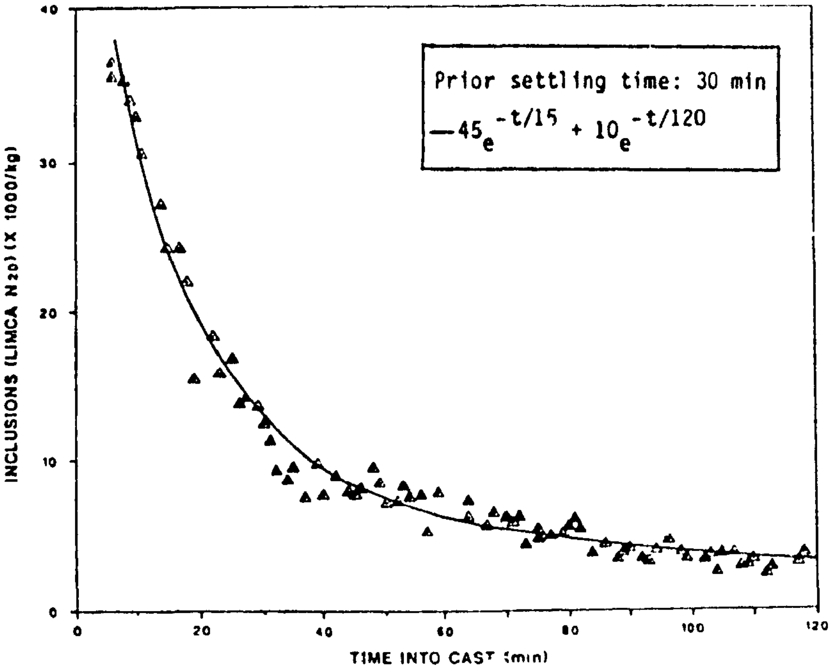

Figure 2 - Effect of settling on inclusion concentration measured by LiMCA at the exit of a tilting furnace. Note the two components observed.

the inclusions present The LiMCA gives more quantitative information about the concentration N_{20} (number of particles above 20 µm of equivalent diameter per kg of aluminum) and the size distribution of these particles.

Metal cleanliness measurements from a number of casting processes lead to the following conclusions (ref 2):

1) Settling of inclusions proceeds during the casting operation and the associated time scale is of the same order of magnitude as the casting time; of course, as we will see in the next section, different inclusions (density and / or size) correspond to different settling rates.

2) A preliminary long settling time prior to casting has a beneficial effect on the cast product since it significantly decreases the level of concentration (N_{20})before the transfer of metal (Fig 2)

3) As a consequence of 1) and 2), the actual settling curve to consider is the one where the abscissa is the total of the two (initial settling time before casting and time into cast) In such a case the global settling curve as shown by Fig 3 consists of three zones Zone A could be observed only at the laboratory level (non zero prior settling time is always encountered in DC (or direct chill) casting centres) and corresponds to a very fast kinetic step: the exponentially decreasing curve has a characteristic time τ between 5 and 10 minutes, defined by:

$$N_{20}(t) = N_{20}(t_0)\ e^{-\frac{t}{\tau}} \tag{1}$$

The curve showing the inclusion content in zones B and C are also exponentially decreasing but with a much slower rate compared to zone A These zones (B and C) generally correspond to a characteristic time of roughly 30 minutes

4) In spite of a controversy about the relative efficiency of stationary furnaces and tilting furnaces, it has been observed in many casting centres that these two types of equipment do not have significantly different

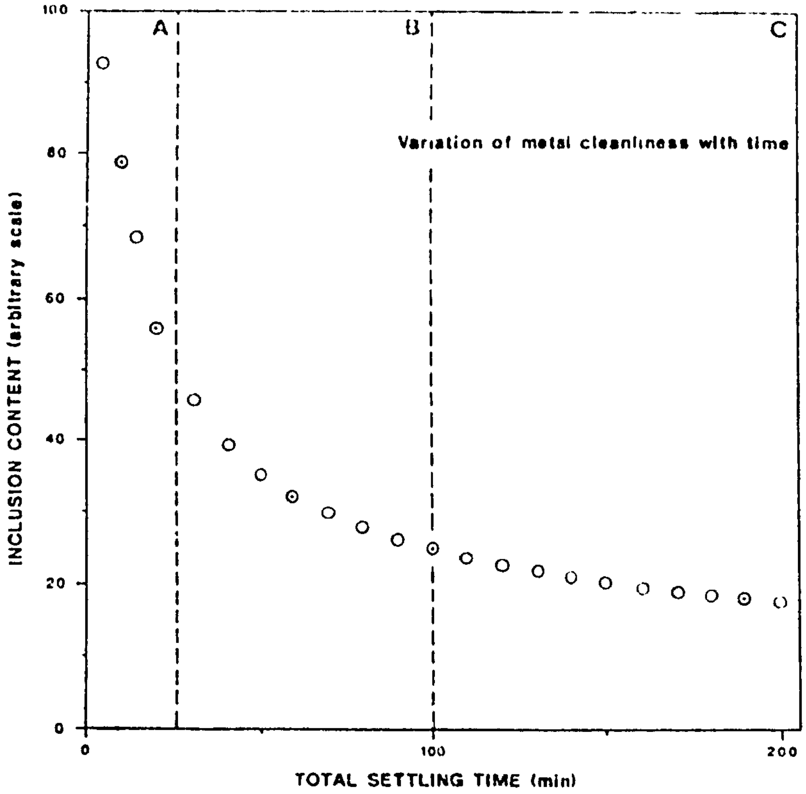

Figure 3 - Variation of metal cleanliness as a function of total elapsed time; region B corresponds to data observed under typical casting conditions.

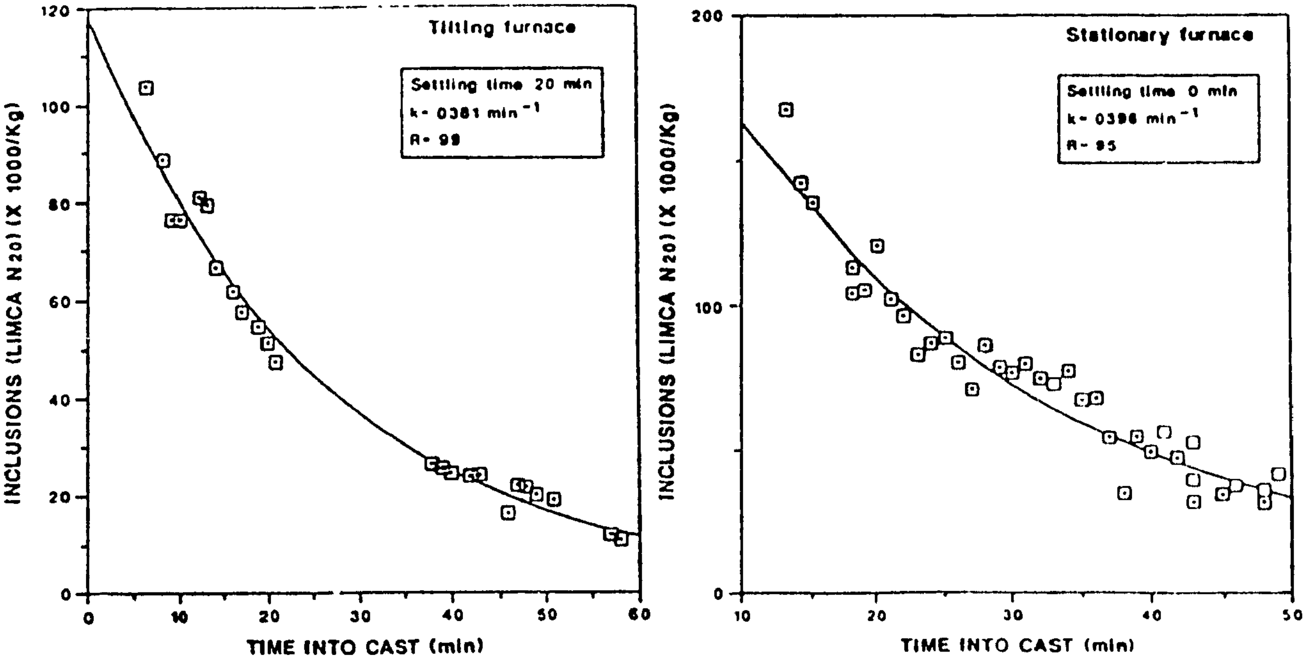

Figure 4 - Rate constants for inclusion removal for a tilting and stationary furnace; the lifetimes (=1/k) are respectively 26 and 25 minutes.[8]

behaviour from the settling point of view. In order to illustrate this, Fig 4 has been plotted. This Figure shows the typical settling curves (zones B and C) of aluminum flowing out of a tilting and a stationary furnace The computed characteristic times were respectively 25 and 26 minutes with a satisfactory exponential curve fitting

5) For very long initial settling times above 100 minutes, statistical data reveal that the average cleanliness level defined as

$$\overline{N_{20}} = \frac{1}{\Delta T} \int_0^{\Delta T} N_{20}(t)\, dt \qquad (2)$$

can still be improved with a longer settling time (Fig. 5) but this effect has a much slower rate (2 to 3 hours of characteristic time). It is not obvious that very long settling times will be economical especially if the furnace holds a relatively clean metal (below 50k particles per kg of aluminum).

In order to provide some interpretation to the above experimental results, a physical model is needed, particularily a model which takes into account the various sizes and densities commonly encountered in DC casting centres.

2 A simple «plug-flow» model

2-1 Introduction

The purpose of this model was to study the displacement of inclusions in holding furnaces at rest as well as during casting The physical mechanisms which take place are essentially settling (for particle densities above the aluminum density), flotation (for lighter particles) and convection. As a first step, convective currents which can be due to external stirring or natural convection effects will be neglected

The inclusions of interest have an equivalent diameter between 20 and 100 microns and are made of chemical compounds given at Table 1, according to the type of alloys produced. The size distribution of these inclusions is now well known and available continuously owing to LiMCA measurements. This

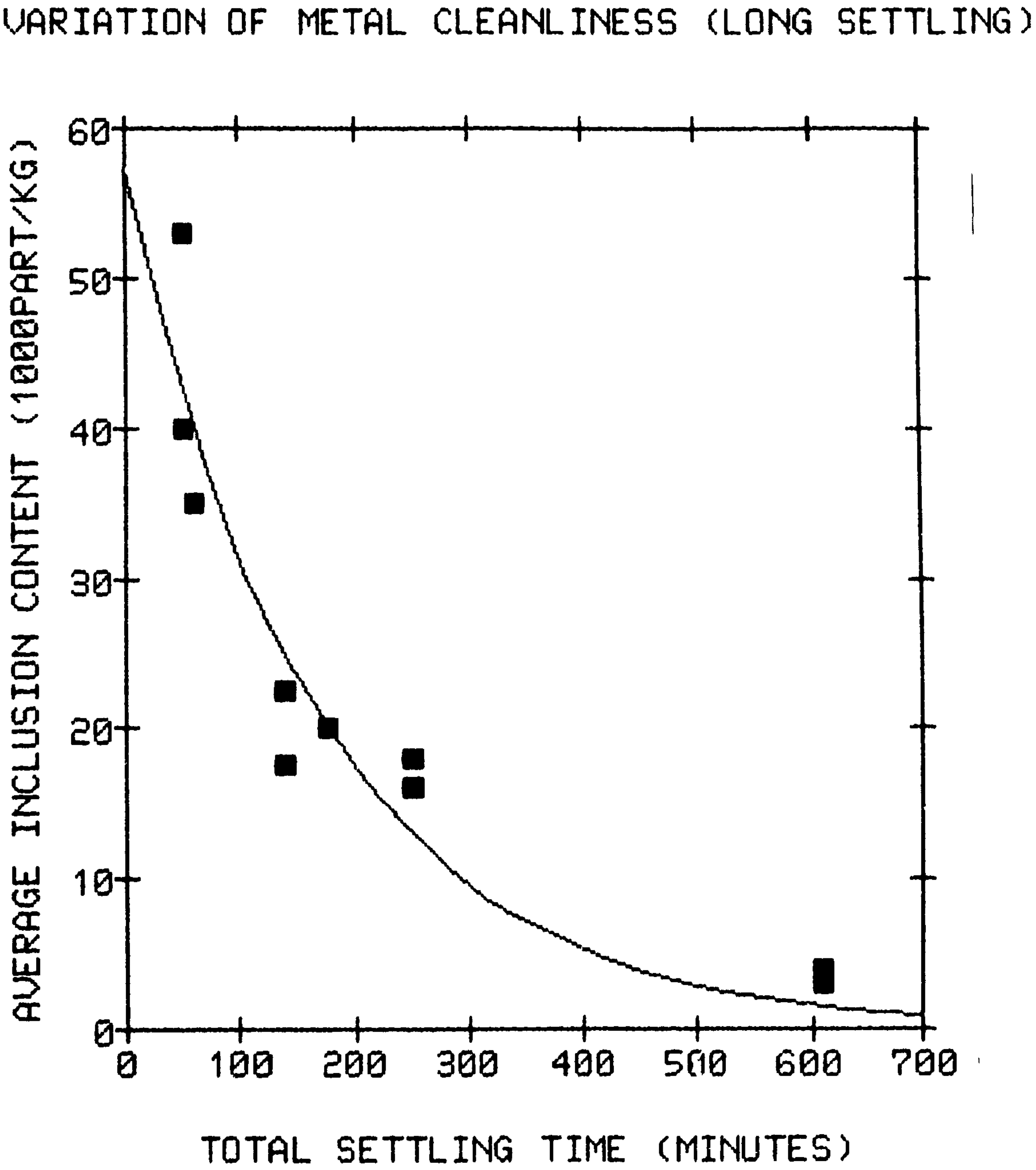
VARIATION OF METAL CLEANLINESS (LONG SETTLING)
AVERAGE INCLUSION CONTENT (1000PART/KG)
60
50
40
30
20
10
0
0
100
200
300
400
500
600
700
TOTAL SETTLING TIME (MINUTES)

Figure 5

distribution does not change significantly within a cast and is typically described by Table 2

inclusions	density 10^3 kg/m^3
α Al_2O_3	3.98
MgO	3.58
TiB_2	4.50
$MgCl_2$	1.80
Al_4C_3	2.36
Al_2MgO_4	3.6
TiVB	4.80

Table 1: Typical Inclusions encountered in holding furnaces

inclusion size (diameter in microns)	frequency (%)
20 to 25	69.0
25 to 30	17.7
30 to 35	7.2
35 to 40	3.7
40 to 45	1.7
45 to 100	0.7

Table 2: Inclusion size distribution

Mathematical model

A one dimensional model is discussed below to obtain the particle concentration as a function of x, abscissa measured from the free surface of aluminium and time t.

We assume a uniform concentration of particles. Their concentration is weak (magnitude of ppm) so the settling velocity (or rising velocity) can be regarded as constant. There is no accumulation of particles in a "cake" that would modify the flow while settling. Even if the shape of some inclusions can be quite irregular, they are considered spherical of equivalent radius R. Depending on the flow regime given by the Reynolds number Re the settling velocity can be computed (ref 3) by three equations:

a) Stokes law

$$Re \leq 2 \quad \Rightarrow \quad V_S = \frac{g D^2 (\rho_p - \rho)}{18 \mu} \tag{3}$$

b) Intermediate law

$$2 \leq Re \leq 500 \quad \Rightarrow \quad V_S = \frac{0.337\, g^{0.71} R^{1.14} (\rho_p - \rho)^{0.71}}{\rho^{0.29} \mu^{0.43}} \tag{4}$$

c) Newton regime

$$Re \geq 500 \quad \Rightarrow \quad V_S = 2.47 \left| \frac{g R (\rho_p - \rho)}{\rho} \right|^{0.5} \tag{5}$$

Because V_S is the unknown, the flow regime can be determined by a factor Z rather than the Reynolds number:

$$Z = 2R \left| \frac{g \rho (\rho_p - \rho)}{\mu^2} \right|^{1/3} \tag{6}$$

This factor Z is actually the cubic root of the Archimedes number Ar defined by Azbel and Cheremisinoff in reference (3) and it can be shown that:

- Stokes regime corresponds to: $Z \geqq 3.3$ (or $Ar \leqq 36$)
- Intermediate regime corresponds to:

  $3.3 < Z < 43.6$ (or $36 < Ar \leqq 83000$)
- Newton regime corresponds to: $Z \geqq 43.6$ (or $83000 \geqq Ar$)

For the settling particles given at Table 1 and radius between 0 and 100µm, the factor Z and velocities are plotted in Figs. 6 and 7. In this case we can note that these inclusions are ruled only by Stokes and intermediate regimes. If d is the depth of aluminum in the furnace, the settling time can be computed by $t = d/V_s$.

In the absence of convective currents, times between 40 and 400 minutes are needed to settle 20 micron particles with densities ranging from 2500 to 4500 kg/m^3

For a given size of particles, settling can be considered as a separation process between a clear phase and a phase of homogeneous concentration (Co initially) With time, the thickness of the clear zone increases as the interface moves with the settling velocity.

In the discrete case, one can consider a finite number of classes of particles of same density (Table 3)

At time *t*, the column of fluid will be formed of 6 "phases" of different concentrations plus a clear zone as explained at Fig. 8.

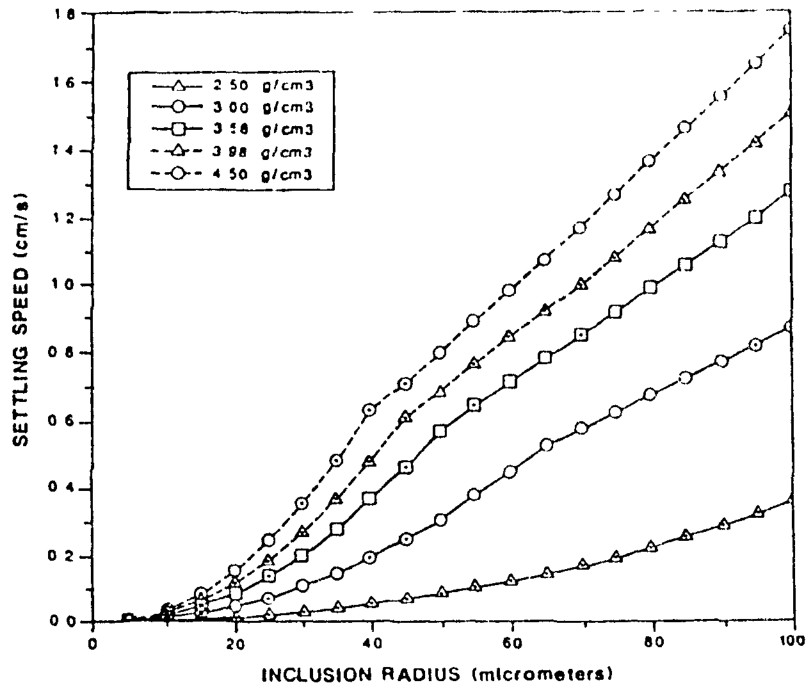

Figure 6 - Settling speeds as a function of inclusion radius for inclusions of various densities. For inclusions in the size range from 20to 50 microns diameter, settling speeds vary from 0.1 to 2.5 mm/s.

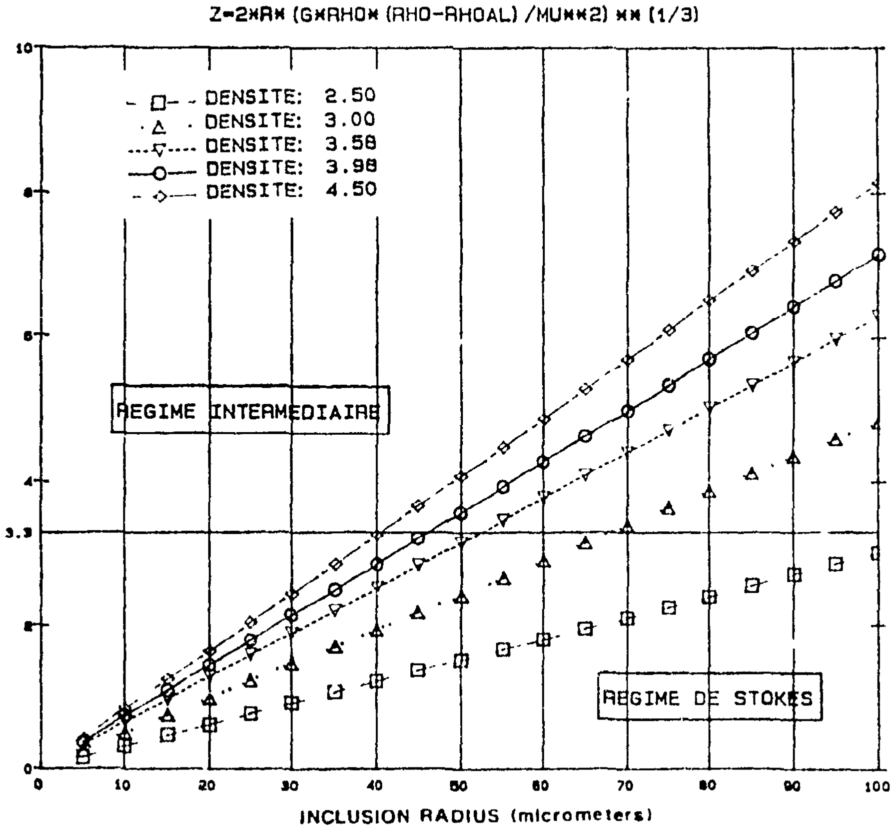

Figure 7: Factor Z as an indication of the flow regime.

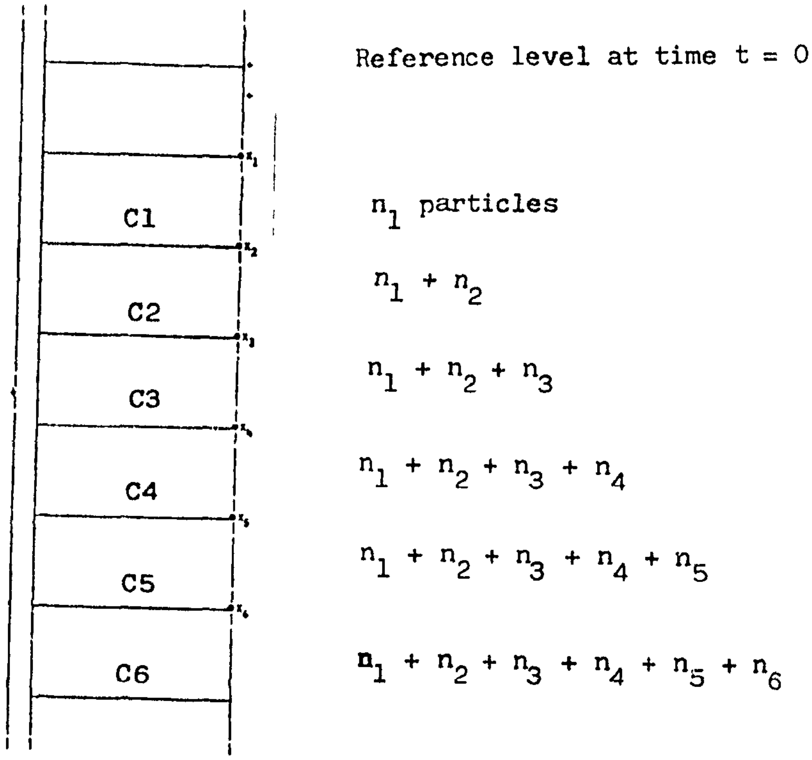

Figure 8: Simple plug flow model: discrete case of various sizes of particles which correspond to distinct layers of concentrations.

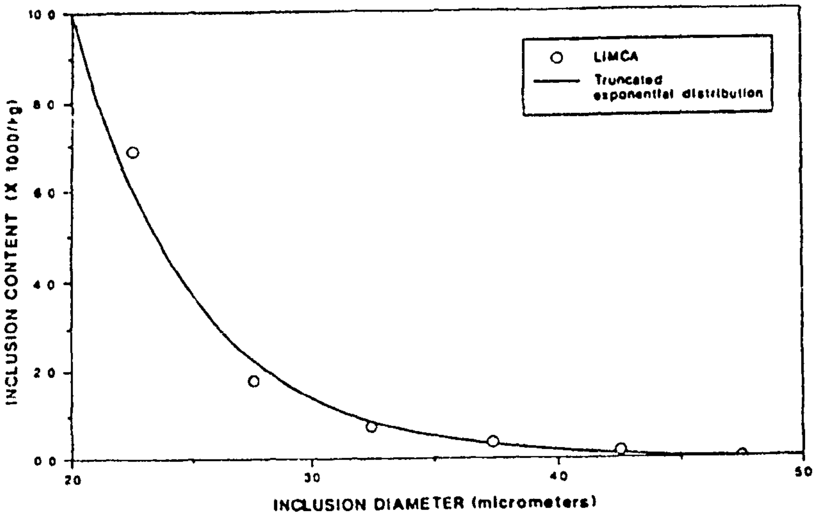

Figure 9 - Comparison of size distribution measured by LiMCA and calculated

particles/kg	class of diameter (μm)
n1	20-25
n2	25-30
n3	30-35
n4	35-40
n5	40-45
n6	45-50

Table 3: discrete distribution of particles

The mass concentration is then:

- for a class of particle.

$$C=n_i\frac{4\pi}{3}\left(\frac{d_i}{2}\right)^3\rho_i=0.524*10^{-15}n_i d_i^3\rho_i \qquad (7)$$

$$or\ C=0.524*10^{-15}n_i d_i^3\rho_i$$

if [di] = μm and [ρi] = g/cm3

- for *n* particles:

$$for\ n\ particles \qquad C=0.524*10^{-15}\sum_{i=1}^{n}n_i d_i^3\rho_i \qquad (8)$$

The interface level $x_n = V_n \times t$ allows one to compute the mass concentrations of inclusions as a function of the settling time.

Practically, the inclusions have a continuous distribution which can be estimated from discrete LiMCA measurements. The continuous probability density function n_λ can be defined as:

$$n_\lambda = P(x = d) = \frac{\lambda e^{-\lambda(x-d_{min})}}{1-e^{-\lambda H}} \quad with \;\; H = d_{max} - d_{min} \tag{9}$$

and is plotted in Fig 9

Where $H = d_{max} - d_{min}$ is the length of the size internal considered. Estimation of the parameter λ from LiMCA data as well as computation of theoretical frequencies are given in appendix A.

2-2 Concentration of particles as a function of x,t

By analogy with the discrete model, the mass concentration in ppm can be expressed as:

$$C(x,t) = 0.524*10^{-9}\rho \int_{dmin}^{D} N\, n_\lambda(y)\, y^3\, dy \tag{10}$$

where:

- N is the total number or particles per kg for a given density ρ (g/cm^3);
- n_λ is the probability density;
- D is a function of the settling velocity according to the type of flow (equations 3-5).

So,

$$C(x,t) = 0.524 * 10^{-9} \rho \frac{N \lambda}{1 - e^{-\lambda H}} \int_{d_{min}}^{D} y^3 e^{-\lambda(y - d_{min})} dy \tag{11}$$

which can be integrated by a triple integration:

$$C(x,t) = 0.524 * 10^{-9} \rho \frac{N \lambda}{1 - e^{-\lambda H}} \left| \Psi(d_{min}) - \Psi(D) \right| \tag{12}$$

where

$$\Psi(y) = -\frac{1}{\lambda} e^{-\lambda(y - d_{min})} \left(y^3 + 3\frac{y^2}{\lambda} + 6\frac{y}{\lambda^2} + \frac{6}{\lambda^3} \right) \tag{13}$$

In the case of a Stokes flow regime, for most particles of interest

$$D = \left| \frac{18 \mu V_S}{g \Delta\rho} \right|^{1/2} \quad where \quad V_S = \frac{X}{t} \tag{14}$$

Computations of C(*x*,*t*) was achieved for several densities of inclusions.

2-3 Simulations with the plug flow model

A population of 10 000 particles/kg of aluminum was considered, the distribution of which is given at Table 2. As specified in appendix A, the parameter λ of the density of probability function n_λ could be computed and estimated as:

λ = 0.189492 with a relative error below 10^{-6}.

For a given depth *x* in the furnace, computation of C(*x*,*t*) was undertaken for the densities given in Table 1. As a first approximation, this "plug flow" type model allows one to simulate settling/flotation phenomena for the two kinds of furnaces.

- Stationary furnace: x = furnace depth since tapping of aluminum takes place from the bottom of the furnace.

- Tilting furnace: x = 0 since the metal is poured out from the top.

In the case of a mixture of two or more particles of different densities, the global mass concentration is the total of the mass concentrations found for each type of particle

2-4 Results of simulation

If we compute concentrations with a given particle size distribution at different densities, at $t=0$ the mass concentrations do not have the same value In order to make rational comparisons more easily we chose to compute volumetric concentrations in ppm (10^{-6} vol/vol)

Figures 10, 11 and 12 show the concentrations at three distinct levels (x) of the furnace. In all cases, concentrations are monotonically decreasing functions of time

Particles heavier than aluminum

For particles heavier than aluminum, concentration decreases all the more rapidly when:

-the density is higher

-the point considered (abscissa x) is near the metal free surface

For example, the times required to get the concentrations down to zero for particles of density 3 58 (i.e. MgO) are given at Table 4.

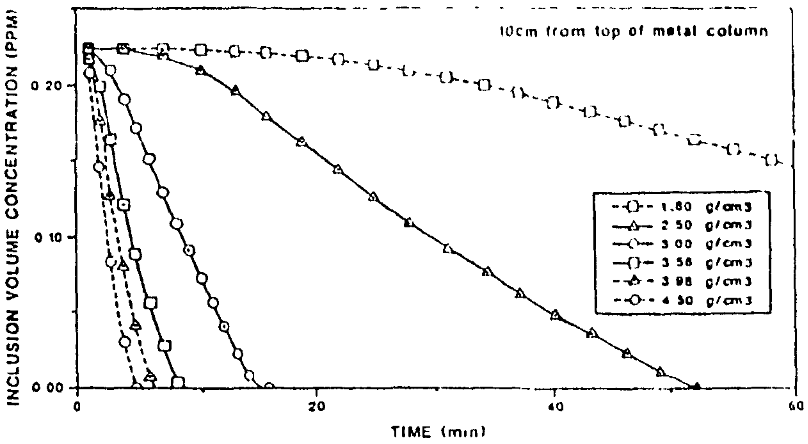

Figure 10 - Inclusion volume concentration predicted by simple model for a position 10 cm underneath the top of the metal bath ("tilting furnace scenario", for a range of species (densities).

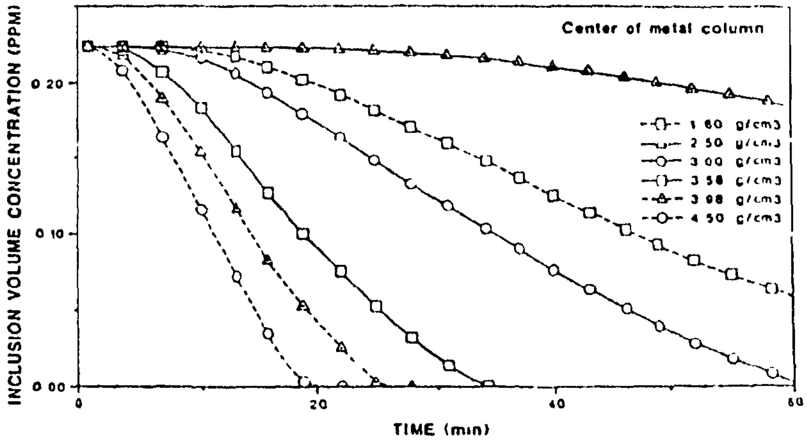

Figure 11 - Inclusion volume concentration predicted by simple model for a position midpoint (45 cm) in the metal bath, for a range of species (densities).

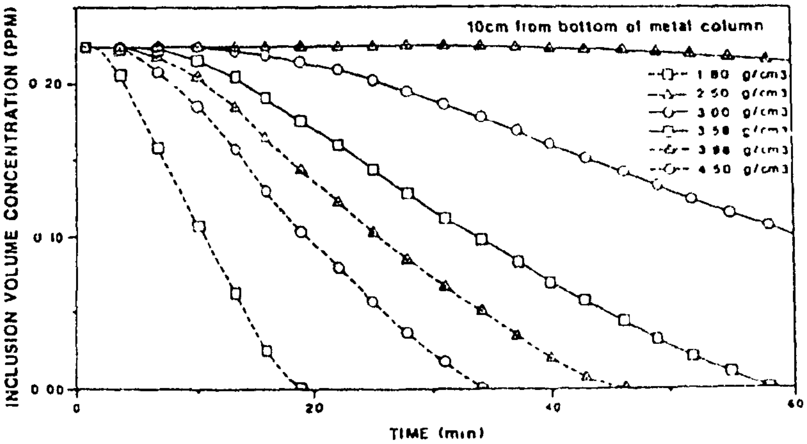

Figure 12 - Inclusion volume concentration predicted by simple model for a position 10 cm from the bottom of the metal bath ("stationary furnace scenario"), for a range of species (densities).

position x (cm)	time (minutes)
11 4 cm (top of furnace)	8
46 4 cm (middle)	32
81 4 cm (bottom of furnace)	58

Table 4: time required to settle out particles for d = 3.58 $*10^3$kg/m^3

At a given position in the holding furnace, the concentration gradients are very dependent on particle densities; to illustrate this point, Table 5 gives the times required so that the concentration C(*t*) reaches zero at a point situated in the middle of the furnace.

density (10^3kg/m^3)	time (minutes)
2 50	213
3 0	60
3.58	33
3 98	25
4 50	20

Table 5: time required to settle out particles at x = 46cm

Particles lighter than aluminium

For example, $MgCl_2$ has a density of 1 8 g/cm^3 at temperatures above 708°C, i e in liquid form This time the concentration decreases less rapidly at the top than at the bottom of the furnace. This inverted tendency is represented through numerical values in Table 6

position x (cm)	time (minutes)
11 4 cm (top of furnace)	147
46 4 cm (middle)	78
81.4 cm (bottom of furnace)	18

Table 6: time required to settle out particles for $d = 1\ 80 \times 10^3$ kg/m^3

A conclusion which can be drawn from this study is that for a simple plug flow model, a tilting furnace would give better results for particles heavier than aluminium whereas a stationary furnace would be of interest for lighter particles ($d < 2.35$ g/cm^3)

Case of a mixture of particles (same size distribution but different densities)

Let's consider a mix of $MgCl_2$ (1 8 g/cm^3) and (Ti-V)B (4 5 g/cm^3) As shown in Figures 13 and 14, the total concentration decreases much faster at the bottom than at the top· only 33 minutes are required for the concentration to drop to a zero value Because of the major role played by the heavier compound, a stationary furnace would produce better effects

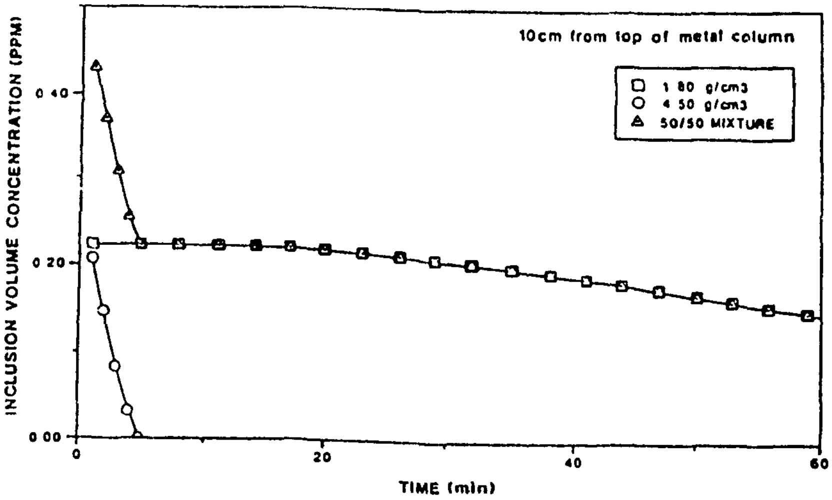

Figure 13 Time variation for the inclusion concentration on a mixture of floating ($MgCl_2$) and sinking (TiB_2) inclusions, at a point 10 cm from the top of the metal bath ("tilting furnace scenario").

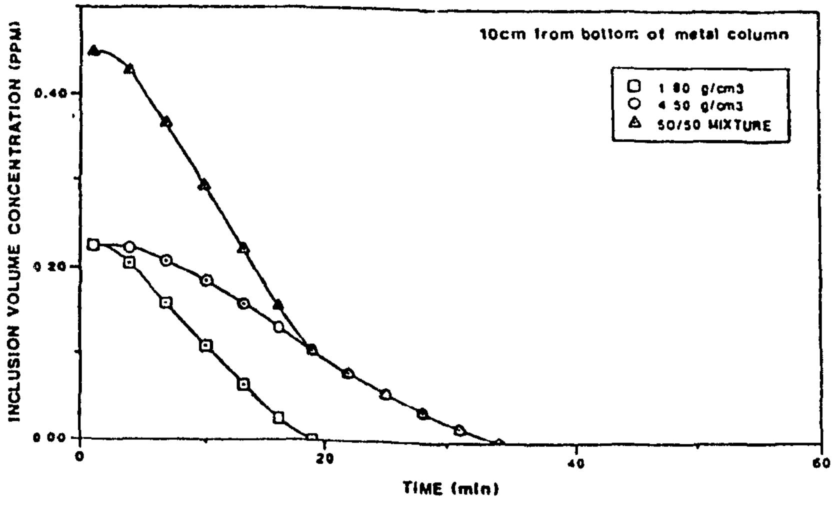

Figure 14 - Time variation for the inclusion concentration on a mixture of floating ($MgCl_2$) and sinking (TiB_2) inclusions, at a point 10 cm from the bottom of the metal bath ("stationary furnace scenario"). For this particular mix of species, the inclusion concentration is initially higher for the stationary furnace, but it decreases towards zero much more rapidly; in this case, after approximately 15 minutes, the performance of the stationary furnace is superior to that of the tilting furnace.

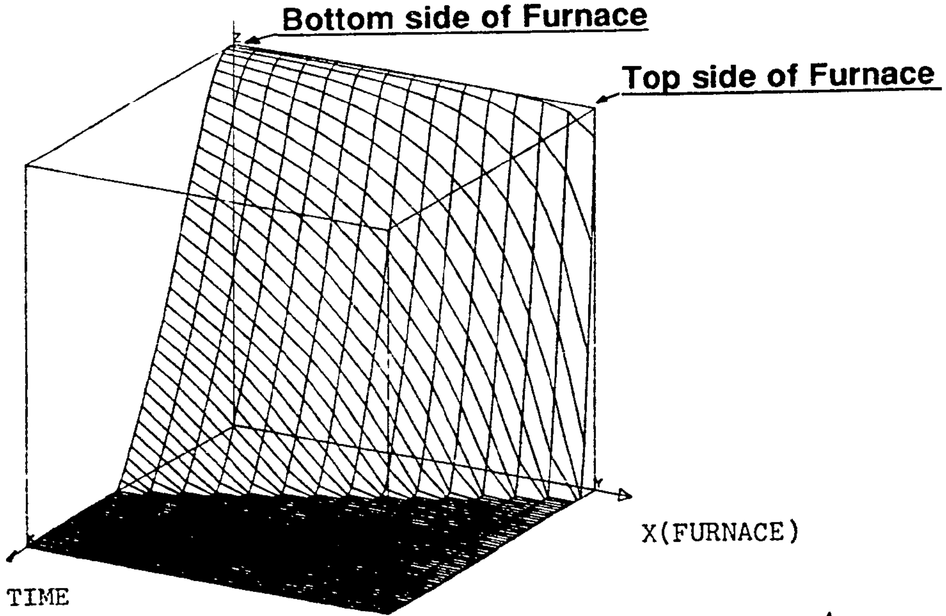

Figure 15: Concentration for particle density = 4500 kg/m^3

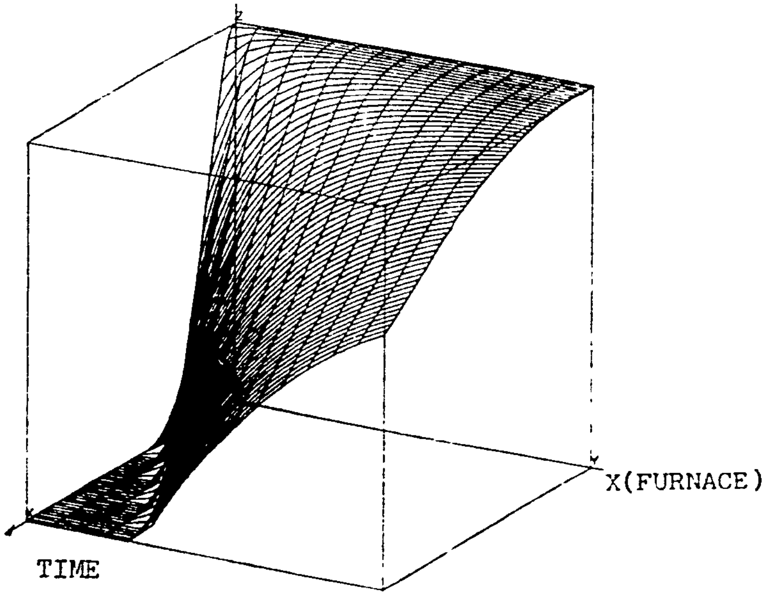

Figure 16: Concentration for particle density = 1800 kg/m^3

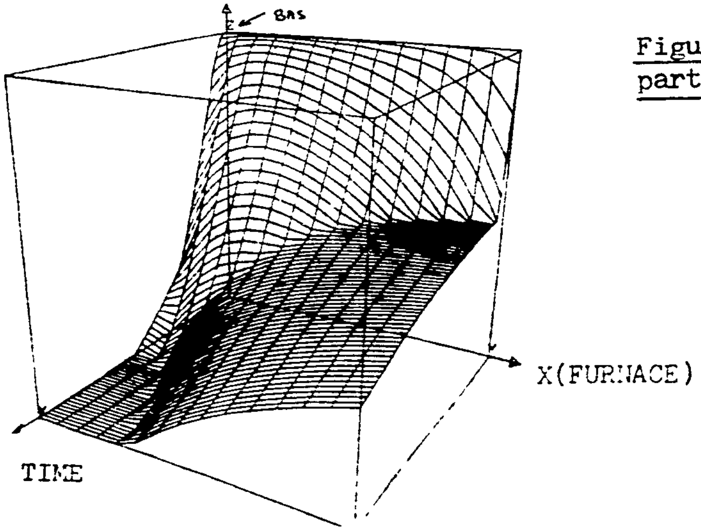

Figure 17

Computed concentration of a mix of two distributions of particles of different densities as a function of time and distance X in the furnace.

For a better visual display, a three dimensional representation has been made for C(*x*,*t*) of each compound and for the overall volumic concentration (Fig 15 to 17).

2-5 Conclusions : "plug flow" model

In all cases, inclusion concentrations are predicted to decrease as a monotonic function of time For particles heavier than aluminum, the concentration decreases faster a) when the density is high b) near the top of the vessel For this scenario the tilting furnaces would be more efficient; for inclusions lighter than aluminum, on the contrary, stationary furnaces should be a favorable choice

Unfortunately, the shapes of the predicted concentrations obtained from the simple model do not match those observed. The curves obtained from LiMCA measurements (Figs 1,2) show neither the initial plateau of the computed curves nor the inflection points present on them.

If one compares the observed results of settling of (Ti-V)B inclusions (d = 4 2 g /cm^3) plotted in Fig 10, the characteristic time of 45 minutes does not agree with the 5-10 minutes predicted by the model Furthermore, exploratory vertical samplings of a 750kg furnace suggest that inclusion concentrations, for a given size range, are relatively independent of depth This is in direct contradiction with the model's predictions This suggests the possibility of non negligible recirculation of metal inside the furnace. In order to account for this movement, the limiting case of a well mixed reactor can be considered as an alternative hypothesis

A well mixed bath model

If we assume a well stirred bath of aluminum of volume V, we can represent the mass transfer from within the bath to a stagnant boundary layer near the floor of the furnace by the equation:

$$V\frac{dn_D}{dt} = -n_D''A \qquad (15)$$

where n_D is the number of particles per unit volume and n_D'' its flux through the stagnant layer. Because of absorption at this boundary, we can write.

$$n_D'' = \alpha U n_D \tag{16}$$

where $0 < \alpha < 1$, α depending on the turbulence level

Then,

$$\frac{dn_D}{n_D} = -\frac{\alpha U A}{V} dt \tag{17}$$

where U is the terminal settling velocity and proportional to D^2.

Hence

$$\frac{dn_D}{n_D} = -k D^2 dt \qquad where \quad k = \frac{\alpha g \Delta\rho}{18 \mu L} \tag{18}$$

Integration gives:

$$n_D(t) = n_D(t_0)\, e^{-k D^2 t} \tag{19}$$

LiMCA data observed at different classes of size diameters were plotted to represent the settling rate constant given by the slope of Log n_D (Fig 18) It can be shown that these rates show a D^n dependence with $0<n<2$ (Fig 19,20). Since $n = 2$ corresponds to Stokes law, other additional phenomena may be attributed to be occuring in the furnace, causing the discrepancy in the mixed vessel involved and LiMCA measurements probable factors for this discrepancy could be capture mechanisms at the boundaries or buoyancy driven flows due to heat transfer, etc. Further,the limiting case of a well stirred bath can represent the physical phenomena in only an approximate way

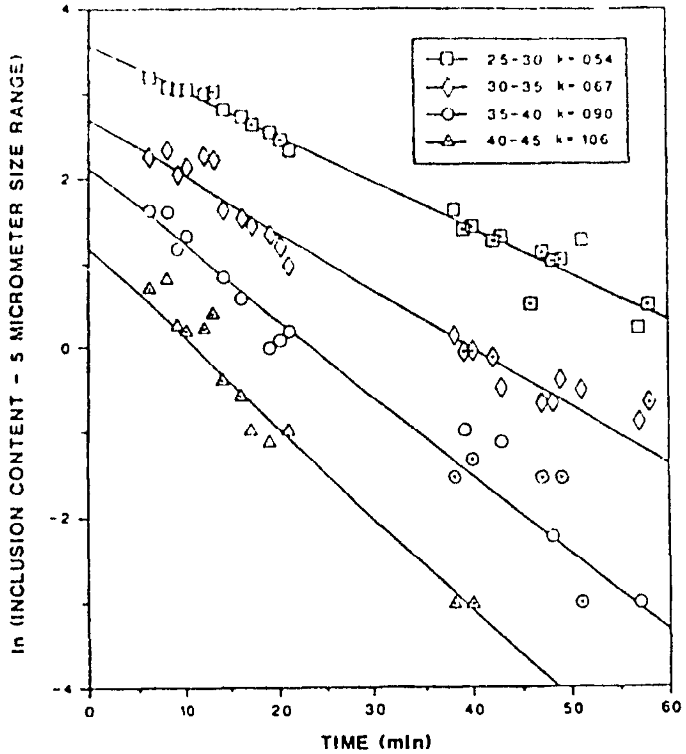

Figure 18 - Variation of settling rate constant for different size ranges; data obtained in a tilting furnace, with a Mg-containing alloy, after extensive Cl_2 furnace fluxing (large quantities of floating inclusions).

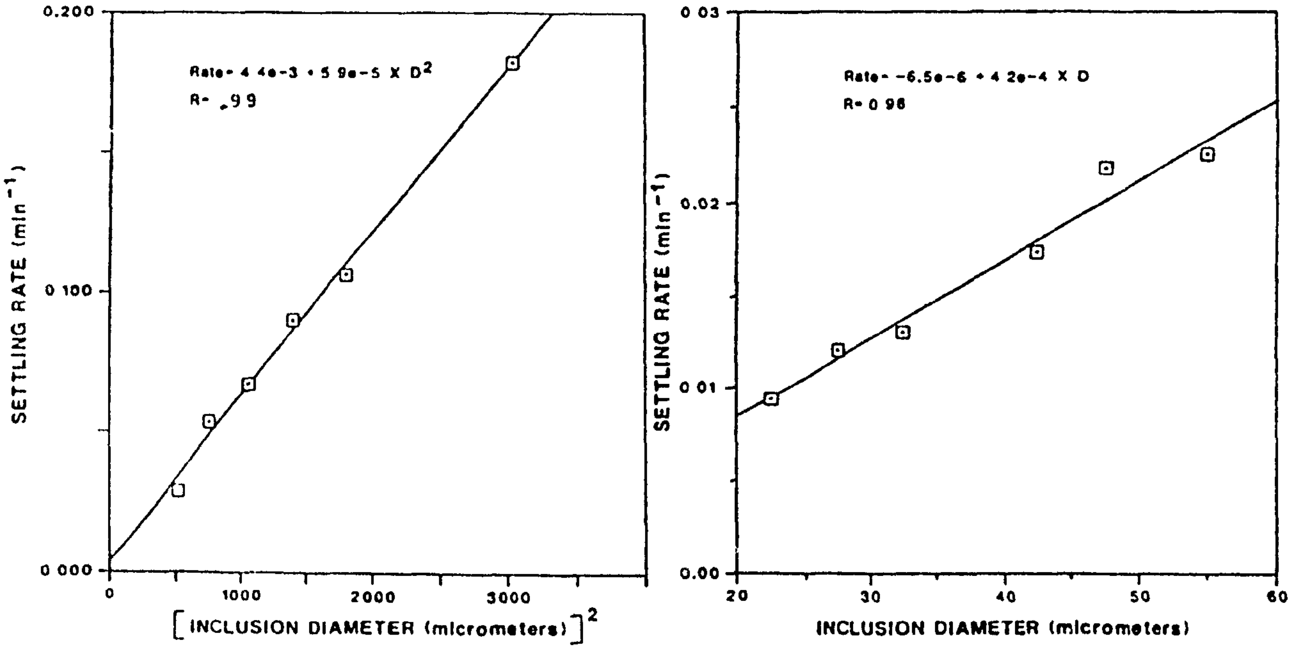

Figures 19,20 - Dependence of settling rate constant on inclusion diameter

3 Conclusions to preliminary work

New possibilities at ALCAN INTERNATIONAL to assess metal cleanliness on both the quantitative and qualitative sides have made it possible to record a significant amount of casting data Comparisons of these data with simple preliminary models allow the following observations to be made·

a) Depending on the size and type of inclusions, settling in reverbatory furnaces can take place for several hours Provided that no other movement is superimposed, a maximum of two hours seem beneficial to the final product

b) Predictions of simplified models based on the limiting cases of a plug flow type reactor or a well mixed bath show discrepancies with data recorded from experiments.

c) The contribution of convective currents inside a metal holding furnace is speculated to be significant This is an additional subject of study of the present thesis Thermal buoyancy driven flows which take place in a furnace prior to casting are due to temperature gradients, heat losses through the side or bottom walls and also due to a non uniform temperature profile at the metal free surface The implications of convective currents are thoroughly studied These currents are in the turbulent regime because of the high Rayleigh numbers involved

CHAPTER III

Mathematical modelling of turbulent natural convection. Literature review.

Transient turbulent natural convection in cavities is of interest to a considerable variety of fields and applications: ventilation of rooms, solar energy collection, environment (dissipation of heat in atmosphere or estuaries .), flow around engineering structures such as turbine blades, circulation of fluid in a nuclear reactor

While a large number of papers are available in the literature for laminar cases, the same is not true for turbulent buoyancy driven flows. Ostrach (1972) and Catton (1978) reviewed the earlier work on the laminar natural convection in cavities. No such a review on turbulent natural convection is found in the literature When turbulent buoyancy flows have to be modelled, the difficulty arises from the concurrent facts:

- •Contrary to pure convective flows, the momentum and enthalpy equations remain interlinked during the simulation process This can eventually lead to some instabilities or divergence and always to a large computing time

- •The behaviour of the flow combines both boundary-layer-like features near the heated and cooled walls and a slower gross circulation elsewhere (generally in the bulk of the cavity).

- •Turbulence modelling was initially developped for convective flows where high Reynolds numbers have to be accounted for: for example, the mixing-length and well known K-E model work very well in forced convection problems In the natural convection problems, the Reynolds numbers generated by buoyancy are relatively lower even if turbulence can be identified While it is possible to modify the generation term of energy (of turbulence) in the turbulent model to take into account the buoyancy effects, the field of turbulent natural convection has not been yet searched extensively at least with respect to liquid metals

Thus, among this class of problem, published work on natural convection in cavities for low Prandtl number fluids and high Rayleigh numbers are very limited (11,12,16)

Despite the importance of buoyancy driven turbulent natural convection in metal processing vessels, this area has received scant attention The main reason for the lack of studies may be due to the fact that experimentally it is very difficult to measure or even qualitatively visualize flow patterns inside big vessels filled with molten metal.

Finally, it should be noted that most of the published works available are concerned with either square or rectangular cavities. In metallurgical industries, processing vessels are rarely square or rectangular shapes For example trapezoidal reverbatory furnaces, ladles and odd-shape tundishes are very common metal processing vessels

The following is a review of turbulent natural convection in cavities The review is limitied to the recent work only.

In the seventies, Jones, Launder and Spalding (4,5) reported the capabilities of the K-E model for near wall as well as for free shear flow Their models compute the turbulent kinematic viscosity by solving two partial differential equations for the turbulent energy and for the rate of dissipation of energy Their transport equations, as for other primary variables, are of convective-diffusive type, generally with a transient term and additional source terms to reflect the production or dissipation of transport quantities At this early stage of development of the turbulent K-E model, two variants were already presented a) high Reynolds number formulations and b) low Reynolds number formulations. With success, the K-E model was able to predict turbulent boundary layer flows with a predominant strong longitudinal acceleration In such a case, reversion towards laminar regime could be computed and a good agreement was made versus experiments, particularily from Moretti & Kays (34). Moreover, the K-E model leads to accurate predictions for flows with recirculation as well as for those of the boundary layer type. The K-E was found to be superior to the mixing length algebric model in providing a substancially greater predictive accuracy.

In 1979, Chan and Banerjee (6) presented a three dimensional analysis of transient turbulent natural convection in rectangular enclosures. A numerical technique based on the MAC (marker and cell technique) was used sucessfully to solve low Rayleigh number cases (10^5) for 2D as well as 3D problems. This technique was used on the conservation equations with primary variables. Discretization of the transport equations was made over a cell using the full upstream formulation for the advective terms to preserve the transportive property Constraints of stability for such an explicit scheme require that the fluid must not cross more than one cell at a (time) step. In this case, convergence was reached for the case of air ($Ra = 10^5$, $Pr = 0.72$) with good agreement with experimental data. The technique is said to work well for turbulent flows

In 1980, Ideriah (7) made predictions of turbulent cavity flows (two dimensional, steady-state) using primitive variables formulation of Navier Stokes equations and adopting a modified K-E model for turbulence. Terms proportional to $\rho g \beta (v\theta')$ were used in the standard K-E equations to take into account the buoyancy effects A high Reynolds number formulation was used and, for all primary variables, the wall regions were modelled through wall functions (log-law for momentum as an example). The *simple* (semi-implicit scheme for pressure linked equations) algorithm developed by Patankar (8) was employed to solve the set of finite difference equations. The predictions of momentum and heat transfer generated by these studies were very good for high Reynolds number cases ($Re = 2 \times 10^5$) while a discrepancy of 10 to 15% was observed for lower Reynolds number ($Re = 10^4$).

In 1982, Fraikin and Portier (9) analyzed the problem of turbulent natural convection in two dimensional enclosures with purely conductive walls for Grashof numbers up to 10^7-10^8. The time averaged forms of the conservation equations were solved using the stream function vorticity approach. Turbulence was modelled by a standard two equations K-E model, including a dissipation term of turbulent energy by buoyancy; this last term is also balanced by a production term of energy by shear. The method used to solve the equations was an alternative direction implicit scheme and a control-volume approach with hybrid differencing for both convection and diffusive terms. For very slow converging simulations with a 25 x 25 non uniform mesh, the heat transfer could be predicted by the correlation: $Nu_H = 0.162*Gr^{0.275}$ valid for Grashof numbers between 6×10^6 and 10^8 Results for momentum and heat transfer could be confirmed by comparing with few experimental data up to $Gr = 5 \times 10^7$. This Grashof number corresponds to the transition region. A sensivity study was also carried out for the constants met in the K-E model. For problems with Grashof numbers higher than 10^8, Fraikin and Portier anticipated a considerable increase of the computing time which would be particularily necessary for the resolution of the turbulent boundary layers.

In 1982, Markatos & Malin (10) studied the problem of turbulent-buoyancy induced-smoke flow in enclosures with an internal heat source term. Primary variables were used to solve momentum, heat, mass and turbulent equations with a *simple* algorithm The formulation of the K-E was standard, except that, for the E equation the source term for shear and buoyancy (GB + GK) was multiplied by a linear function of the Richardson number $Rf = -GB/GK$. Boundary conditions were set up with the wall function approach of Launder and Spalding (ref 5) Two dimensional steady-state simulations were achieved at Grashof $Gr = 10^{12}$ for which almost no experimental data was available Nevertheless, good numerical comparisons could be made with studies held at University of Notre-Dame (Yang & Chang). Moreover, Markatos and Malin highlighted the importance of the buoyancy term at least in the K equation of the turbulent model which was found to improve the realism of the predictions

In 1983, Bejan (11) discussed transition to turbulence from scale analysis considerations on a vertical heated wall. Particularily, he provided correlations for the momentum and thermal boundary layer thicknesses for extreme Prandtl number fluids ($Pr << 1$ and $Pr >> 1$). Bejan also pointed out criterions for transition to turbulence for isothermal as well as uniformly heated walls.

In 1984, Markatos and Pericleous (12) solved numerically the problem of highly turbulent natural convection in square cavities (Rayleigh numbers from 10^3 to 10^{16}). They used the high Reynolds number formulation of the K-E model to predict at steady state buoyancy driven flows in two dimensional cavity configurations A generation term

$$G_B = -\beta g \frac{\mu_T}{\sigma_T}\left(\frac{\partial T}{\partial Y}\right) \tag{20}$$

was included to reflect the buoyancy dissipation in the K equation. Wall functions were used during the computations. From the numerical point of view, the "*simplest*" algorithm which is a variant of the "*simple*" algorithm was used: a Jacobi (point by point) procedure was used for convective terms and a line-by-line one for diffusive terms. Computations were achieved with the PHOENICS code with non uniform meshes from 30 x 30 to 80 x 80. The procedure was found to be strongly convergent and final results proved to be grid independent. Moreover, the use of the K-E model in this work lead to reasonable predictions of the overall flow at high Rayleigh numbers. Validity versus experimental data was checked up by the authors to $Ra = 10^8$ and extrapolated up to $Ra = 10^{12}$.

In 1985, Vanka (13) proposed a new algorithm based on a fully coupled solution of the Navier Stokes equations. Integration by finite differences was made with the control volume approach using a staggered grid and an "exact" scheme for the internode variation of the dependent variables. To retain the coupling between the momentum and continuity equations, an iterative process was used to update simultaneously velocity and pressures and subsequently the K and E together. The equations for U,V,P were considered as a block-structured matrix F(x) = 0 and solved by a genaralized Newton method The Jacobian matrix involved is a block-pentadiagonal one so that the solving procedure had to set up using splitting techniques to save computer storage. Vanka assessed the performance of the algorithm for four recirculating flow situations under various flow conditions. For the coaxial jet-case studied, the program converged 10 times faster than the initial "*simple*" program with a much higher accuracy (since the "exact" scheme was used)

In 1985, Ozoe Churchill and Lior (14) computed turbulent natural convection in rectangular channels filled with water subject to an horizontal thermal gradient (Rayleigh number $Ra = 10^{10}$ and 10^{11} and Prandtl $Pr = 6.7$). They used a two dimensional formulation of stream function and vorticity coupled with a K-E model that in the Fraikin's studies (9) They used the hybrid finite-difference scheme during their computations, a highly non uniform grid for the discretization (very fine near the walls and coarse in the bulk of the cavity) As expected, most of the movement occurs near the vertical walls while the middle of the cavity remains almost stagnant with stable sinusoidal oscillations for the time averaged velocity, turbulence fields and temperatures. The computed Nusselt numbers were in good agreement with the correlations from Churchill and optimisation of the K-E constants (σt and C1) could lead to improved results Patterns and orders of magnitude of most variables could be well predicted with this approach but a lack of turbulence experimental data is to be noted at high Rayleigh numbers

On the experimental side two papers of interest were published in 1986 on turbulent natural convective flows in cavities

Giel and Schmidt (15) studied a water filled enclosure subject to an horizontal thermal gradient between its vertical walls. Measurements were achieved at high Rayleigh number 8×10^{10} mainly for velocity components and enthalpy in two dimensions Copper-constantan and chromel-alumel thermocouple probes were used for temperature measurements and laser-Doppler anemometer techniques were used for mean velocities Spectral analysis (using the Fast Fourier Transform) of the fluctuating velocities made it possible to distinguish four flow regimes in the cavity laminar, transitional, turbulent and relaminarization

The other interesting experimental study was made by Viskanta (16) for 3-D natural convection in a rectangular cavity and is one of the very rare studies of low Prandtl number fluids: liquid gallium Numerical studies generated by a *simpler* algorithm (using TDMA or tridiagonal matrix algorithm) were consistent with earlier studies of free convection with ordinary fluids. But for low Prandtl numbers, the computed Nusselt numbers for 2D and 3D simulations were found to be significantly different (overprediction for the 2D) The correlation which resulted from that study was:

$$Nu = 0.16\, Ra^{0.31} Pr^{0.14}$$

so for Pr = 0.01 $\quad$ $\mathrm{Nu} = 0.084\ \mathrm{Ra}^{0.31}$

This sort of correlation was also found in a separate study by researchers Chiesa and Guthrie (33) Three dimensional patterns were found to reflect convective heat transfer to the walls as well as in the core of the cavity. In general a finer grid was found necessary for low Prandtl number fluids.

In 1986, Humphrey and To (17) presented a comparison of turbulence modelling for free convection along a flat plate using two different approaches: a K-E model (adapted for low Reynolds numbers) and an algebric stress model (ASM). Performance of both models was found satisfactory for momentum and heat transfer and conformed to experimental data. The role of the buoyancy term in the K equation was discussed. In spite of moderate effects (a 7% error is observed if omitted), this term is predominant in the wall region where the production of energy by shear is balanced by its dissipation by buoyancy, which has a dampening effect In a follow-up paper, Humphrey and To (17) tested the former K-E model with a cavity problem. The low Reynolds formulation was used with variable physical properties instead of the classical Boussinesq approximation which is limited to low overheat ratios ($\Delta T/T_0$). The buoyancy source term for the turbulent energy equations was chosen to be:

$$G = \overline{\rho' U'_i}\, g_i = \frac{1}{T}\frac{\mu_T}{\sigma_T}\left(\frac{\partial \overline{T}}{\partial X_i}\right) g_i \tag{21}$$

No wall function was used for the boundary conditions but computations of the variables were achieved everywhere in the domain including the viscous sublayer region. Consequently the grid used was highly non uniform with at least five points within this sublayer region. For wall boundary conditions, the following asumptions were made ($U_i = 0$; $T = T_W$; $K = 0$) and

$$\frac{\varepsilon}{\nu} = 2\left(\frac{\partial k^{1/2}}{\partial n}\right)_W \tag{22}$$

For building the mesh an estimate of the boundary layer thickness was taken from George and Capp (32): $1.7 = y/\eta_t$ where η_t is the inner region length scale given by:

$$\eta_t = \left| \left(\frac{V_\infty}{Pr} \right)^2 - (g\,\beta\,\Delta T) \right|^{1/3} \qquad (23)$$

Extensive testing of their model was achieved for number of free convection situations encountered in the relevant literature and grid independent results were checked carefully. Validation versus experimental work was done and discrepancies between measurements and computations were attributed only to the lack of experimental knowledge about turbulence, especially in the viscous sublayer.

In 1987, Coulter and Guceri (18) provided computational solutions of laminar and turbulent natural convection in irregularly shaped geometries. They used the boundary fitted coordinates approach (BFCS). This is a mapping technique which transforms the partial differential equations of transport phenomena into a computational domain of regular shape. Discretization and solution of these equations are then made by classical methods. The K-E model from Jones and Launder was used in conjunction with the stream function-vorticity approach for momentum. Integration was made by a control volume technique using upwind differencing for the convective terms. A grid control technique was set up to ensure a sufficient number of nodal points near the walls and where turbulence is the more likely to develop. Valid results were obtained up to Rayleigh numbers of 10^8.

In 1987, Thompson et al (19) modelled buoyancy-driven turbulent flow and heat transfer in rectangular cavities using two turbulence models: an eddy viscosity model and a high Reynolds formulation of the K-E model. Simulations were carried out for water with Rayleigh numbers between 10^{12} and 10^{13}, using the Boussinesq approximation and constant physical properties of the fluid. Velocity profiles were successfully compared in the boundary layer zone with other models results. The eddy viscosity model was found much less time consuming than the K-E model and proved to be a good help for grid refinement purposes.

In 1988, Farouk (20) undertook the study of high Rayleigh number transient natural convective flows in a cavity with an internal heat source (Ra from 10^6 to 10^8 and Prandtl number 6.5). A two dimensional approach with a stream function and vorticity formulation were applied to the equations describing the problem. A KE model from Jones and Launder was chosen with a turbulent viscosity functions of K,E but also of the local Reynolds number. All equations were solved for the whole domain (laminar, transitional and turbulent regions) with a finite difference (control-volume with hybrid scheme) method. Non uniform meshes up to 81 x 51 grid points were tested. Interesting flow behaviour patterns could be observed which ranged from a multicellular structure to a unique recirculation vortex as the Rayleigh number increases. Average Nusselt numbers at boundaries compared well with other authors' studies (measurements of Kulacki and Nagle).

In 1989, Ince and Launder (21) reported computations for turbulent natural convection in rectangular enclosures. They chose a K-E eddy viscosity model with an adapted low Reynolds model formulation. In Particular, the coefficients C_μ and C_E were taken as functions of the turbulent Reynolds number, defined as $Rt = \rho K^{**}2/\mu/E$. A new buoyancy term was included into the generation term of the K differential equation:

$$\frac{\beta\rho g}{T}\overline{U'_i\theta'} = \frac{3}{2}\frac{C_\mu}{\sigma_\theta}\frac{K}{E}\,\frac{\beta\rho g}{T}\,\overline{U'_iU'_k}\,\frac{\partial\overline{T}}{\partial X_k} \quad \textit{where} \quad \overline{U_i\,U_k} = \frac{2}{3}\delta_i^k K - \nu_T\left(\frac{\partial U_i}{\partial X_k} + \frac{\partial U_k}{\partial X_i}\right) \qquad (24)$$

Instead of using wall functions, they proposed a modification of the E equation through the addition of a non linear source term S_C, which is a function of K,E and y the distance to the wall. This term mainly models the rate of energy dissipation in the inner region (close to the wall), while it decreases in the outer region. The classical control-volume elliptic solver for primary variables was used jointly with a staggered grid. Two dimensional square cavity problems were solved with intermediate Rayleigh numbers between 3×10^7 and 2×10^9. Correlations with Nusselt were found to be of the type $Nu = c\ Ra^{1/3}$. Near wall profiles of the vertical velocity and temperatures were plotted and compared to the formulae of George and Capp. In the enthalpy profiles close to the walls were fitted very well with the above formulae, the velocity was closer to the profiles proposed by Humphrey and To (17). In the present studies, the Rayleigh numbers considered were not high enough for the viscous stresses to be negligible in the region of the wall

Conclusion of the Literature review

Summing up, the K-E model is recognized to be an efficient mean of computing turbulence not only in forced flow situations as it was initially created for but also for buoyancy driven flows inside cavities Some authors, in the latter cases recommend the use of a buoyancy term in the K and/or E equations (12,17,21) although some other investigators find these terms negligible in their calculations (17) This type of turbulence modelling will be considered at Chapter 4.

CHAPTER IV

Computation of buoyancy driven flows

1 Basic equations. the laminar case and turbulence modelling

1-1 Laminar equations

In the laminar case, the four general equations necessary to represent convective heat and mass transfer due to buoyancy driven flows are.

- the continuity equation

$$\frac{\partial \rho}{\partial t} + \nabla \cdot (\rho V) = 0 \qquad (25)$$

- the momentum equation

$$\frac{\partial}{\partial t}(\rho V) + (V \cdot \nabla)(\rho V) = -\nabla P - \nabla \cdot \tau + \rho F \qquad (26)$$

- the internal energy equation

$$\frac{\partial}{\partial t}(\rho H) + \nabla(\rho V H) = -\nabla(P V) - \tau.(\nabla V) - \nabla q + q''' \qquad (27)$$

- the concentration equation

$$\frac{\partial}{\partial t}(\rho C) + \nabla(\rho V C) = -\nabla \cdot J + m''' \qquad (28)$$

The tensor and vector notation is that used in Bird , Stewart and Lightfoot (ref 22) In most cases, the enthalpy H is related to the temperature field so that the computation of the thermal gradients is then possible.

1-2 Hypotheses made

We are mainly interested in the problem of natural convection in a rectangular or trapezoidal cavity because this is the ordinary shape of ALCAN INT. reverbatory or holding furnaces (Figs 48,75-76). Let us note that this problem exists because of the gravitational field g so that the outside force on the closed cavity is equal to ρg. We suppose that no other field (magnetic, electric field) exists. Moreover we suppose that the following assumptions are fulfilled:

1. The fluid inside the cavity is incompressible; its density ρ is independent of the space coordinates and will be only a function of T. We assume the Boussinesq approximation so that in the right hand side of the momentum equation only.

$$\rho = \rho_o \left| 1 + \beta(T - T_o) \right| \tag{29}$$

where β is the thermal expansion coefficient

2. The thermal conductivity of the fluid is constant

$$q = -k \nabla T \tag{30}$$

3. The mass diffusivity of the fluid is constant

$$J_A = -D \, \nabla C$$

4. The pressure and gravity forces are predominant in comparison with the viscous dissipation effects

5. The molecular viscosity μ of the fluid is constant

6. While the natural convection in finite enclosures is necessarily a three dimensional problem, the cavities which we consider in this work will be assumed to be sufficiently extended so that the time

averaged motion can be approximated as being two dimensional. Practically, the 2D plane considered is a plane situated far from the two end walls of the cavity.

7 The viscous dissipation term for incompressible two dimensional flow is $\mu\Phi$ where:

$$\Phi = 2\left[\left(\frac{\partial U}{\partial X}\right)^2 + \left(\frac{\partial V}{\partial Y}\right)^2\right] + \left(\frac{\partial U}{\partial Y} + \frac{\partial V}{\partial X}\right)^2 \tag{31}$$

Under the above hypothesis, the system of equations for the laminar case is equivalent to:

$$\nabla \; V = 0 \tag{32}$$

$$\rho_o \frac{\partial V}{\partial t} + \rho_o \left[(V \;\; \nabla)(V)\right] = -\nabla P + \mu \nabla^2 V + \rho g \tag{33}$$

$$\rho_o C_P \frac{\partial T}{\partial t} + \rho_o C_P \left[\nabla T \cdot V\right] = k \nabla^2 T + q''' + \mu\Phi \tag{34}$$

$$\frac{\partial C}{\partial t} + \nabla C \;\; V = D \nabla^2 C + m''' \tag{35}$$

$$\rho = \rho_o \left[1 + \beta(T - T_o)\right] \tag{36}$$

All these equations are in the scalar form except equation (33) which is of a vectorial form The quantities q''' and m''' represent the volumetric rates of heat and mass generation, which in our case will be zero in the whole domain except at the boundaries It is approximate to note that for this type of problem, equations (33) and (34) remain strongly coupled.

1-3 The turbulent equations for momentum and enthalpy

For thermal natural convection problems, two dimensionless numbers are of interest. the ratio of buoyancy forces to viscous forces i e the Grashof number (Gr_H)

$$Gr_H = \frac{g\beta\Delta T H^3}{\nu^2} \qquad (37)$$

based on the temperature gradient ΔT. And the Rayleigh number

$$Ra_H = Pr^* Gr_H = \frac{g\beta\Delta T H^3}{\nu\alpha} \qquad with\ Pr = \frac{\nu}{\alpha} \qquad (38)$$

where $Pr = \nu/\alpha$ is the Prandtl number. When the Grashof or Rayleigh number is very high, it becomes more and more difficult to get sensible solutions for equations (32) to (35) The more common attitude in such a case is to define some time-averaged variables (defined by an over-bar) For example in our case.

$$U = \overline{U} + U' \ , \ V = \overline{V} + V' \ , \ C = \overline{C} + C' \ , \ T = \overline{T} + T' \qquad (39)$$

In a general way $\Phi = \Phi + \Phi'$ for each primary variable with

$$\overline{\phi} = \frac{1}{\tau}\int_0^{\tau} \phi(t)\,dt \qquad and \qquad \int_0^{\tau} \phi'(t)\,dt = 0 \qquad (40)$$

where τ is a period of time.

One has to transform the equations (32) to (35) with these new variables After Bejan (28), we have in two dimensions and cartesian coordinates

Eq (32) becomes.

$$\left(\frac{\partial \overline{U}}{\partial X} + \frac{\partial \overline{V}}{\partial Y} \right) = 0 \tag{41}$$

Eq (33) can be split in two scalar equations

$$\rho_o \frac{\partial \overline{U}}{\partial t} + \rho_o \left| \left(\overline{U} \frac{\partial \overline{U}}{\partial X} + \overline{V} \frac{\partial \overline{U}}{\partial Y} \right) \right| = - \frac{\partial \overline{P}}{\partial X} + \mu \left(\frac{\partial^2 \overline{U}}{\partial X^2} + \frac{\partial^2 \overline{U}}{\partial Y^2} \right) + \rho g_Y \tag{42}$$

$$- \frac{\partial}{\partial X} \left(\overline{\rho U'^2} \right) - \frac{\partial}{\partial Y} \left(\overline{\rho U' V'} \right)$$

$$\rho_o \frac{\partial \overline{V}}{\partial t} + \rho_o \left| \left(\overline{U} \frac{\partial \overline{V}}{\partial X} + \overline{V} \frac{\partial \overline{V}}{\partial Y} \right) \right| = - \frac{\partial \overline{P}}{\partial Y} + \mu \left(\frac{\partial^2 \overline{V}}{\partial X^2} + \frac{\partial^2 \overline{V}}{\partial Y^2} \right) + \rho g_Y \tag{43}$$

$$- \frac{\partial}{\partial X} \left(\overline{\rho U' V'} \right) - \frac{\partial}{\partial Y} \left(\overline{\rho V'^2} \right)$$

Eq (34) leads to

$$\rho_o \frac{\partial \overline{T}}{\partial t} + \rho_o \left| \left(\overline{U} \frac{\partial \overline{T}}{\partial X} + \overline{V} \frac{\partial \overline{T}}{\partial Y} \right) \right| = \rho_o \alpha \left(\frac{\partial^2 \overline{T}}{\partial X^2} + \frac{\partial^2 \overline{T}}{\partial Y^2} \right) - \frac{\partial}{\partial X} \left(\overline{\rho U' T'} \right) - \frac{\partial}{\partial Y} \left(\overline{\rho V' T'} \right) \tag{44}$$

Eq (35) leads to

$$\rho_o \frac{\partial \overline{C}}{\partial t} + \rho_o \left| \left(\overline{U} \frac{\partial \overline{C}}{\partial X} + \overline{V} \frac{\partial \overline{C}}{\partial Y} \right) \right| = \rho_o D \left(\frac{\partial^2 \overline{C}}{\partial X^2} + \frac{\partial^2 \overline{C}}{\partial Y^2} \right) - \frac{\partial}{\partial X} \left(\overline{\rho U' C'} \right) - \frac{\partial}{\partial Y} \left(\overline{\rho V' C'} \right) \tag{45}$$

As one can see, some new terms appear in the right hand side of equations (42) to (45)·

$$-\frac{\partial}{\partial X}\left(\overline{U'\Phi'}\right)\ and\ \frac{\partial}{\partial Y}\left(\overline{V'\Phi'}\right) \qquad (46)$$

which are actually new unknowns of the problem For the closure purposes we can define:

a) the eddy shear stress

$$The\ eddy\ shear\ stress \qquad \tau_{XY} = -\rho\overline{U'V'} = \rho\varepsilon_M \left| \frac{\partial \overline{U}}{\partial Y} + \frac{\partial \overline{V}}{\partial X} \right| \qquad (47)$$

b) the eddy heat flux

$$The\ eddy\ heat\ flux. \qquad \Psi_{XY} = -C_p\,\rho\overline{V'T'} = \rho C_p\varepsilon_H \frac{\partial \overline{T}}{\partial Y} \qquad (48)$$

c) the eddy mass flux

$$The\ eddy\ mass\ flux \qquad M_{XY} = -\overline{V'C''} = \varepsilon_m \frac{\partial \overline{C}}{\partial Y} \qquad (49)$$

In these equations E$_M$, E$_H$ and E$_m$ are, respectively, the momentum eddy diffusivity, the thermal eddy diffusivity and the mass eddy diffusivity. Though these quantities have some analogy with the standard diffusivities, they are in fact not a property of the fluid but are flow dependant With the equations (47-49), the system(42-45) simplifies to give.

$$\rho_o\frac{\partial \overline{U}}{\partial t} + \rho_o\left(\overline{U}\frac{\partial \overline{U}}{\partial X} + \overline{V}\frac{\partial \overline{U}}{\partial Y}\right) = -\frac{\partial \overline{P}}{\partial X} + \frac{\partial}{\partial X}\left((\mu + \rho_o\varepsilon_M)\frac{\partial \overline{U}}{\partial X}\right) + \frac{\partial}{\partial Y}\left((\mu + \rho_o\varepsilon_M)\frac{\partial \overline{U}}{\partial Y}\right) \qquad (50)$$

$$+\ \rho g_X + S_U$$

$$\rho_o\frac{\partial \overline{V}}{\partial t} + \rho_o\left(\overline{U}\frac{\partial \overline{V}}{\partial X} + \overline{V}\frac{\partial \overline{V}}{\partial Y}\right) = -\frac{\partial \overline{P}}{\partial Y} + \frac{\partial}{\partial X}\left((\mu + \rho_o\varepsilon_M)\frac{\partial \overline{V}}{\partial X}\right) + \frac{\partial}{\partial Y}\left((\mu + \rho_o\varepsilon_M)\frac{\partial \overline{V}}{\partial Y}\right) \qquad (51)$$

$$+\ \rho g_Y + S_V$$

where:

$$S_U = \frac{\partial}{\partial X}\left((\mu + \rho_o \varepsilon_M) \frac{\partial \overline{U}}{\partial X} \right) + \frac{\partial}{\partial Y}\left((\mu + \rho_o \varepsilon_M) \frac{\partial \overline{V}}{\partial X} \right) \tag{50a}$$

and

$$S_U = \frac{\partial}{\partial X}\left((\mu + \rho_o \varepsilon_M) \frac{\partial \overline{U}}{\partial Y} \right) + \frac{\partial}{\partial Y}\left((\mu + \rho_o \varepsilon_M) \frac{\partial \overline{V}}{\partial Y} \right) \tag{51a}$$

$$\rho_o \frac{\partial \overline{T}}{\partial t} + \rho_o \left(\overline{U} \frac{\partial \overline{T}}{\partial X} + \overline{V} \frac{\partial \overline{T}}{\partial Y} \right) = \rho_o \left| \frac{\partial}{\partial X}\left((\alpha + \varepsilon_H) \frac{\partial \overline{T}}{\partial X} \right) + \frac{\partial}{\partial Y}\left((\alpha + \varepsilon_H) \frac{\partial \overline{T}}{\partial Y} \right) \right| \tag{52}$$

$$\rho_o \frac{\partial \overline{C}}{\partial t} + \rho_o \left(\overline{U} \frac{\partial \overline{C}}{\partial X} + \overline{V} \frac{\partial \overline{C}}{\partial Y} \right) = \rho_o \left| \frac{\partial}{\partial X}\left((D + \varepsilon_m) \frac{\partial \overline{C}}{\partial X} \right) + \frac{\partial}{\partial Y}\left((D + \varepsilon_m) \frac{\partial \overline{C}}{\partial Y} \right) \right| \tag{53}$$

The above equations constitute a system of six equations requiring eight unknown variables (U,V,P,T,K,E,C,ε_M,ε_H,ε_m). In order to bridge the gap between equations and variables, additional equations are needed to model the turbulence. Over the past twenty years numerous turbulence models have been developed by various researchers Among these models the KE model is the most tested and is very popular in Engineering Science (23,24).

1-4 The K-E model

In the KE model, the kinetic energy of turbulence per unit of mass of fluid is defined by:

$$k = \frac{1}{2} \left(\overline{U'^2} + \overline{V'^2} \right) \tag{54}$$

for 2D flows while the dissipation rate of energy can be represented by:

$$E = C_D \frac{K^{1.5}}{L} \tag{55}$$

where L is the length scale, C_D a constant

The momentum eddy diffusivity is taken to be

$$\varepsilon_M = C_\mu K^{0.5} L \tag{56}$$

and the turbulent viscosity μ_T:

$$\mu_T = \rho\varepsilon_M = \rho C_\mu C_D \frac{K^2}{E} \tag{57}$$

$$\frac{\mu_T}{\sigma_T} = \rho\varepsilon_H \quad and \quad \frac{\mu_T}{\sigma_C} = \rho\varepsilon_m \tag{58}$$

The variables σ_T and σ_C are respectively the turbulent Prandtl and Schmidt numbers. The new variables K ,the kinetic energy of turbulence and E, the rate of dissipation of energy per mass of liquid are driven by two partial differential equations:

The K equation:

$$\rho_o \frac{\partial \overline{K}}{\partial t} + \rho_o \left(\overline{U} \frac{\partial \overline{K}}{\partial X} + \overline{V} \frac{\partial \overline{K}}{\partial Y} \right) = \frac{\partial}{\partial X} \left(\frac{\mu_T}{\sigma_K} \frac{\partial \overline{K}}{\partial X} \right) + \frac{\partial}{\partial Y} \left(\frac{\mu_T}{\sigma_K} \frac{\partial \overline{K}}{\partial Y} \right) \tag{59}$$

$$+2\mu_T\left|\left(\frac{\partial \overline{U}}{\partial X}\right)^2+\left(\frac{\partial \overline{V}}{\partial Y}\right)^2\right|+\mu_T\left(\frac{\partial \overline{U}}{\partial Y}+\frac{\partial \overline{V}}{\partial X}\right)^2+S_{G1}-\rho\,\overline{E}$$

The E equation.

$$\rho_o\frac{\partial \overline{E}}{\partial t}+\rho_o\left(\overline{U}\frac{\partial \overline{E}}{\partial X}+\overline{V}\frac{\partial \overline{E}}{\partial Y}\right)=\frac{\partial}{\partial X}\left(\frac{\mu_T}{\sigma_E}\frac{\partial \overline{E}}{\partial X}\right)+\frac{\partial}{\partial Y}\left(\frac{\mu_T}{\sigma_E}\frac{\partial \overline{E}}{\partial Y}\right) \tag{60}$$

$$+2\mu_T C1\frac{\overline{E}}{\overline{K}}\left|\left(\frac{\partial \overline{U}}{\partial X}\right)^2+\left(\frac{\partial \overline{V}}{\partial Y}\right)^2\right|+\mu_T C1\frac{\overline{E}}{\overline{K}}\left(\frac{\partial \overline{U}}{\partial Y}+\frac{\partial \overline{V}}{\partial X}\right)^2+S_{G2}-C2\rho_o\frac{\overline{E}^2}{\overline{K}}$$

where S_{G_1} and S_{G_2} are additional production terms; for turbulent natural convection, they account for the buoyancy effects:

$$S_{G1}=-\,g\,\beta\,\frac{\mu_T}{\sigma_T}\,\frac{\partial \overline{T}}{\partial Y} \tag{61}$$

$$S_{G2}=-C_3\,\frac{\overline{E}}{\overline{K}}\,g\,\beta\,\frac{\mu_T}{\sigma_T}\,\frac{\partial \overline{T}}{\partial Y} \tag{62}$$

The first term was found to have a moderate influence on the flow field especially when stratification is predominant while the second term was found to be negligible by Markatos and Malin (10). This topic will be disscussed later.

For the constants, Launder and Spalding (5) recommended the values given in Table 7 Fraikin & al (9) recommended the value: $C_3 = 0\ 7$ for the buoyancy term Although there exists in the literature many variants of the KE model, the standard "high Reynolds" formulation was adopted in our work

Table 7: Values of parameter for the KE model

$C_\mu = 0.09$	$C_D = 1.0$	$C_1 = 1.44$	$C_2 = 1.92$	$\sigma_k = 1.0$	$\sigma_\varepsilon = 1.3$
$\sigma_T = 0.9$	$\sigma_C = 1$				

As the cavities to be considered were of large size in which strong flow patterns are likely to develop at least in a transient state, it was decided to adopt the above formulation in our computations

2 Numerical methods

2-1 Form of differential equations

The transport equations for the variables U, V, T, C, K, E, can be put in the following general form.

$$\frac{\partial \rho \Phi}{\partial t} + div(\rho \overline{U} \Phi) = div(\Gamma grad(\Phi)) + S_\Phi \tag{63}$$

[evolution] [convection] [diffusion] [source]

From the above equation, various transport equations can be derived by approximately defining Φ, S_Φ and Γ. For example.

- for the continuity equation $\Phi = 1,\ S_\Phi = 0$
- for the momentum equation $\Phi = U,\ S_\Phi = \rho g - grad(P) + S_U,\ \Gamma = \mu + \mu_t$
- for the energy equation $\Phi = T,\ S_\Phi = 0,\ \Gamma = \rho(\alpha + \alpha_t)$

- for the species continuity equation: $\Phi = C$, $S_\Phi = 0$, $\Gamma = \rho(D + D_t)$

2-2 Use of the staggered grid

With the classical methods of finite differences when solving the Navier Stokes equations, some difficulties arise from the first derivatives when classical grids are used Let's consider the cell at Fig 21.

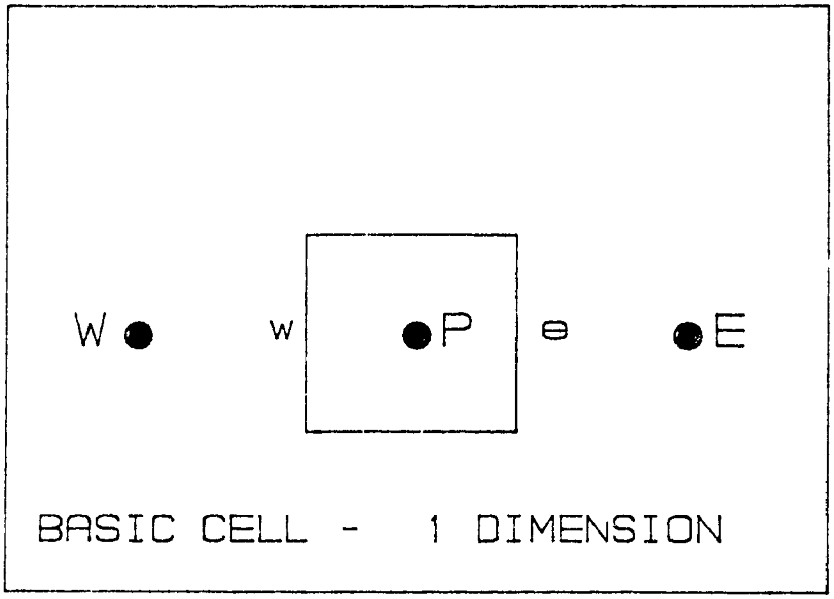

Figure 21

If we use

$$\left(\frac{dP}{dX} \right)_P = \frac{P_E - P_W}{2\,\Delta_X} \tag{64}$$

in the momentum equation

$$\left(\frac{dU'}{dX} \right)_P = \frac{U'_E - U'_W}{2\,\Delta_X} \tag{65}$$

then the method could bear alternate pressure on velocity fields For example in the case a numerical pressure field would be [100, 300, 100, 300, 100] for neighbour points, one would detect no gradient ($\Delta U / \Delta X = 0$ in one dimension) The continuity equation might not be satisfied at all Therefore the concept of finite volume is useful so that.

$$\left(\frac{\partial P}{\partial X} \right)_P = \frac{P_e - P_w}{2\,\Delta_X} \; and \; \left(\frac{\partial U}{\partial X} \right)_P = \frac{U_e - U_w}{2\,\Delta_X} \qquad (66)$$

Velocities and pressures are therefore computed at the interface of the control volume and interpolations are needed to deduce properties inside the control volume, at its center, where the energy equation is to be solved

Two different grids have then to be superimposed (see Figure 22)

the main grid: computation of T, K, E

the secondary grid: (interface of control volumes according to *x* and *y*) computation of U_x and U_y.

Let us note that the Δx and Δy are not necessarily equal between all the points; the program has to keep these data in memory

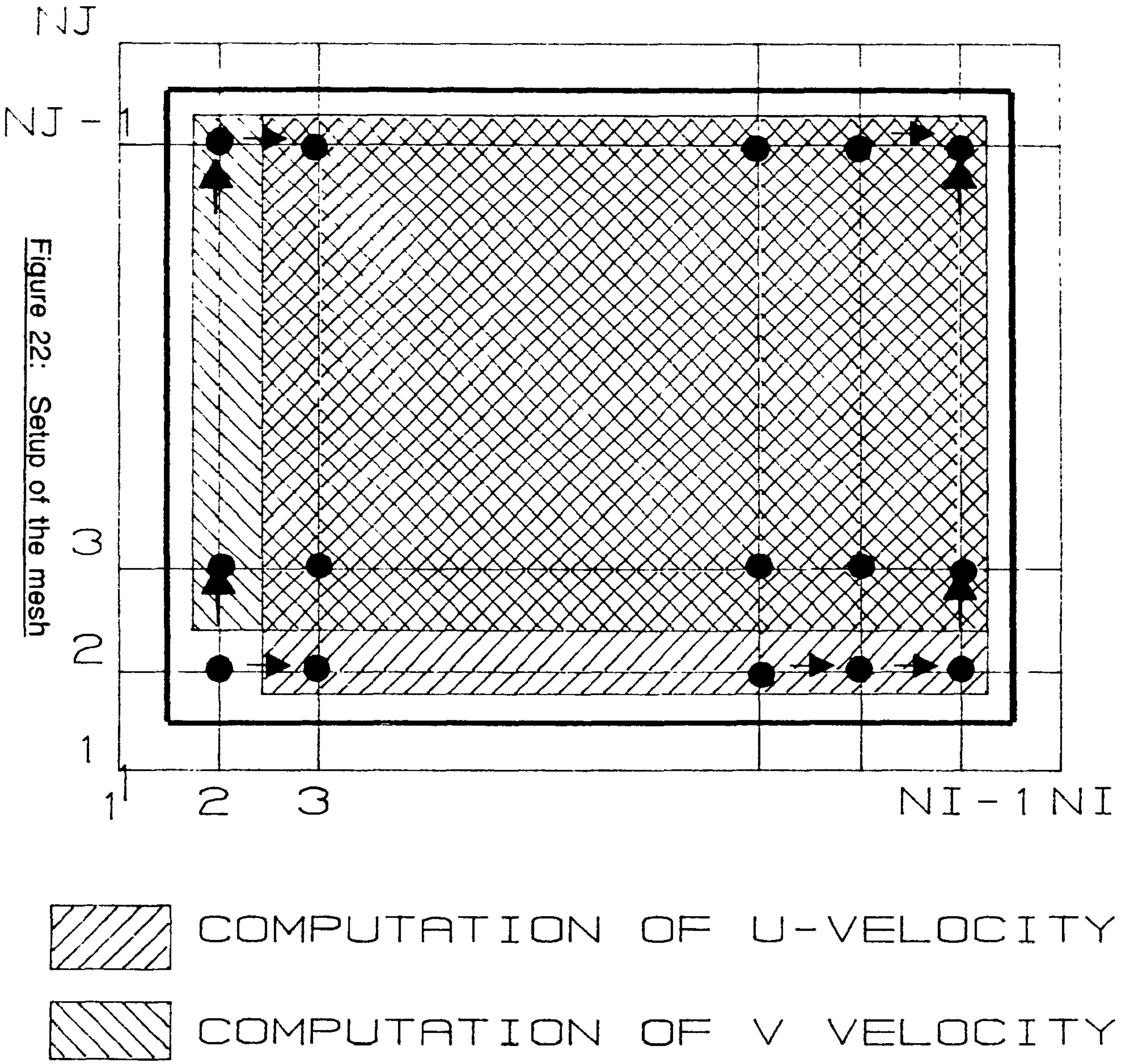

Figure 22: Setup of the mesh

2-3 Profile to be set up

As noted in 2 2, it is important to find a convenient way to derive a profile for U and V velocities on the control volume Patankar (8) recommends the "Power law profile": according to the value of Peclet number ($Pe = \rho UL/\Gamma$ = ratio convection/diffusion) different interpolations can be set up

Consider the cell drawn in Fig 23,

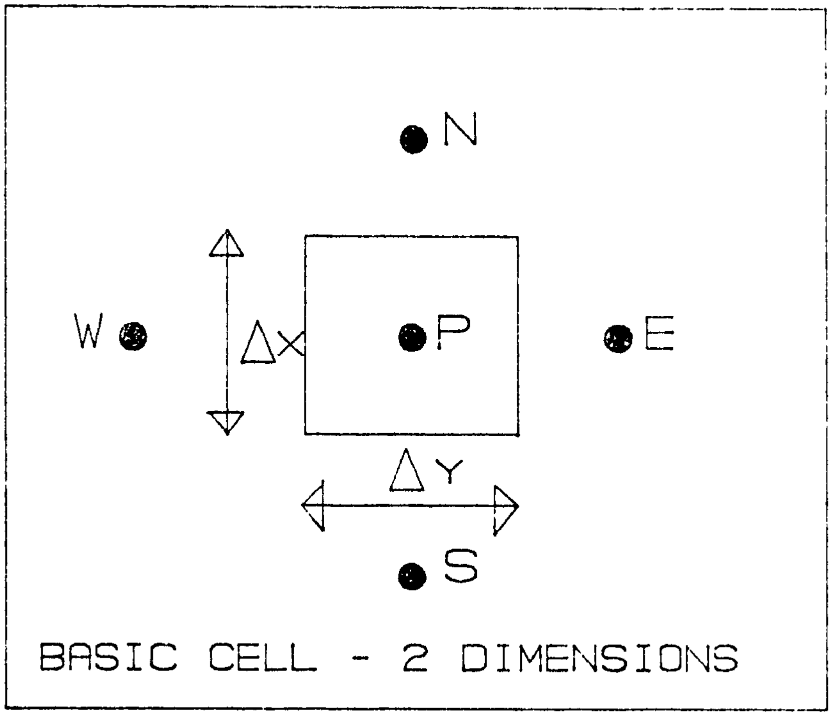

Figure 23

The discretized form of equation (63) can be expressed by

$$a_P\Phi_P = a_E\Phi_E + a_W\Phi_W + a_S\Phi_S + a_N\Phi_N + b \tag{67}$$

where.

$$a_E = D_e A(|P_e|) + Max(-F_e, 0.) \tag{68}$$

$$a_W = D_w A(|P_w|) + Max(+F_w, 0.) \tag{69}$$

$$a_S = D_s A(|P_s|) + Max(+F_s; 0.) \tag{70}$$

$$a_N = D_n A(|P_n|) + Max(-F_n, 0.) \tag{71}$$

$$b = S_C . \Delta X \Delta Y \quad with \quad \Delta X = X_e - X_w \quad and \quad \Delta Y = Y_n - Y_s \tag{72}$$

where

$$F_i = (\rho u)_i \Delta S \ , \ D_i = \Gamma_i \Delta S/(\delta s)_i \quad and \quad P_i = F_i / D_i \tag{73}$$

The choice of the profile corresponds to the choice of the function A (IPI) for "power-law"profile·

$$A(|P|) = Max[0., (1 - 0.1|P|^5)] \tag{74}$$

Actually in the Teach-T code, the hybrid scheme is used so that:

$$A(|P|) = Max[0., (1 - 0.5|P|)] \tag{75}$$

Less precise than the power law scheme, the above function requires less computation time and seems to give good results in most practical situations (8).

2-4 The SIMPLE algorithm

This algorithm used in the TEACH-T code is defined as a semi-implicit method for pressure linked equations. The main steps are the following.

1. guess a pressure field P*;
2. solve momentum equations and find U* and V*; the line method with alternating directions is used until convergence;
3. search for a new pressure field from the continuity equation;
4. correction on velocities on the basis of this new pressure field;

(5) solve the other equations with primary variables such as T, K, E, the line method with alternated directions is still used,

(6) with the updated pressure field return to step (2) until convergence is achieved

2-5 Structure of the TEACH-T program

As one can see from Figure 24, the TEACH-T program comprises 3 different parts.

2-5-1 Preprocessing

Preprocessing is achieved via START, reading of DATA CARDS and PROPS subroutines (fluid properties)

2-5-2 Solver

The SOLVER itself uses

- as many subroutines CALCΦ as primary variables (U,V, P, T, K, E...). The subroutine CALCT was not initially in the teach T and had to be constructed by the author.
- a LISOLV sub program that solves the tridiagonal linear system of equations for each iteration and each variation. For this purpose an iterative method rather than a direct method is used; the TDMA or Thomas algorithm also has the advantage of saving memory as much as possible and is more stable than methods such as Gauss Seidel.
- a PROMOD subprogram which is called from each CALCΦ to modify source terms and also to set up boundary conditions.

2-5-3 Post processing

Post processing is finally achieved through the PRINT subprogram at both intermediate iterations and final convergence

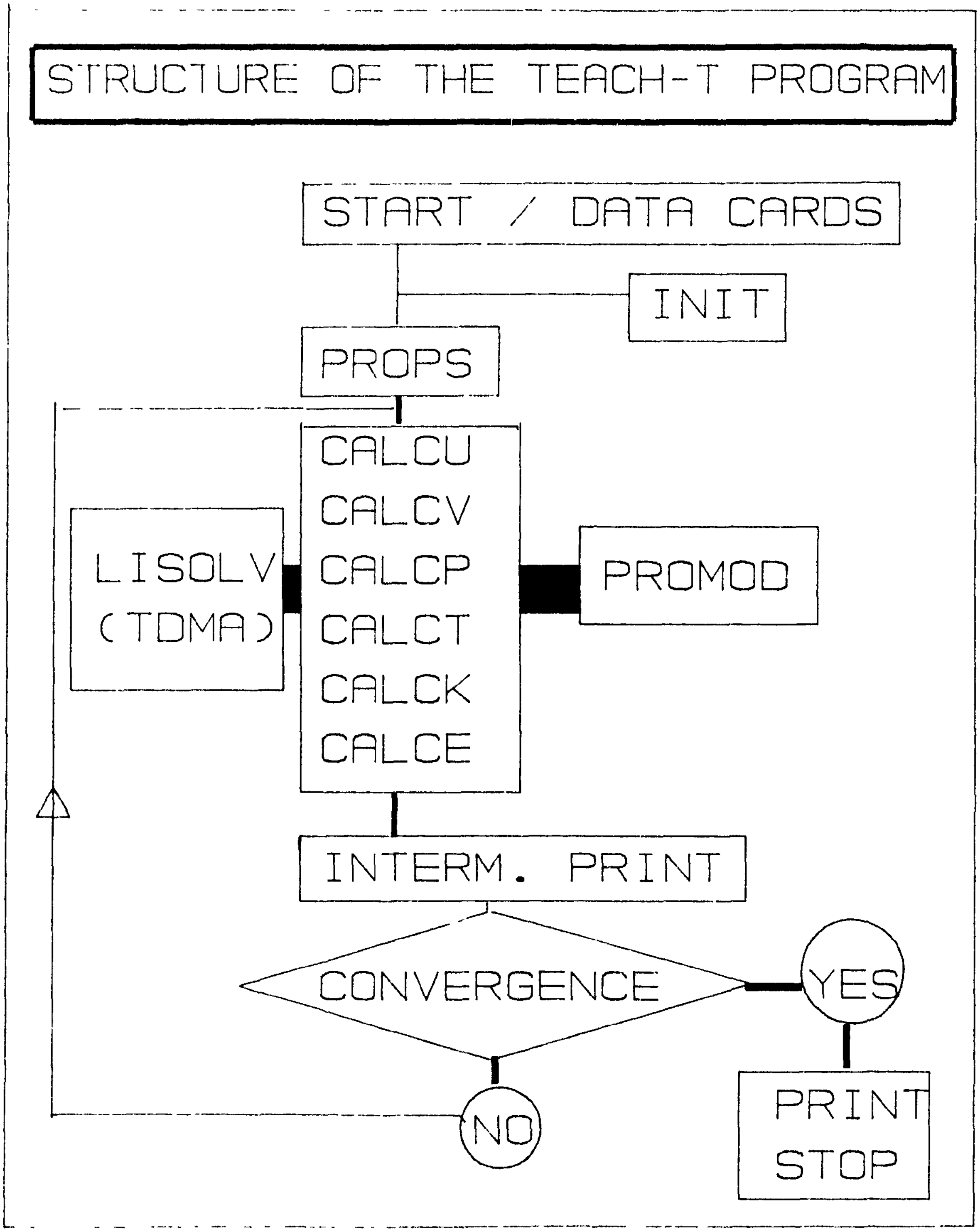
STRUCTURE OF THE TEACH-T PROGRAM
START / DATA CARDS
INIT
PROPS
CALCU
CALCV
CALCP
CALCT
CALCK
CALCE
LISOLV
(TDMA)
PROMOD
INTERM. PRINT
CONVERGENCE
YES
NO
PRINT
STOP

Figure 24

2-6 Boundary conditions and other topics

Boundary conditions have to be specified for the mathematical problem to be well defined.

2-6-1 Boundary conditions for momentum

Velocity components U and V normal to the walls are zero at the wall, the tangential components have to be computed so that friction can be expressed at the wall-liquid interface.

Turbulent flow near a wall is distinguished in two ways from flow far from the wall: the effect of the molecular viscosity becomes predominant because of the damping effect of the wall on turbulence; secondly, some properties show large gradients in the vicinity of the wall. To take into account the different behaviours of fluid in the bulk and close to a wall, a now standard way, developped by Launder and Spalding (5), is to incorporate wall functions. Let's now consider the turbulent boundary layer equation (76) for momentum close to the wall (Fig. 25).

$$\overline{U}\frac{\partial \overline{U}}{\partial X} + \overline{V}\frac{\partial \overline{U}}{\partial Y} = -\frac{1}{\rho}\frac{\partial \overline{P}}{\partial X} + \nu\frac{\partial^2 \overline{U}}{\partial Y^2} - \frac{\partial}{\partial Y}\left(\overline{U'V'}\right) \tag{76}$$

If E_M is the momentum eddy diffusivity, if we neglect the longitudinal pressure gradient and if the convective terms can be neglected near the wall

$$(\nu + \varepsilon_M)\frac{\partial \overline{U}}{\partial Y} = \frac{\tau_0}{\rho} \tag{77}$$

where τ_0 is the shear stress

The friction velocity is by definition:

$$U^* = \left(\frac{\tau_0}{\rho}\right)^{0.5} \tag{78}$$

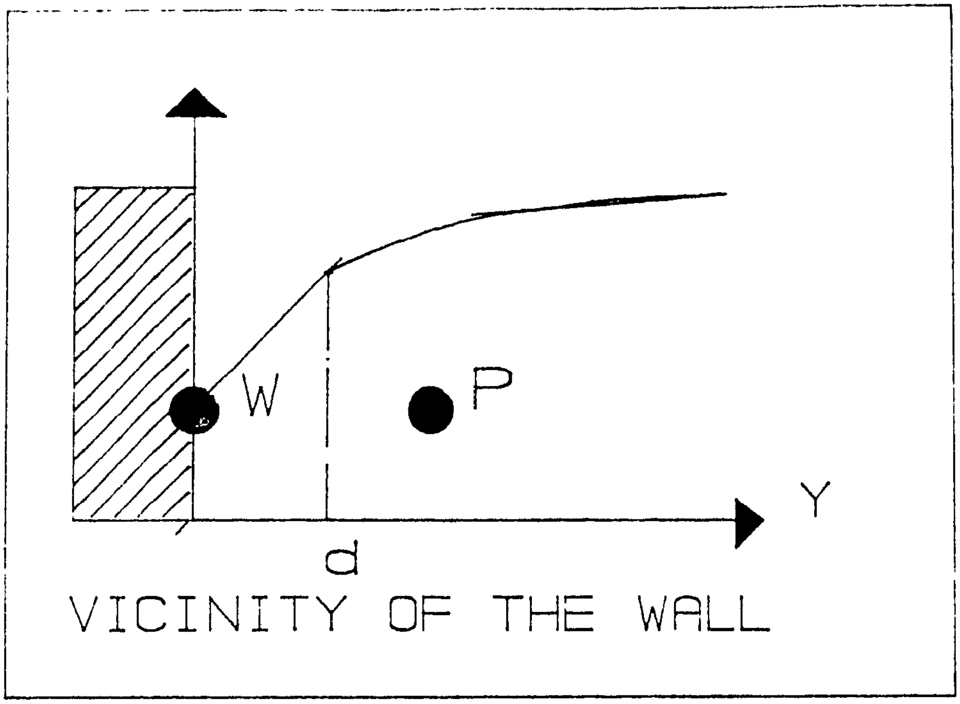

Figure 25: vicinity of the wall

So, dimensionless variables can be used:

$$U^+ = \frac{\overline{U}}{U^*} \quad V^+ = \frac{\overline{V}}{U^*} \quad x^+ = x\frac{U^*}{\nu}, \quad y^+ = y\frac{U^*}{\nu} \tag{79}$$

to transform equation (53) near the wall:

$$\left(1 + \frac{\varepsilon_M}{\nu}\right)\frac{\partial U^+}{\partial Y^+} = 1 \tag{80}$$

The momentum eddy diffusivity ε_M can be related to the velocity gradient

$$\varepsilon_M = l^2 \left|\frac{\partial \overline{U}}{\partial Y}\right| = \kappa^2 y^2 \left|\frac{\partial \overline{U}}{\partial Y}\right| \tag{81}$$

where l is the length scale proportional to y (κ is the Von Karman Constant)

•Inside the viscous sublayer

$$\frac{\varepsilon_M}{\nu} \ll 1 \quad \Rightarrow \quad U^+ = Y^+ \tag{82}$$

•Inside the turbulent sublayer

$$\frac{\varepsilon_M}{\nu} \gg 1 \quad \Rightarrow \quad \frac{\kappa^2 y^2}{\nu^2} U^{*2} \left(\frac{\partial U^+}{\partial Y^+}\right)^2 = 1 \tag{83}$$

$$\kappa Y^+ \frac{\partial U^+}{\partial Y^+} = 1 \tag{84}$$

$$\frac{\partial Y^+}{Y^+} = \kappa \, \partial U^+ \tag{85}$$

$$U^+ = \alpha Ln Y^+ + \beta \tag{86}$$

Prandtl and Taylor (ref 28) have found $\alpha = 1/\kappa = 2.5$ and $\beta = 5.5$

and the limit between the two layers was found to be for $y^+ = 11.6$

The log law for the wall is then expressed by

$$0 < Y^+ < 11.6 \Rightarrow U^+ = Y^+ \quad and \quad Y^+ > 11.6 \Rightarrow U^+ = 2.5 Ln Y^+ + 5.5 \tag{87}$$

S, the skin friction coefficient reflecting the shear stress on the wall is by definition

$$S = \frac{\tau_0}{0.5\rho U_\infty^2} \tag{88}$$

so that for $y^+ > 11.6$ the relation.

$$for\ Y^+ > 11.6 \quad \frac{\overline{U}}{U^*} = 2.5 Log\left|\frac{YU^*}{\nu}\right| + 5.5 \tag{89}$$

leads to

$$\frac{S}{2} = \left|\frac{0.43}{Log(9Re\sqrt{(S/2)})}\right|^2 \quad with\ \ Re = \frac{Y\overline{U_s}}{\nu} \tag{90}$$

The Reynolds number being based on y: Re = YU/v

Practically, the skin friction coefficient can then be computed from the Reynolds number by solving a non linear equation through an iterative process

One should note that other relations are available in the literature for linking the Reynolds number to skin friction. A comparison of Prandtl, Prandtl-Taylor and Schultz-Grunow's approaches is given at Fig. 26 As seen, there are no significant differences to be observed among these relations for high Reynolds numbers (10^5-10^{10}).

2-6-2 Boundary conditions for enthalpy

- If the wall heat flux is specified, no modification is required since this flux is used directly at the wall boundary.

- If the wall temperature is specified as a boundary condition, wall functions are required since temperatures, like velocity components, U or V, may vary steeply in the vicinity of the wall.

The heat flux q_w is expressed by:

$$q_w = \frac{\mu_t}{\sigma_t}\frac{dT}{dY} \tag{91}$$

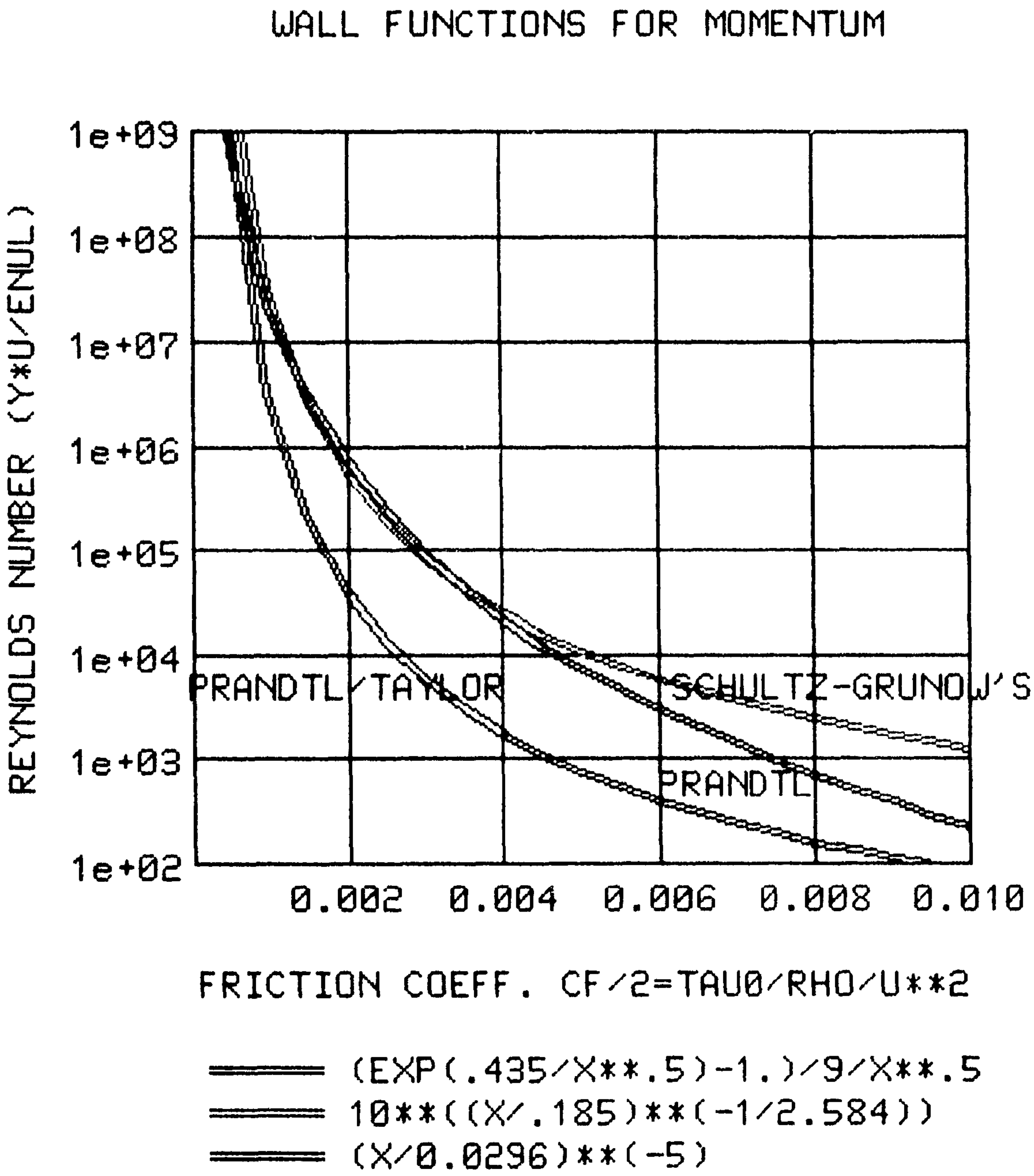
WALL FUNCTIONS FOR MOMENTUM
REYNOLDS NUMBER (Y*U/ENUL)
1e+09
1e+08
1e+07
1e+06
1e+05
1e+04
1e+03
1e+02
PRANDTL/TAYLOR
SCHULTZ-GRUNOW'S
PRANDTL
0.002
0.004
0.006
0.008
0.010
FRICTION COEFF. CF/2=TAU0/RHO/U**2
(EXP(.435/X**.5)-1.)/9/X**.5
10**((X/.185)**(-1/2.584))
(X/0.0296)**(-5)

Figure 26

where

$$\frac{dT}{dY} = \frac{T_p - T_W}{Log\,(EY^+) + kH} \tag{92}$$

with

$$H = 9\left(\frac{\sigma}{\sigma_T} - 1\right)\left(\frac{\sigma}{\sigma_T}\right)^{-\frac{1}{4}} \tag{93}$$

For convective heat transfer, the Stanton number (dimensionless) can be defined locally as:

$$St = \frac{h}{\rho C_p U_\infty} \tag{94}$$

and computed from the skin friction coefficient S:

$$St = \frac{S/2}{\sigma_T \left| 1 + 9\left(\frac{\sigma}{\sigma_T} - 1\right)\left(\frac{\sigma}{\sigma_T}\right)^{-\frac{1}{4}} \sqrt{(S/2)} \right|} \tag{95}$$

2-6-3 Boundary conditions for K and E

The kinetic energy and its gradient normal to the wall is assumed to be zero The production of kinetic energy is a source term in the K equation This source term is computed from velocity gradients, using the log law of the wall

$$K_P = \frac{U^{*2}}{C_\mu^{0.5}} \tag{96}$$

Since the characteristic length of turbulence as well as the kinetic energy are zero at the wall

$$\varepsilon = \frac{K^{3/2}}{l} \tag{97}$$

These factors make it impossible to specify the dissipation rate at the wall Therefore, the procedure commonly used is to take the first node of the grid close enough to the wall where convective terms of turbulence are negligible In this region, the production of turbulent energy is balanced by its dissipation and:

$$\varepsilon_p = \frac{U^{*3}}{y\,\kappa} \quad where \quad U^* \quad C_\mu^{0.25}\,K^{1/2} \tag{98}$$

κ = Von Karman constant

and y is the first node to the wall distance (Launder and Spalding 1972)

In order to apply the non zero tangential traction boundary condition $\tau^* = \rho U^2$ and the above condition on K, the value of the friction velocity U^* must be computed This is obtained from the log law velocity profile $U^* = \kappa U / \mathrm{Log}(EyU^*/v)$ (from eq 90) where U is the most recent estimate of the tangential velocity This last equation is solved for U^* in order to specify the boundary condition for the next iteration

2-6-4 Boundary conditions for concentrations

Generally the profile of concentration is not known at the boundaries of the computational domain Either it is a zero mass flux condition (impermeability) or it is a flux of a given value· it can be an input of material or a sink of mass For example, if the normal component of velocity close to the wall is V_N and if the concentration at this point is C^P, the sink of mass can be computed as:

$$S_C = \alpha\, V_N^P\, C^P\, A^P \tag{99}$$

where α is a coefficient $(0<\alpha<1)$ and A^P is the cell area normal to V_N

2-6-5 The pressure field

Pressure is a relative variable which is computed by reference to a point arbitrarily chosen within the computational domain In the case of natural convection of molten metals, this relative pressure is generally very small compared to the hydrostatic component

2-7 Initial conditions

During the INIT phase, all the variables have to be initialized before the first time step and iteration As an example, one can give the reasonable values·

- U = V = 0 (no initial movement)
- T = Tref (reference or average temperature)
- P = 0
- K = 10^{-5} m^2/s^2 (very small turbulence)
- E = 10^{-5} m^2/s^3
- C = 1 (uniform concentration)

2-8 Convergence of the algorithm

The mathematical criteria for convergence are based on equilibrium being achieved for each variable in each and all control volumes. For instance, we must have for the variable Φ:

$$a_P \Phi_P = a_E \Phi_E + a_W \Phi_W + a_S \Phi_S + a_N \Phi_N + b \qquad (100)$$

The absolute residual source term is defined as

$$RESOR\Phi = \sum_{CELLS} \left(a_P \Phi_P - \sum_{neighbours} a_{nb} \Phi_{nb} - b \right) \qquad (101)$$

For some variables, this computed quantity has to be normalized to take into account the gross flow coming in or out of the system The mathematical conditions (necessary and sufficient) for the convergence at each time step is:

RESORU
RESORV
RESORM
RESORT -> 0 with the respect to the
RESORK computer accuracy when
RESORE the number of iterations
RESORC increases

For each iteration at each time step, it is also useful to print the values of the Φ at a monitoring location. when these values do not change significantly, it is often because we are close to the solution but it is not a sufficient criterion of convergence

2-9 Type of grid and parameters to adjust

Some parameters have to be adjusted for each case , especially.

-the type and size of grid: the geometry can be set up with a regular grid but also with a non uniform grid for example the grid can be fine close to the wall so as to pick up the high gradients of the boundary layer and coarser in the middle of the cavity

-the relaxation factors. these factors defined for each primary variable ensure the stability of the computations but modify the convergence speed. They are of two types:

* the linear relaxation factor is mainly used for variables such as pressure. For the variable Φp we have the identity

$$\Phi_P = \frac{\sum a_{nb}\Phi_{nb} + b}{a_P} \tag{102}$$

then the relaxation factor (α) relevant to Φ is defined by

$$\Phi_P = \Phi_P^{*} + \alpha\left[\frac{\sum a_{nb}\Phi_{nb} + b}{a_P} - \Phi_P^{*}\right] \tag{103}$$

- the "false time step" relaxation factor This possibility corresponds to an addition of a source of the variable Φ in each cell

  Mass in cell/$\Delta T^{*}[\Phi]$.

  Small values of this factor correspond to a large slowing of numerical changes in the variable Φ from one iteration to the next iteration.

This tactic is adopted mainly for steady-state simulations. In transient simulations, there is already a source of this kind because of the real time step.

2-10 Treatment of sloping wall boundaries

As the computational geometry was of cartesian nature, there are two distinct approaches that can be used to treat irregular physical geometries using the finite difference technique

The first possibility which is certainly the more difficult to set up is based on grid generation systems: they are various procedures for generating the curvilinear coordinate system which defines the grid. The BFCS (boundary fitted coordinate system) falls into two basic classes. a) algebraic systems in which the coordinates are computed by interpolation and b) partial differential equation systems which have to be solved to determine the coordinates These techniques have been thoroughly reviewed by Thompson (25) and will not be considered here.

Another possibility is to keep the entire rectangular mesh around the cavity for computational purposes and to use a blockage and porosity approach All cells of the mesh outside the actual boundaries of the cavity are blocked off such that no flux can cross any of the cell limits Cells entirely inside the physical domain are not subject to any blockage but cells which are situated on the boundary itself are subjected to a partial blockage depending on their location on the boundary In the PHOENICS code, three porosity coefficients (two in 2D) have to account for the fluxes which can cross each of these boundary cells along the East-West, North-South and High-Low directions If applied correctly, this technique can very efficient in representing inclined walls Nevertheless it presents two drawbacks.

a) If the required grid is very large and particularly for non uniform meshes, it takes a considerable amount of programming time to specify all porosity factors These factors are dependent on the grid system employed and therefore problem specific

b) The resolution of the boundary layer at the inclined walls often leads to non uniform grids unless a very large number of cells (with an associated high computing time) is attempted

Although local wall shear stresses and heat fluxes on such a simulated wall may not generally agree closely with measurements, this approach is quite acceptable and have been found to be very promising (26) provided one is interested mainly in general trends of the flow patterns, the enthalpy field and species concentration behaviour

2-11 Numerical code used

2-11-1 The TEACH-2E program

Until 1986, the computer code available to the author was a greatly extended version of the "TEACH-2E" code, a modified version of the TEACH-T code This code is based on the control volume approach and uses primitive variables along with the SIMPLE algorithm (Semi-Implicit method for pressure linked equations of Patankar (ref 8)) The "TEACH-2E" program was built mainly for forced convection fluid flow problems in a rectangular or cylindrical cavity with an enlargement Of modular type, this program works basically with the primary variables which have to be solved sequentially The variables available in "TEACH-2E" were originally

U: velocity in the *x*-direction
V: velocity in the *y*-direction
P: pressure field
K turbulent kinetic energy
E: turbulent energy dissipation rate

The last two variables come from the well-known KE model Thus, this code was originally two dimensional and default options were set up for steady-state forced convection problems

In order to study natural convection and to go further than some models which use a variation of density within a forced convection code, a new subprogram was incorporated in the TEACH-T code which takes into account the enthalpy variable In this case, contrary to problems where forced convection is predominant, the momentum equation and enthalpy equation are interlinked. This means basically that H (or T) is a full primary variable in itself and will have to be solved at each iteration after U, V and P.

2-11-2 The PHOENICS code

The other code used during this work was a commercial CFD code called PHOENICS released by CHAM LTD, England. PHOENICS stands for Parabolic Hyperbolic or Elliptic Numerical Integration Code System This code was made available through ALCAN INT LTD on their Kingston computer facilities. Similar to the "TEACH-2E" code, PHOENICS is based on the control volume based primitive variables approach PHOENICS provides the option to solve systems of partial differential equations with up to fifty variables. A large number of "built-in" features are available with this code at numerous levels. The basic algorithm to integrate the equations over the control volumes was modified from "SIMPLE" to"SIMPLEST" for better efficiency: in this latter approach, "the coefficients for momenta contain only diffusion contributions, the convective terms being added to the linearized source terms of the equations This implies that, in the absence of diffusion the momentum equations are solved by a point by point Jacobi equation and not by the line by line procedure" (26) The effect of this modification is to prevent a worsening of convergence as the grid becomes finer

Among the numerous features of this CFD code it is worth mentioning four of its elegant features These are the ability of the code to handle

-two or three dimensional transient turbulent fluid flow problems in arbitrary geometries,

-two phase flow problems,

-set up of cartesian or curvilinear coordinates to treat non standard geometries with the boundary fitted coordinates approach,

-turbulence modelling with the mixing-length and KE models

Practically, the PHOENICS code embodies three main subroutines

- **The SATELLITE data items** which are the pre-processing part of the code Specification of the geometry, the space and time meshes, initial and boundary conditions, properties of the fluid and solving parameters (iterations to perform, relaxation) are required there from the user (QI DAT file written in PIL language)

- **The EARTH program** is the solver of the code Starting from the EARDAT.DAT file produced by the SATELLITE, this part usually requires most of the computing time of the problem It actually runs the number of iterations needed to reach convergence with a pre specified convergence This solver then produces three output files RESULT.DAT which traces each step of the solving routine, PHIDA DAT which contains data for graphic purposes and PHOENICS LOG to monitor the residual sources of the primary variables computed

- **The graphic packages** PHOTON and GRAFFICS enable the user to plot the results in terms of profiles, contours or vectors for each variable

3 Numerical testing simulations natural convection results and validation

3-1 Simulations with the TEACH-T code

3-1-1 Academic example case of a gas (air)

a) description of the problem

In order to test the capabilities of a version of the TEACH T program, extended for natural convection, the classical case of a rectangular cavity filled with air at the room temperature (Fig 27) was solved

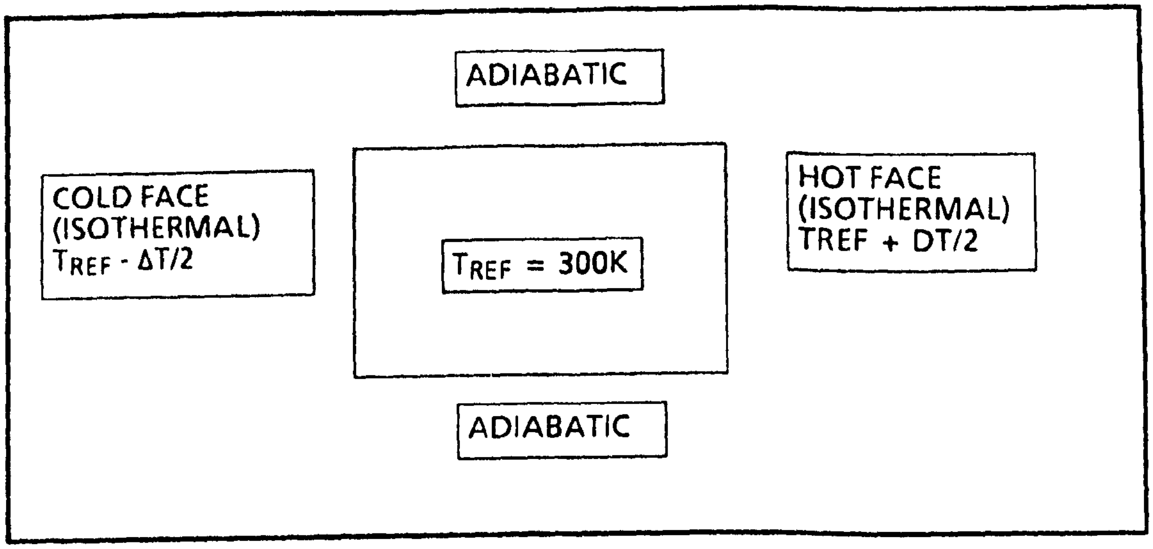

Figure 27: Classical case of natural convection in a closed cavity.

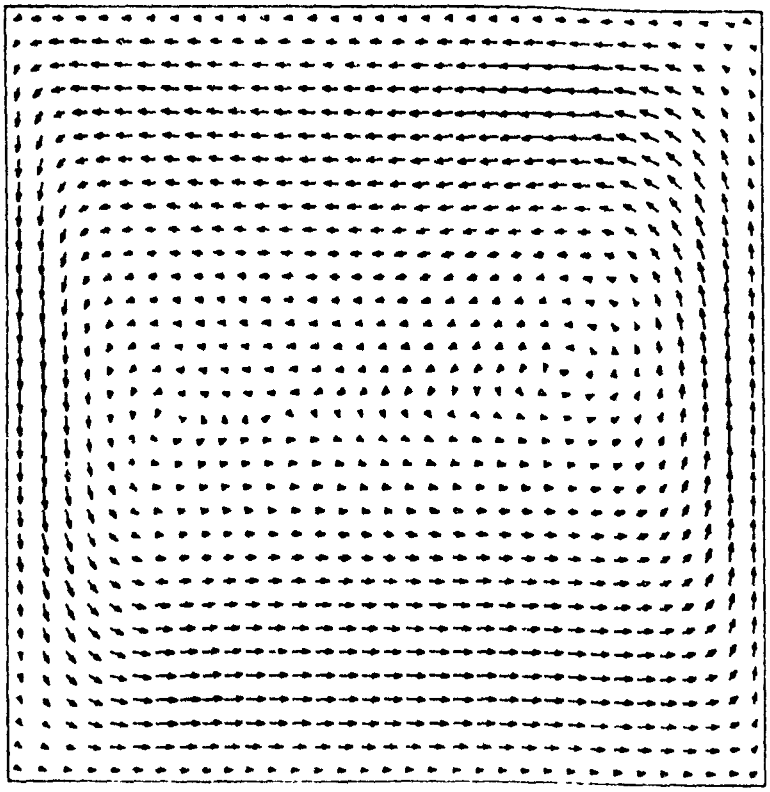

Figure 28: Typical natural convection flow pattern

The following parametric values were used during the simulation

- gravity field: $g = 9.805\ ms^{-2}$
- coefficient of thermal expansion: $\beta = 1/Tref = 3.33 \times 10^{-3}\ K^{-1}$
- thermal diffusivity. $\alpha = k/\rho Cp = 2.216 \times 10^{-5}\ m^2 s^{-1}$
- molecular viscosity: $\mu = 1.846 \times 10^{-5}$ Pa s
- density: $\rho = 1.77\ kg\ m^{-3}$
- geometric dimensions, L = 0.0625m H = 0.05m

For the case of natural convection the dimensionless numbers of interest are:

Prandtl number

$$Pr = \frac{\nu}{\alpha} = 0.708 \tag{104}$$

Grashof number

$$Gr_H = \frac{g\beta\Delta T H^3}{\nu^2} \tag{105}$$

Rayleigh number

$$Ra_H = \frac{g\beta\Delta T H^3}{\nu\alpha} \tag{106}$$

A temperature gradient of $\Delta T = 12.750K$ was first considered, so that $Gr_H = 2.12 \times 10^5$ and $Ra_H = 1.5 \times 10^5$. Several ranges of Rayleigh numbers were next simulated: Ra/1000, Ra/100, Ra/10, 10Ra, 100Ra where $Ra = 1.5 * 10^5$, this was done by changing the boundary condition ΔT which is proportional to Ra_H

b) computations and profiles; Nusselt number, correlations

For $Ra = 1.5 \times 10^5$, the converged solution with the TEACH T code is very similar to those given in the literature (3) For each primary variable, the output is a matrix (NI*NJ)

- From U & V the velocity vectors were plotted in order to have an idea of the movement within the cavity

- Using the T matrix, isotherms were plotted

For $Ra = 1.5 \times 10^5$, the results are presented in Figures 28 and 29. As in the literature, the flow field shows one main recirculating loop in the anti-clockwise way, (the cold face is at the left of the cavity, the hot face at the right), some secondary vortexes also begin to appear

Computation of Nusselt number

By definition, the Nusselt number is equal to the ratio of the heat transfer by convection to transfer by conduction across a fluid layer of thickness *l*.

$$Nu = \frac{h\,\Delta T}{k\,\frac{\Delta T}{l}} = \frac{hl}{k} \tag{107}$$

For example, the flux through the wall can be expressed by:

$$q_w = h_y (T_w - T_a) = -k\left(\frac{\partial T}{\partial Y}\right) \tag{108}$$

where h_y is the local heat transfer coefficient (Fig. 30). The mean heat transfer coefficient over the height H is:

$$h = \frac{1}{H}\int_0^H h_y\,dy \tag{109}$$

As

$$h_y = -\frac{k}{(T_w - T_a)}\left(\frac{\partial T}{\partial X}\right)_{X=0} \tag{110}$$

We have

$$h = -\frac{k}{H}\int_0^H \frac{1}{(T_w - T_a)}\left(\frac{\partial T}{\partial X}\right)_{X=0} dy \tag{111}$$

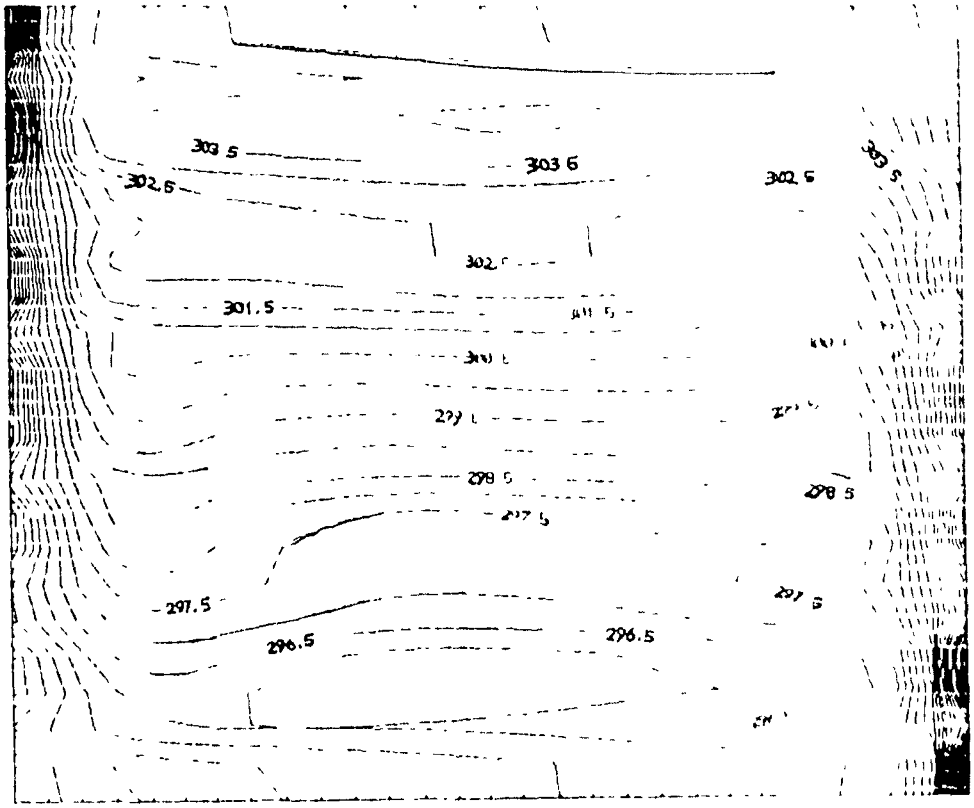

Figure 29: Computed temperature field (Run T050387)

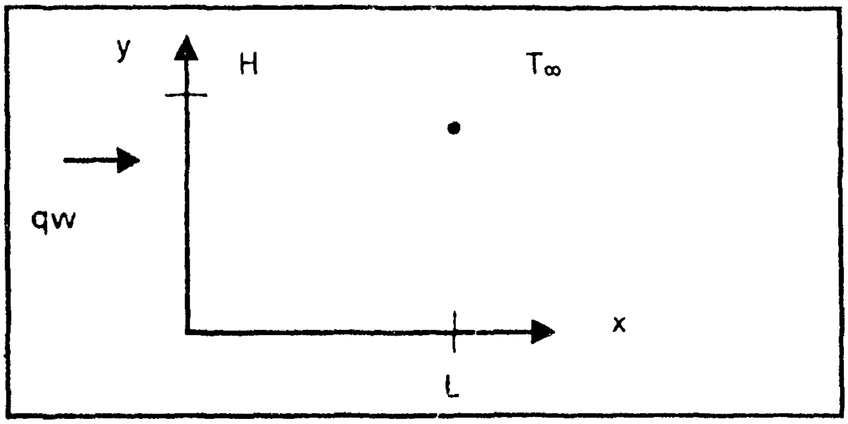

Figure 30: Heat flux computed through the side wall.

(we consider a constant coefficient K)

Replacing (111) in (107), the formula stands

$$Nu = \frac{L}{H}\int_0^H \frac{1}{(T_w - T_c)} \left(\frac{\partial T}{\partial X}\right)_{X=0} dy \qquad (112)$$

From the output matrix T(I,J), the different profiles T(I,J) as functions of x (corresponding to different values of Y [OR J]) were interpolated by spline functions of 3rd order. Similar interpolation was done for the component V_y versus x. The results of these interpolations are presented in Figures 31 and 32.

For a Rayleigh number $Ra = 1.5 \times 10^5$, the maximum vertical velocity component was found to be located at 5% of the length of the cavity. This observation and the velocity profiles are in good agreement with previous studies carried out by De Vahl Davis (27).

Once T(I,J) is approximated analytically, one can compute ($\Delta T/\Delta x$) for $X = 0$ for each value of y and finally integrate (88) using Simpson's rule.

For the conditions given in 3-1-1, which correspond to a Rayleigh number $Ra_H = 1.5 \times 10^5$, the average Nusselt number over the cavity was found to be 8.671. Bejan showed in reference (3) that the Nusselt number can be analytically expressed in the case of natural convection in a cavity by the formula.

$$Nu = 0.364 \frac{L}{H} Ra_H^{1/4} \qquad (113)$$

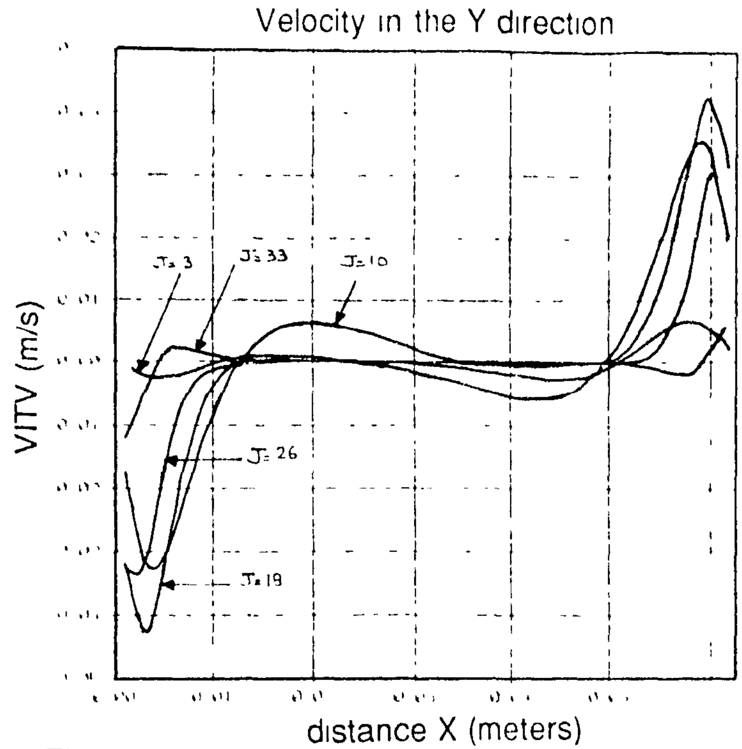

Figure 31: **Velocity profiles (meters/second)**

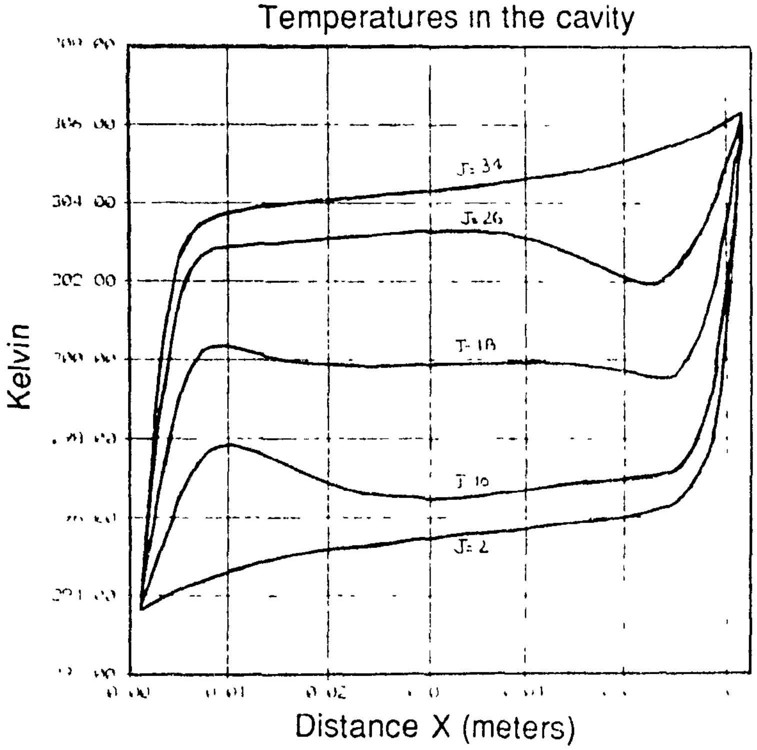

Figure 32: **Temperature profiles (Kelvin)**

This formula was however compared with good agreement to experiments from Seki et al, Eckert & Carlson, MacGregor & Emery, Jakob & Yin et al In the case of $Ra_H = 1.5 \times 10^5$ and

$$\frac{L}{H} = \frac{0.0625}{0.05} = 1.25 \qquad (114)$$

we find $Nu = 8.95$

The value given by the TEACH-T is 8.671 which is also a very good agreement

A variety of examples of natural convection within this cavity were simulated by changing the value of the Rayleigh number. the quantity ΔT was chosen to vary from $\Delta T_{ref}/100$ to $\Delta T_{ref}*100$ Thus, the Rayleigh number which is proportional to ΔT, changes in the same proportion The observed results are shown at Table (8)

We noticed that the thermal boundary layer was thinner and thinner as the Rayleigh number increased (Figs 33 and 34) At the same time, and as observed elsewhere in the literature, the flow field began to show partial instabilities with the formation of secondary vortexes

Note the last test did not lead to a converged solution after 1000 iterations, this is due in the author's view to the high level of turbulence within the cavity For all the other cases, good results were found after a reasonable number of iterations

It is interesting to obtain a correlation between the Rayleigh and Nusselt numbers Log (Nu) versus Log (Ra) was therefore plotted in Figure (35). This graph is linear with a coefficient of correlation of 99.9%, the linear regression can be expressed by:

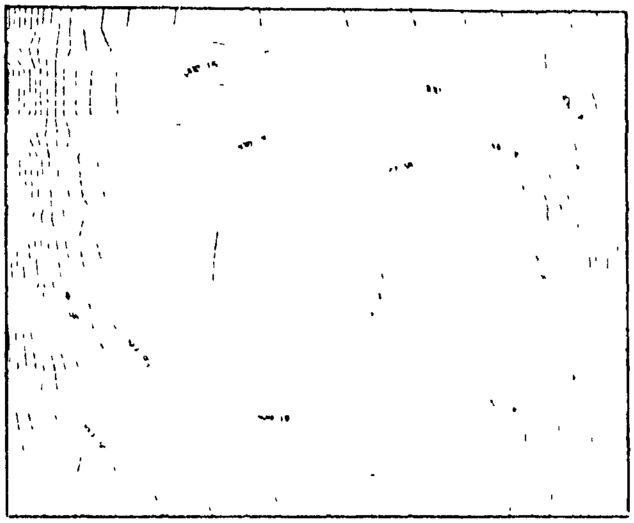

Figure 33: Temperature field (Ra = 1,5 X 10^4)

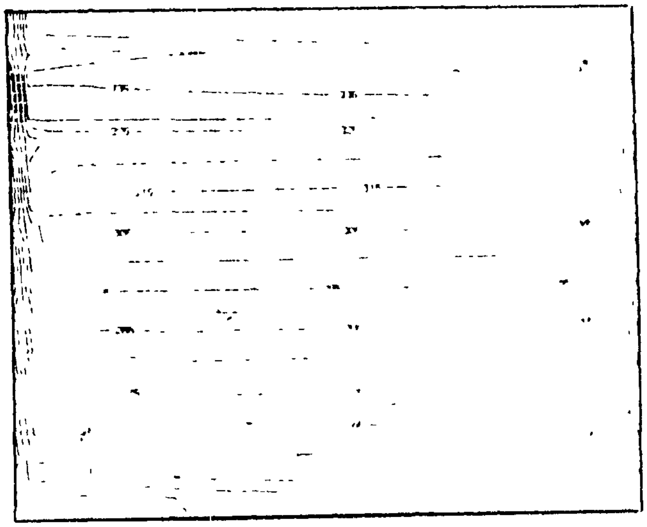

Figure 34: Temperature field (Ra = 1,5 X 10^6)

Test No	ΔT/K	Ra Iterations	Nusselt	Flux W/m2
06042	0 12751	1 5 x 10^3 386	2 778	1 49 x 10^{-1}
06041	1 2751	1 5 x 10^4 387	3 848	2 065
06046	12 751	1 5 x 10^5 413	8 671	46 5
06043	127 51	1 5 x 10^6 510	19 25	1 03 x 10^3
06044	1275 1	1 5 x 10^7 1000 not conv	29 53	

Table 8 summary of computations achieved

$$Nu = 0\ 3309\ Ra_{H}^{0\ 2752} \tag{115}$$

This formulation (equation 115) is relatively close to that found theoretically and given by Bejan (28).

c) convergence of the TEACH-T code

As seen in section 2.8, the residual sources of the primary variables were computed at each iteration and kept in memory for every 20 iterations A stop test was set up when Max (RESORU, RESORV, RESORM) was less than 5 x 10^{-6} The residual sources were then plotted versus the number of iterations As we can see on the graphs in semi-log coordinates, the RESORΦ are exponentially decreasing functions (Figures 36 to 38) Concerning RESORT, its final value is slightly bigger than the other RESORΦ, (9 x 10^{-5} versus 1 x 10^{-6} for RESORU) This can be explained by the fact that RESORT would have to be normalized by the heat flux crossing the cavity As this heat flux was computed only after one had obtained the output fields and at the same time as the Nusselt number it was not possible to normalize it from the beginning (Actually the heat flux computed was around 50 watts/m2).

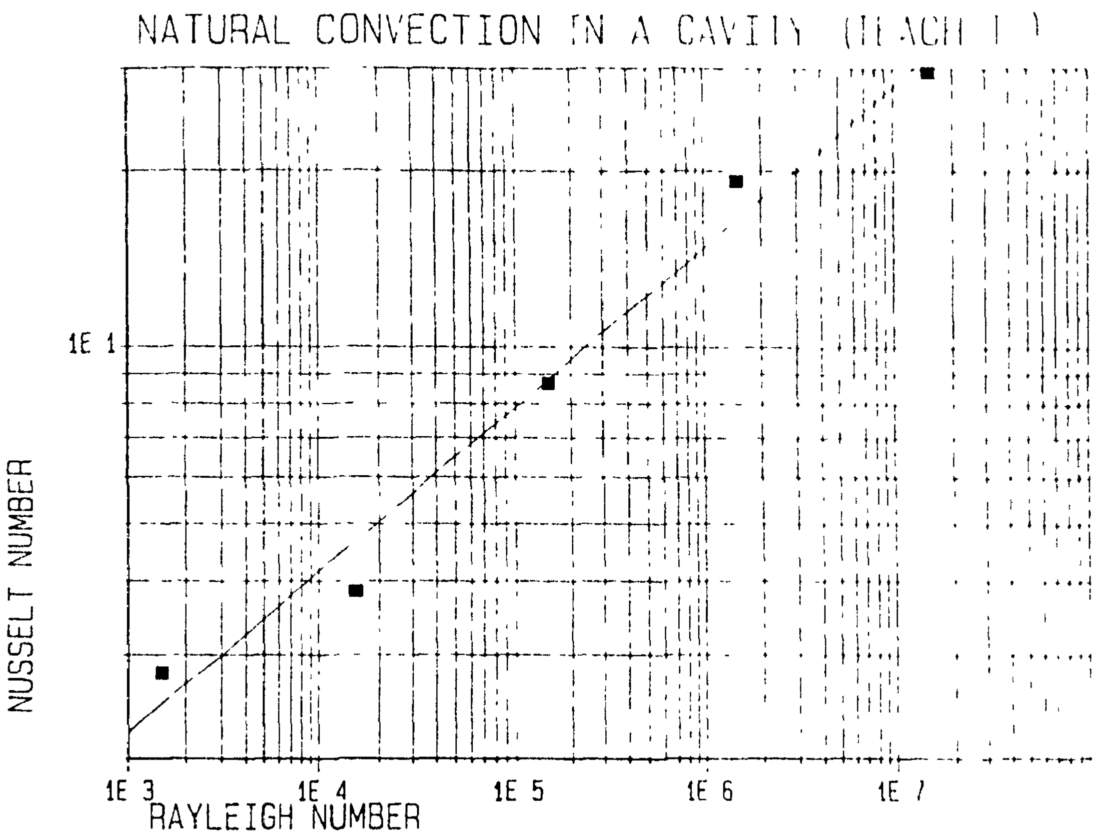

Figure 35: Correlation Nusselt/Rayleigh

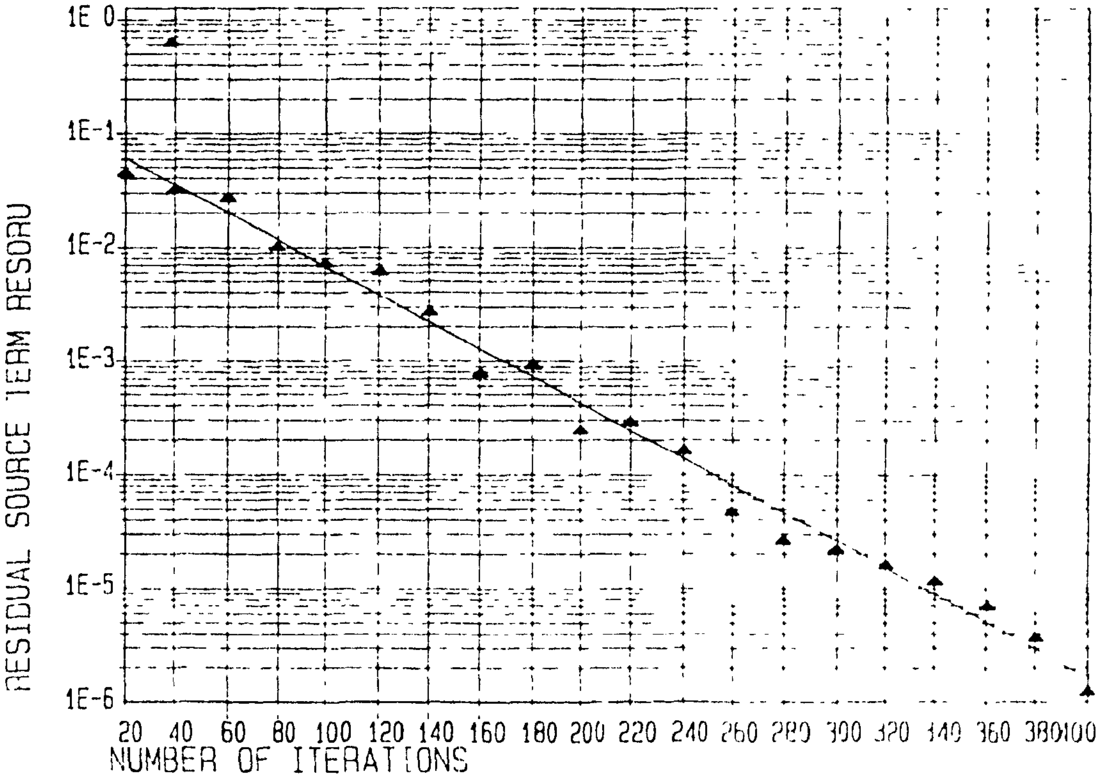

Figure 36: Convergence of primary variable U

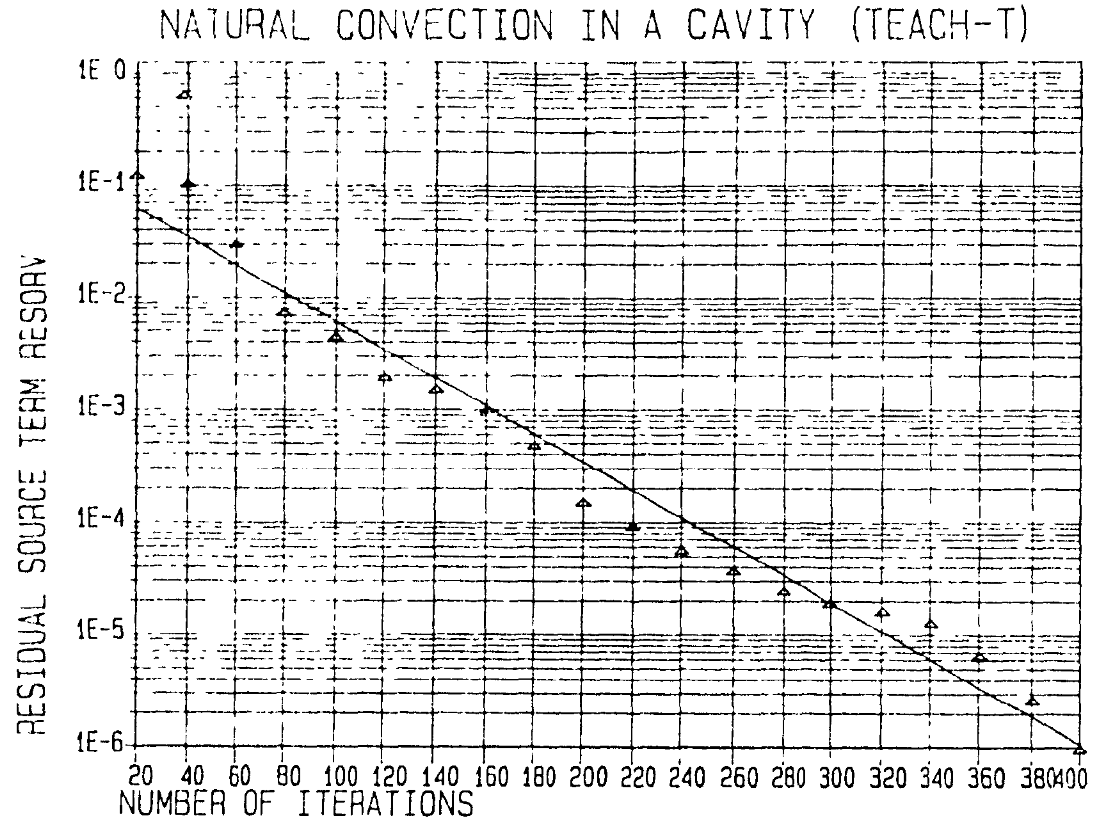

Figure 37: Convergence of primary variable V

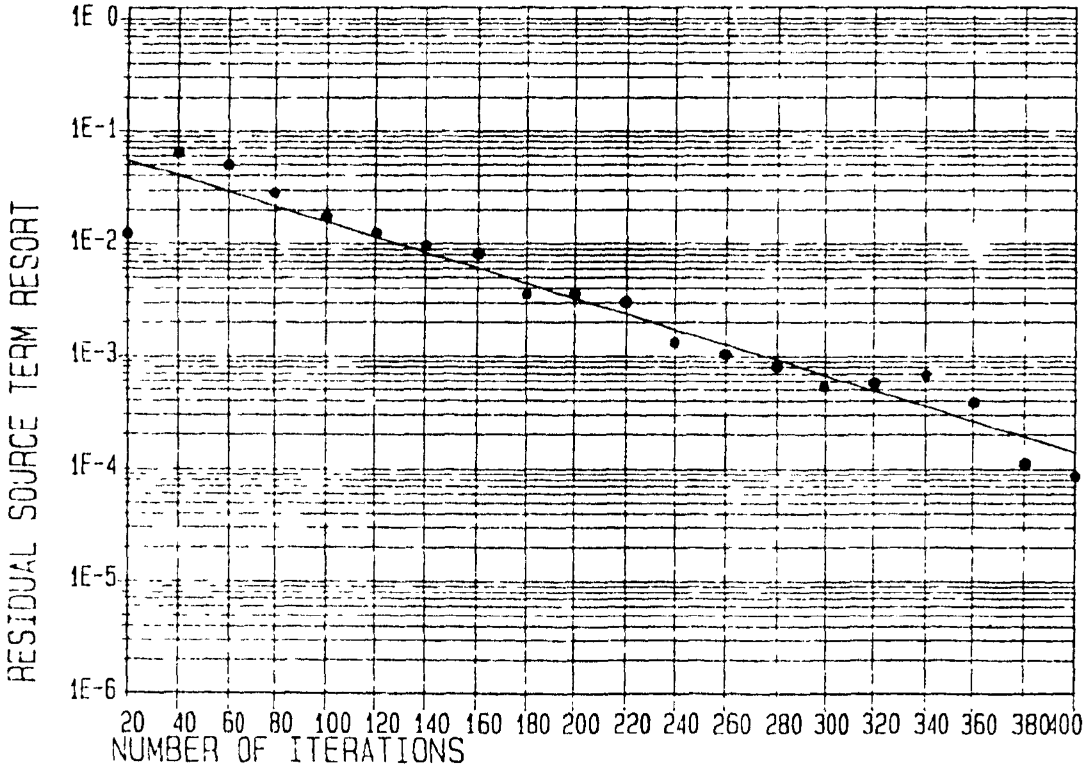

Figure 38: Convergence of primary variable T

In conclusion, one can say that the code converged for all tests except for the last one (06044) which appears to have a high level of turbulence

d) grid used

Several meshes were used for the same Rayleigh number (1.5×10^5), it turned out that for this type of laminar problem in a closed cavity, a grid of 33×33 was sufficient to give realistic results. A finer grid did not improve these numerical solutions of laminar flow problems and futhermore involved much more CPU time. For example, computations were achieved on a PC XT turbo (8MHz clock) using the professional FORTRAN compiler (FORTRAN 77), the CPU time required was plotted versus the number of cells in the X or Y directions; See Figure 39

So one can say that

$$CPU_{mn} = 4.028\, e^{0.1056*NI} \qquad (with\ NI = NJ) \tag{116}$$

3-1-2 Tests and adaptation of the TEACH T to natural convection of molten metal in a cavity

a) description of the problem

At the request of the ALCAN research center in November 1986, the following problem was set up. A rectangular cavity filled with molten aluminum, heated from the top and whose dimensions are not too far from a those of a slice of a real reverbatory furnace (Fig 40). As a first approximation one can say that the temperature at the top has to be maintained some ΔT over the temperature at bottom and on the sidewalls. The following properties were considered:

- density of molten metal	$\rho = 2357$ kg/m^3
- molecular viscosity	$\mu = 1.252 \times 10^{-3}$ Pa S
- thermal diffusivity	$\alpha = 4.36 \times 10^{-5}$ m^2/s

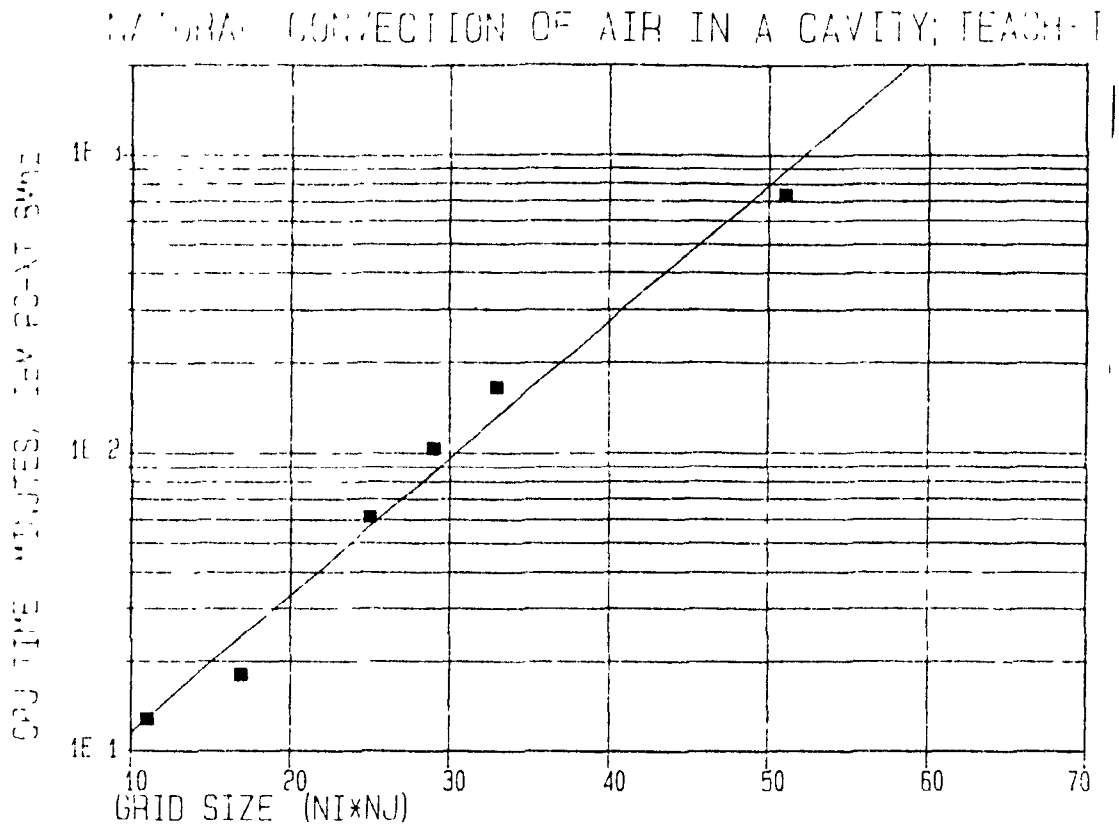

Figure 39: Computing time as a function of grid size

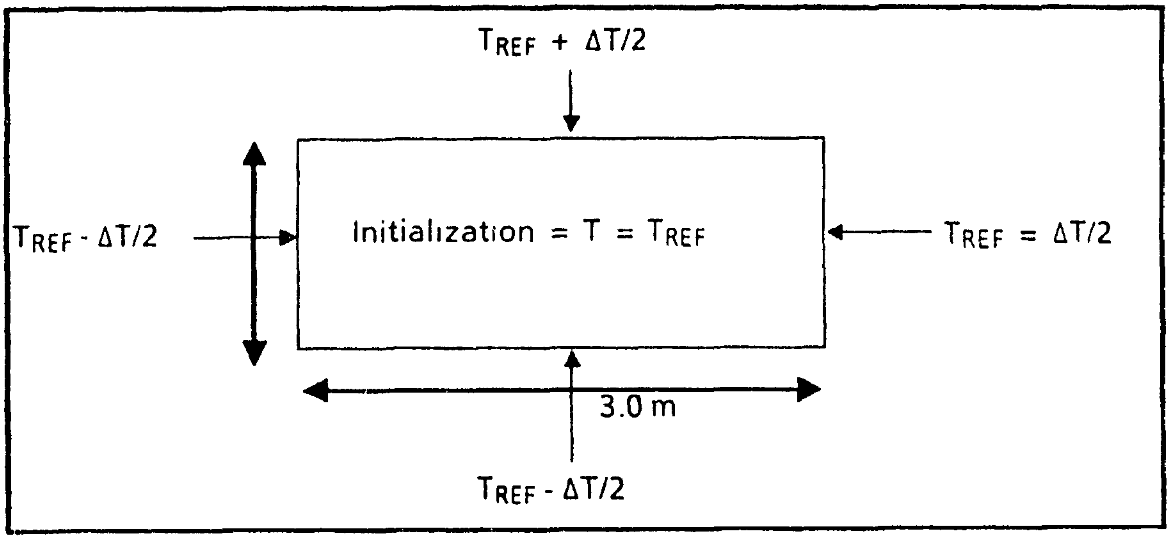

Figure 40: Boundary conditions applied on the cavity filled with molten aluminium

- coefficient of thermal expansion $\beta = 1.65 \times 10^{-4} K^{-1}$
- reference temperature Tref = 973K
- temperature gradient $\Delta T = 50K$

From these values one can compute the Rayleigh number (based on the longest dimension)

$$Ra_L = \frac{g\beta\Delta T L^3}{\nu a} = \frac{9.805*1.65*10^{-4}*50*3^3}{\frac{1.252*10^{-3}}{2357}*4.36*10^{-5}} = 9.1*10^{10} \qquad (117)$$

This basically indicates that the flow field takes place in a highly turbulent regime; therefore one has to activate the turbulence subprograms CALCK and CALCED.

b) computations and profiles

Two different grids were used for this problem.

- a regular grid with constant ΔX and ΔY (NI = NJ = 35)
- a non uniform grid (NI = NJ = 35), set up as it follows

In order to take into account the small thickness of the boundary layers close to the walls, it was decided that a coarse grid be used in the middle of the cavity and a fine grid near the side walls. The ΔX values were actually set up in a geometric progression starting form each side towards the middle of the cavity as shown in Fig. 41.

The length L and the number of grid points NI being given, one has only to choose a value for the geometric parameter q to define a grid in the x direction. In this problem qx = 1.2 was chosen and the same procedure was adopted for the y-direction (qy = 1.2).

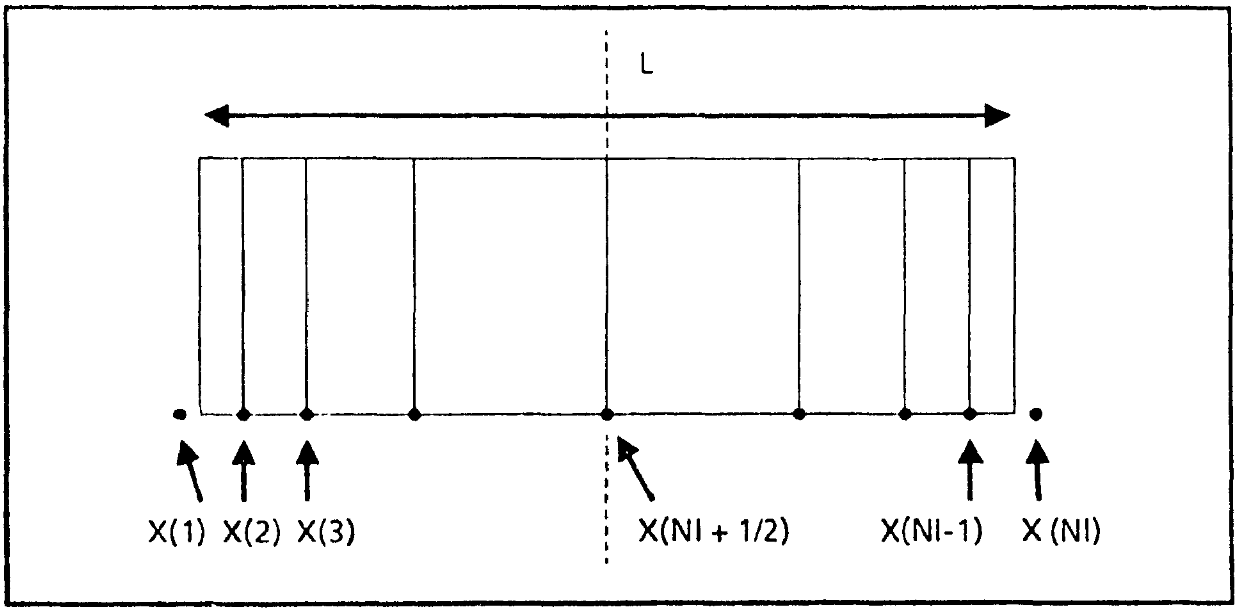

Figure 41: Definition of non uniform mesh

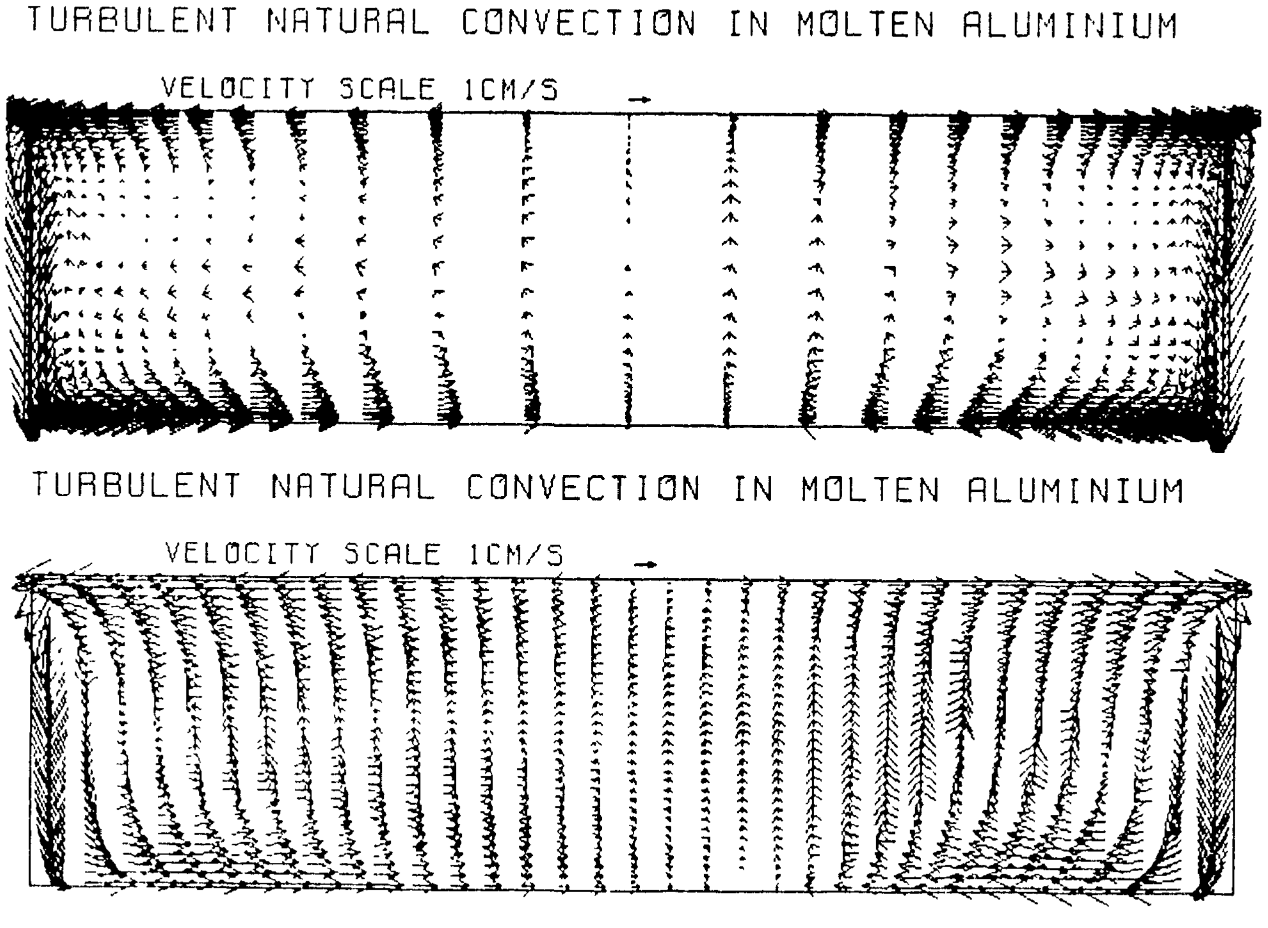
TURBULENT NATURAL CONVECTION IN MOLTEN ALUMINIUM

TURBULENT NATURAL CONVECTION IN MOLTEN ALUMINIUM

Figure 42: Computed flow field with both uniform and non uniform meshes.

The relaxation factors used for the primary variables were the following

- velocity U&V = 0.5
- pressure: 1.0
- temperature: 1.0
- kinetic energy and rate of dissipation. 0.7

The velocity profiles obtained for this problem are given at Fig 42 for both uniform and non uniform meshes.

c) convergence of code

In the same way as in Chapter 3.1 1, the residual sources of primary variables were computed at each iteration to check convergence of the code For numerical values, see Table 9 for simulation with a uniform mesh and Table 10 for simulation with non-uniform mesh. These residual sources are plotted respectively in Figures 43 and 44.

For the first case (uniform grid), residuals decrease from the range [10^9, 10^{16}] to [10^{-2}, 10^2]; if RESORK and RESORED are monotonically decreasing with respect to the number of iterations, it is not the same for the other variables; moreover the sources RESORM, RESORU, RESORV seem to increase again after 2500 iterations.

As for the second case (non uniform grid), the residual sources decrease much faster (Fig. 40) but after around 1500 to 2000 iterations they reach some kind of plateau, the range of which is situated between 10^{-2} and 10^3, after 3000 iterations it becomes very expensive and almost impossible to get down from these "plateau", the precision of 5×10^{-6} that we required in the program to stop the iterative process can then never be reached, one should note that this value of 5×10^{-6} is not utopic because this was achieved during computations achieved for the laminar problem

Nevertheless, it would appear from Fig 42, that the velocity profiles are realistic and contain two recirculating vortexes The maximum velocities recorded after 3000 iterations were

RESIDUAL SOURCES OF PRIMARY VARIABLES
UNIFORM MESH (35*35)

ITERATIONS	RESORU	RESORV	RESORM	RESORT	RESORK	RESORE
10	5.39×10^{12}	1.20×10^{3}	4.33×10^{8}	1.13×10^{9}	3.21×10^{13}	7.26×10^{16}
100	5.37×10^{10}	1.73×10^{10}	2.43×10^{5}	9.64×10^{6}	1.06×10^{13}	5.45×10^{16}
200	1.65×10^{10}	8.16×10^{9}	1.62×10^{5}	2.52×10^{6}	4.96×10^{12}	2.87×10^{16}
500	1.99×10^{9}	1.64×10^{9}	1.096×10^{4}	8.04×10^{5}	1.26×10^{12}	1.05×10^{15}
750	2.03×10^{8}	1.41×10^{8}	2.01×10^{3}	7.26×10^{4}	9.05×10^{10}	2.56×10^{13}
1000	1.34×10^{7}	1.52×10^{7}	6.93×10^{2}	1.98×10^{4}	3.73×10^{9}	3.34×10^{11}
1500	5.69×10^{4}	6.89×10^{4}	2.83×10^{1}	9.22×10^{2}	4.50×10^{6}	4.00×10^{7}
2000	2.36×10^{2}	3.05×10^{2}	1.203×10^{0}	8.88×10^{1}	5.28×10^{3}	5.29×10^{3}
2500	$4.11\times10^{\ 1}$	3.13×10^{-1}	4.03×10^{-1}	5.45×10^{1}	5.80×10^{0}	1.02×10^{0}
3000	1.01×10^{2}	9.28×10^{1}	9.80×10^{2}	3.84×10^{2}	$7.08\times10^{\ 3}$	$5.03\times10^{\ 3}$

Table 9

RESIDUAL SOURCES OF PRIMARY VARIABLES

NON UNIFORM MESH (35*35)

ITERATIONS	RESORU	RESORV	RESORM	RESORT	RESORK	RESORE
10	1.03×10^{11}	1.43×10^{11}	7.13×10^{7}	6.61×10^{7}	1.19×10^{12}	4.31×10^{15}
100	2.45×10^{9}	5.51×10^{3}	1.87×10^{6}	1.04×10^{7}	7.93×10^{9}	1.59×10^{13}
200	2.44×10^{8}	5.35×10^{7}	6.95×10^{5}	1.27×10^{5}	3.31×10^{9}	1.99×10^{12}
500	5.47×10^{5}	1.53×10^{5}	4.46×10^{3}	8.97×10^{3}	1.87×10^{6}	5.12×10^{7}
750	3.03×10^{4}	4.82×10^{3}	2.25×10^{2}	7.81×10^{2}	4.63×10^{4}	4.16×10^{5}
1000	1.85×10^{3}	2.43×10^{2}	7.25×10^{0}	5.24×10^{2}	6.64×10^{2}	2.79×10^{3}
1500	1.34×10^{1}	3.73×10^{0}	3.70×10^{0}	4.47×10^{2}	$2.24\times10^{\ 1}$	$6.99\times10^{\ 1}$
2000	6.37×10^{1}	2.55×10^{2}	1.96×10^{3}	1.51×10^{3}	$1.42\times10^{\ 2}$	$3.89\times10^{\ 1}$
2500	4.75×10^{1}	1.97×10^{2}	1.64×10^{3}	1.44×10^{3}	$1.24\times10^{\ 2}$	$6.08\times10^{\ 1}$
3000	5.00×10^{1}	1.98×10^{2}	1.51×10^{3}	1.66×10^{3}	$1.48\times10^{\ 2}$	$4.96\times10^{\ 1}$

Table 10

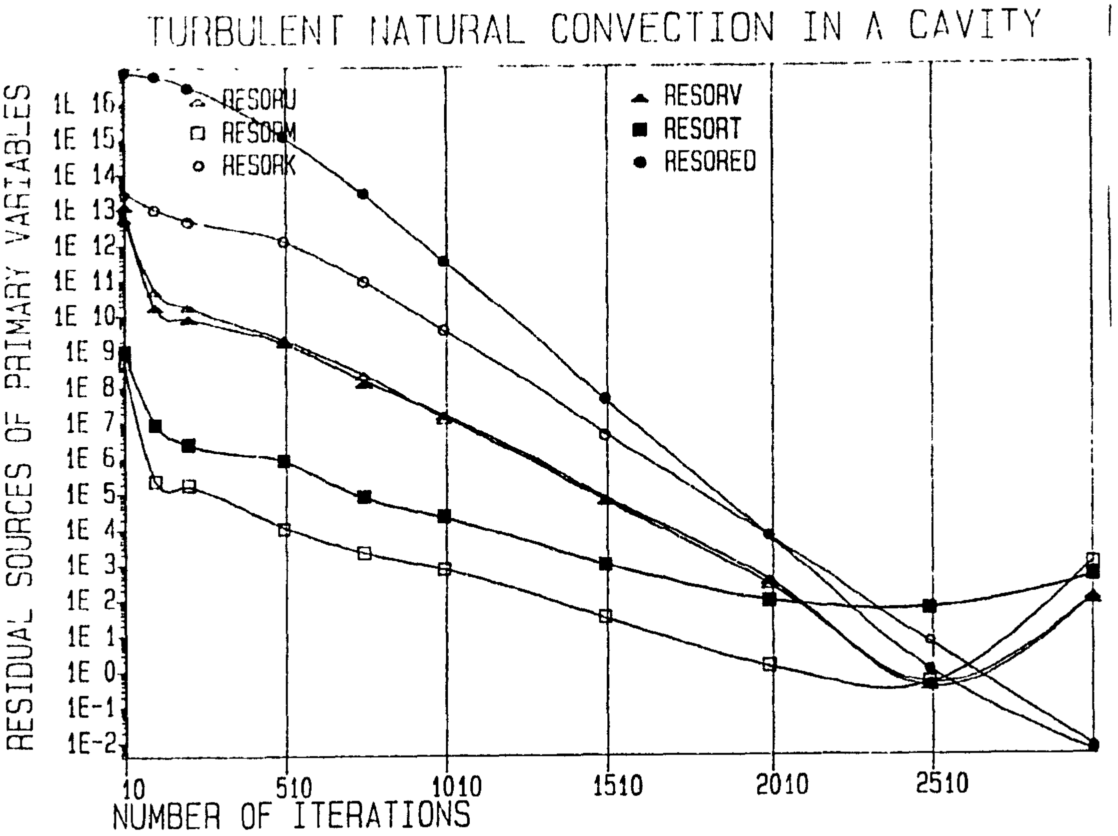

Figure 43: Code convergence = uniform mesh

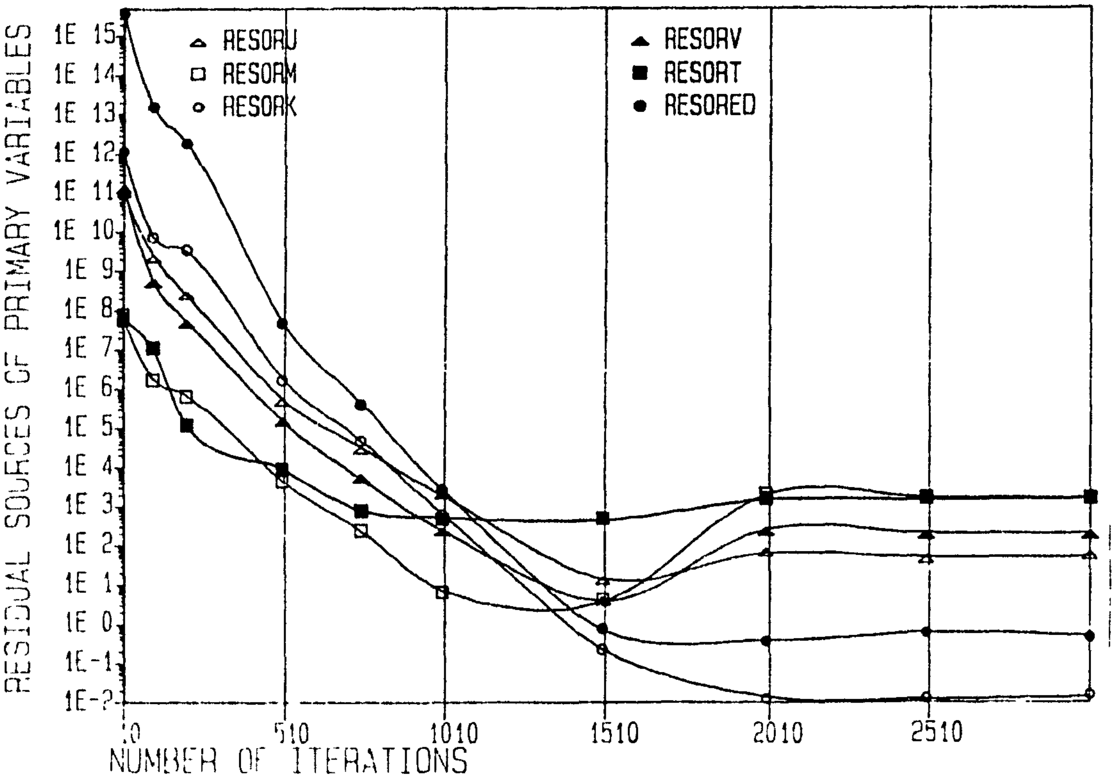

Figure 44: Code convergence = non uniform mesh.

$\| V \|_{max} = 32.2$ mm/s with the uniform grid

$\| V \|_{max} = 56.3$ mm/s with the non uniform grid

The average velocity was equal to $\| V \|_{AV} = 7.57$ mm/s with the uniform grid

$\| V \|_{AV} = 11.5$ mm/s with the non uniform grid

Although the order of magnitude is the same for both grid cases, the difference between the values of $\| V \|$ can be explained: in the case of the non uniform mesh, the velocity was computed closer to the wall than in the case of a uniform mesh which, in the case of a boundary layer flow, leads to a higher value of $\| V \|$.

Even if the field values (U, V, P, T, K, E) at the monitoring location do not move too much after 2500-3000 iterations, it is difficult to strictly conclude convergence of the code for this problem on a theoretical point of view; if strict convergence is obtained, the limit of all the residual sources should be zero, with respect to the precision of the computer. This requirement is particularly not fullfilled with RESORM, which reflects mass imbalances.

3-1-3 Computers used during the simulation

In the Department of Mining and Metallurgical Engineering the author have access to the McGill mainframe and particularly to an AMDAHL 580. Unfortunately, user operating costs were very high, even for research purposes and when using the lowest priority. As an example, the program DT6 used for computations explained in Chapter 3 required 62.5 minutes of total elapsed time and cost around $140 for 3000 iterations

As a result, other possibilities for running the programs were explored:

- IBM PC XT with the PROFESSIONAL FORTRAN COMPILER
- IBM PC XT turbo (8 MHZ clock instead of 4.77)
- IBM PC XT with a special board (DEFINICON SYSTEMS) including a 68020 processor for FORTRAN-77 applications; this enables us to work in 16 MHZ and 32 bits words.

- CRAY II of University of Toronto was also used for the purpose of a bench mark free of charge!

To give a good idea of the results of the bench mark, the reader is referred to the folowing Table..

	AMDAHL 580 McGILL	CRAY II UNIV.OF TORONTO	IBM PC-XT		IBM PC-XT + 68020
			STANDARD	TURBO	
DT 52 (Denis Frayce)	CPU 12 min	0.6 min	1450 min	865 min	159 min
HOON 2 (S Joo)	CPU 18 min 12s	2.27 min			

Table 11: computing time of simulations on various installations

NOTE: In the case of using CRAY II, the CPU could be reduced by a further 30%, if all the sub-programs were to be vectorized.

- DT5 was the natural convection program used in Chapter 3 (grid 35*35, 2000 iterations)

- HOON 2 was a 3D forced convection program simulating recirculating flows in metallurgical reactor vessels (tundishes).

From Figure 41, one can define some ratios:

$$\frac{\text{CRAY}}{\text{AMDAHL}} = 20 \qquad \frac{\text{AMDAHL}}{\text{PC TURBO}} = 72 \qquad \frac{\text{AMDAHL}}{(\text{PC} + 68020)} = 13$$

NOTE: on AMDAHL 580: 1 time unit (CPU) = 10^7 instructions

3-1-4 Comparison of results given by TEACH-T and other work on the boundary layer point of view

In order to test the boundary layer predictions for the momentum and thermal boundary layers δ_V and δ_T, one can compare TEACH-T predicted values with those applying to isothermally heated vertical plates in a semi-infinite medium. Bejan (28) gives the following correlations for boundary layer thicknesses:

$$\delta_V = H * Pr^{0.25} * Ra_H^{-0.25} \tag{118}$$

$$\delta_T = H * Pr^{-0.25} * Ra_H^{-0.25} \tag{119}$$

where δ_V and δ_T are respectively the momentum and thermal boundary layers for natural convection. Such formulae show that the ratio δ_V/δ_T is independent of the Rayleigh number and is only a function of the fluid properties (Prandtl number). For the present situation, the Prandtl number for liquid aluminium is about 0.01 so that:

$$\delta_V / \delta_T = \sqrt{Pr} = 0.1 \tag{120}$$

This expectation is born out by the computations shown in Fig. 45, where the thermal boundary layer is seen to be about 50 mm thick compared to the momentum boundary layer thickness of 5 mm.

3-1-5 *Influence of the buoyancy term in the K equation for the turbulent situations*

For the previous rectangular cavity filled with molten metal, two simulations were run under the same boundary and initial conditions

- Test 1: a buoyancy term in the kinetic energy of turbulence, K, equation (eq 61); while for Test 2: the buoyancy term was omitted from the K equation

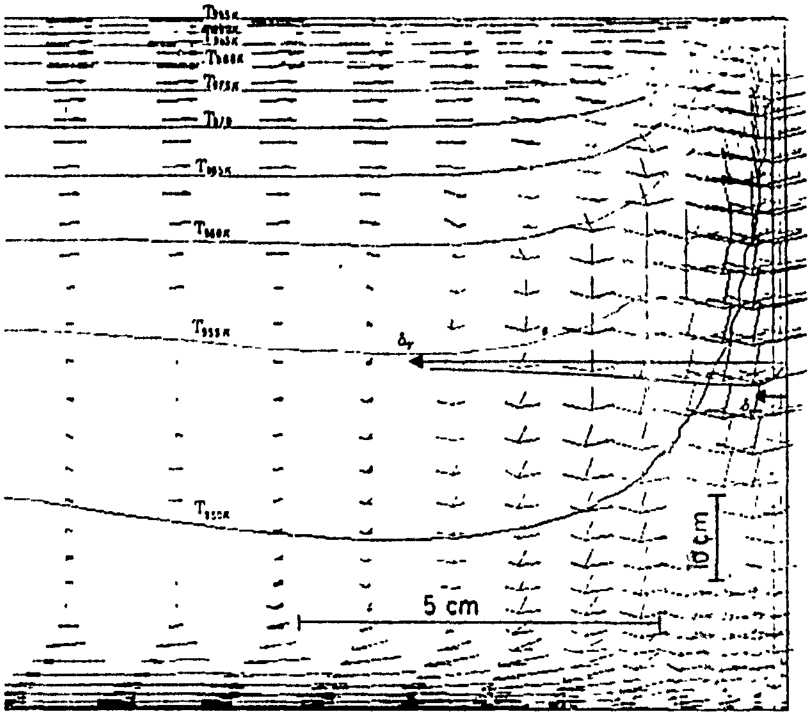

Boundary layer thicknesses at wall (note the expanded scale in the x (horizontal) co-ordinate system)

Figure 45

U VELOCITY COMPONENT (M/S) - WITH BUOYANCY TERM IN K EQ.

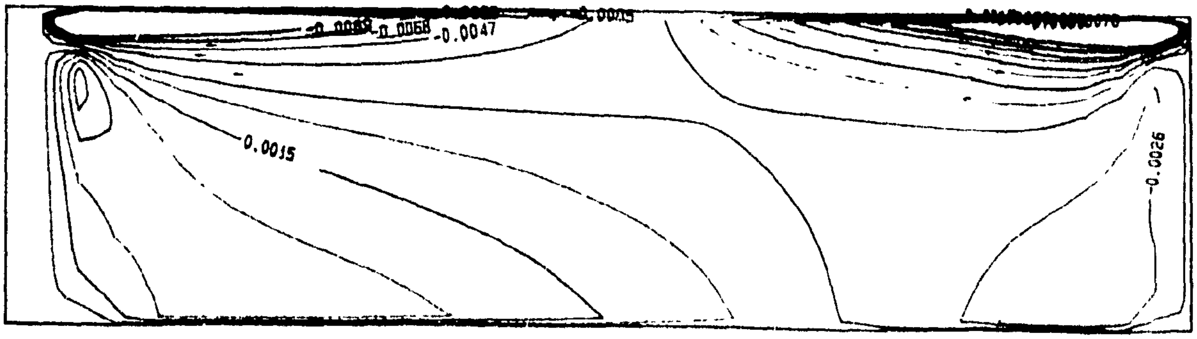

U COMPONENT OF VELOCITY (M/S) - NO BUOYANCY TERM IN K EQ.

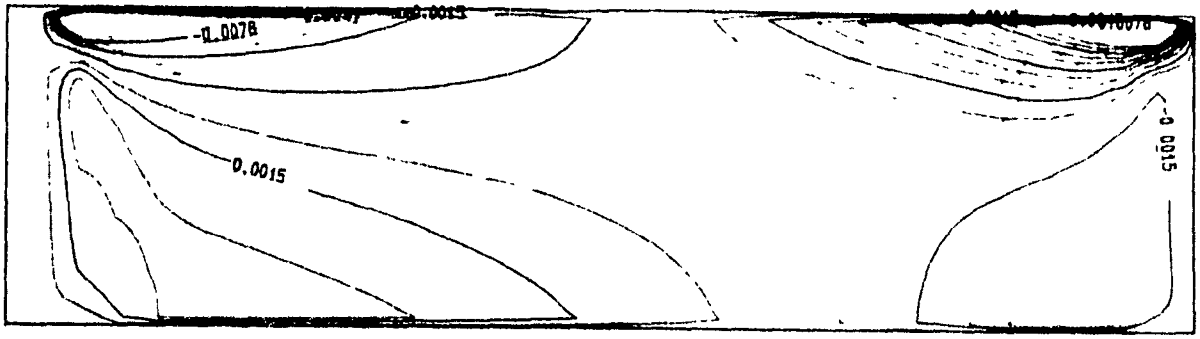

V VELOCITY COMPONENT (M/S) -WITH BUOYANCY TERM IN K EQ.

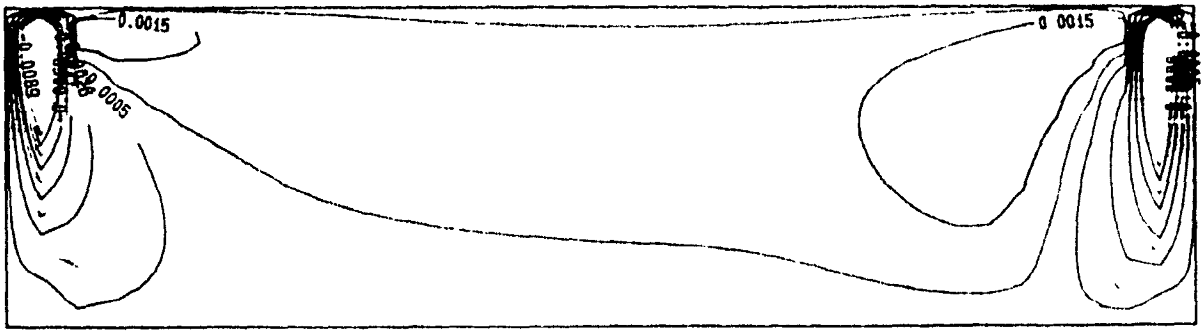

V VELOCITY COMPONENT (M/S) - NO BUOYANCY TERM IN K EQ.

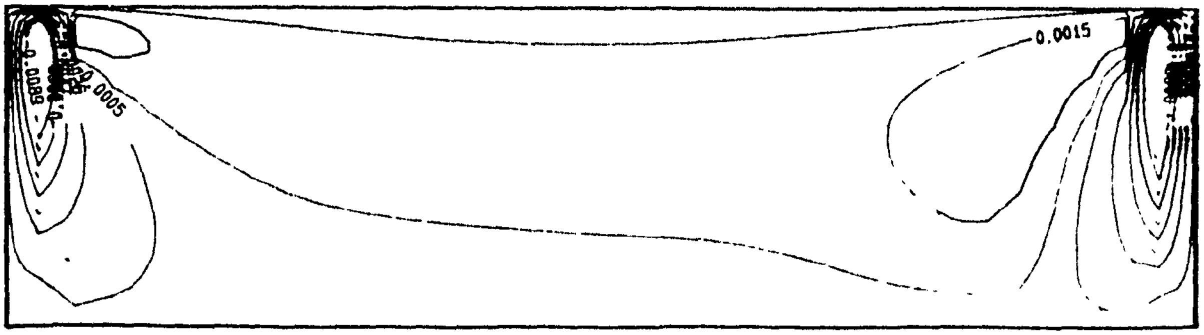

Figure 46: Influence of a buoyancy term in the K equation on the computations (U and V components)

STREAM FUNCTION - WITH BUOYANCY TERM IN THE K EQUATION

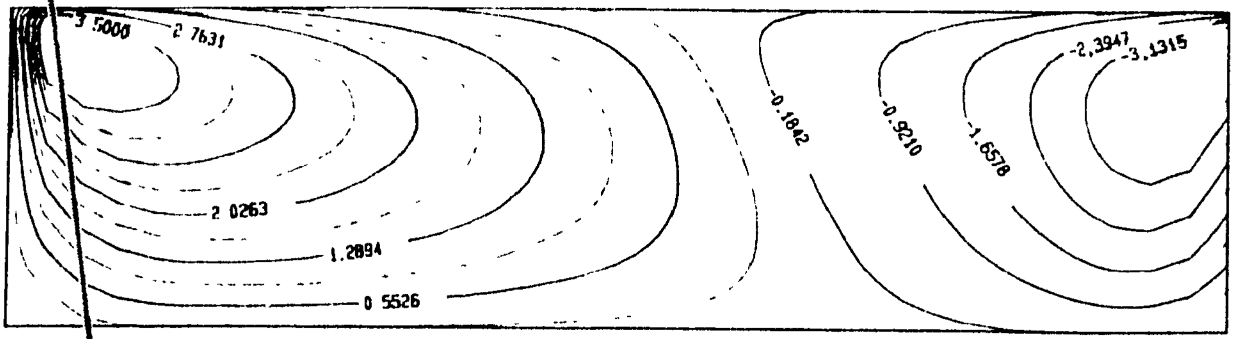

STREAM FUNCTION - NO BUOYANCY TERM IN THE KE EQUATION

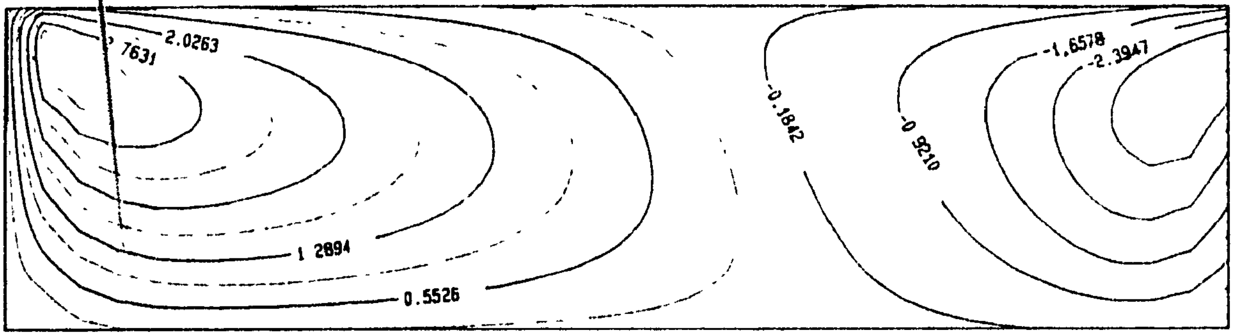

TURBULENT KINETIC ENERGY (M2/S2) - WITH BUOYANCY TERM

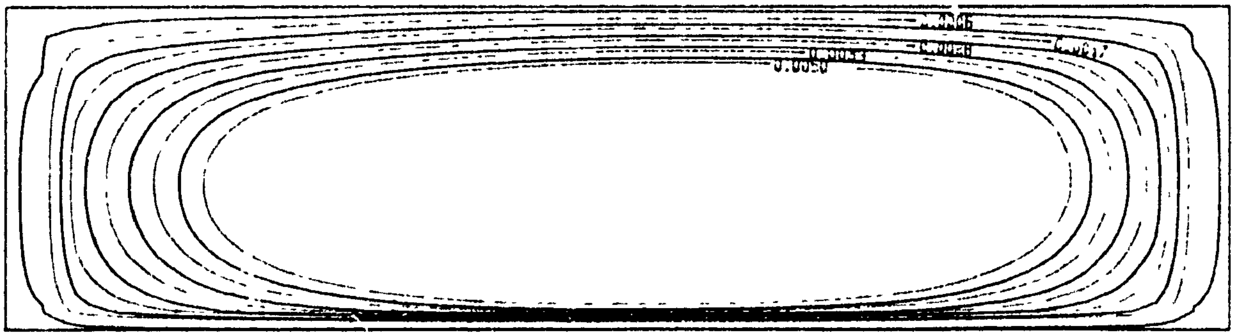

TURBULENT KINETIC ENERGY (M2/S2) - NO BUOYANCY TERM

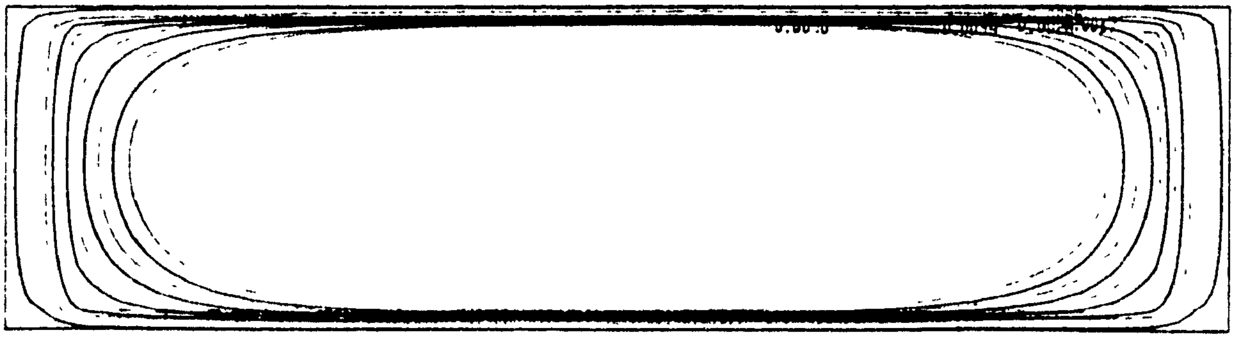

Figure 47: Influence of a buoyancy term in the K equation on the computations (Steam function and turbulent energy)

Figures 46 and 47 clearly show that the source term in the K equation leads to much higher gradients in the kinetic energy of turbulence close to the walls (side, top and bottom walls). Nevertheless, and in spite of the coupling of the variables of momentum, energy, K and E, the velocity fields and computed stream functions are very similar for both cases Thus, for the particular natural convection problem at hand, omission the buoyancy source term in the K equation did not lead to any significant error in the flow patterns predicted by the model (less than 1% of difference for the average velocity)

This sensitivity study to the present situation was undertaken because of existing controversy encountered in the literature (10,12,17) on the importance of this additional source term in the K and E equations

3-2 Simulations with the PHOENICS code

Numerical simulations were carried out with the PHOENICS code to model two dimensional, transient, turbulent natural convection in two reverbatory furnaces filled with molten aluminum. The first one was a full scale industrial holding furnace (50 ton capacity) while the second one was a reverbatory laboratory furnace having an aluminum melting capacity of 6 25 ton The laboratory furnace at the ALCAN Research Centre was available for the experimental verification of the computed results.

3-2-1 Description of the process and objectives

The process simulated is depicted schematically in Fig 48 A trapezoidal cavity of "infinite" length along the vertical Z axis is heated from the top by a flat flame gas burner providing a uniform flux. As the side and bottom walls are not perfectly insulated, heat losses from these walls due to conduction and radiation are taken into account. Following the recommendation of the group at UQAC, heat losses can be precisely modelled by an overall heat transfer coefficient and a temperature of reference (303K) Owing to the presence of oxide films such as (Al_2O_3) on the top of the melt, the top boundary was considered as a rigid wall rather than a free surface A no slip condition was thus applied to all boundaries The molten metal in the furnace

EXPERIMENTAL 6.25 TON HOLDING FURNACE

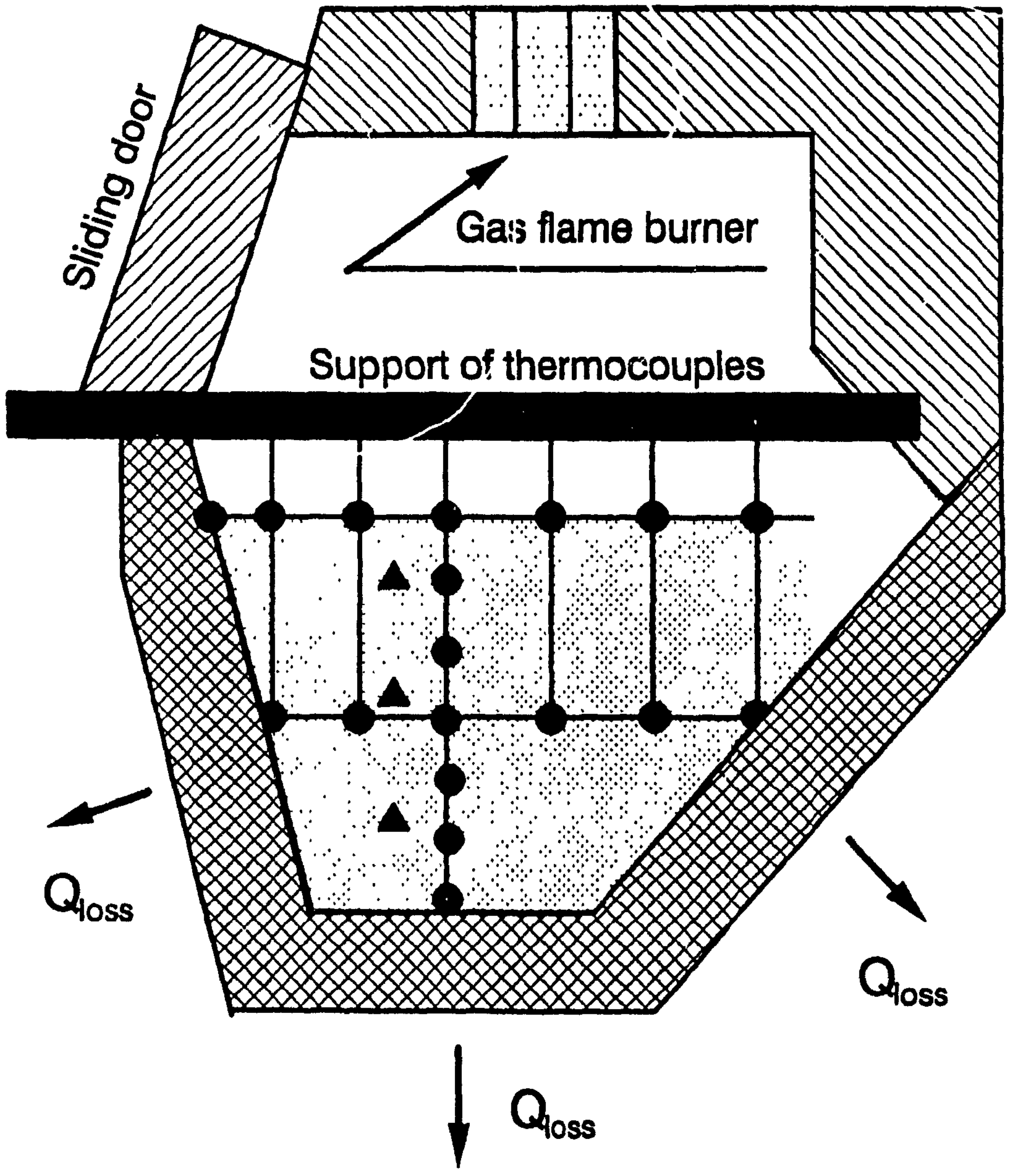

▲ Concentration measurements (LIMCA)
(Through side wall of furnace)

● Temperatures measurements

Figure 48

is assumed to be at a fixed uniform temperature initially Heat transfer through the walls then causes density changes within the molten metal in the cavity and leads to buoyancy driven recirculation As mentioned in Chapter 1, movement in the fluid is not negligible in terms of inclusions settling/rising velocities and has a direct bearing of the metal quality The latter can be quantified by concentrations of inclusions.

Because of their very small sizes , quantity, and volume fraction within the melt, the inclusions were not considered as a second phase but were assumed to follow the general flow patterns which they do not modify The inclusions are thus subjected to both the local flow velocities and the Stokes law Computing the concentration C1 of particles of a given diameter and of a given density (Stokes velocity V_S) needs to take the vector $(U,V + V_S)$ rather than (U,V) when solving this C1 convection/diffusion equation This approach was successfully followed by Tacke and Ludwig in the case of steel tundishes and ladles (ref 29). The settling velocity V_S is the only parameter in the model which characterizes the particle. For particles heavier than aluminium $|V_S| = -V_S$(majority of cases). For the light particles such as $MgCl_2$, $|V_S| = V_S$ For the heavier particles, a no-flux wall boundary condition was assumed for the top surface. As for the side and bottom walls, absorption condition was expressed by:

$$m''' = \alpha * V_S * C_p \tag{121}$$

where m''' is the particle flux density in the downward direction at the wall (number of particles leaving the surface per unit area and unit time), C_P is the particle concentration close to the wall (taken at the closest grid point) and α a coefficient $(0<\alpha<1)$ reflecting absorption of particles to the wall. Ideal absorption conditions can be considered in the absence of reliable data $(\alpha = 1)$

On the other hand, for the buoyant particles, zero (mass) flux boundary conditions were assumed for the side and bottom walls, and an equivalent relation to the equation 121 was proposed for the top surface of the melt comprising solid dross.

The objective of this work was to demonstrate how a general CFD package such as PHOENICS can be used to provide a solution of two dimensional transient turbulent buoyancy driven flow in cavities The motivation for this work was to obtain flow patterns along with enthalpy and the particle concentration fields, and thereby decide on the optimum design of such vessels, and the best place from which liquid metal should be withdrawn during DC casting operations.

It is now appropriate to describe modifications to the PHOENICS code needed in order to mathematically simulate the problem just mentioned.

3-2-2 Satellite data items-the input QI DAT file [group 1 to 24]

Thus, the QI DAT input file is divided into 24 groups in order to provide all information needed by the EARTH program. The detail of every group is provided at appendix B.

3-2-3 Runs achieved-typical output

Successive runs were achieved in the transient mode and are described at tables (12, 13). There the number of time steps and iterations per step can be found as well as the ranges of the field of the variables U1, V1, H1, P1, K, E, C1 and C3 (concentrations of inclusions of densities 3500 kg/m^3 and 1800 kg/m^3) and the computing time on a VAX/785 computer.

3-2-4 Graphical output-field of variables

The behaviour of the fluid flow in a cavity can be displayed by plotting the velocity field V, the contours of enthalpy H1, the turbulent kinematic viscosity, the relative pressure fields P1 and concentrations at several stages of the simulation. These plots are given in Figures (50-69) for the two cases of furnaces considered in this thesis.

3-2-5 Transient output-profile of variables

At selected points the temporal plots of the main variables can project a representative picture of the behaviour of the process To this end, in the case of the experimental 6 25 ton furnace, the monitoring points chosen were:

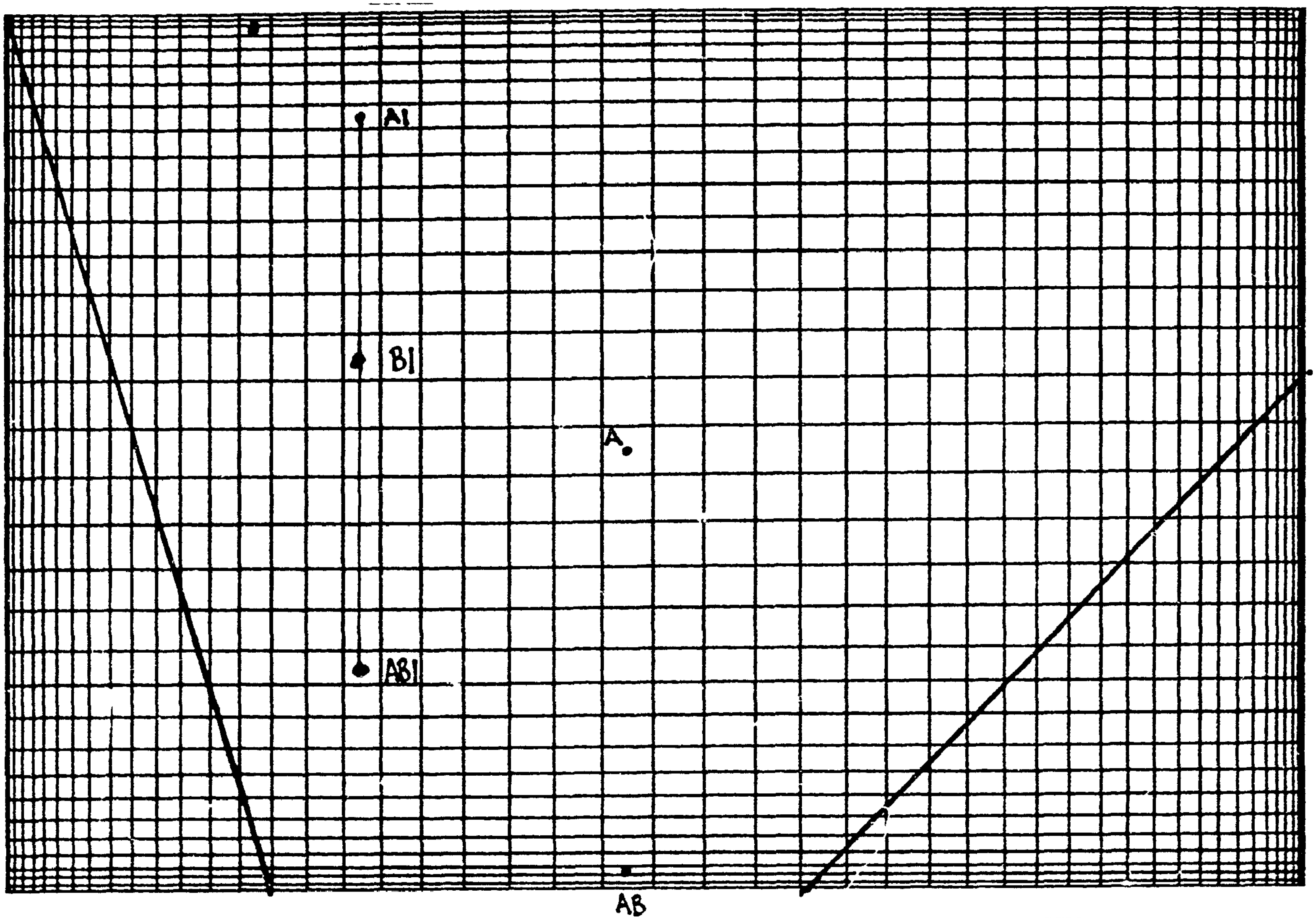

Figure 49: Grid set up and monitoring points for both computations and experimental data (concentrations mainly)

RUN	STEP	DT (s)	TABS (s)	SWEEPS	CPU (hour)	U1 (cm/s)	V1 (cm/s)	H1 (Joules/Kg)	ENUT (m^2/s)
A1	5	2	10	250	1H57	[-0.42, 0.25]	[-0.67, 0.71]	[9.515×10^{5}, 9.538×10^{5}]	[0, 0.746×10^{5}]
A2	50	2	110	100	7H29	[-1.76, 1.41]	[-1.41, 0.70]	[9.447×10^{5}, 9.546×10^{5}]	[0, 0.647×10^{-4}]
A3	100	2	310	50	7H44	[-1.15, 1.01]	[-1.16, 0.29]	[9.440×10^{5}, 9.552×10^{5}]	[0, 0.882×10^{-4}]
A4	150	2	610	40	9H10	[-0.92, 0.85]	[-0.86, 0.15]	[9.408×10^{5}, 9.554×10^{5}]	[0, 0.887×10^{-4}]
A5	150	2	910	40	9H10	[-0.82, 0.80]	[-0.84, 0.10]	[9.382×10^{5}, 9.553×10^{5}]	[0, 0.68×10^{-4}]
A6	150	2	1210	40	9H11	[-0.75, 0.77]	[-0.84, 0.08]	[9.359×10^{5}, 9.55×10^{5}]	[0, 0.56×10^{-4}]
A7	550	2	2310	10	9H19	[-0.63, 0.78]	[-0.79, 0.11]	[9.306×10^{5}, 9.535×10^{5}]	[0, 0.52×10^{-4}]
A8	550	2	3410	10	9H19	[-0.58, 0.76]	[-0.78, 0.11]	[9.254×10^{5}, 9.516×10^{5}]	[0, 0.519×10^{-4}]

Table 12 : Typical sequence of simulations for the full scale reverbatory furnace

RUN	STEP	DT (s)	TABS (s)	SWEEPS	CPU (hour)	U1 (cm/s)	V1 (cm/s)	H1 (Joules/Kg)	ENUT (m^2/s)
E1	5	2	10	250	2H13	[-0.66, 0.18]	[-0.40, 0.19]	[9.821×10^5, 1.012×10^6]	[0, 0.776×10^{-5}]
E2	50	2	110	100	8H12	[-1.26; 0.65]	[-1.69, 0.64]	[9.803×10^5, 1.012×10^6]	[0, 0.129×10^{-3}]
E3	100	2	310	50	8H20	[-1.40, 0.74]	[-1.30, 0.17]	[9.782×10^5, 1.012×10^6]	[0, 0.574×10^{-4}]
E4	150	2	610	40	9H50	[-1.52, 0.90]	[-1.66, 0.18]	[9.758×10^5, 1.012×10^6]	[0, 0.74×10^{-4}]
E5	150	2	910	40	9H36	[-1.57, 0.83]	[-1.85, 0.22]	[9.74×10^5, 1.012×10^6]	[0, 0.828×10^{-4}]
E6	150	2	1210	40	9H24	[-1.60, 0.86]	[-1.95, 0.24]	[9.727×10^5, 1.012×10^6]	[0, 0.907×10^{-4}]
E7	550	2	2310	10	9H14	[-1.64, 0.87]	[-2.10, 0.26]	[9.710×10^5, 1.012×10^6]	[0, 0.103×10^{-3}]
E8	550	2	4310	10	9H25	[-1.66, 0.86]	[-2.17, 0.29]	[9.725×10^5, 1.012×10^6]	[0, 0.109×10^{-3}]

Table 13 : Typical sequence of simulations for the 6.25 ton laboratory furnace

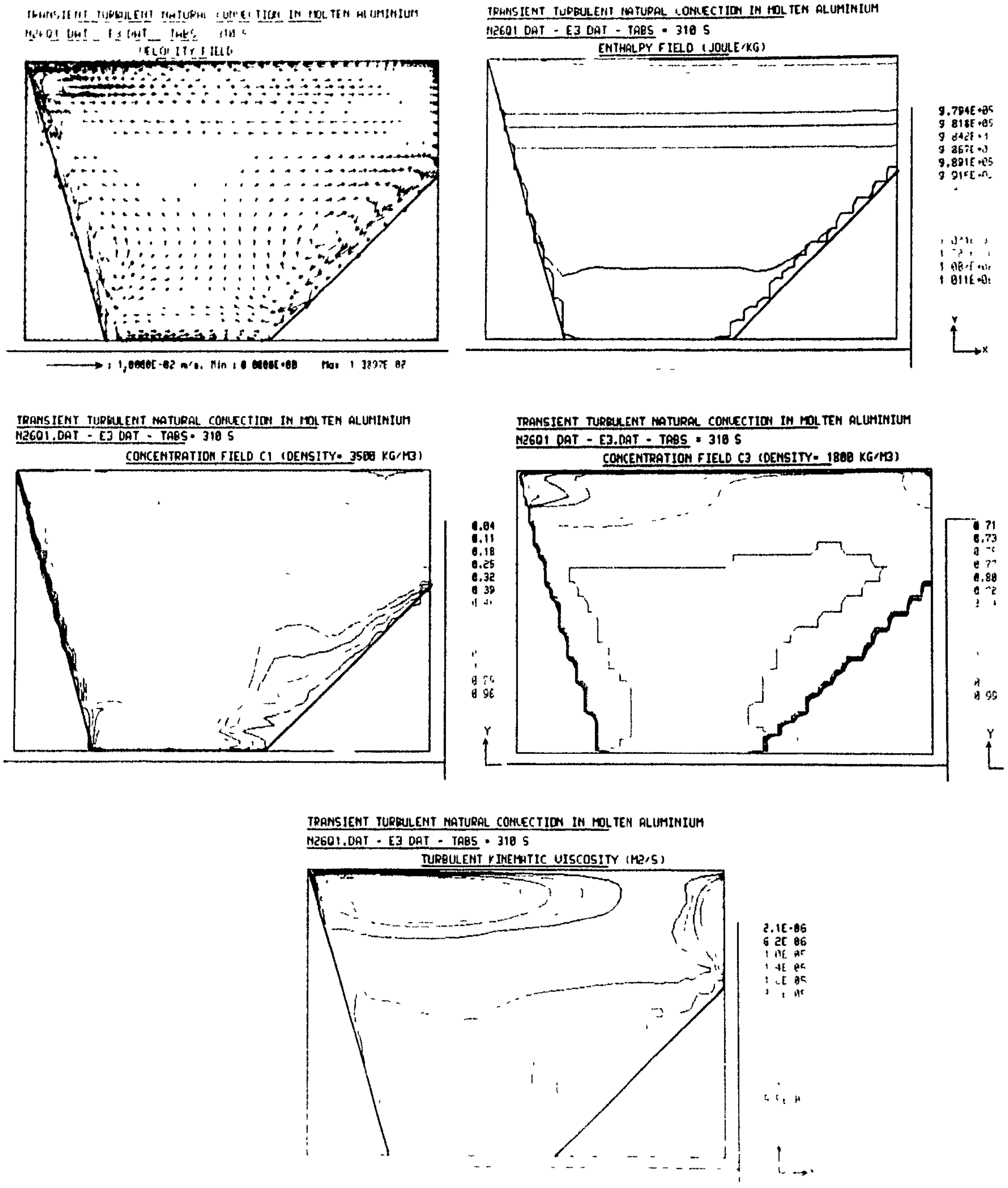

Figures 50-54: Fields of primary variables in 6.25 ton furnace (t=310 s).

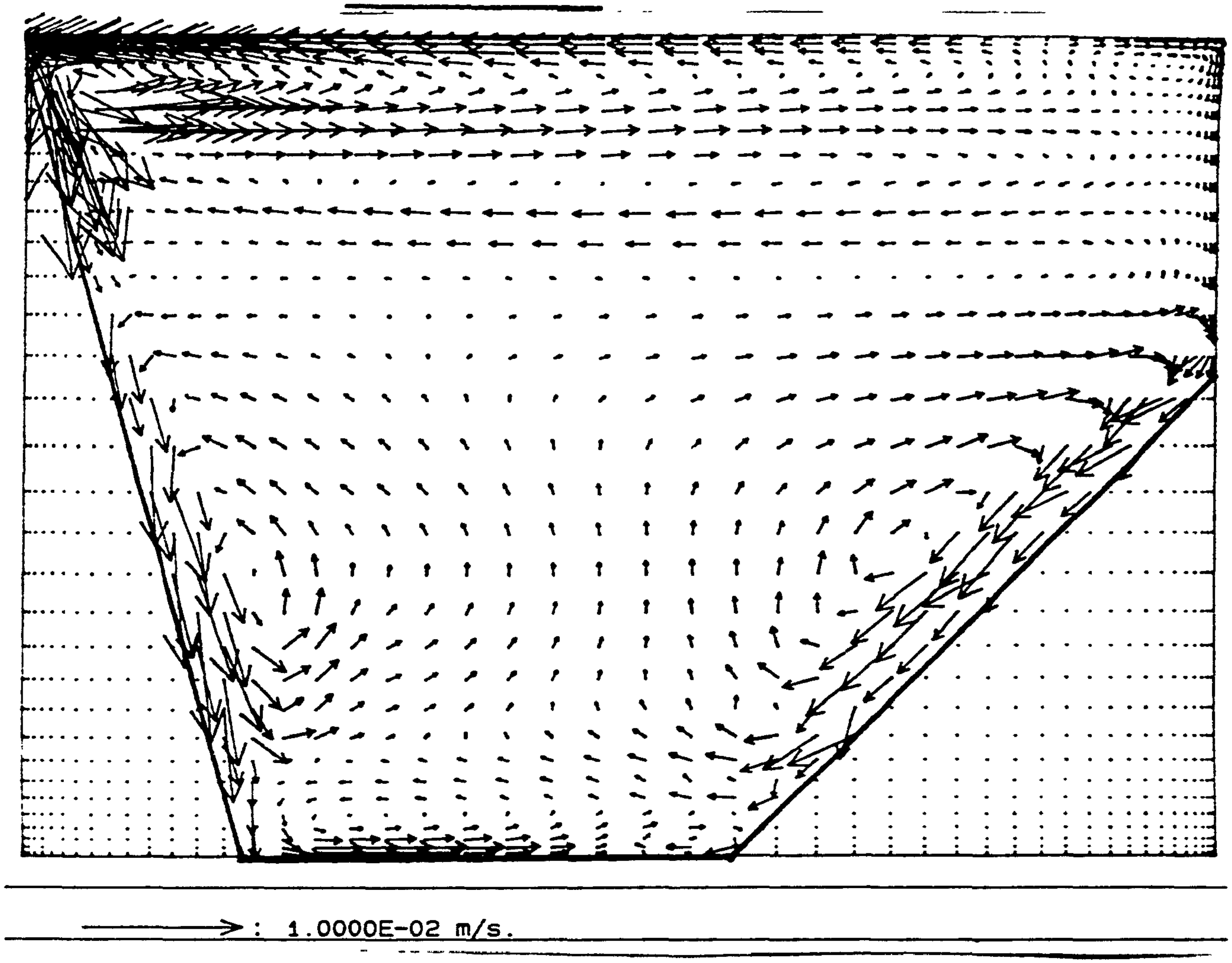

TRANSIENT TURBULENT NATURAL CONVECTION IN MOLTEN ALUMINIUM

N26Q1.DAT - E3.DAT - TABS = 310 S

VELOCITY FIELD

Figure 50

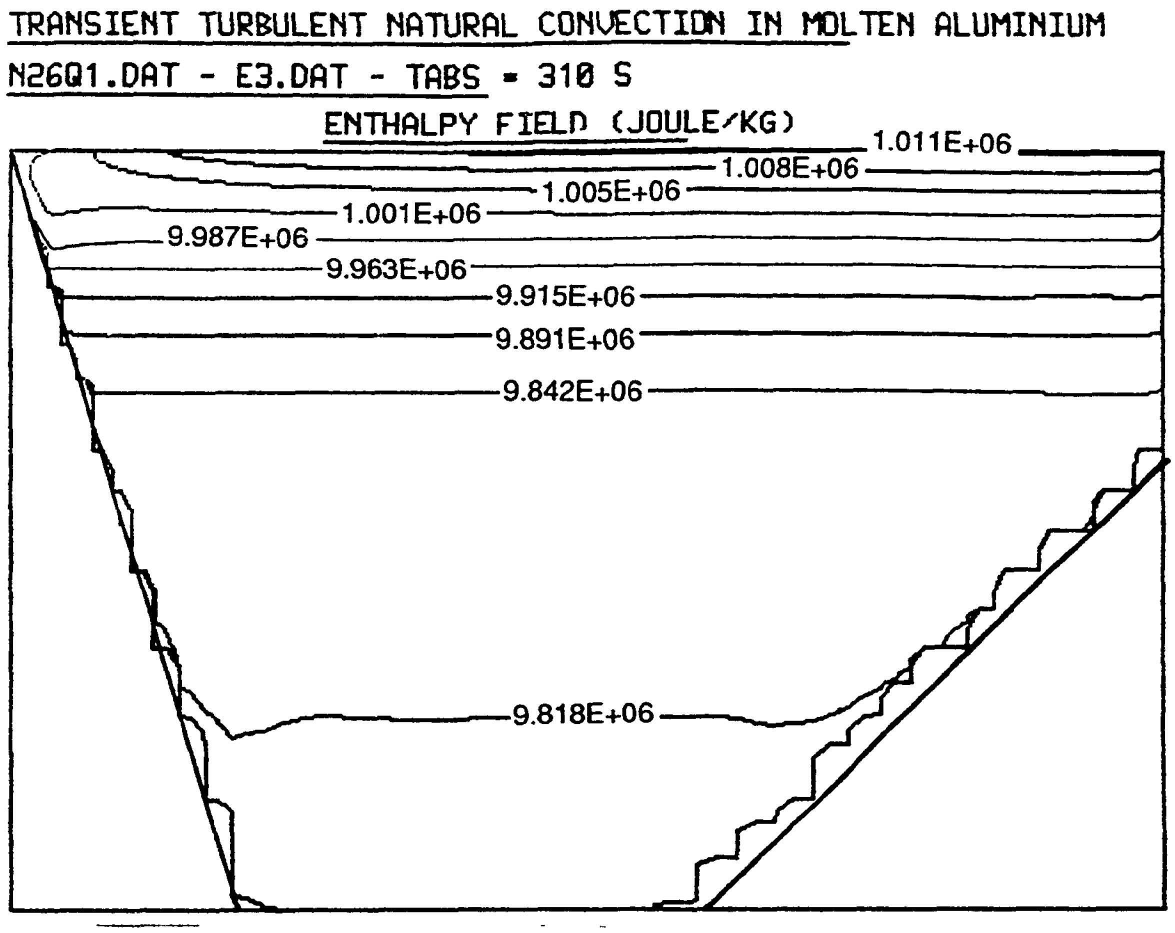
TRANSIENT TURBULENT NATURAL CONVECTION IN MOLTEN ALUMINIUM
N26Q1.DAT - E3.DAT - TABS = 310 S
ENTHALPY FIELD (JOULE/KG)
1.011E+06
1.008E+06
1.005E+06
1.001E+06
9.987E+06
9.963E+06
9.915E+06
9.891E+06
9.842E+06
9.818E+06

Figure 51

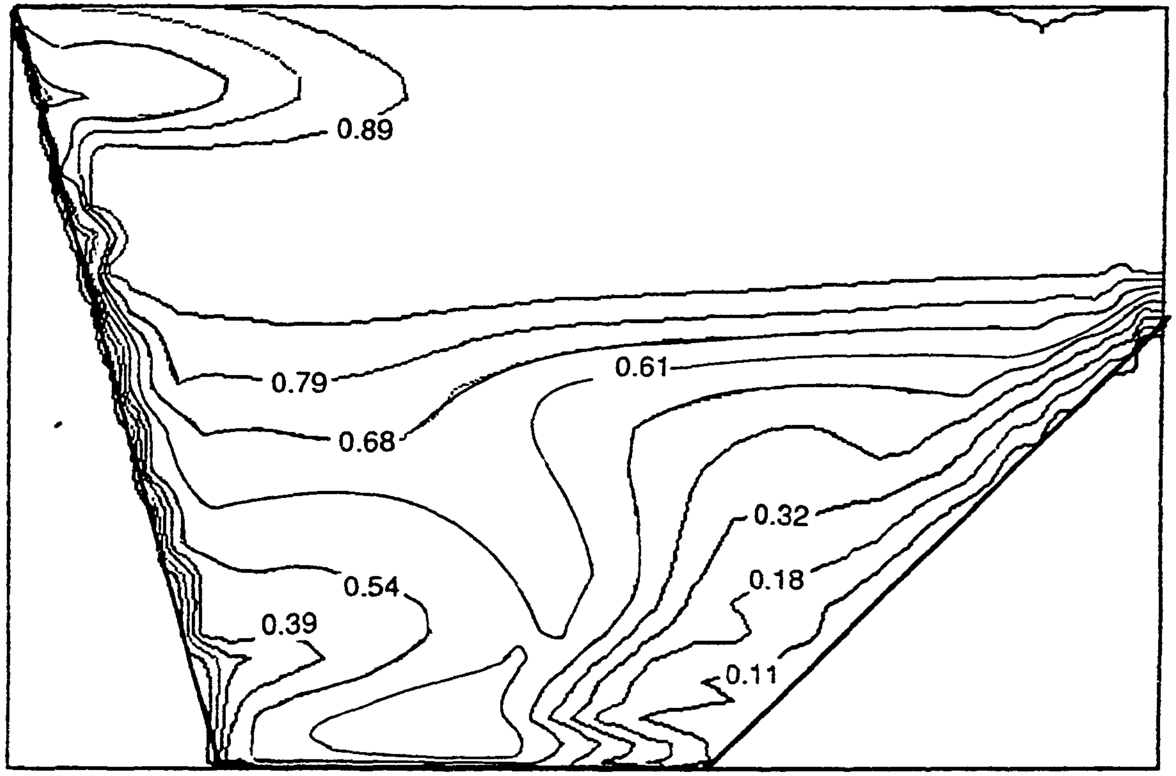

TRANSIENT TURBULENT NATURAL CONVECTION IN MOLTEN ALUMINIUM

N26Q1.DAT - E3.DAT - TABS= 310 S

CONCENTRATION FIELD C1 (DENSITY= 3500 KG/M3)

Figure 52

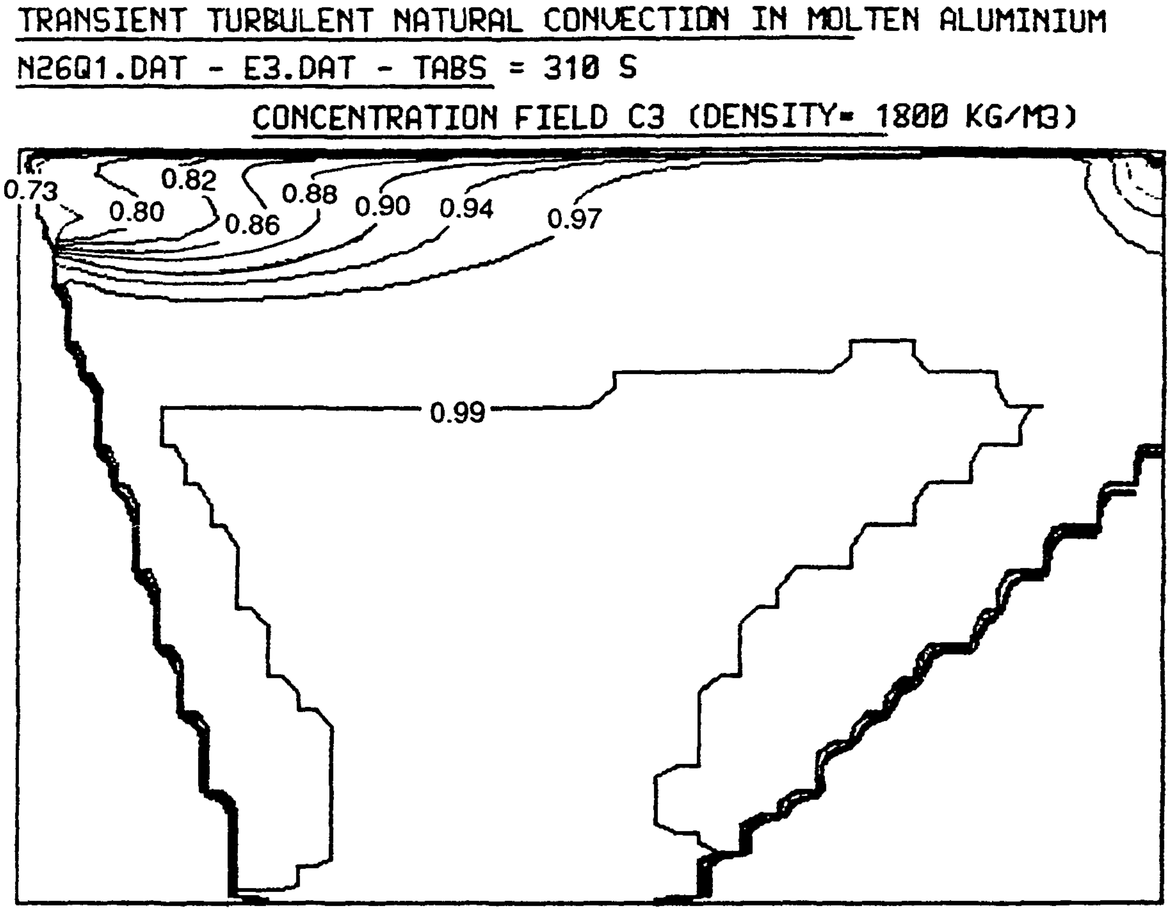
TRANSIENT TURBULENT NATURAL CONVECTION IN MOLTEN ALUMINIUM
N26Q1.DAT - E3.DAT - TABS = 310 S
CONCENTRATION FIELD C3 (DENSITY= 1800 KG/M3)
0.73
0.80
0.82
0.86
0.88
0.90
0.94
0.97
0.99

Figure 53

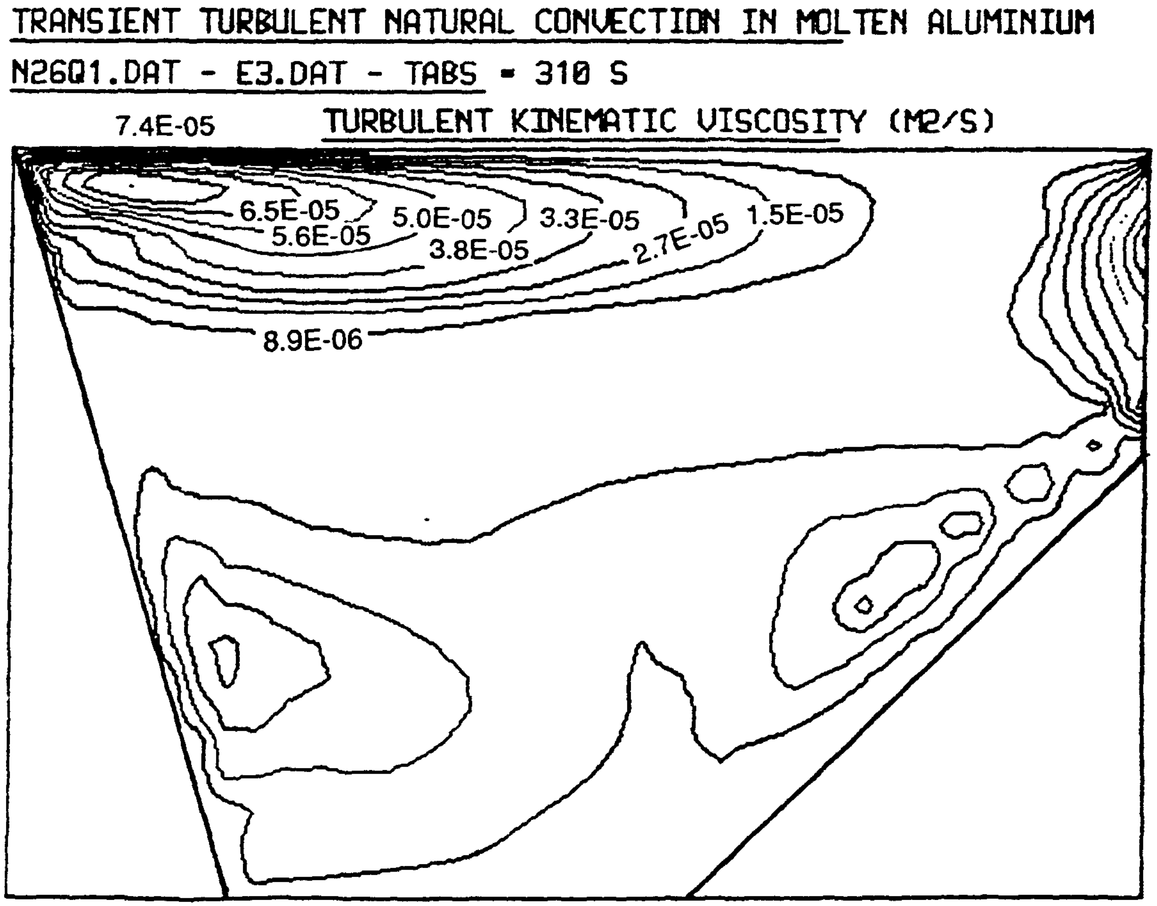
TRANSIENT TURBULENT NATURAL CONVECTION IN MOLTEN ALUMINIUM
N26Q1.DAT - E3.DAT - TABS = 310 S
TURBULENT KINEMATIC VISCOSITY (M2/S)
7.4E-05
6.5E-05
5.6E-05
5.0E-05
3.8E-05
3.3E-05
2.7E-05
1.5E-05
8.9E-06

Figure 54

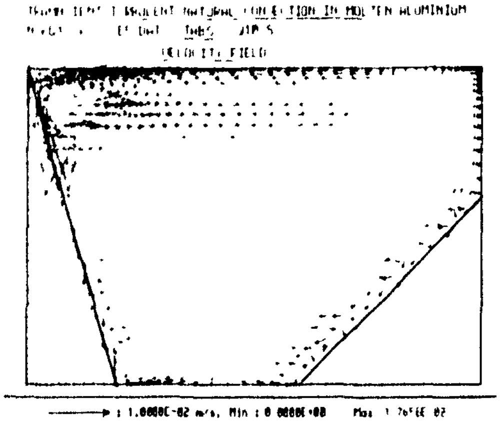

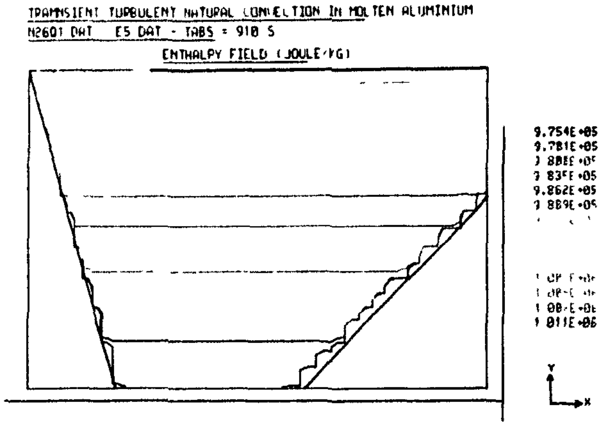

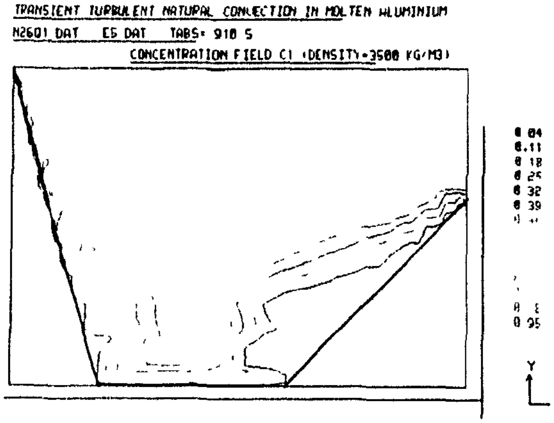

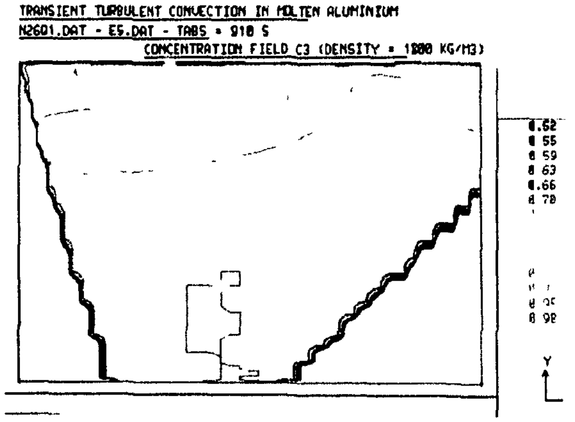

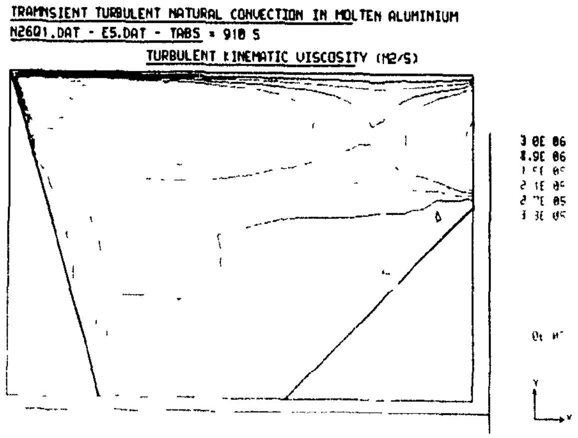

Figures 55-59: Fields of primary variables in 6.25 ton furnace (t=910 s).

TRANSIENT TURBULENT NATURAL CONVECTION IN MOLTEN ALUMINIUM

N26Q1.DAT - E5.DAT - TABS = 910 S

VELOCITY FIELD

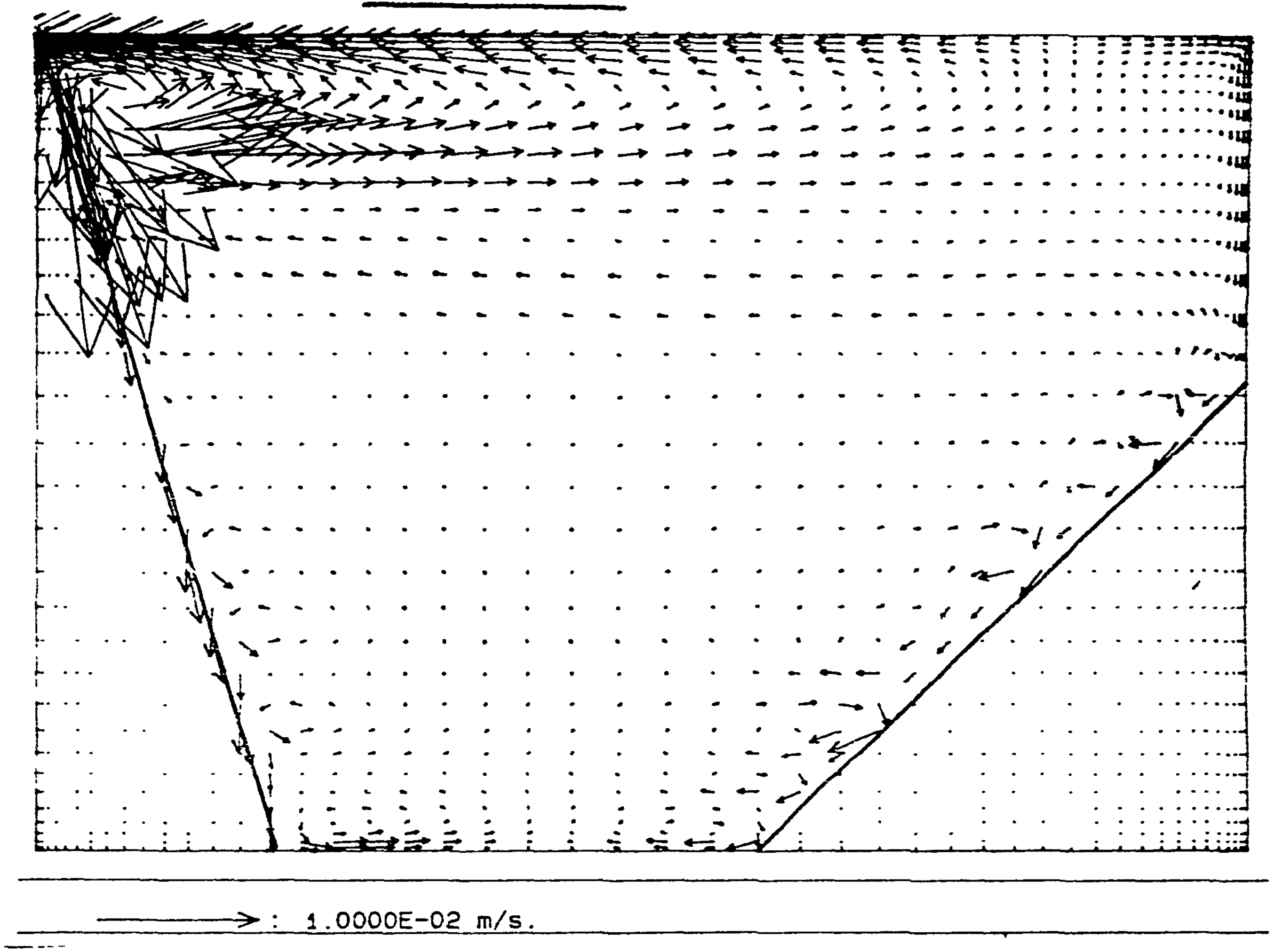

Figure 55

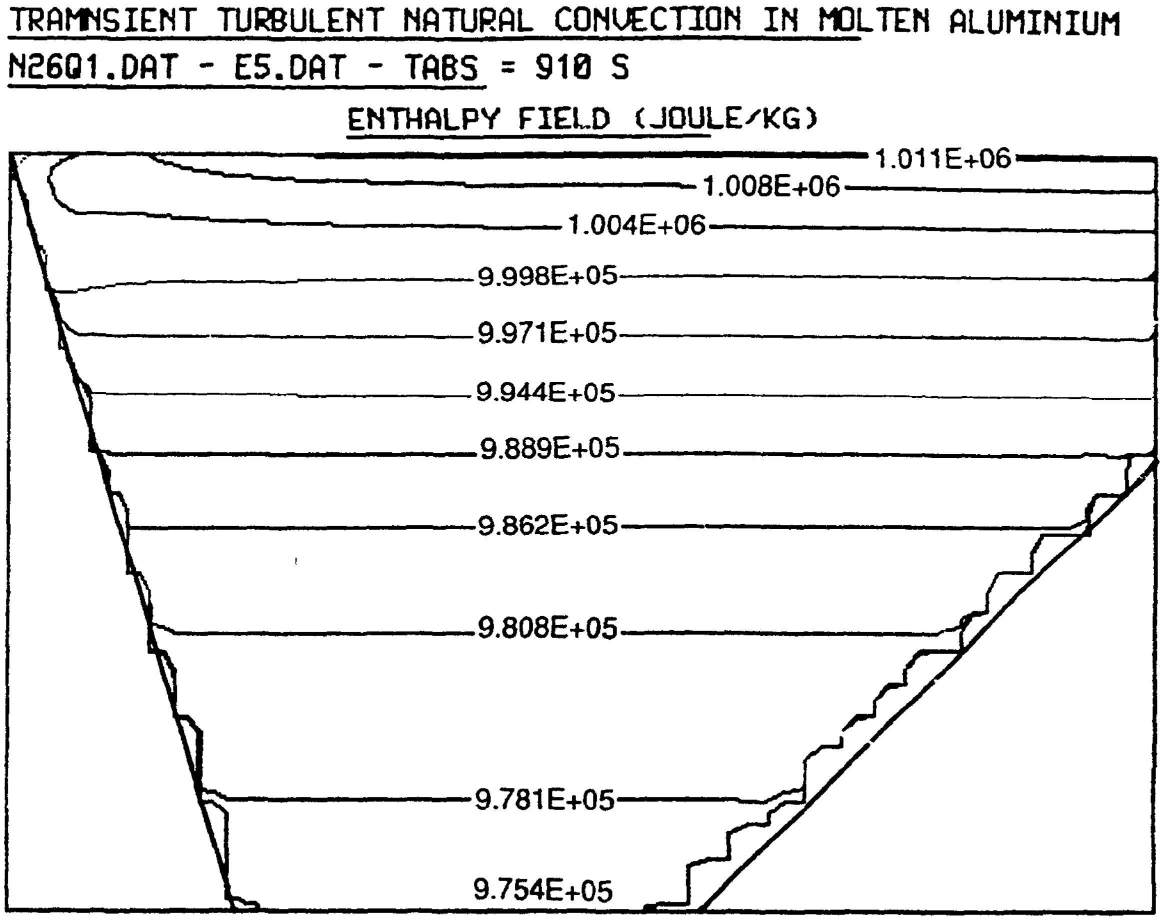
TRAMNSIENT TURBULENT NATURAL CONVECTION IN MOLTEN ALUMINIUM
N26Q1.DAT - E5.DAT - TABS = 910 S
ENTHALPY FIELD (JOULE/KG)
1.011E+06
1.008E+06
1.004E+06
9.998E+05
9.971E+05
9.944E+05
9.889E+05
9.862E+05
9.808E+05
9.781E+05
9.754E+05

Figure 56

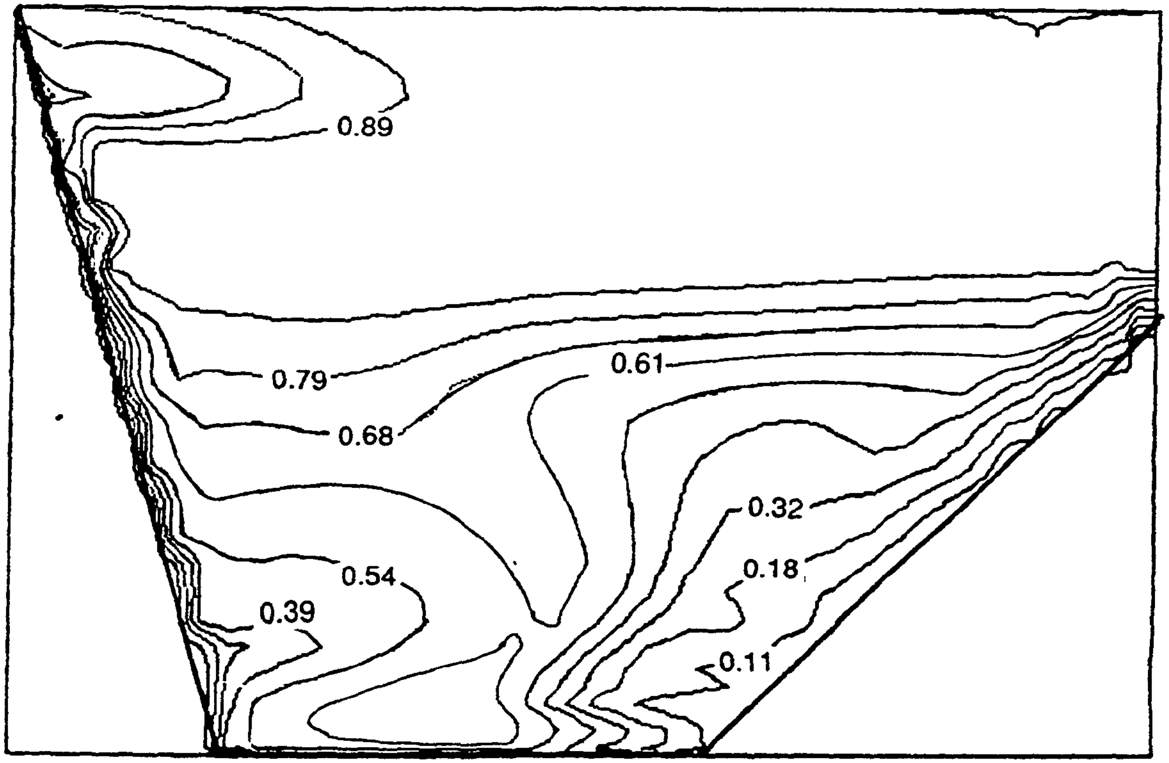
TRANSIENT TURBULENT NATURAL CONVECTION IN MOLTEN ALUMINIUM
N26Q1.DAT - E3.DAT - TABS= 310 S
CONCENTRATION FIELD C1 (DENSITY= 3500 KG/M3)

Figure 57

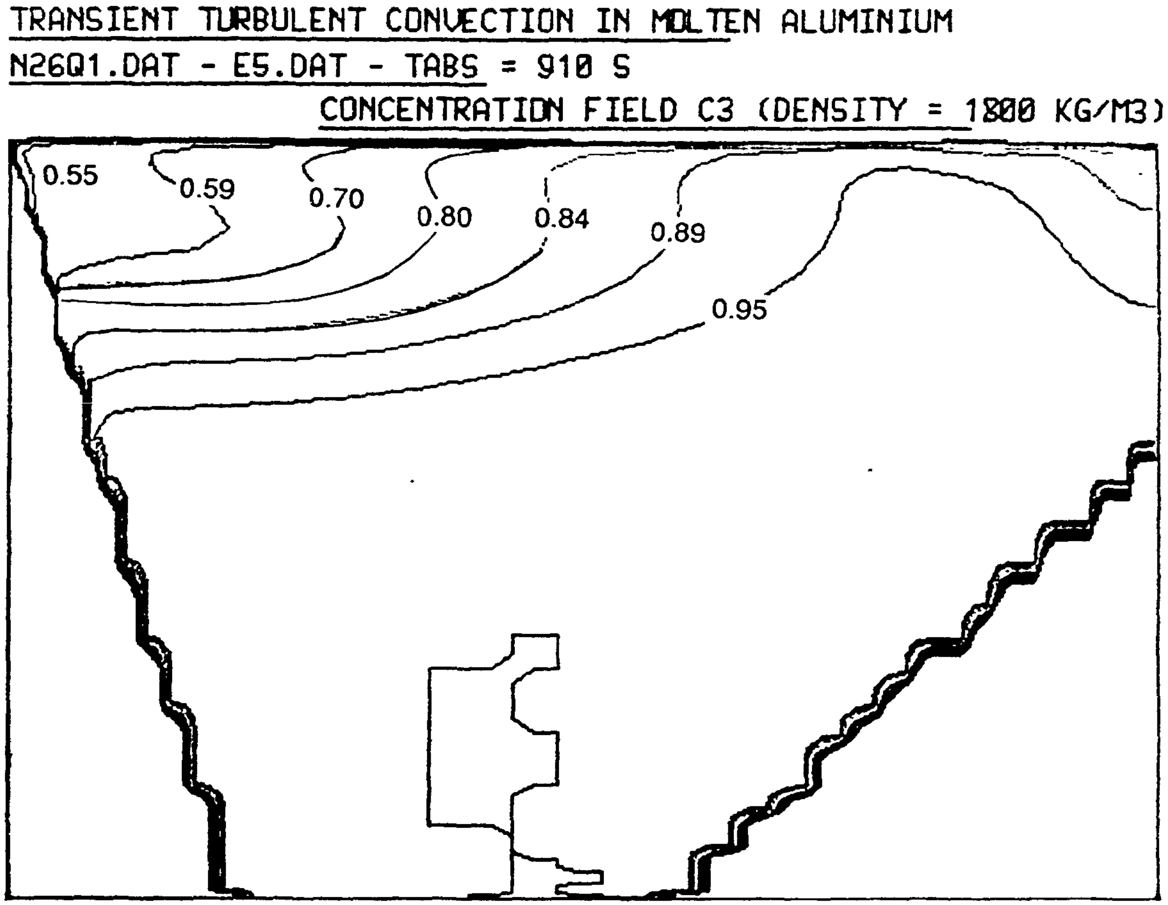

TRANSIENT TURBULENT CONVECTION IN MOLTEN ALUMINIUM

N26Q1.DAT - E5.DAT - TABS = 910 S

CONCENTRATION FIELD C3 (DENSITY = 1800 KG/M3)

Figure 58

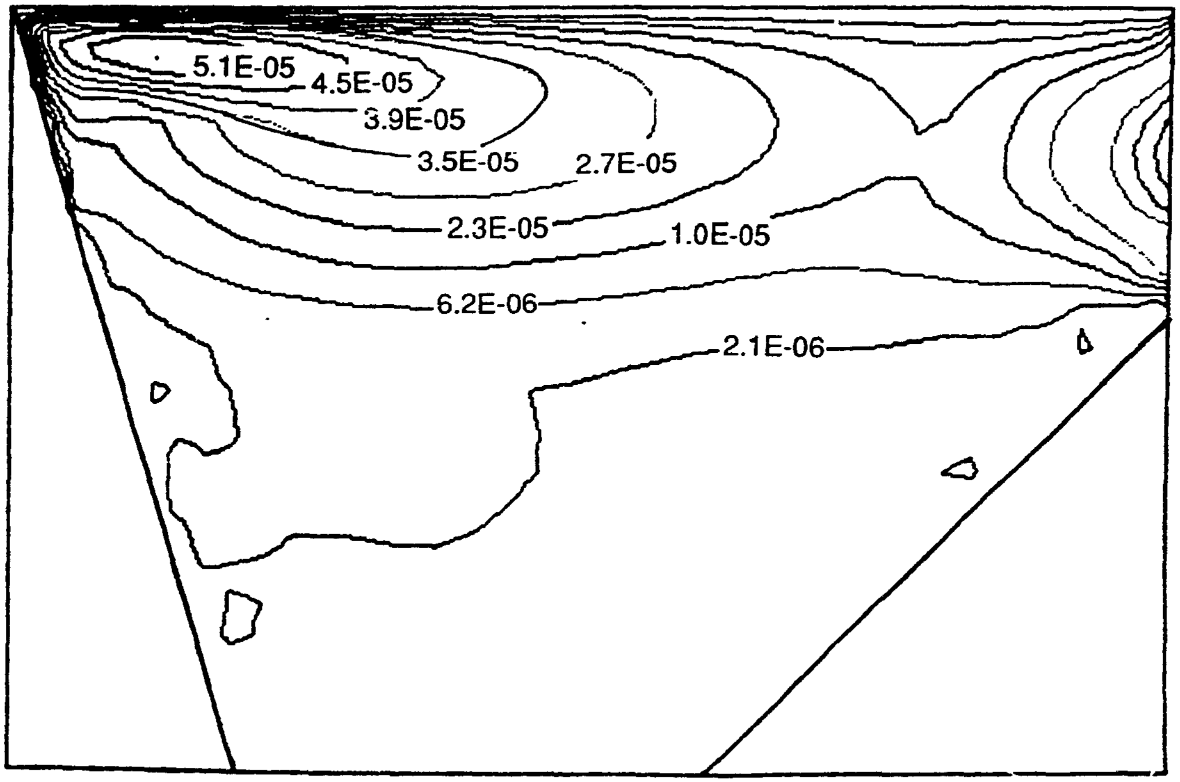
TRAMNSIENT TURBULENT NATURAL CONVECTION IN MOLTEN ALUMINIUM

N26Q1.DAT - E5.DAT - TABS = 910 S

TURBULENT KINEMATIC VISCOSITY (M2/S)

Figure 59

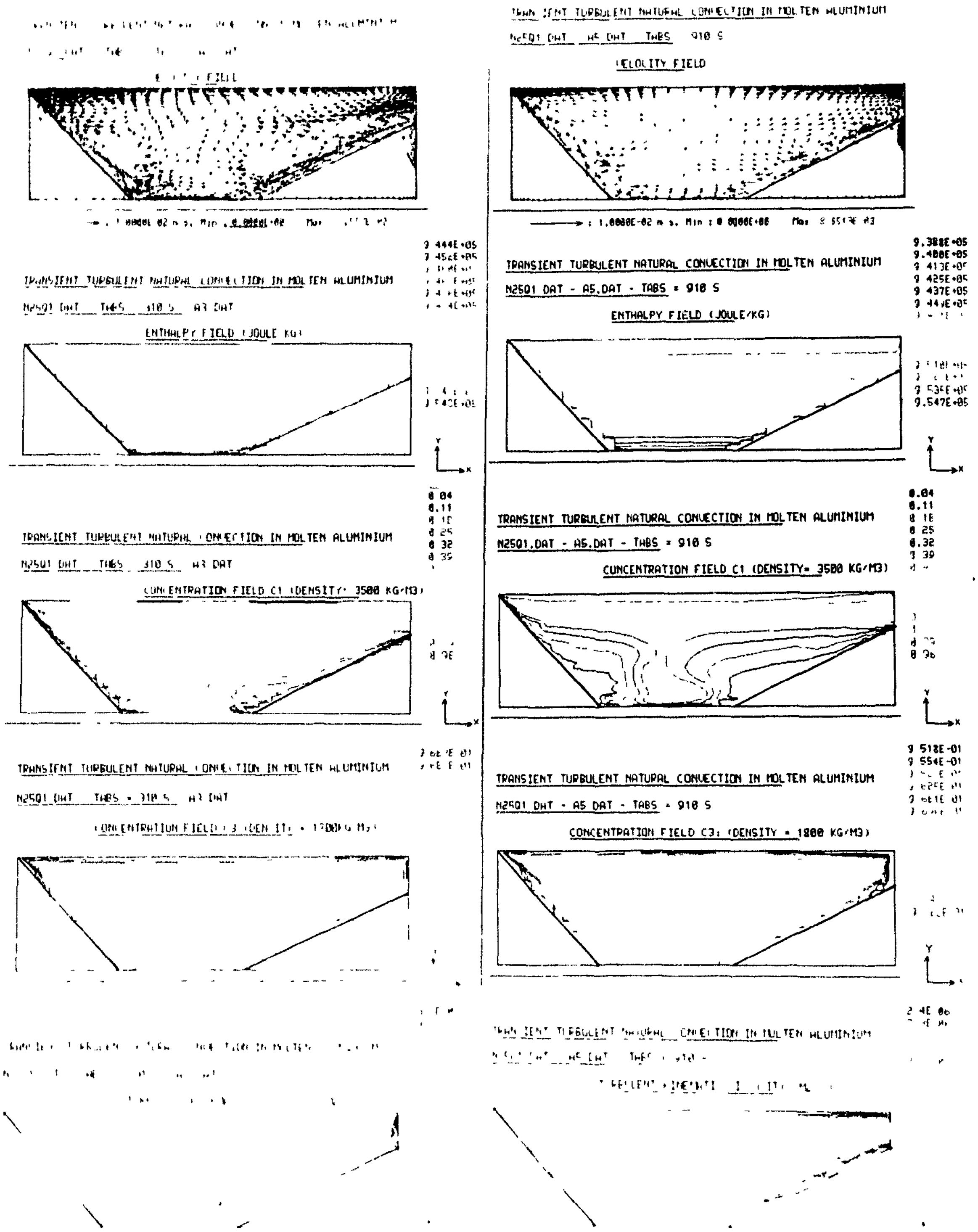

Figures 60-69: Fields of primary variables in full scale industrial furnace. (t=310 s and 910 s).

TRANSIENT TURBULENT NATURAL CONVECTION IN MOLTEN ALUMINIUM

N25Q1.DAT - TABS = 310 S - A3.DAT

VELOCITY FIELD

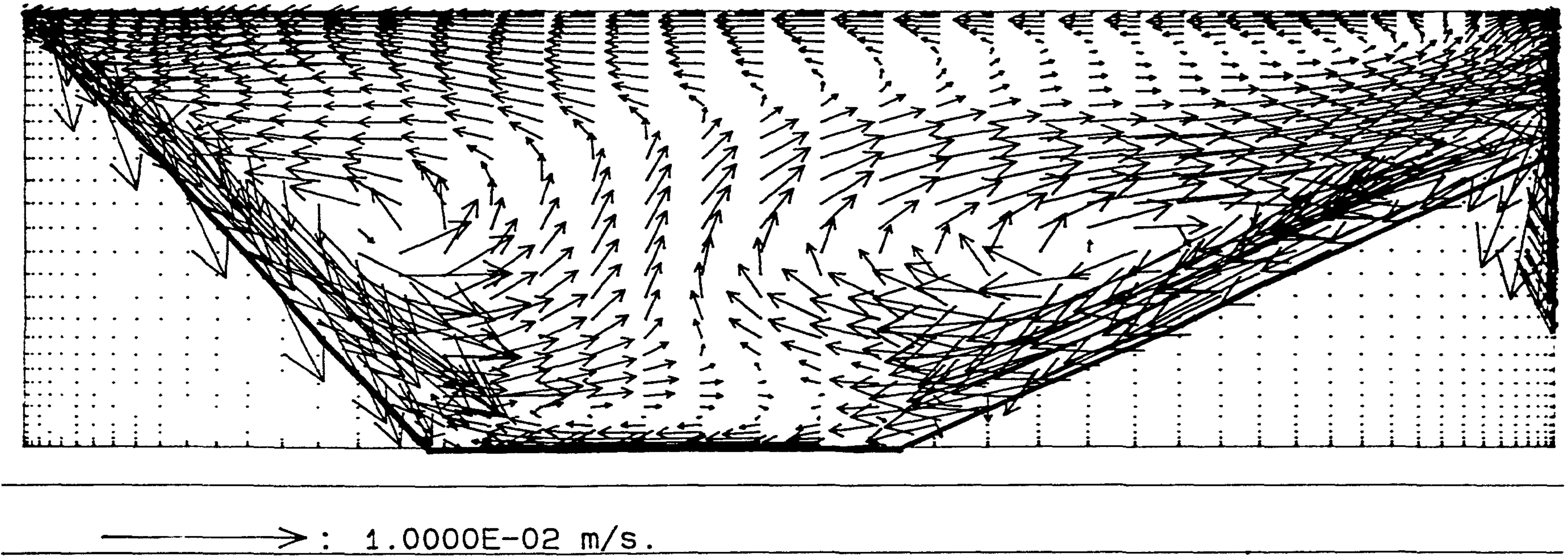

Figure 60

TRANSIENT TURBULENT NATURAL CONVECTION IN MOLTEN ALUMINIUM

N25Q1.DAT - TABS = 310 S - A3.DAT

ENTHALPY FIELD (JOULE/KG)

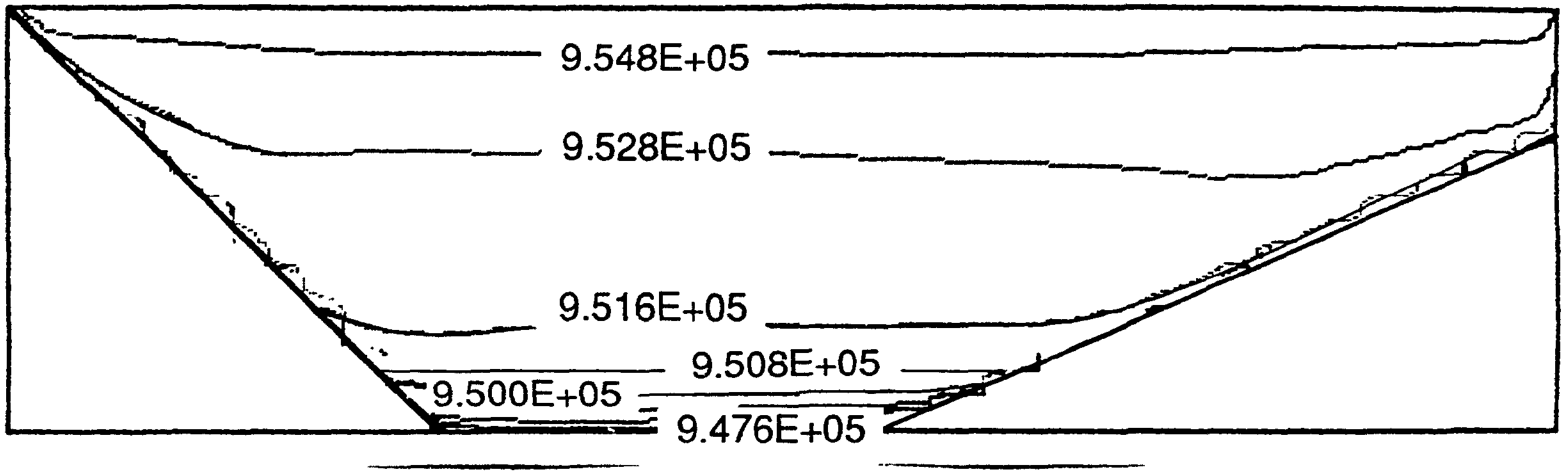

Figure 61

TRANSIENT TURBULENT NATURAL CONVECTION IN MOLTEN ALUMINIUM

N25Q1.DAT - TABS = 310 S - A3.DAT

CONCENTRATION FIELD C1 (DENSITY: 3500 KG/M3)

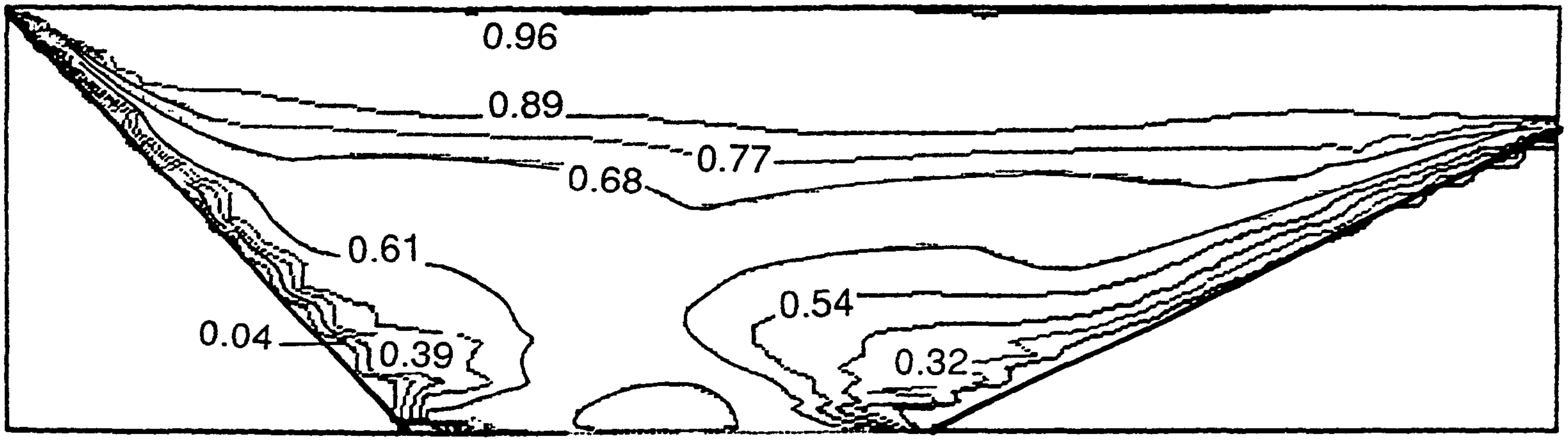

Figure 62

TRANSIENT TURBULENT NATURAL CONVECTION IN MOLTEN ALUMINIUM

N25Q1.DAT - TABS = 310 S - A3.DAT

CONCENTRATION FIELD C3 (DENSITY = 1800KG/M3)

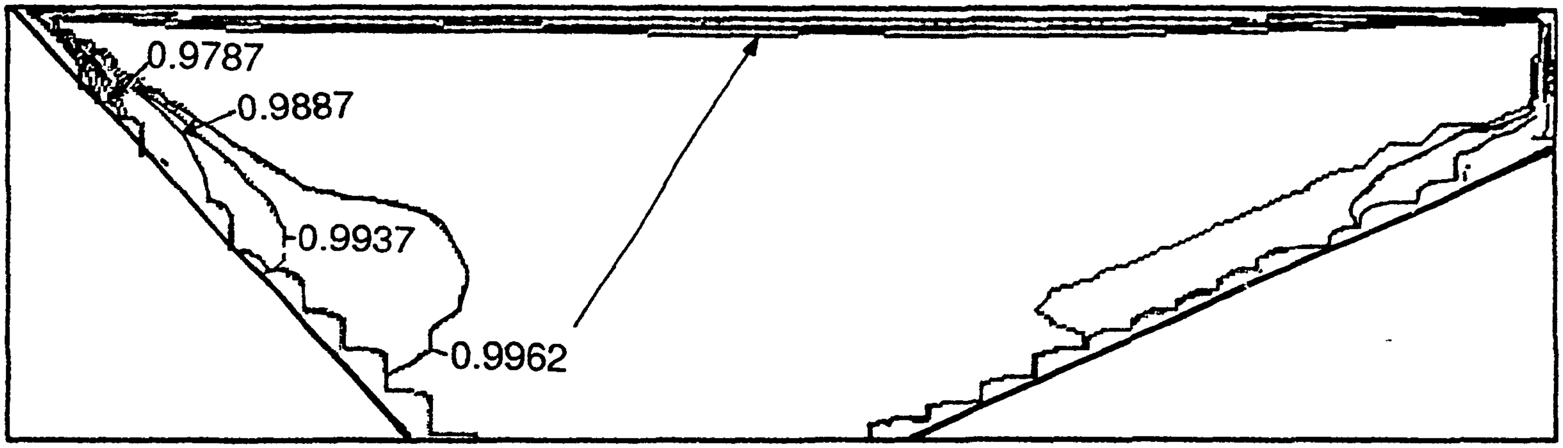

Figure 63

TRANSIENT TURBULENT NATURAL CONVECTION IN MOLTEN ALUMINIUM

N25Q1.DAT - TABS = 310 S - A3.DAT

TURBULENT KINEMATIC VISCOSITY (M2/S)

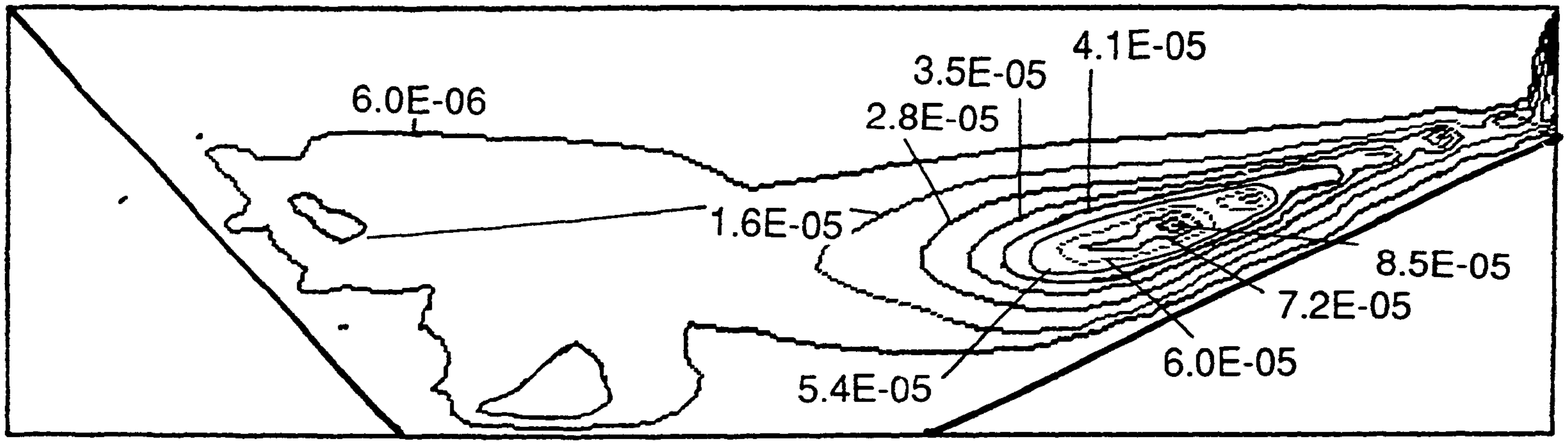

Figure 64

TRANSIENT TURBULENT NATURAL CONVECTION IN MOLTEN ALUMINIUM

N25Q1.DAT - A5.DAT - TABS = 910 S

VELOCITY FIELD

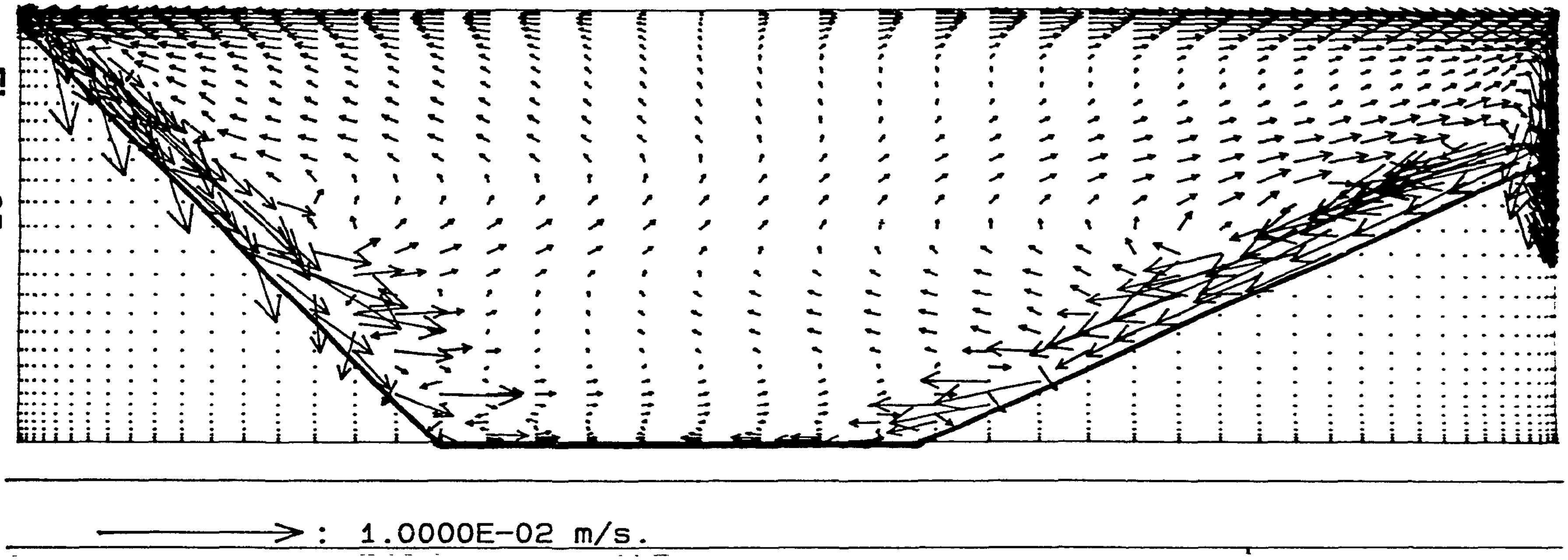

Figure 65

TRANSIENT TURBULENT NATURAL CONVECTION IN MOLTEN ALUMINIUM

N25Q1.DAT - A5.DAT - TABS = 910 S

ENTHALPY FIELD (JOULE/KG)

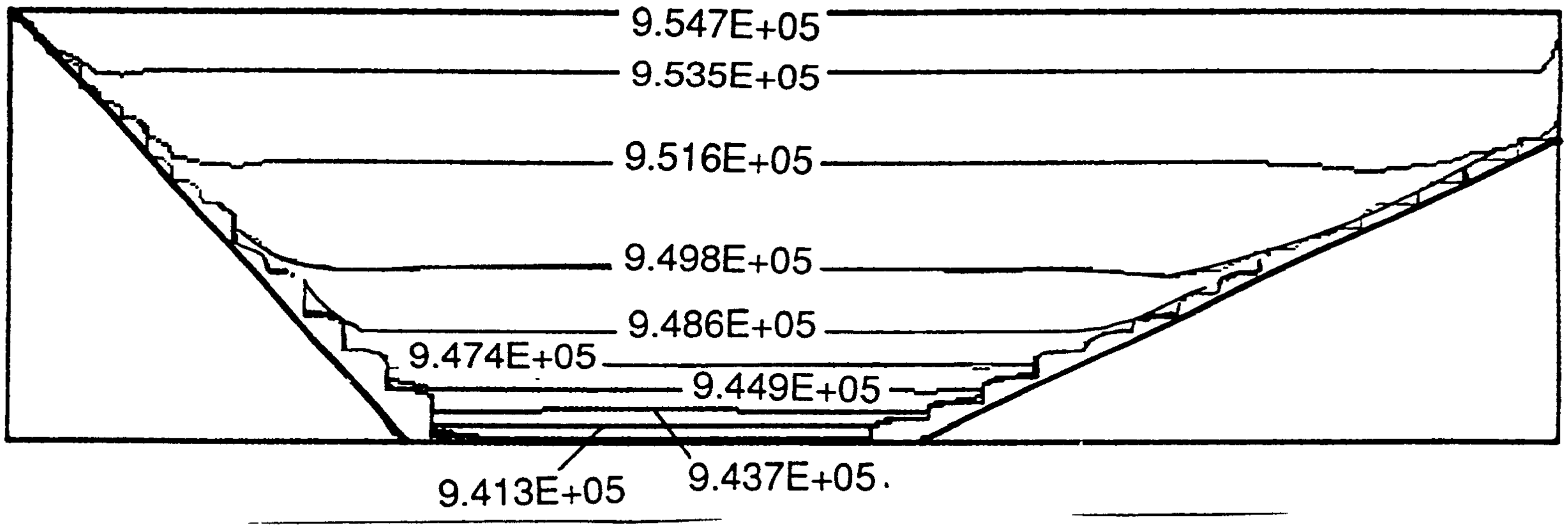

Figure 66

TRANSIENT TURBULENT NATURAL CONVECTION IN MOLTEN ALUMINIUM

N25Q1.DAT - A5.DAT - TABS = 910 S

CONCENTRATION FIELD C1 (DENSITY= 3500 KG/M3)

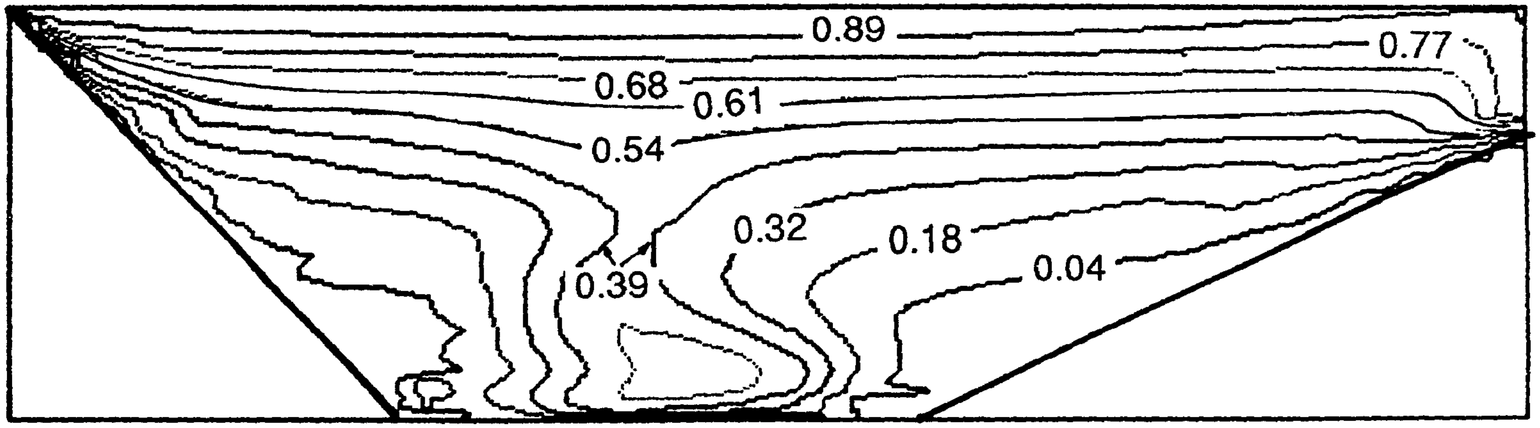

Figure 67

TRANSIENT TURBULENT NATURAL CONVECTION IN MOLTEN ALUMINIUM

N25Q1.DAT - A5.DAT - TABS = 910 S

CONCENTRATION FIELD C3: (DENSITY = 1800 KG/M3)

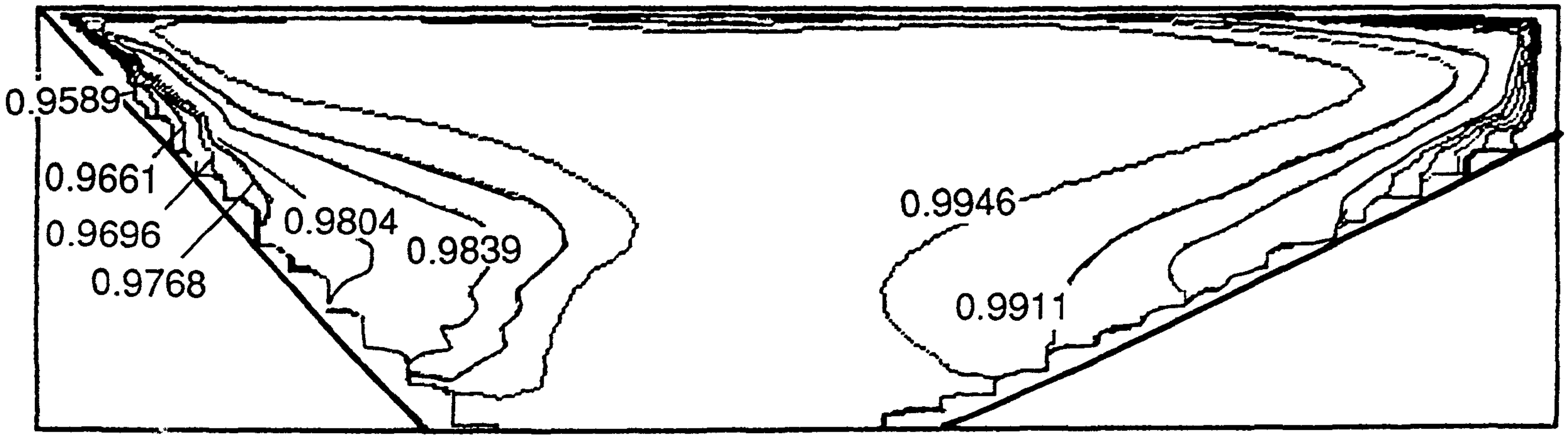

Figure 68

TRANSIENT TURBULENT NATURAL CONVECTION IN MOLTEN ALUMINIUM

N25Q1.DAT - A5.DAT - TABS = 910 S

TURBULENT KINEMATIC VISCOSITY (M2/S)

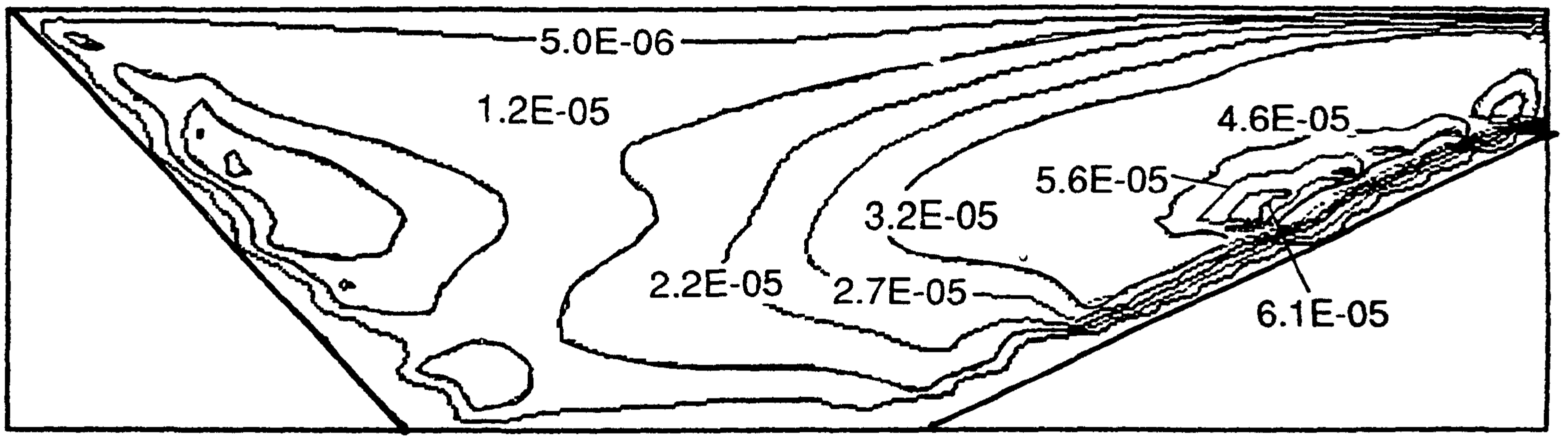

Figure 69

A = (25,25,17,17,1,1)
B = (16,16,33,33,1,1)
AB = (25,25,3,3,1,1)
AI = (19,19,26,26,1,1)
BI = (19,19,19,19,1,1)
ABI = (19,19,12,12,1,1)

These points are a good reference for comparing computations to experimental measurements (especially concentrations) These profiles are presented at Figures (70-72).

An inspection of the above Figures reveals that the turbulent natural convection within the furnaces starts with a relatively strong movement, with maximum velocities in the order of 2 cm/s. The velocity vectors seem to be mostly directed down the inclined side walls. In both furnaces, two opposite patterns of recirculation are observed at the onset of the simulation The components of the velocity are then damped down with time and the temporal profiles clearly show that velocity field changes very little after 30 minutes of simulation in real time. Contrary to the dampening of velocity fields, the enthalpy H1 is seen to take a much longer time to stabilize This may be attributed to the conductive effects of aluminum in relatively shallow cavities. It is therefore natural to expect that the time necessary for complete thermal stratification will be unduly long for this type of problem. Once thermal stratification is achieved in the furnace, the velocity field was no longer influenced by the thermal gradients. Under these circumstances, the liquid aluminum remains motionless in the core of the cavity A little recirculation can still be observed very close to the inclined side walls In the case of the experimental furnace, the persistent recirculation vortex located at the top left of the furnace is only due to a non uniform heat flux from the top As mentioned before, extra heat losses were inevitable near the sliding door through which the thermocouples were installed during experiments. This creates an horizontal gradient of temperature at the top surface of the molten aluminum, which in turn causes this supplementary movement (Fig. 55).

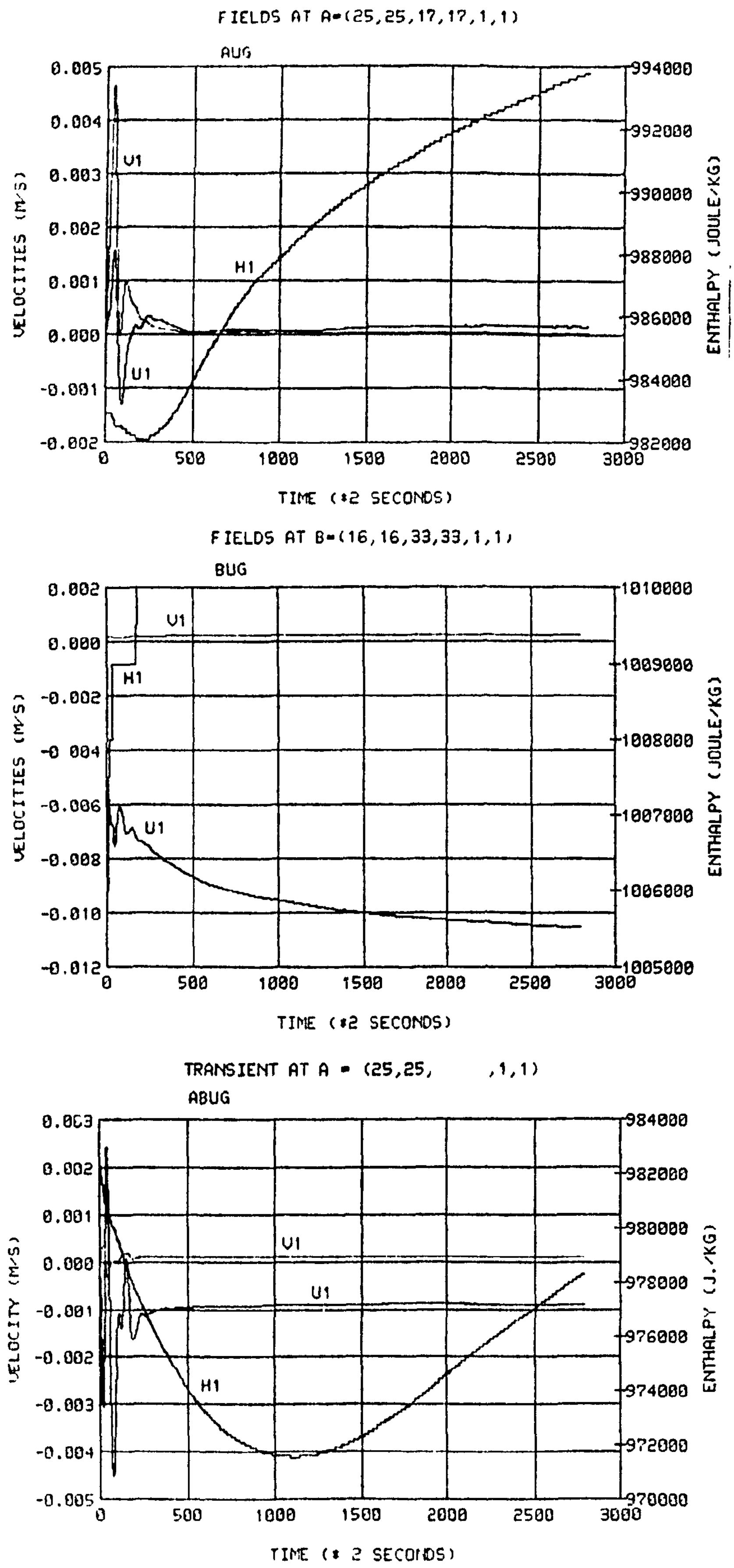

Figure 70 : Profiles of primary variables at points indicated on Fig. 49

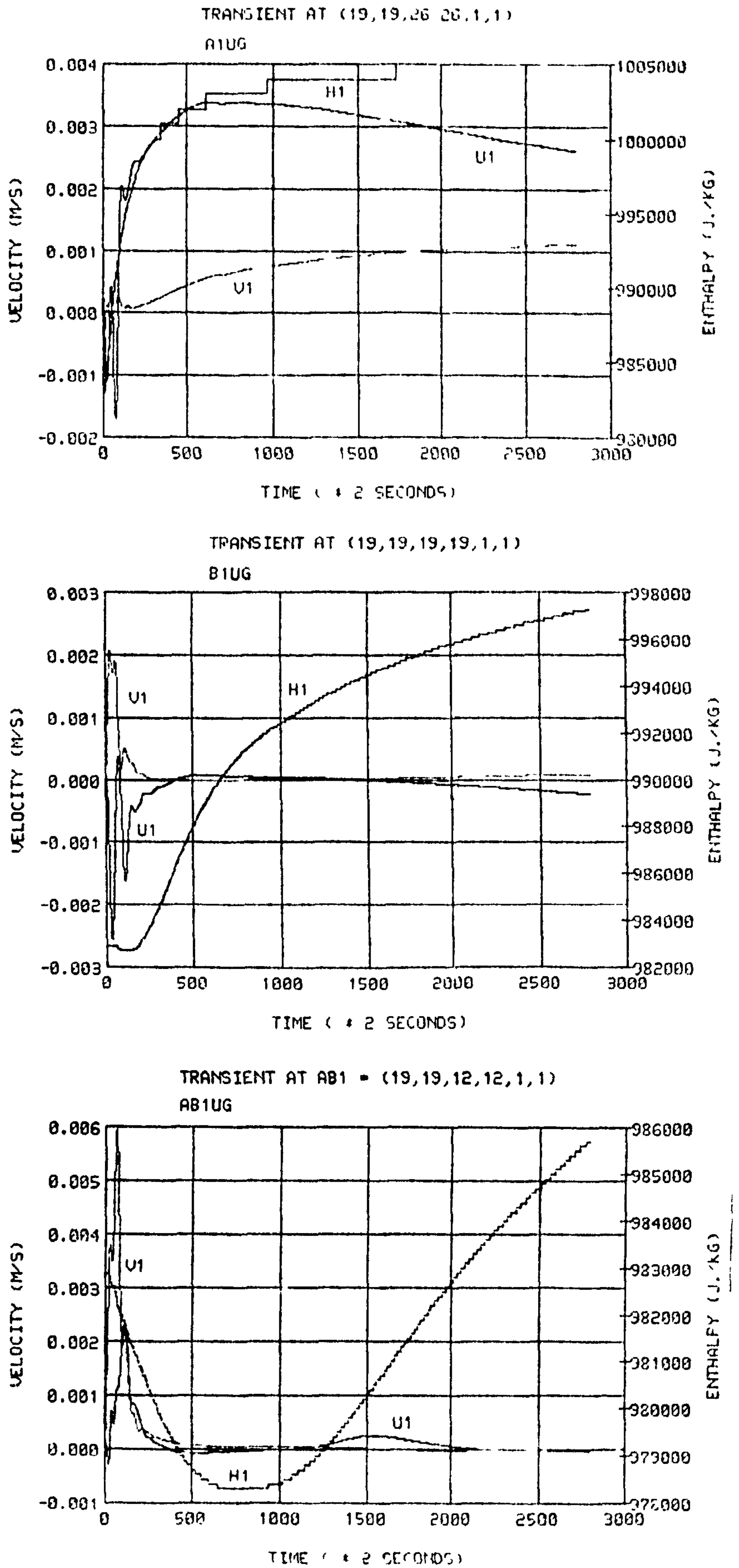

Figure 71 : Profiles of primary variables at points indicated on Fig. 49

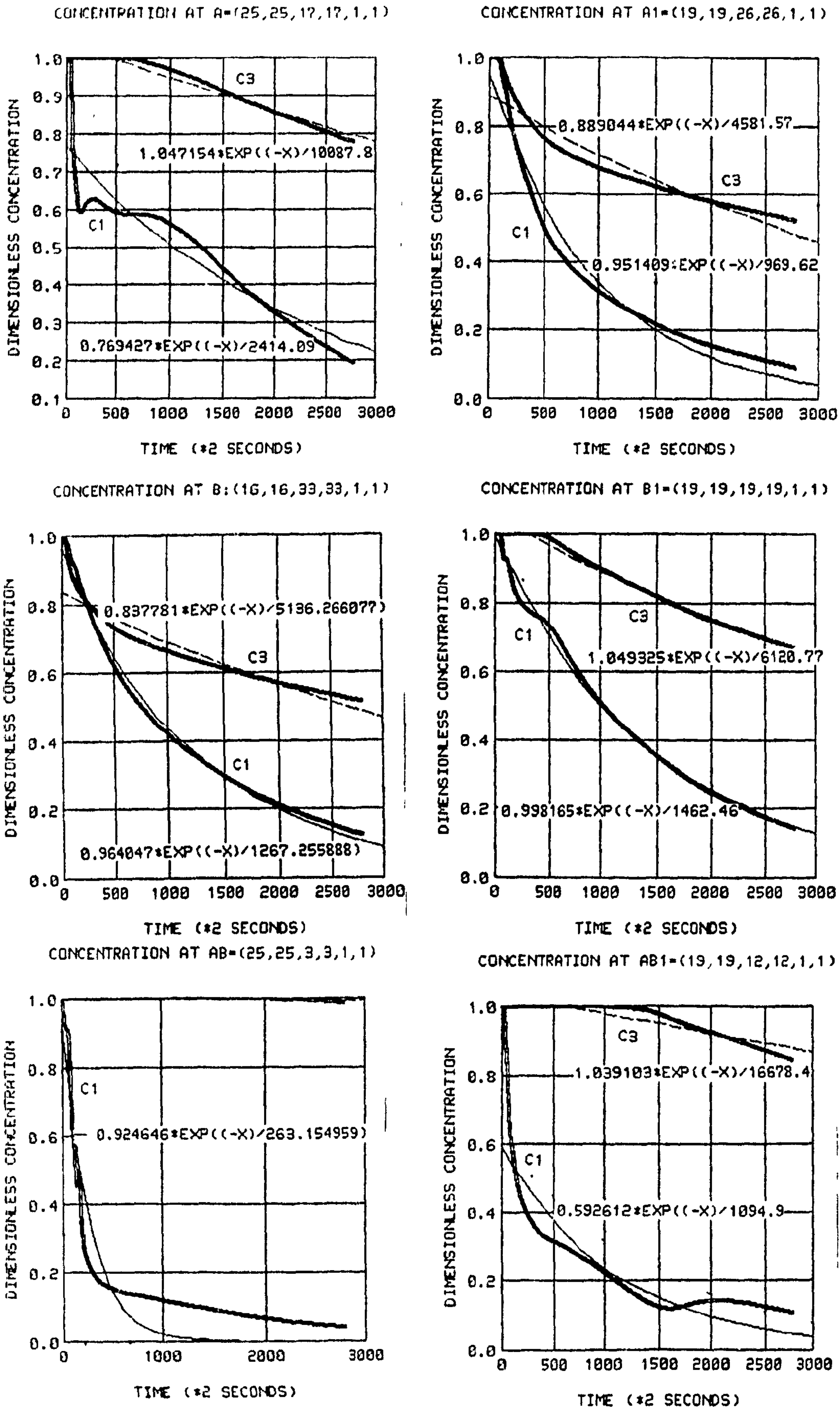

Figure 72: Computed concentrations
C1 (density = 3500 kg/m^3) and C3 (density = 1800 kg/m^3)

The computed kinematic (turbulent) viscosity ranged between 0 and 10^{-4} m^2/s; the highest value was encountered in the bulk of the cavity. The maximum kinematic turbulent viscosity was 200 times the value of its laminar counterpart (5×10^{-7} m^2/s).

3-2-6 Convergence and computer time

For each time step of the transient simulation, the convergence of the full set of variables is necessary before proceeding to the next step. From the initial conditions, the numbers of iterations or "SWEEPS" needed to attain convergence depends on many factors. The strategy adopted was to fix very small values of the residual references (RESREF: 10^{-6}) and to monitor the residual sources versus SWEEPS. In general a decrease of about 3-5 order of magnitude was needed to reach convergence. This corresponds to a plateau of the residual sources versus sweeps.

As an example, the exponents n of the order of magnitude of the residual sources (proportional to 10^n) are given in table (14) along with the number of sweeps. Mass continuity errors, or more precisely volumetric flow imbalances, are of the order of $10^{-2} \times 10^{-6}$ (cf RESREF(P1)) and therefore are not significant.

SWEEPS	PI	U1	VI	K	E	HI	CI
1	3	4	5	4	3	10	6
10	2	3	3	3	3	7	2
25	0	1	1	3	2	7	1
50	0	0	1	2	1	7	1
100	-2	-1	0	1	0	7	1
200	-2	-1	0	-2	-3	7	1
250	-2	-1	0	-2	-3	7	1

Table 14: convergence monitoring at Tabs = 10s.

For this type of recirculating flow, the residual sources for momentum were below 10^{-6} and, for turbulence variables, residual sources were below 10^{-8}

For enthalpy, they were below 10^1 (Watts), which has to be normalised by the input heat flux:

$$q_{inp} = 10 / 1500 / 3.76 = 2 \times 10^{-3} \quad \text{(dimensionless)}$$

For concentration this residual source stays below 10^{-5}.

It should be noted that a progressively smaller number of SWEEPS were needed as computations marched forward in time since results from the previous time step served as very reliable guesses for the present time step. A run with 250 sweeps required an average of 23 minutes of CPU time on the VAX/785 minicomputer for a 50 × 35 grid. For a 60 × 40 grid mesh, this time extended from 23 minutes to 32 minutes.

3-2-7 Grid independence and computer storage

To obtain grid independent results, two types of grid independence tests had to be performed; namely space and time grids had to be optimized.

3-2-7-1 Time grid independence

For a given geometry and given initial conditions, a simulation lasting 100s was carried out for 100s under the same conditions for a set of time steps, numbering 2,5,10,20,50 and 100. These non dimensional time step numbers correspond respectively to 50s, 20s, 10s, 5s, 2s and 1s (a linear time grid was taken for all simulations). For all variables, a comparison was then made of the transient behaviour of the system. As an example, Figure 73 indicates the profiles of U1, the horizontal component of velocity. It is seen that the evolution of U1 obtained with LSTEP = 100 and that computed with LSTEP = 50 are very similar; the same is true for the other primary variables computed. The above results lead the author to choose a time step of 2 seconds for all simulations.

If this choice of a small time step is necessary to provide adequate solutions and if we consider the slow conductive phenomena in a large cavity filled with molten aluminum, this means that the computing cost will be prohibitively expensive to simulate the process at an industrial time scale. In practice the

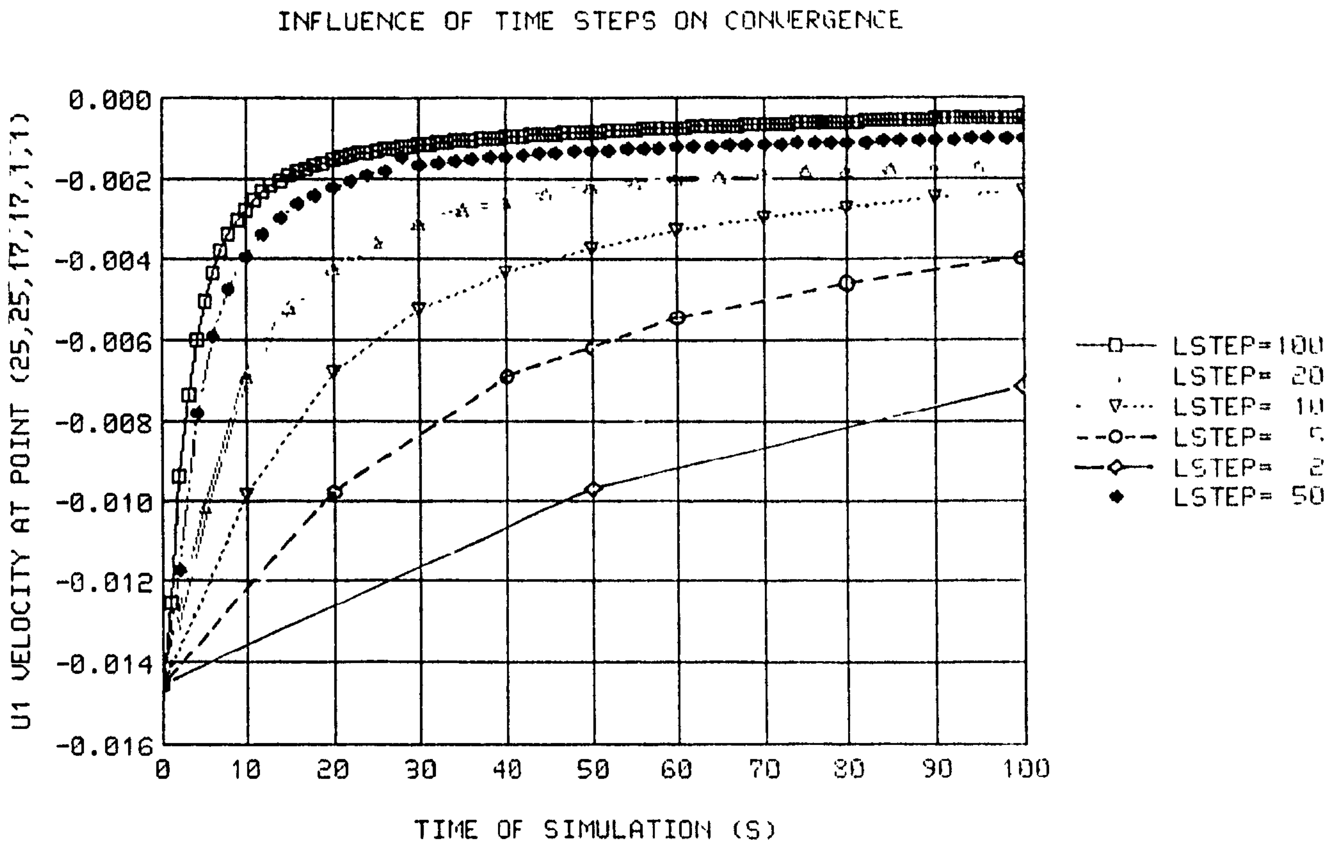

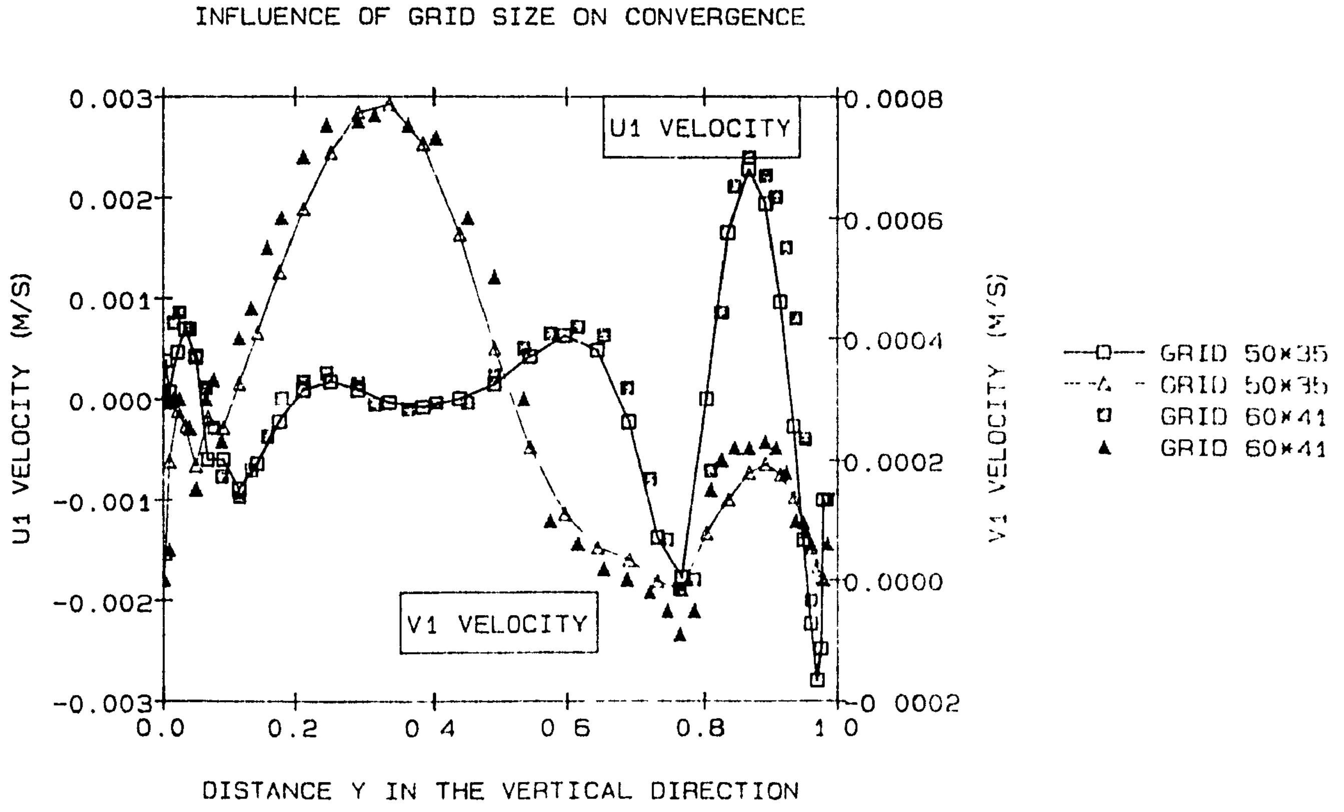

Figures 73-74: Time and space grid independence tests

computing time encountered for a typical simulation of the problem can be counted in terms of days on a VAX system, while the total elapsed time sometimes reached more than a week (because of time-sharing accesses).

3-2-7-2 Space and grid independence

A test similar to that for time step independence was undertaken to ensure that the results reported in this thesis are independent of the space mesh. For this purpose, several sets of grids were chosen to compute the field variables. It has been seen in Fig. 74 that the finest grid 60 x 40 yielded results that were not significantly different from the 50 x 35 grid system. While a 60 x 40 or even finer grid should have provided better resolution of the inclined walls, treated by the blockage and porosity approach, it was nevertheless decided, for computational economy, to run all simulations with the 50 x 35 non uniform mesh defined earlier.

3-2-8 Comparison with exact or other solutions

This type of comparison could not be achieved for such a problem. The problem tackled in this thesis is a non linear, second order fully elliptic problem and does not admit to any known analytical solution . Because of the unique geometrical shape, no direct comparison could be made with other related works found in the literature. As mentioned in the literature review, these are very few works which have tackled turbulent natural convection at high Rayleigh numbers as reported here.

3-2-9 Comparison with experiment

This type of comparison has been carried out at the ALCAN research centre situated in Jonquiere, Quebec. The results will be discussed in the next chapter.

3-2-10 Difficulties encountered and means of overcoming them

Two main difficulties were encountered while solving the problem of turbulent natural convection in cavities filled with molten aluminum.

First, the irregular geometry of the holding furnace made it very difficult to treat the inclined walls very accurately. Although the treatment of the sloping walls by the blockage and porosity approach did not provide a very good resolution of the momentum and thermal boundary layers It, nevertheless, gives a reasonably good approximation of the flow field generated due to buoyancy in the furnace. If the exact treatment of irregular geometries is found to be necessary for specific purposes it is recommended that the BFCS (boundary fitted coordinates (25) approach) should be used. Unfortunately, the author had major problems with the BFCS supplied with the PHOENICS package.

The second difficulty encountered to carry out the simulations was the inadequacy of computational resources. The computations achieved were quite time consuming, especially to obtain converged results of high precision. The computer used was a VAX/785, kindly provided by ALCAN, on a time sharing basis. Typically, the computing time required for a simulation represented only 20% of the total elapsed time. A complete run for one case often required more than a week to accomplish.

While this was a limitation, our research groups use of our METFLO code on a CRAY computer seems to be very promising.

Although the CRAY supercomputer facilities were available during the finishing stage of this work, budgetary and software constraints did not allow these computations to be transported to a CRAY environment.

CHAPTER V

Experiments of validation on 750 kg and 6 .25 ton furnaces held at Alcan Research Centre

1. Introduction

The following chapter reports efforts and results achieved at the Alcan Research Center during the summer of 1988 aimed at testing our mathematical model of aluminum behaviour in reverbatory furnaces. The work involved the presence of a cooperative stagiaire from Université de Sherbrooke, Mr JP Gaudreault as well as the help of an experienced technician Mr S Munger from the Alcan labs for three months.

As for the equipment, some existing facilities in the Alcan Arvida Research Center were fortunately available. There were two main furnaces:

-firstly, a 6.25 ton furnace (Figs. 48,75-76) built in the same way as a real industrial furnace; of trapezoïdal geometry, heated from the top by a gas flat-flame burner which keeps the metal far above the metling point; the side inclined walls, made of refractory material, are cooled by heat losses (conductive and radiative effects have been extensively studied in the past and heat fluxes were known for these experiments).

Secondly, a Bickeley-modified type furnace of 750 kg capacity of square section and heated uniformely by an electrical resistance (top cover). As no inclined wall exists in such a furnace and insulation is very good at the walls, this type of equipment is more likely to lead to thermal stratification within a relatively short time. Even if it does not represent the industrial process itself, this furnace was mainly used for preliminary tests of sedimentation of solid particles (kinetics of settling) and for the preparation of the concentration measurement apparatus (LiMCA). In no case was this smaller furnace used for validation of the mathematical model. However the results of settling of inclusions in this furnace revealed to be much more reliable and reproducible than those initially obtained within a 150 kg Bickeley crucible used as a very first step.

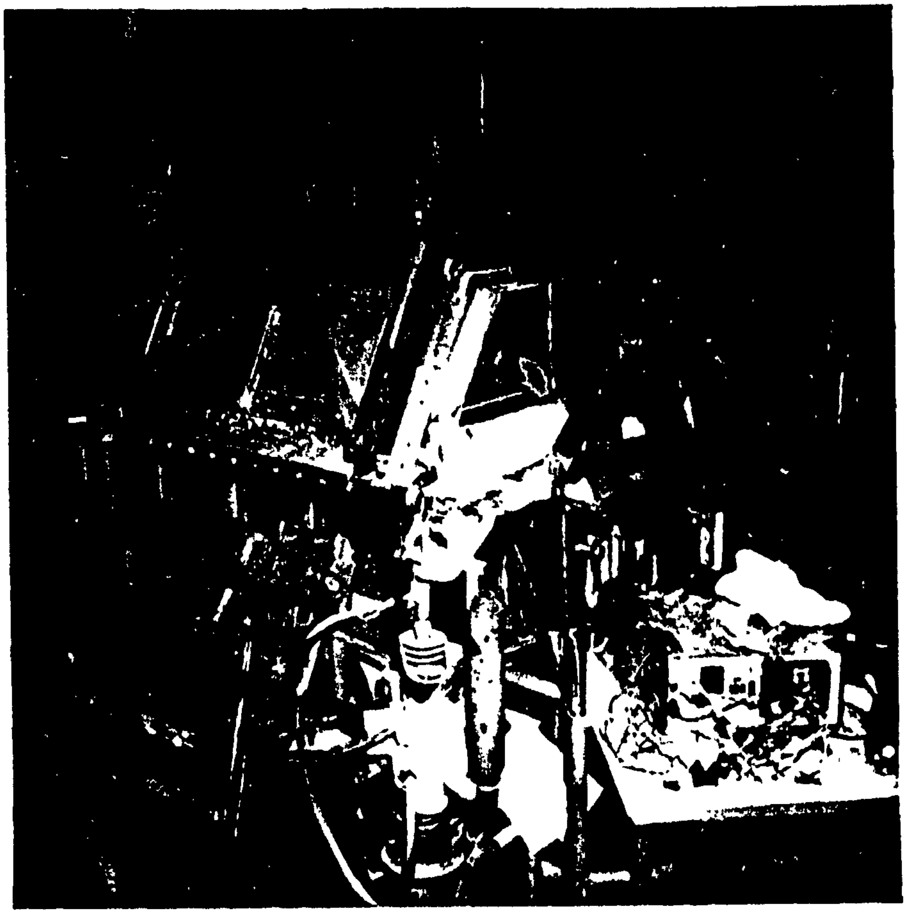

Figure 75: Experimental setup at ALCAN research laboratories.

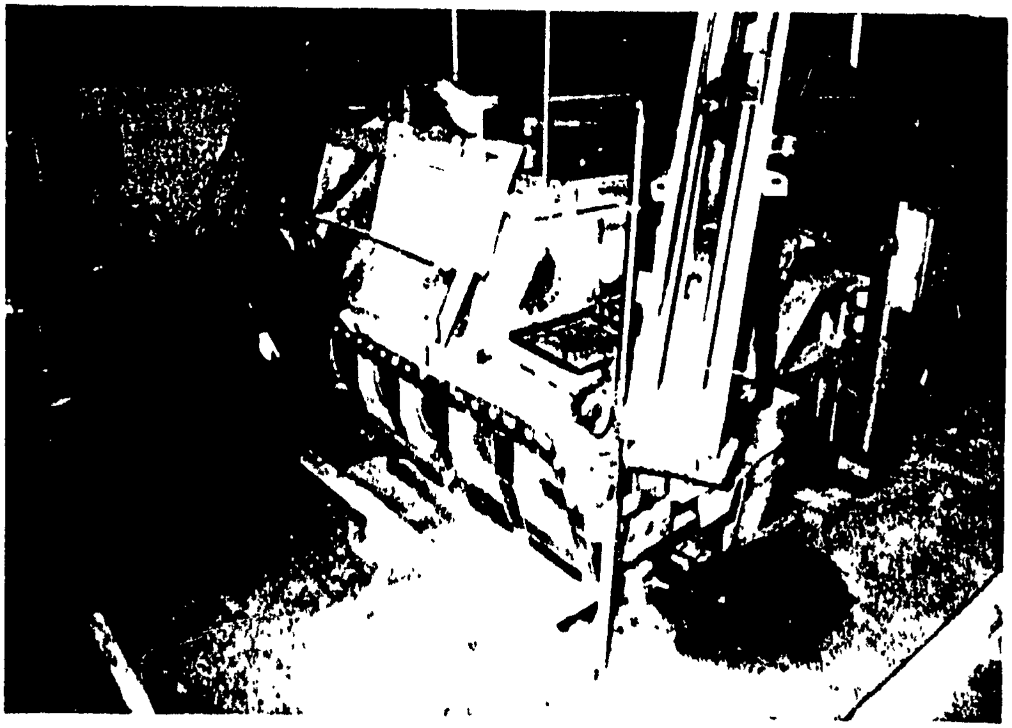

Figure 76: Experimental setup at ALCAN research laboratories.

2. Goals of experiments

The main goal of these experiments was to set up a well controlled situation (a hot, physical, model) as close as possible to the industrial process to enable us:

-to define precisely the boundary conditions of the system, mainly for the enthalpy variable which is the key variable of a natural convection problem. This part corresponds to on line transient measurements of temperatures at various spots on the boundaries of a "slice" of the furnace.

-to predict, once the boundary conditions are known, the transient turbulent natural convection phenomena: mainly the hydrodynamic flow field, the enthalpy field everywhere in the computational domain, as well as the turbulence variables K and E.

-to predict also, owing to the mathematical model, the effects of the convective currents on the behaviour of the particles. That is to compute the convective-diffusive mass transport equation for each type of particle (several densities and equivalent diameters of particles assumed to be of spherical shape).

-to measure, at various points in the core of the aluminum furnace the variables temperature and concentration (via thermocouples and Liquid Metal Cleanliness Apparatus) in order to validate the predictions generated by the model and to verify in the transient mode as well as at steady state, if the predicted variables make sense in terms of order of magnitude and gradients.

-to measure, in parallel, the magnitude of the flow field in molten aluminum: unfortunately, this last step could not be achieved, a new electromagnetic velocity probe supposed to measure both axial and longitudinal velocities in molten aluminium and recently developped at the University of Avignon could not be available to us at that time

-to have, if possible, a good idea of the particle densities dealt with (micrographic analysis for TiB_2 or [Ti-V-B] inclusions).

3. Techniques and apparatus used to achieve these goals

Two distinct quantities had to be measured: temperatures above the melting point of aluminum and concentrations of particles initially suspended in pure molten aluminum.

3-1 Temperatures measured

Standard K-type thermocouple measurements were simultaneously made at 17 points along a given cross sectional plane of the furnace (Fig. 48). Each thermocouple rod was set up from the top of the furnace through the sliding door and positioned correctly by using an horizontal steel support laid 15 cm above the molten metal free surface. This support was cooled by air to prevent it from bending due to the high enthalpy produced by the burner. Each immersed thermocouple rod was insulated and protected from erosion by "MICA WASH" and ceramic layers. For data acquisition of temperatures, a data-logger (Fluke 2280A) was connected to pick up measurements every minute (Fig. 76).

3-2 Concentration measurements

Suspended particles in pure commercial aluminum (99.7 %) could be quantified at 2 or 3 locations in the furnace owing to a relatively new method for assessing the metal cleanliness: the LiMCA (Liquid Metal Cleanliness Analyzer) was first developped at McGill University in 1980, in cooperation with ALCAN INTERNATIONAL (30,1); this system is able to provide online, both the concentration and the size distribution of inclusions larger than 20 µm equivalent diameter. The probe is based on the resistive pulse or ESZ principle (Electric Sensing Zone): when a small non conductive particle crosses an electrically insulated orifice situated at the base of the probe, the electrical resistance of the molten metal flowing through this orifice increases in proportion to the particle's volume, (Fig. 77). The corresponding change in resistance ΔR due to this non conductive particle was found by De Blois (1977) to be:

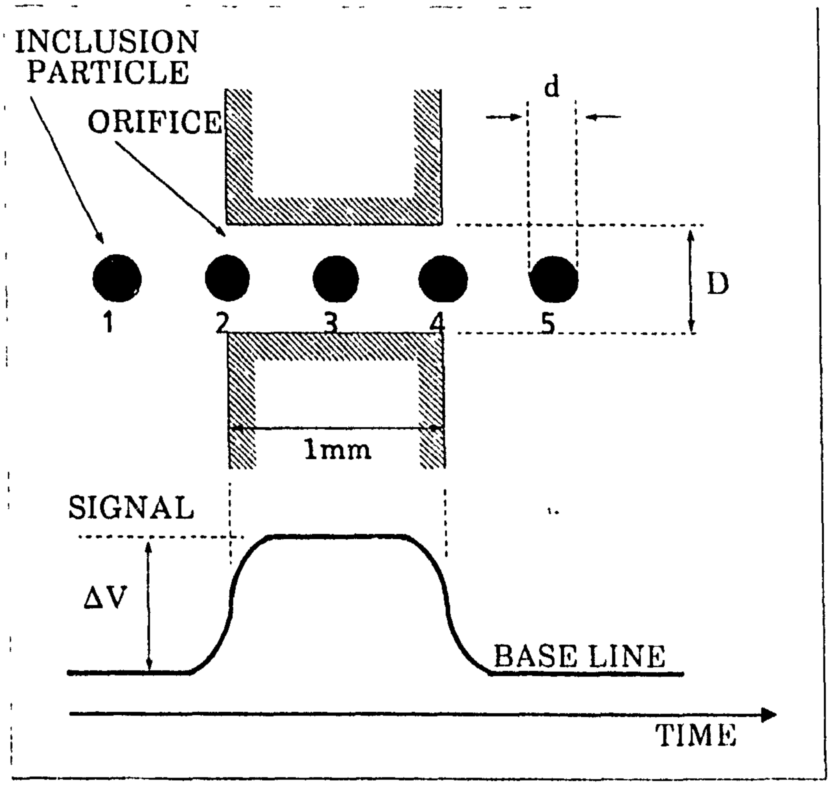

Figure 77 Principle of particle detection by the Electric Sensing Zone technique: the signal produced consists of a steady voltage baseline with a bell shape transient.

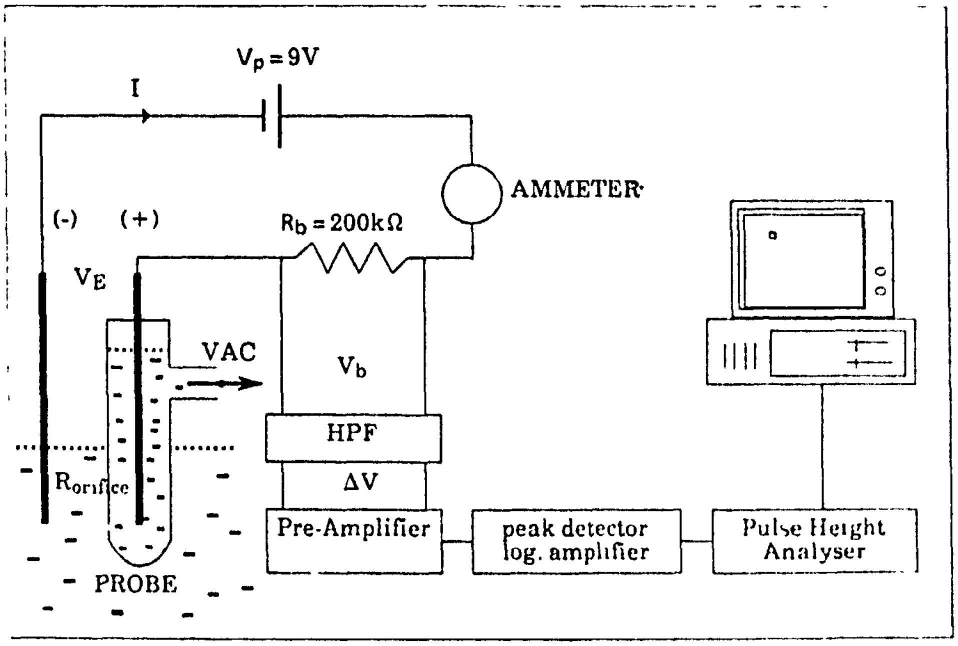

Figure 78 Schematic diagram of the ESZ system.

$$\Delta R = \frac{4\rho d^3}{\pi D^4} F\left(\frac{d}{D}\right) \quad with \quad F\left(\frac{d}{D}\right) = \left|1 - 0.8\left(\frac{d}{D}\right)^3\right|^{-1} \tag{122}$$

where: ρ is the electrical resistivity of aluminum
($\rho = 2.5 \times 10^{-7}$ Ω•M at 700•C)

d is the particle diameter
(generally between 20 and 100 µm for the range of practical interest)

D is the orifice diameter
(300 µm for example)

F is a function of d/D; De Blois proposed: $F(d/d) = [1-0.8(d/D)^3]^{-1}$
but F is often taken to be unity in practice

Voltage pulses due to the presence of an electric current allow one to measure the number of particles and their sizes, by reference to a base line (when no particle crosses the orifice).

In any case, and in absence of blockage of the orifice (for which d/D = 1),by undesired particles, the maximum error of the method is in the order of 5%. Further treatment of the electric voltage is done via signal processing analysis equipment. As seen in Fig. 78, the signal is filtered through a high-pass filter, then preamplified, before going through a log-amplifier able to detect accurately very small particles. Then a peak detector recognizes pulses which are thus counted and sorted by categories to provide the particle size distribution. Data acquisition disc and hard copy of the final results are achieved by the terminal micro-computer.

Alcan Int. has built several generations of prototype LiMCA models and is using them extensively in casting centers to check the metal cleanliness prior to casting, as well as in the laboratory environment. The latest model of LiMCA is fully integrated and packaged in an easy carriable and "ready to use" unit

4. Experimental procedure

The experimental procedure involved the following steps:

4.1 Installation of thermocouples which had to stay permanently in the furnace during all experiments (6.25 ton furnace only). An air cooling system for the suspension bars was then switched on.

4.2 The furnace was filled with pure commercial aluminum (99.7%) at 750°C coming directly from the potline division.

4.3 The Data acquisition device was turned on to record every ten minutes temperatures at 17 points.

4.4 A preheated impeller fixed to a rotor was then set down into the furnace through the side well. A chlorine-argon mixture (10% Cl_2) was fluxed through the axis of the impeller to free the metal from any solid particles (aluminum oxydes for example). Dross was removed and the metal is then considered as clean.

4.5 The LiMCA, (Liquid Metal Cleanliness Analyzer) was set to read at a given depth within the furnace (from 15 cm to 75 cm). The melt was sampled every minute, yielding a 5 ml quantities of molten metal provided no problem was encountered. The particle concentration was then immediately recorded, as well as its size distribution for further analysis. In the absence of particle additions, it was found that the recorded concentration was very low and stable at around 5000 particles per kg of aluminum. After extremely long settling time, such counts could even decrease below 1000 part/kg

4.6 Known particles were then introduced into the furnace and well mixed until a maximum of the measured concentration is reached. Two types of particles were used during our experiments: (TiB_2) and $(Ti\text{-}V)B_2$

●(TiB_2) is generally formed by a chemical reaction from KBF_4 and Ti.

Used as a grain refiner in the fabrication of aluminum alloys, (Ti B_2) is available as rod shape refiner Al - 5% Ti 1% B. Once mixed with aluminum, the elementary size of Ti B_2 is generally of 2 to 3 µm order but aglomerates can be made in the range [10 - 100µm].

- [Ti-V]B_2 is chemically a chrystal wetted by aluminum and consists of elementary cells between 20 and 30 microns of diameter. A "master alloy" containing 4% boron was used. This compound reacted with minor amount of dissolved Ti and V already contained in the furnace, to produce [Ti-V]B_2.

An example of the two distinct particles used is given at Figure 79. Assuming an average diameter of particles of 25 microns, a concentration of the order of one ppm will provide a LiMCA measured concentration of typically 50 to 100 thousand particles per kg of aluminum.

5. Results and discussion

A resume of the most significant experiments is given at Table 15. For each experiment, the settling curves showed a quasi exponential decay for the concentration measured by the probe. The following correlation can be made for each size of particle:

$$Nd_i = Nd_i^0 \; exp\left(- \frac{t - t^0}{\tau} \right) \tag{123}$$

- Nd_i is the concentration of inclusions per kg of aluminium
- Nd_i^0 is the concentration at t = to
- t_0 is the initial time of settling; generally the measured concentration is maximum at this time.
- τ is the characteristic time of the process.

The two important parameters Nd_{i0} (also noted A) and τ are statistically estimated from data for each size of particle at each experiment. A compilation of values, standard deviations and limits of confidence interval of these parameters is reported at appendix (C). The average value of Nd_i is also

** RAPPORT D'ANALYSE **

NO. DE LA DEMANDE CRDA : 82509

DOSAGE	ID ECHANTILLON	NO REFERENCE	NOM COMPOSE	RESULTAT	UNITES

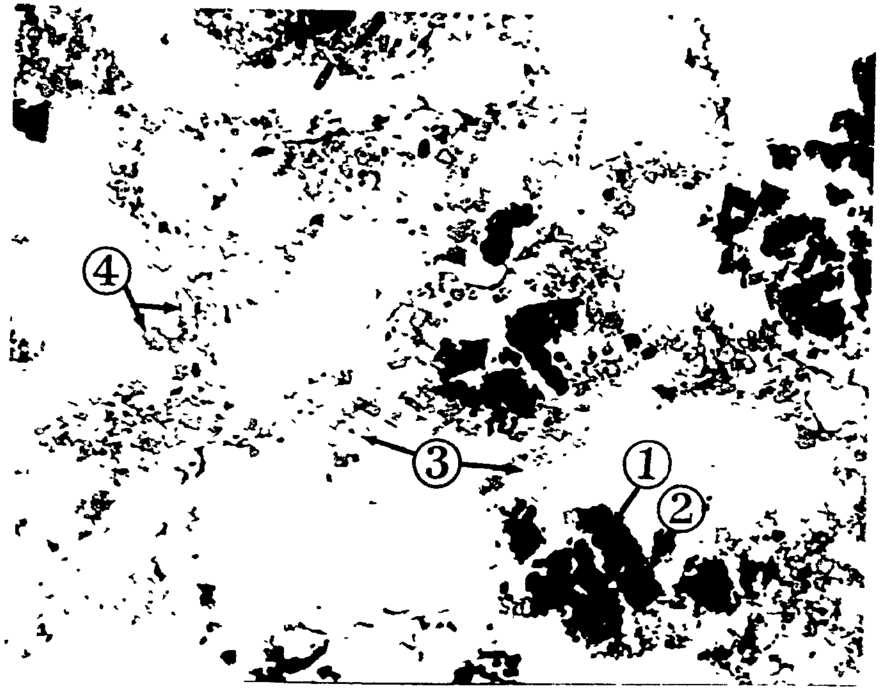

2785 Figure I 500X
NO RAPPORT: 82447 20-05-1
#1: SiC
#2: Al4C3
#3: TiB2
#4: TiV6

Figure 79: Sorts of particles encountered in molten aluminium.

EXP NUMBER	FURNACE TYPE	DEPTH LIMCA PROBE	PARTICLE TYPE	τ_{min} [20-300]	σ_{min} [20-300]	$N_{20}(t=0)$ (Kpart./kg)	σ (N_{20})	N_{20}(av.) (Kpart./kg)	TEMP MEASURED ?	TMAX PLANE (1) °C	TMAX PLANE (2) °C	ΔTMAX PLANE (3) °C
G2006	CRUCIBLE 140 Kg	40 cm	TiB2 (rod)	11.4	0.87	39.8	2.4	6.75 (8.3)	N	740		
G2106	CRUCIBLE 140 Kg	40 cm	Tib2 (rod)	15.4	1.44	9.20	0.64	2.31 (2.3)	N	740		
G2306	CRUCIBLE 140 Kg	40 cm	Ti-V-B (master)	68.0	22.5	33.8	2.04	27.3 (4.7)	N	740		
G2906	BICKELEY 750 Kg	50 cm	Ti-V-B	20.3	4.75	94.2	12.2	19.0	N	740		
G1208	6.25 TON	75 cm	Ti-V-B	52.7	3.81	43.8	1.72	16.5	Y	760	740	30
G1508	6.25 TON	15 cm	Ti-V-B	50.0	1.56	47.6	0.79	19.6	Y	760	740	30
G1608	6.25 TON	45 cm	Ti-V-B	52.6	6.46	61.2	3.76	26.7	Y	744	729	17

Table 15: Summary of the most significant experiments carried out at ALCAN Research Centre

of importance when settling is studied, since it gives a broad measure of the metal cleanliness. This variable was computed as:

$$N[20-300] = \frac{1}{t^{\infty}-t^{0}} \int_{t^{0}}^{t^{\infty}} N^{0}[20-300]\, exp\left(-\frac{t-t^{0}}{\tau}\right) dt \qquad (124)$$

5-1 Experiments on Ti B_2

Two experiments on (Ti B_2) rod grain refiner were carried out in a crucible containing only 140 kg of aluminium. The settling curves are given in graphs [G2006B, G2006B2, G2006B3] and [G2106B, G2106B2, G2106B3] for each experiment (Fig. 80). The average metal cleanliness indices, N_{20}, were low in both cases (6800 and 2300 particles per kg). The characteristic times τ for the total number of particles above 20 µm are typically in the range [10-15] minutes.

Particles greater than 40 µm in diameter show an even sharper decay in concentration, with time constants of only 5 minutes.

Agglomerates of (TiB_2) therefore represent very "heavy" particles which settle rapidly (5 to 15 minutes) in an insulated crucible and give little chance to elaborate on the impact of natural convection on metal quality.

This is one of the main reasons why all the following experiments were carried out using (Ti-V-B). However, experiments with (Ti B_2) were helpful to get familiarise personnel with LiMCA instruments and for equipment calibration . Experimental details are given in section 4 of this chapter

5-2 Experiments on (Ti-V-B)

Test G2306 (Fig. 81) was run on the same 140kg capacity crucible with (Ti-V-B) introduced as a master alloy 4% boron. Typical time constant for this type of inclusion generated in the bulk of the metal was found to be $\tau = 68$min ($\sigma = 22$) for all sizes of particles (20-300 microns); it was only 30min for particles in the range (40-45 microns) and 6min for particles above 50 microns The level of cleanliness after the addition of (Ti-V-B) was around 40 K particles/kg. The same procedure as in 5-1 was followed.

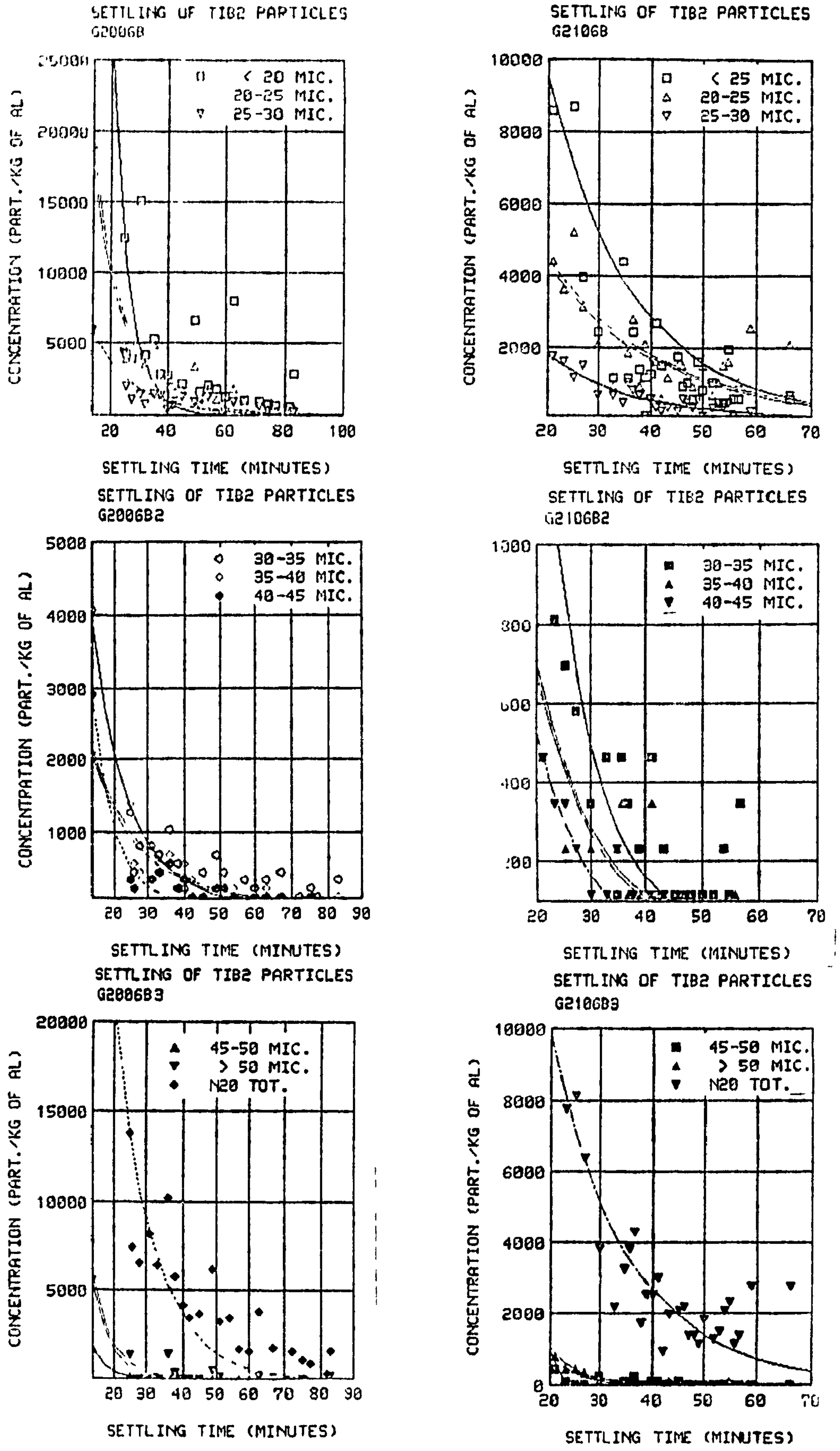

Figure 80 : Online measured concentrations with LIMCA into 750 kg furnace.

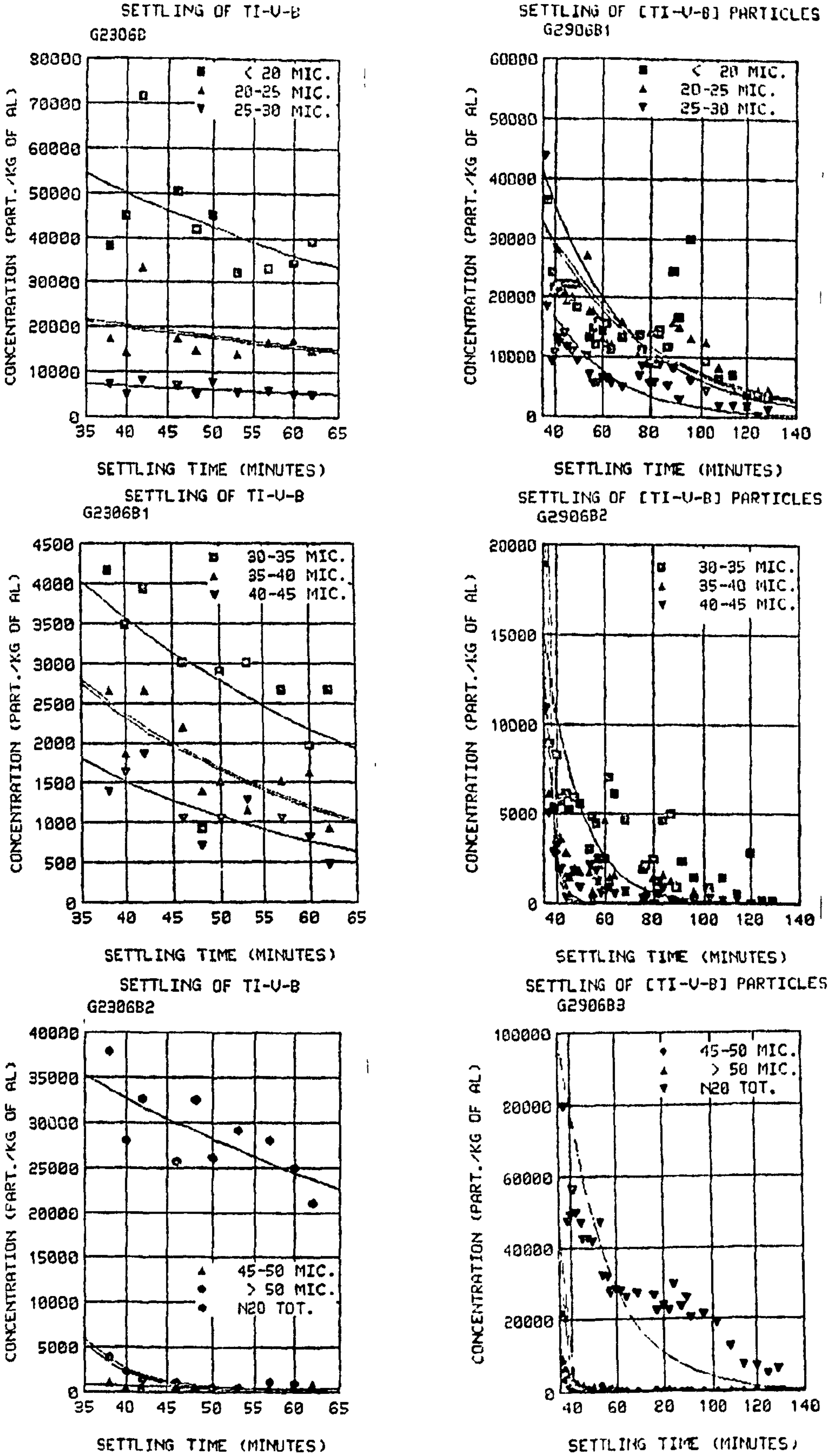

Figure 81 : Online measured concentrations with LIMCA into 750 kg furnace.

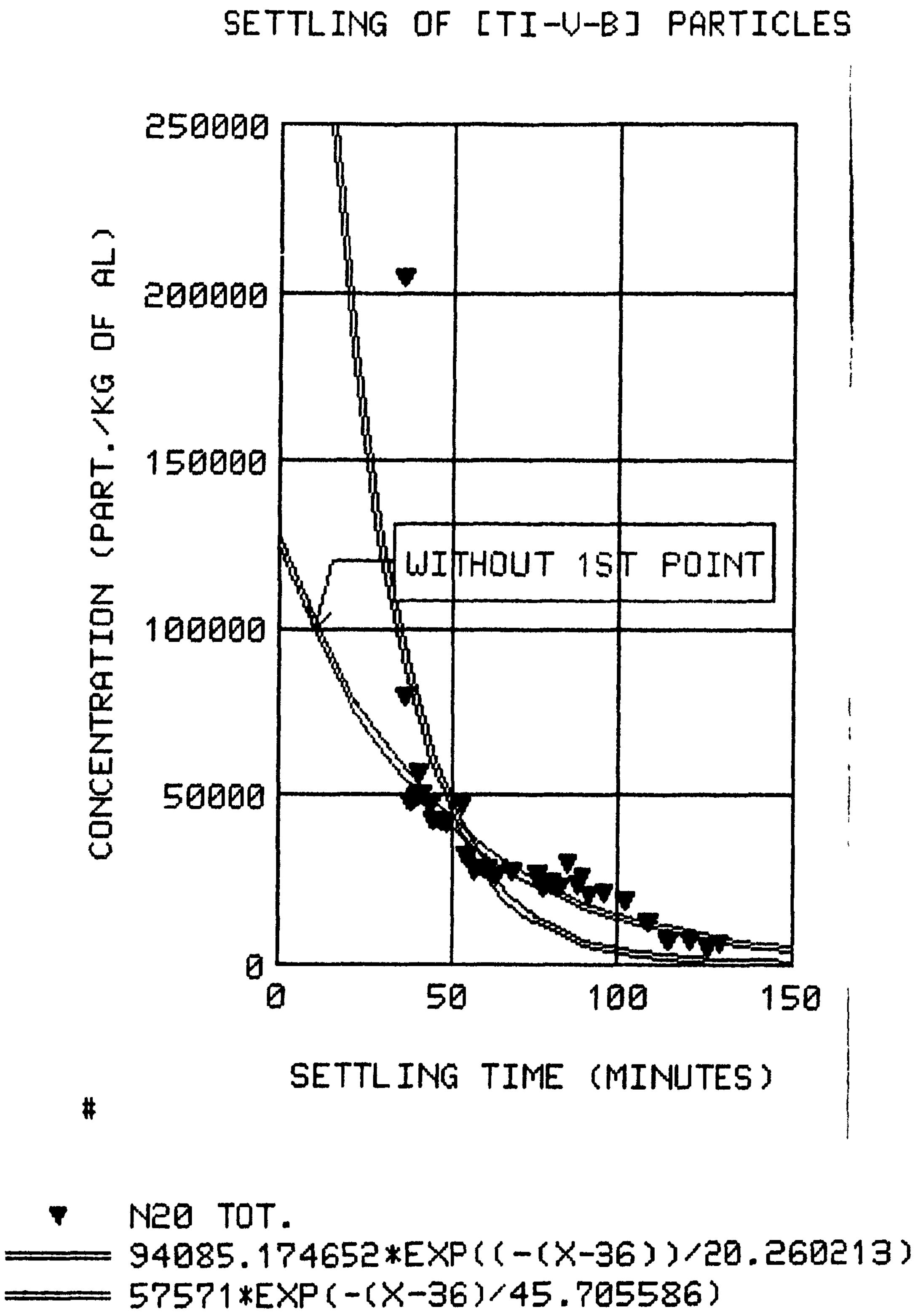

Figure 82: Two steps kinetic in settling of Ti-V-B Particles

A similar test, G2906 (Fig. 81) was achieved on a bigger furnace (modified Bickeley of 750 kg capacity) of square base with very thick insulated vertical side walls. Once melted, the metal was heated from the top so that a steady thermal stratification prevails at the beginning of the experiment After metal cleaning by an Ar/Cl_2 mixture, the introduction of inclusions lead to an extremely high value of concentration (205 K particles / kg) going down to 80 000 a minute later and around 45 000 the following minute These observations correspond to a characteristic settling time of only 20 minutes ($\sigma = 4.8$) only. Insofar as one considers the inital peak concentration of 200 K particles/kg as being valid, it seems that not only one, but two, distinct phenomena of sedimentation occur within the melt with two quite different kinetics: an extremely fast decay followed by a more often encountered sedimentation process with a time constant typically around 45 minutes This is well illustrated in Fig. 82. If we consider all the points of the curve versus time, data fitting gives the above mentioned settling time of 20.2 minutes but the exponential correlation is not as good as the one obtained when the first point (200K part./kg) is not taken into account: in this last case, all the points show perfectly an exponential behaviour (45 minutes of settling time)

As for particles bigger than 20 microns, the characteristic time as a function of the equivalent diameter decreases to values as low as 1 to 5 minutes (for d>50 microns). See Fig. 81 and appendix C.

Experiments made on the 6.25 ton lab furnace

These experiments on a semi-industrial furnace with (Ti-V B) particles provided the most interesting results. The LiMCA measurements of concentration at various locations within the furnace melt were actually coupled with temperature measurements at many points on a cross sectionnal plane of the furnace.

Retaining only the more characteristic behaviour of the furnace, experimental results are now presented for three separate well controlled experiments: G1208, G1508 and G1608. Because of the availability of one LiMCA probe at a time only, these experiments were sequentially run in the same week. Nomenclature of experiments refers to the date each experiment was run. Statistical data recorded during settling is summed up in Table 15. The first two ones reflect measurements of concentration (Figs. 83-84) at two different levels of the furnace, respectively 75 and 15 centimeters below the free surface of the metal. Their average cleanliness levels were similar being in the range [15-20 K part./kg]. Moreover, the levels of concentration at $t = 0$ were also similar (43.8 ± 1.74 and 47.6 ± 0.79 K particles./kg). Surprisingly, the characteristic inclusion settling time at these two levels was found to be very similar: 52.7 min (± 3.8) for G1208 and 50 min (± 1.6) for G1508.

As for experiment G1608, the settling process seems to be of the same magnitude since a characteristic time of 52.6 min (± 6.5) is computed from the data (Fig. 85). In the meantime, the average cleanliness level shows that 50% more inclusions were contained in G1608 than before.

A similar sedimentation pattern of particles above 20 micron at three different levels of the furnace suggests that the overall state of the fluid in the furnace is that of a well mixed reactor at least in the core of the molten metal.

If we make the same comparison for the characteristic settling times (Appendix C) according to the size of the particles involved, Fig. 85 shows that a similar conclusion can be drawn for all classes of particles above 20 microns.

Settling curves measured at three distinct locations of a holding furnace show identical patterns with reliable statistical data in all ranges of particle sizes. This finding indicates that the settling process was not that of a simple sedimentation front of plug flow type as that presented in Chapter 1; moreover, some mixing may and has to occur. This conclusion was first reached by Doutre (31) following an independent campaign of experiments carried out at ALCAN Saguenay works on a study of the kinetics of inclusion settling in a 750 kg furnace.

It is now appropriate to directly compare this experimental data against equivalent results predicted by the mathematical modelling analysis.

5-3 Experimental validation for the mathematical model

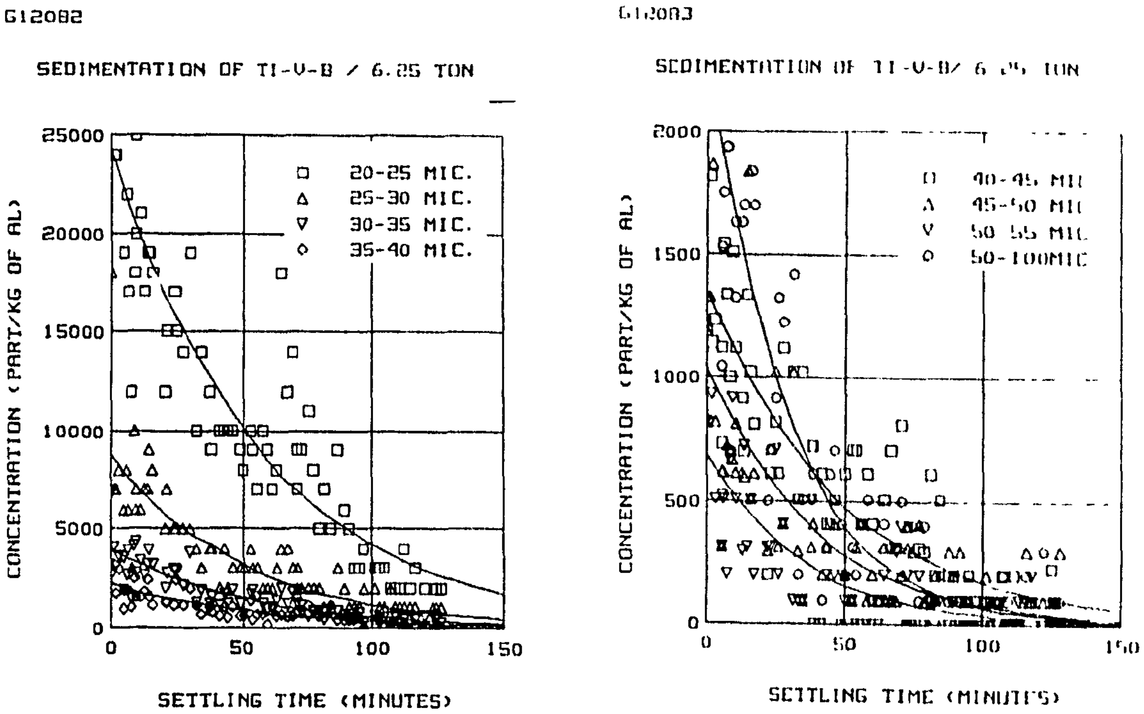

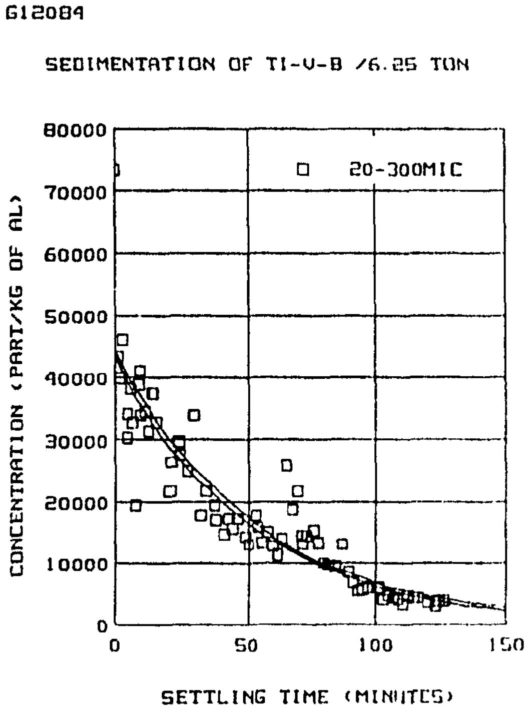

Figure 83: Experiment G1208: Online inclusion concentrations measured with Limca in 6.25 ton furnace.

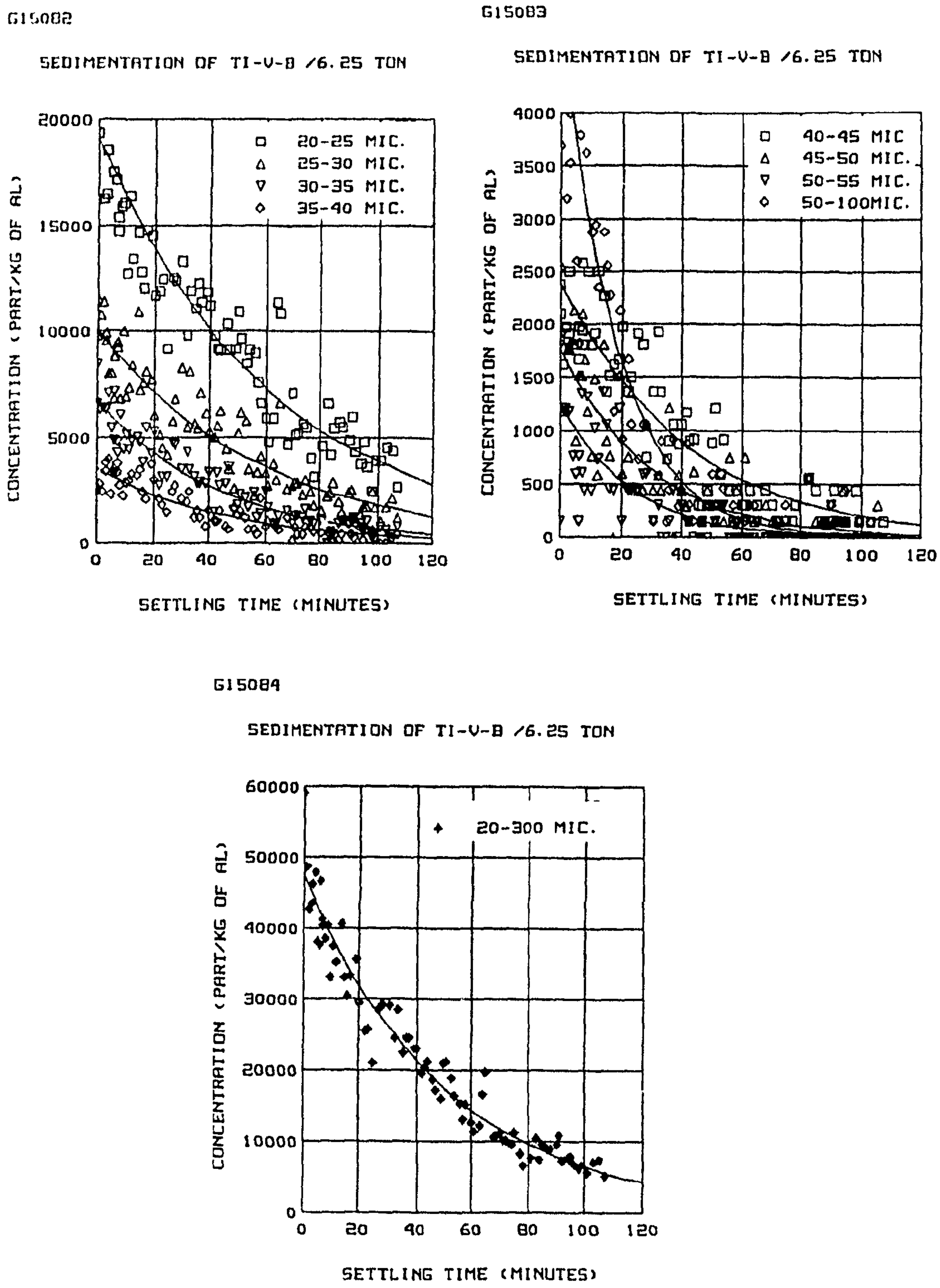

Figure 84: Experiment G1508: Online inclusion concentrations measured with Limca in 6.25 ton furnace.

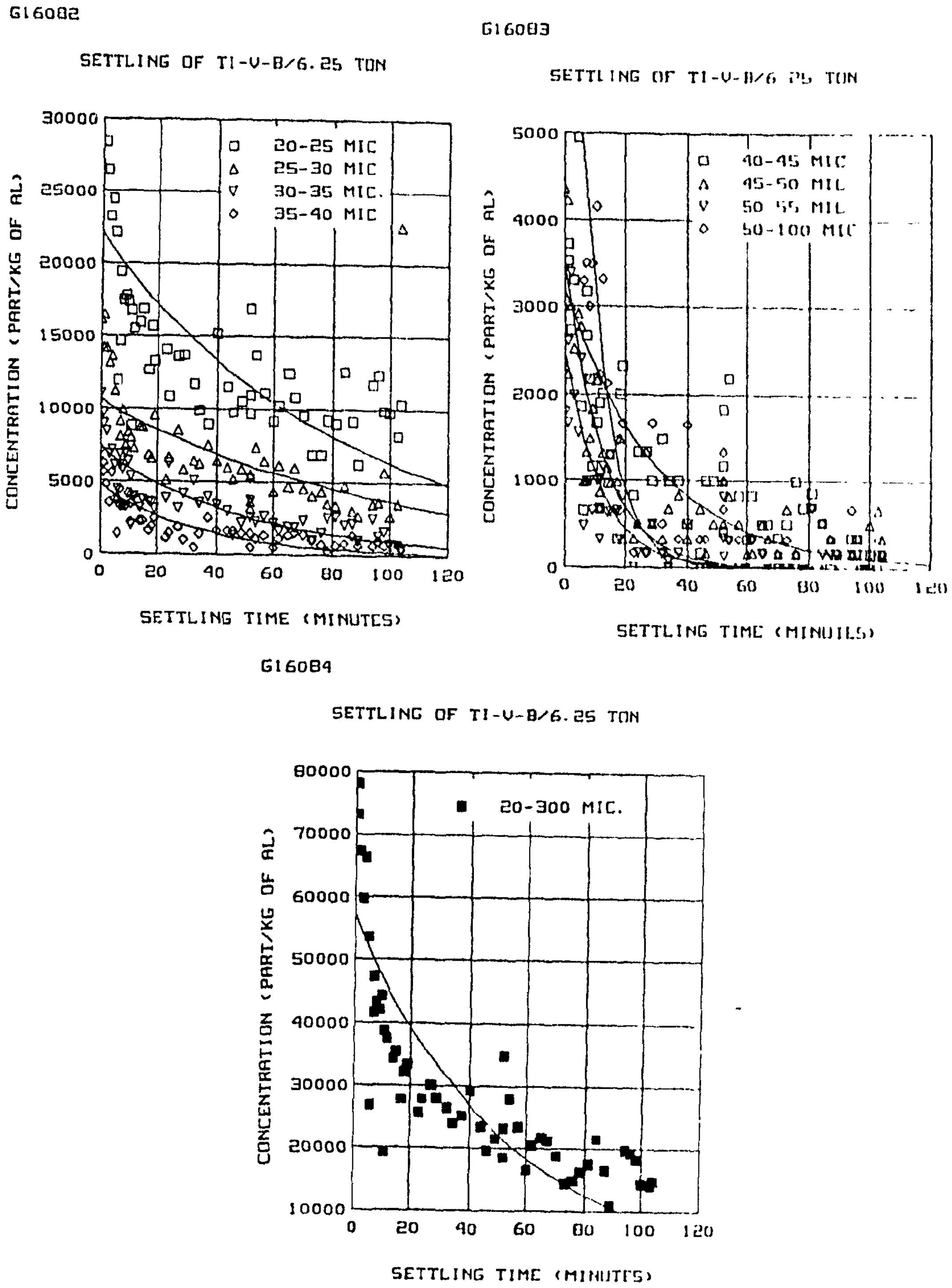

Figure 85: **Experiment G1608: Online inclusion concentrations measured with Limca in 6.25 ton furnace.**

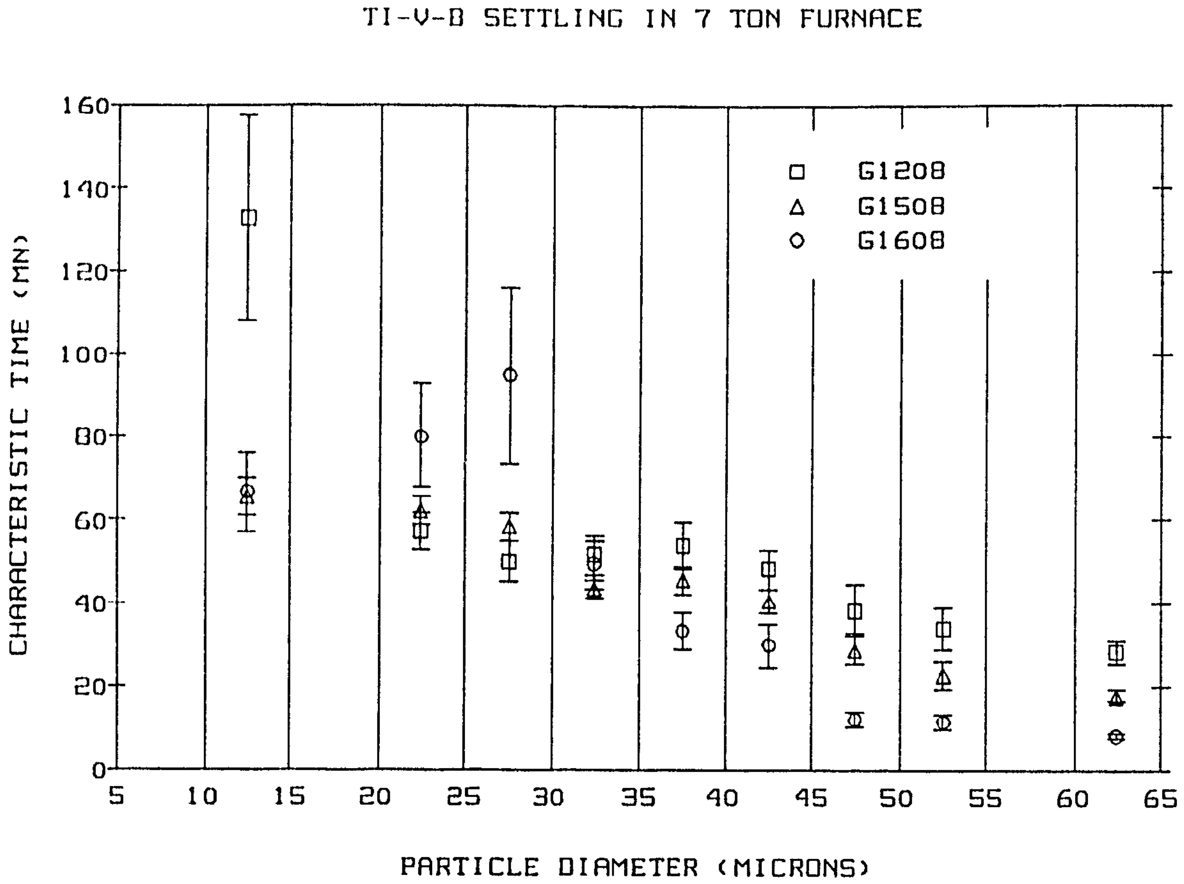

Figure 86: Comparison of settling kinetics of the three experiments: G1208, G1508 and G1608.

In order to compare the experimental results just presented against the mathematical analysis provided at Chapter 3, local concentration-time curves at the three different levels mentioned previously:

- upper section of the furnace A1 = (19,19,26,26,1,1)
- medium section of the furnace B1 = (19,19,19,19,1,1)
- lower section of the furnace AB1 = (19,19,12,12,1,1)

These curves were previously presented in Figures 72 (for computations) and 84-85 (for the LiMCA measurements). Those of them corresponding to inclusions of average diameters around 25 microns were normalized so that concentrations remain in the range [0;1] and the abscissae were also transformed by a scaling factor. Comparison between computations and experimental data up to more than 6000 seconds of simulation is thus much easier as seen from Figures 87-89. Some exponential fitted curves are also provided for the computational results so as to give a quantitative idea of the kinetics of the process.

Comparison between experiment and model (Figs. 87-89) is seen to be very good for two of the three determinant experiments (also see G1208 and G1508 of Table 15). These two settling curves were obtained under well controlled conditions and reflected similar levels of cleanliness in the operating furnace: initially around 45 000 particles per kg of metal, the average cleanliness levels, following settling, showed averages around 17 000 particles per kg with low standard deviations (less than 4%).

In the case of the last experiment G1608 (Fig. 89), the concentration decay versus time seem to be much faster in a first step (150 s) with a smaller rate thereafter. As shown on Figure 89, the process involved here is not a unique exponential process as it was the case of experiments G1208 and G1508 Moreover, this last experiment was achieved under somewhat different conditions than G1208 and G1508:

- first, the initial cleanliness level was monitored to be 61 200 particles per kg (variance of 3760) while the average level measured over the settling curve was 27 000 particles/kg. This constitutes a melt much dirtier than before, by a factor of 50% (Table 15)

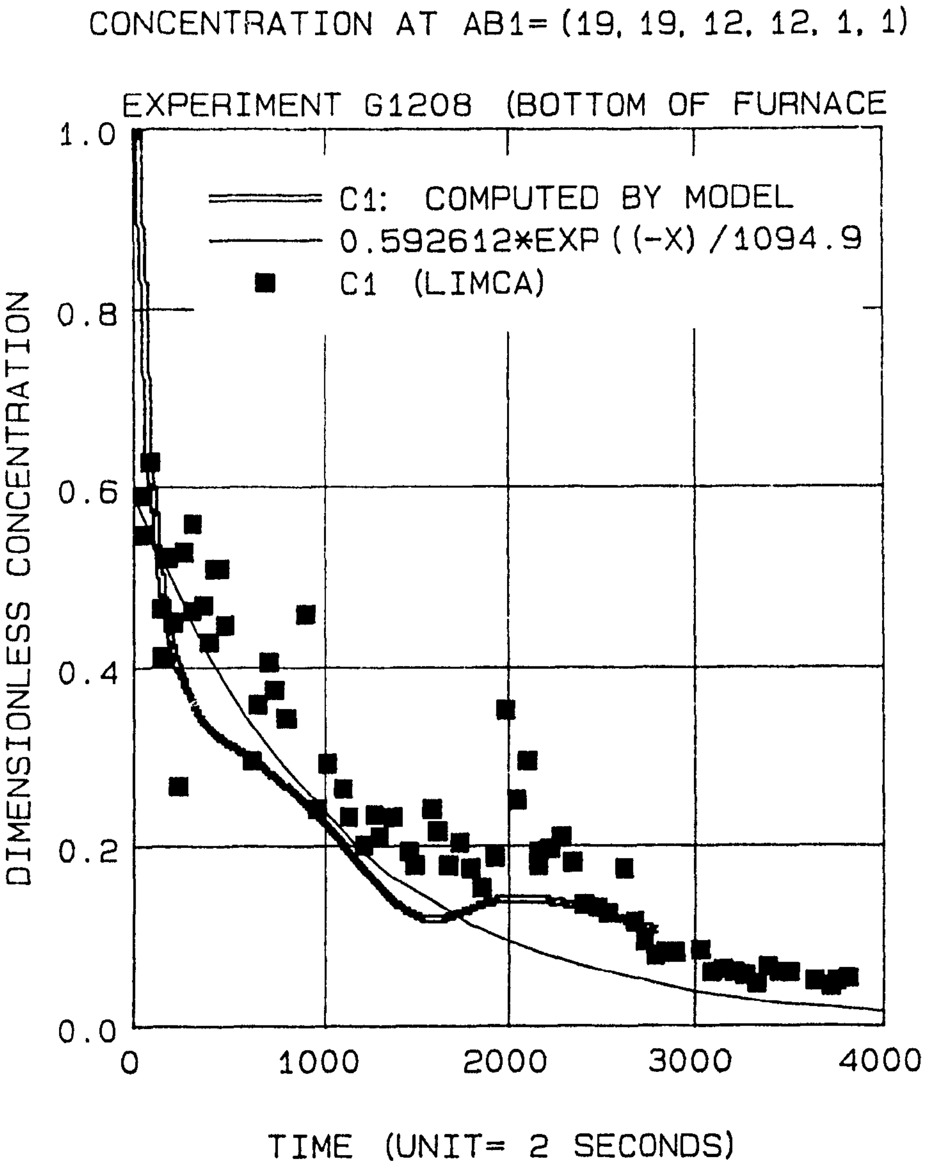

Figure 87: Comparison between experiments and numerical simulations (Bottom of furnace- Exp. G1208)

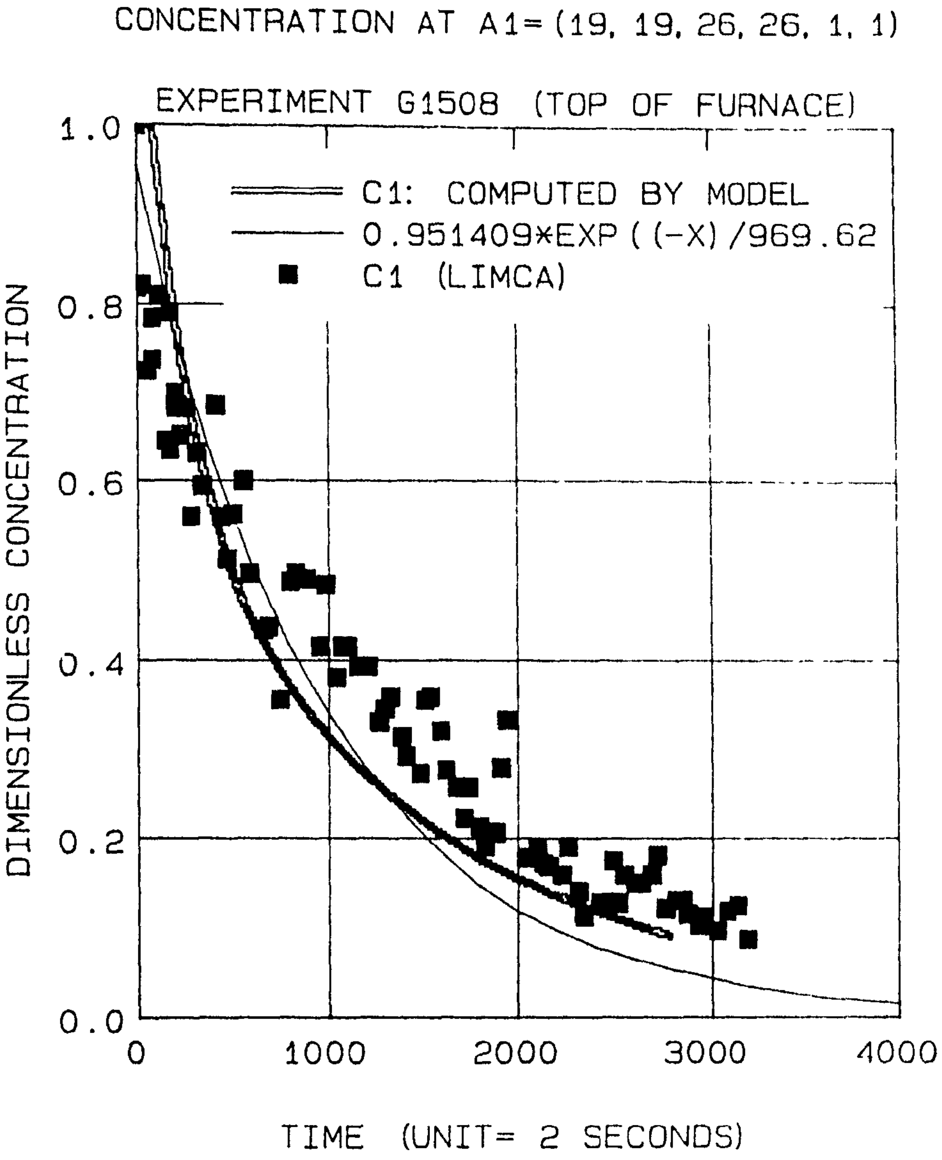

Figure 88: Comparison between experiments and numerical simulations (Top of furnace- Exp. G1508)

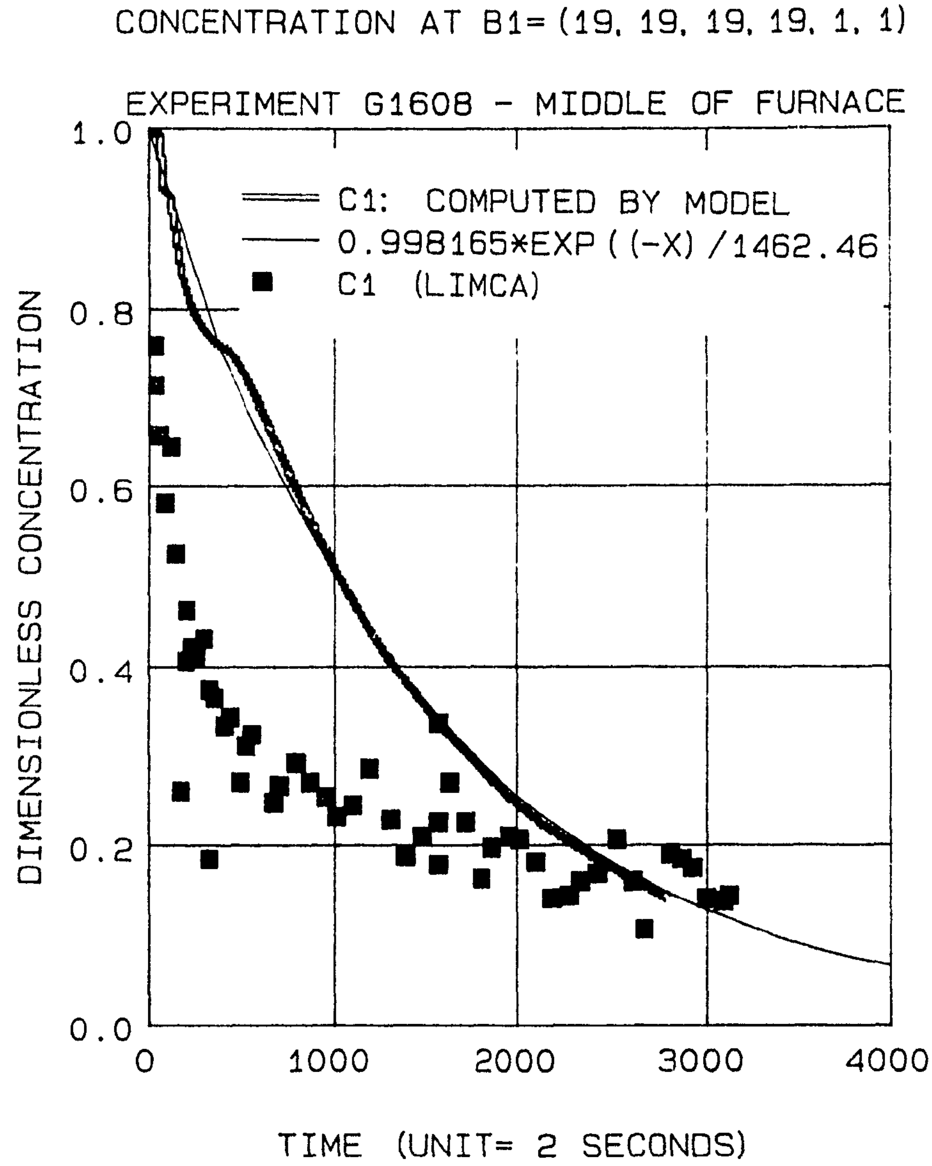

Figure 89: Comparison between experiments and numerical simulations (Middle of furnace- Exp. G1608)

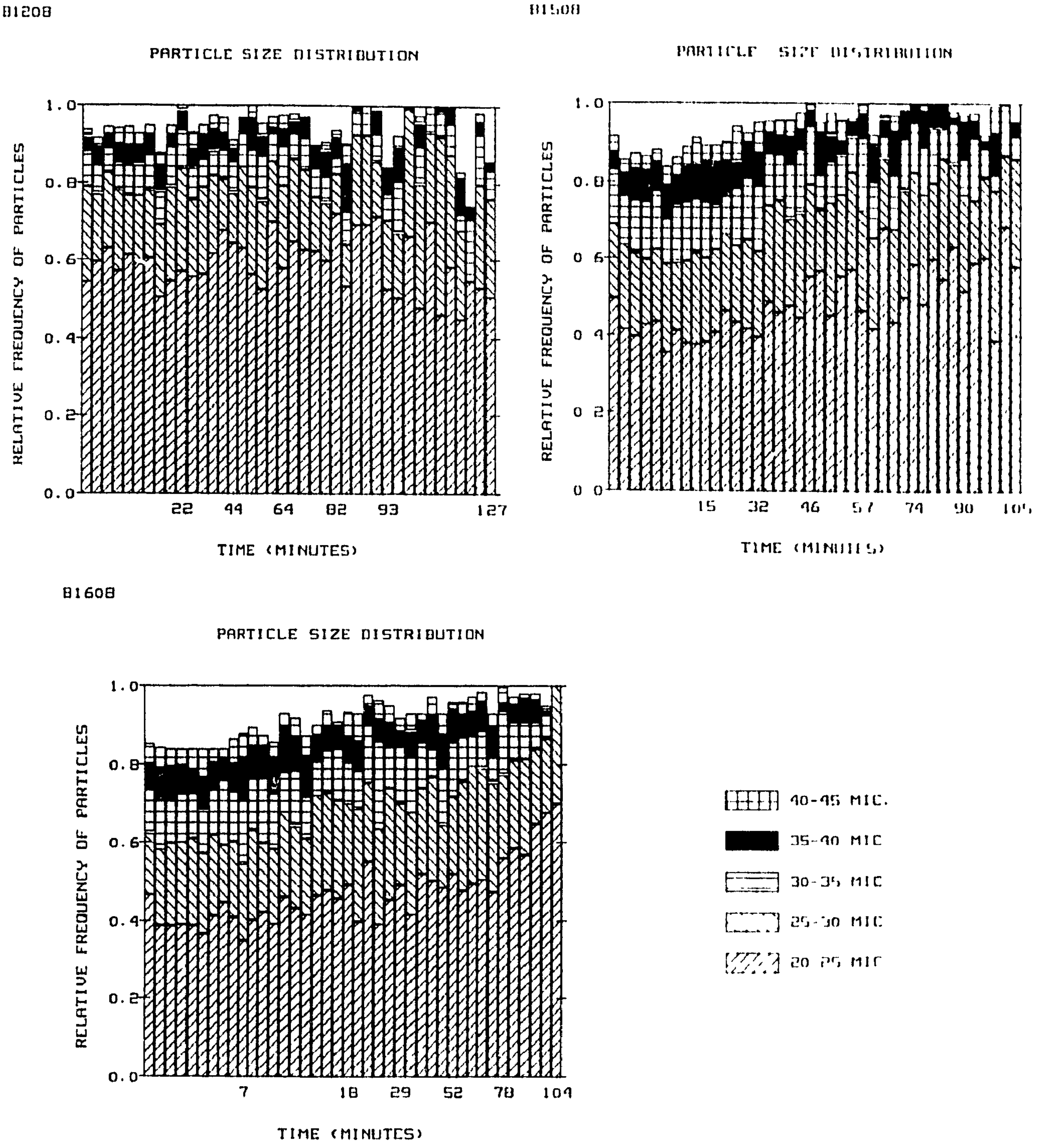

Figure 90: Comparison of transient evolution of particle distribution between the three experiments: G1208, G1508 and G1608.

- second, let us note that because of some problems with the temperature controller, a gradient of only 17°C was set up instead of the 30°C vertical gradient used during the computations and measured during experiments G1208 and G1508

- third, a higher proportion of large particles (above 40 microns of diameter) was monitored by the LiMCA probe during G1608: 12% versus 8.4% and 10% during experiments G1208 and G1508. Figure 90 illustrates the relative particle size distribution in each case for six ranges of diameter.

Among these three findings, the last two suggest that a weaker flow motion due to smaller vertical thermal gradients and a particle size distribution weighted by larger particles should give a stronger component of the Stokes velocity. Actually, this relatively stronger component may well be the cause of the steep decrease in the measured particle concentration in experiment G1608. The second part of this curve could then be regarded as the settling curve once the largest particles have settled out after around 5 to 10 minutes.

Industrial significance of the experiments

In the present set of experiments, some interesting features and similarities with full scale industrial furnaces were kept with the 6.25 ton laboratory furnace: depth of the bath (around 1 meter), temperature gradients (order of magnitude: 30 K) and order of metal cleanliness or inclusion concentrations (range of 5-100 K particles per kg of aluminum) were all physically modelled to be very close to equivalent full scale counterparts; moreover, the quantity of molten aluminum considered was sufficiently large to observe and compute:

Unsteady turbulent natural convective currents, until now not appreciated by other researchers (35) ;

Concentration decays relatively similar in range to those observed in the troughs at the exit of tilting or stationary furnaces encountered at the industrial scale.

The main findings of these studies are:

1) Due to the high thermal conductivity of aluminum ,thermal stratification of the melt takes up to two hours to stabilize.

2) In spite of the vertical thermal stratification patterns observed, there exists major convective currents in places where "additional " heat losses are encountered : this was the case at the top left side of the furnace, close to the sliding doors left partially open during experiments due to the presence of the support of thermocouples.

3) Convective currents are significant with velocities in the order of 1 to 10 centimeters per second. A similar order of magnitude was found by other investigators in a totally indepent study sponsored by Pechiney, France (35), even though their work addresses this problem only for the steady state regime. These authors used a finite element commercial code in two dimensions, adopting a Lagrangian formulation for particle tracking but were not able to publish validating results through measurements within the melt. Convective currents are now recognized to play a major role in assessing molten metal quality in the Aluminum Industry.

4) Owing to two key experiments, it has been proved that the behaviour of inclusions do not obey either:

-- A "plug flow" reactor law: in such a case, the hypothesis of the stagnant bath becoming progressively cleaner from the top down would be valid. It should be noted that this long believed and false hypothesis more or less implicitely made industrial people prefer tilting furnaces to stationnary furnaces (in the case, as it was in this study, of inclusions heavier than aluminum);

-- A "well mixed" reactor type of flow. In such a case,uniform concentrations would be ultimately encountered and first order kinetic would be the law governing concentration fields.

5) As represented in concentration isocontours (Figs 55-59), the spatial gradients of mass transfer occur not only vertically but also in the horizontal

direction. For example in the top third part of the the furnace, the metal remains much cleaner on the left hand side rather than on the right of the trapezoid shape furnace. At this last place, heat losses induce strong convective currents circulating away a part of inclusions in a large vortex.

6) Taking into acount the above mentioned boundary conditions and heat losses and assuming that pouring molten metal from the furnace would be achieved from its top right side, a tilting furnace would definitely deliver a less clean metal than if tapping from the lower part of the furnace would be achieved (case of a stationnary furnace). The speculation has to be made in this example that the slow tilting rate would not modify the flow field, which is not necessarily true in all industrial situations. The problem of "tilting" or "pouring" is in this case very complex since it invloves spatial representation of a free surface and moving boundaries. This difficulty superimposes to the other complex phenomena discussed in this thesis (the fully coupled set of Navier-Stokes equations wih heat and mass transfer) and and would require a global Eulerian-Lagrangian approach. However, this challenge has not been adressed in the present work.

CONCLUSIONS

The primary aim of this work was to study the hydrodynamic behaviour of metal and entrained inclusions in aluminum casting or holding furnaces and to develop a mathematical model capable of describing such flows and their role on metal quality. The role of natural convective currents neglected until now in furnace design has been proved to exert a definite influence on metal flow field and thus, on concentration fields encountered.

1) As a first step, molten metal cleanliness statistics of ALCAN's many casting centres were analysed. A static 1D model was proposed in an attempt to explain the trends observed at the exit of a furnace in terms of metal quality. A second "well stirred reactor" type model provided a much better qualitative picture in that the experimental data' s exponential like time decay could be minimized, albeit empirically. It thus appeared that the contribution of metal currents inside the furnace are significant.

2) In order to achieve our main goal the fully non isothermal interlinked system of Navier Stokes equations was solved transiently in two dimensions (for economic reasons) to simulate a slice of an industrial reverbatory furnace subject to external heat sources Turbulence modelling was accounted for by solving two additional partial differential equations for the turbulent energy (K) and its rate of dissipation (E).

   Various simulations on both a full scale furnace and a reduced scale laboratory furnace (6.25 ton) were successfully achieved, for this purpose, the robust finite difference commercial code "PHOENICS" was used mostly on a VAX computer and to a smaller extent on a CRAY XMP machine. Verification tests such as space and time grid independence were carefully accomplished to ensure precision of the results.

3) On the reduced scale furnace, experimental validation was done in a controlled set of experiments. Boundary and initial conditions of the problem were carefully measured while inclusions were introduced in pure molten aluminum. A new technology developped at McGill was used: the Electric Sensing Zone appartus LiMCA allowed to track the concentrations of the particles introduced at distincts levels of the furnace. Until this work, only measurements of this type had been carried out by other investigators at the exit of the furnace (more often in the trough). Remarkable progress in online measurements of metal quality both qualitatively and quantitatively made it possible to assess a precise knowledge of transport phenomena within the furnace itself. Fluid flow coupled with turbulence, heat transfer and mass concentrations could be fairly modelled. In two cases among three, the experimental data did validate very well the mathematical predictions mentioned above.

4) One other conclusion of this study is that both tilting and stationary furnaces behave in a similar way since the kinetics of the concentration field remains the same at the top and the bottom of the furnace.

5) Finally, mathematical modelling is a useful and economic tool for the industrial practitionner for optimizing his cost function which is metal quality at each step of the process. Via Mathematical Modelling of deterministic processes such as natural convection in metallurgical vessels, the cost function can be assessed at any point of the geometric domain involved provided all the constraints that boundary conditions represent are known. It should be noted that the quality of predictions is highly dependent of the quality of input data which has to be carefully checked and validated. A special effort has been done during this work to meet these essential needs.

Given that these requirements are fulfilled, it is felt that the model could be usefully extended to predict the performance of existing industrial furnaces and to explore the merits of other possible designs or operating procedures which would enhance melt quality during the settling period, and henceforth in the cast product.

APPENDIX A

ESTIMATION OF PARAMETER λ FOR THE PARTICLE SIZE DISTRIBUTION

This Appendix provides the details and method used for estimation of the parameter λ in the inclusion size distribution distribution (Chapter II)

The probability density is given in Fig 91

$$n_\lambda = P(x = d) = \frac{\lambda e^{\lambda(x - d_{min})}}{1 - e^{\lambda H}} \qquad (125)$$

The cumulative form of the population of diameters is

$$d_{min} \le x \le d_{max} \qquad N(d) = P(x \le d) = \int_{d_{min}}^{d} n_\lambda(x)\,dx \qquad (126)$$

One easily verifies that N(d_{min}) = 0 and N(d_{max}) = 1

The parameter λ needs to be estimated from historical data The maximum likehood estimation method (35) was retained first, the mathematical expectation is.

$$E(x) = \int_{d_{min}}^{d_{max}} x\, n_\lambda(x)\,dx = \int_{d_{min}}^{d_{max}} x \frac{\lambda e^{\lambda(x - d_{min})}}{1 - e^{\lambda H}}\,dx \qquad (127)$$

Integration gives

$$E(x) = \frac{1}{1 - e^{\lambda H}} \left| d_{min} + \frac{1}{\lambda} - \left(d_{max} + \frac{1}{\lambda}\right) e^{\lambda H} \right| \quad with \quad d_{max} - d_{min} = H \qquad (128)$$

where d_{max}-d_{min} = H

For an unbiased estimation of λ, one has to take.

$E(x) = \mu$

where μ is the sample statistical mean

Resolution of a non linear equation has then to be done:

$$F(\lambda) = \mu[1 - e^{-\lambda H}] - [d_{min} + \frac{1}{\lambda}] + (d_{max} + \frac{1}{\lambda})\, e^{-\lambda H} = 0 \tag{129}$$

This can be achieved graphically as shown on Fig. 93 or numerically by a second order method (Newton) which is quadratically convergent. The scheme is.

$$G(\lambda) = \lambda - \frac{F(\lambda)}{F'(\lambda)} \tag{130}$$

and one iterates the process

Once λ is estimated, the theoretical frequencies for each interval (d_i; d_{i+1}) can be computed

$$\pi_i = \int_{d_i}^{d_{i+1}} n(x)\,dx = \frac{\lambda}{1 - e^{-\lambda H}} \int_{d_i}^{d_{i+1}} e^{-\lambda(x - d_{min})}\,dx \tag{131}$$

Measured frequencies can be compared to computed frequencies (Fig. 92) and the proposed statistical adjustement can be verified from the chi-square test

$$\chi^2_{obs} = 2 \sum_{1}^{n} n_i\, Log\left(\frac{n_i}{n\,\pi_i}\right) \tag{132}$$

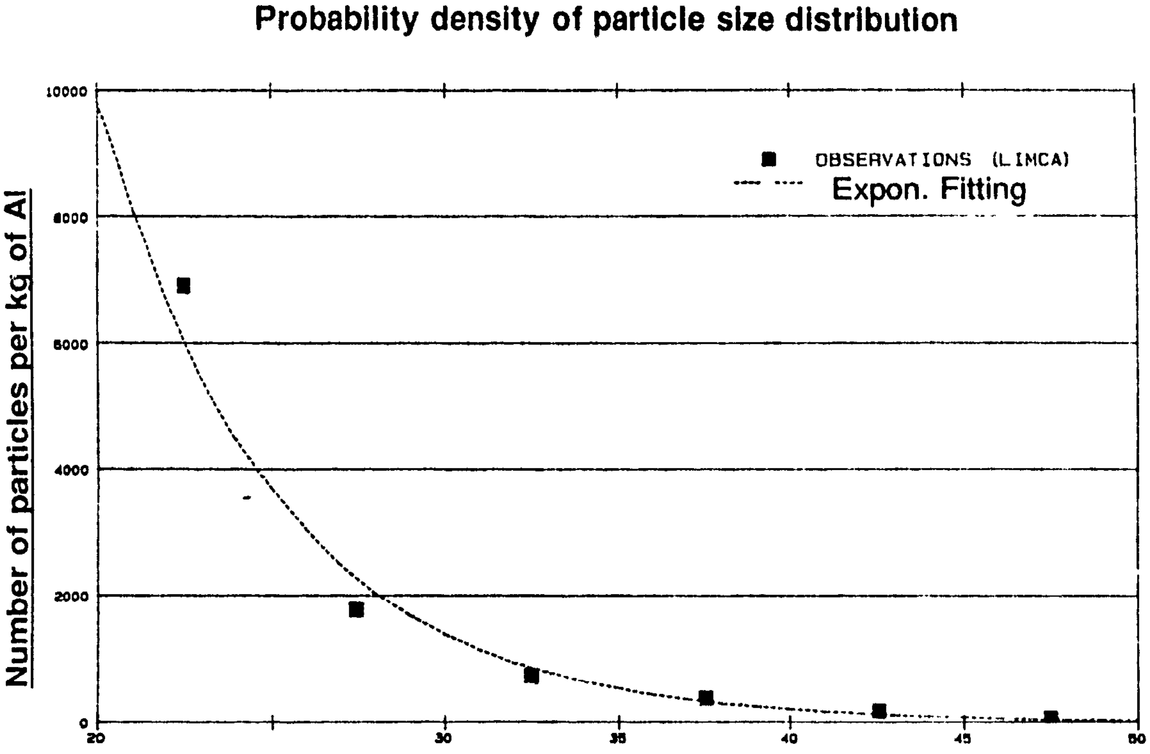
Probability density of particle size distribution

Figure 91:

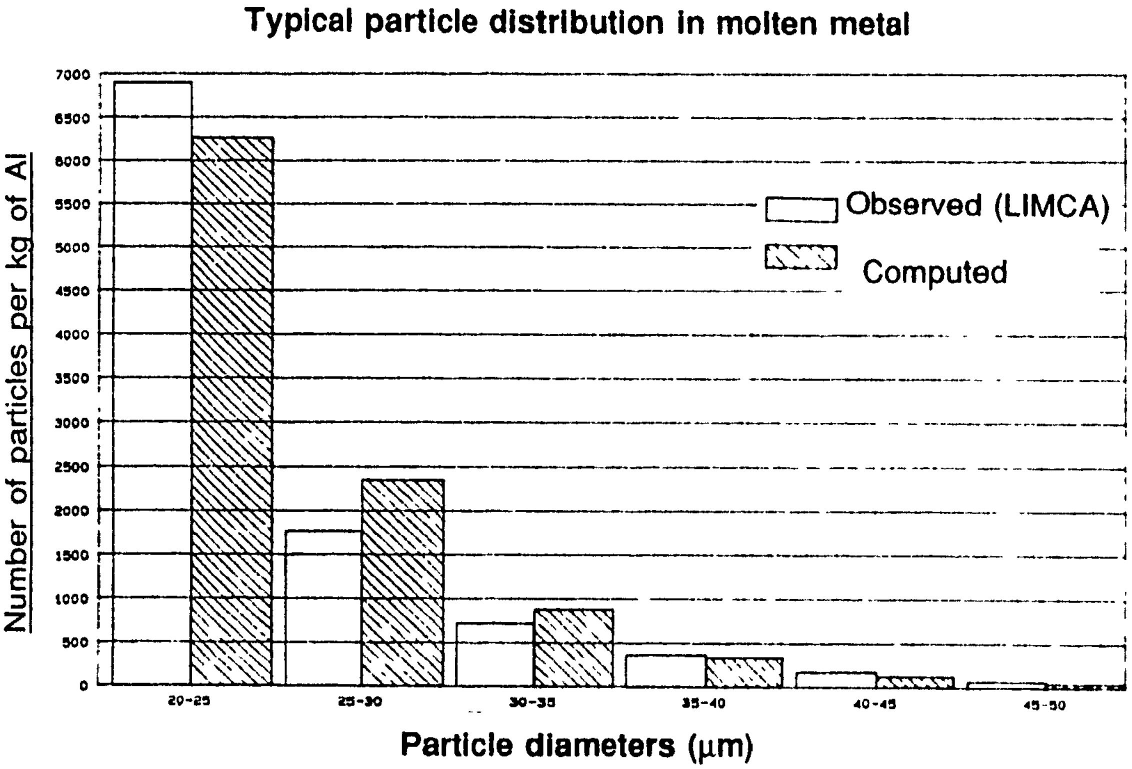
Typical particle distribution in molten metal

Figure 92:

Estimation of parameter LAMDA.

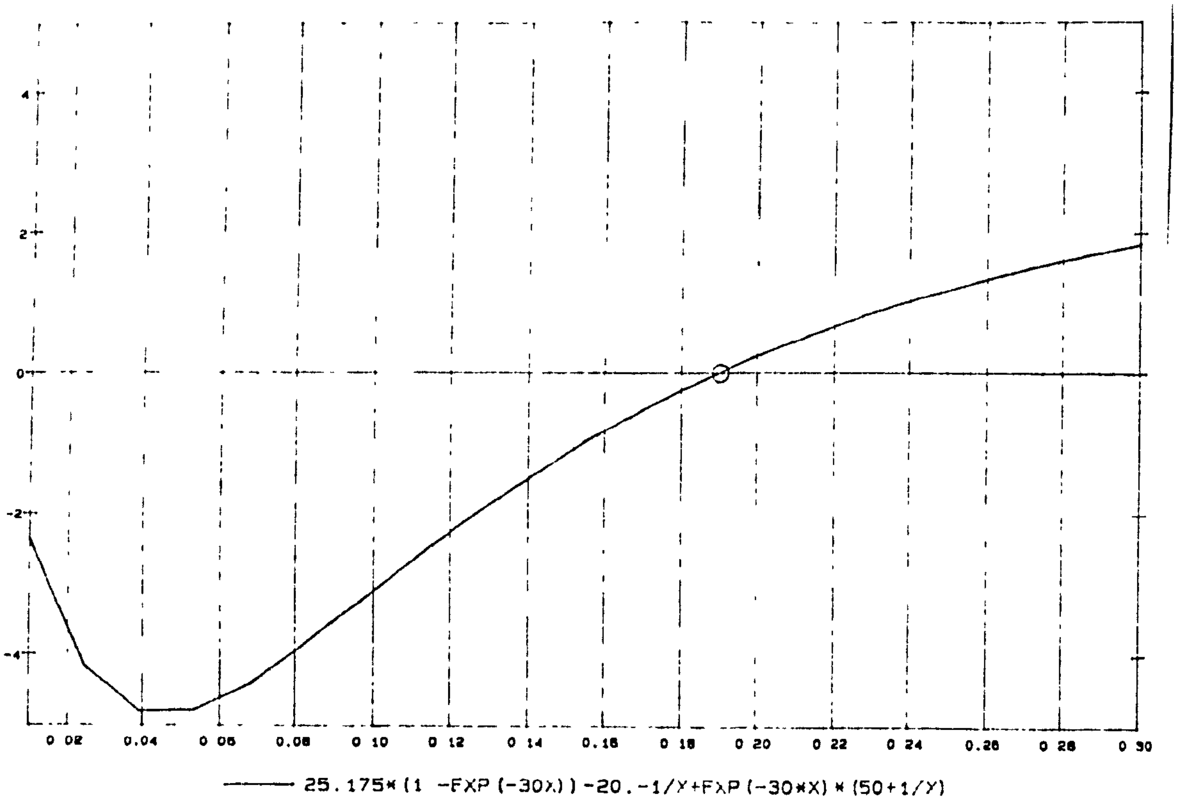

Figure 93

APPENDIX B

DETAIL OF THE *PHOENICS* INPUT FILE: SATELLITE DATA GROUPS

GROUP 1

Title and dimension statements

GROUP2

Specification of the mode (transient) and time step A time step as small as 2 seconds was found necessary to obtain grid independent results (see Section 3.2 7)

GROUPS 3 to 5

Several meshes were considered to set up the geometry of the problem The basic mesh finally adopted was a non uniform 50 x 35 x 1 points See section 3.2.7 for grid space independence

GROUP 6

Not used during the work, this group is linked to body fitted coordinates or grid distortion However, the BFCS method was tried with no success by the author for a six month period

GROUP 7

Specifies the variables to be solved Here we used P1, U1, V1, H1, KE, EP, C1

GROUP 8

This group determines which terms are active in the balance equation for variables solved we need to use both convective and diffusive terms, transient terms and to activate built-in sources for the pressure gradient source for U1 and V1. One phase is considered only so no interphase transport is activated. For the concentration equation, additional Stokes velocity is added in the vertical (y) direction by the statement V1AD = GRND where V1AD is specified through the GROUND subroutine.

GROUP 9

It dictates the properties of the medium i.e molten aluminum:

- density: RH01 = 2357 kg/m^3
- thermal expansion coefficient: B = $1.65 \times 10^{-4} K^{-1}$
- enthalpy of reference: HREF = 973 × CP
- specific heat: CP = 980J $kg^{-1} K^{-1}$
- laminar viscosity: $\mu = 1.252 \times 10^{-3}$ PaS
- kinematic viscosity: ENUL = μ / RH01
- Prandtl number PRNDTL (TEMP) = 1.218×10^{-2}
- Schmidt number PRNDTL (C1) = ENUL / 10^{-9}
- Overall heat transfer coefficient: HBA = $4Wm^{-2}K^{-1}$

GROUP 10

This group is not used since it models interphase transfer processes.

GROUP 11

Indicates the initial physical conditions of the system

- U1 = V1 = 0
- H1 = HREF
- C1 = 1.0 (uniform concentration)
- KE = $10^{-5} m^2 s^{-2}$
- EP = $10^{-5} m^2 s^{-3}$

(very small non-zero turbulence initially to avoid overflow problems)

When doing a sequence of transient simulations, it is possible in this segment to restart the program from the file of the previous computed variables

Also in this group, the blockage and porosity factors are set up on the mesh (fig. 49) to take into account the inclined boundaries

Zero porosity factors are fixed to block off the cells outside the physical domain. Factors between zero and one are used for the cells crossing the inclined walls; as it is a 2D simulation, two factors (NORTH and EAST or NORTH and WEST) are needed for such cells.

GROUP 12

This group is not active for the current problem (one phase only)

GROUP 13

This is one of the biggest groups and describes the boundary conditions of the system of differential equations Boundary conditions are those applied to the furnaces for which computations are illustrated at Figures 50-69

-for momentum.

no slip conditions were considered for the tangential velocities in conjunction with the wall-function approach to specify friction (see section 2-6-1) to each wall boundary The top free surface of the metal bath was also considered as a wall because of the presence of dross (reduced scale furnace as well as real full scale furnace)

An additional source term for the body force has to be taken into account to specify gravity on the whole domain This is done in conjunction with group 19 for the V1 variable The Boussinesq approximation implies a source term.

$$S_{V1} = -VOL \times RH01 \times g \times BETA/CP \times (H_{ref}-H) \qquad (133)$$

There are two other options other than Boussinesq approximation to incorporate the buoyancy force term in the momentum equation.

for heat transfer

- For the industrial full scale furnace, a constant heat flux is applied to the top to represent the gas burner. No special wall boundary friction is needed The value of the flux is 1500 W/m^2

- For the 6 25 ton lab furnace, the temperature profile was measured at the surface as described in Section (2-6-2). Because of non negligible heat losses through the side door, the measured temperature profile was introduced as a top boundary condition instead of a constant heat flux As for the inclined and horizontal bottom walls, the heat fluxes are expressed with an overall heat transfer coefficient:

$$q = h(Tp-T_0) \qquad (134)$$

As mentioned in GROUP 9 of the same Appendix, h was chosen to 4 Watt/m^2/K for most computations For inclined boundaries, h was modified as seen in Fig 94

The flux Φ on the physical boundary can be split in two components $\Phi 1$ and $\Phi 2$ so that

$$\Phi * A = \Phi_1 * A_1 + \Phi_2 * A_2 \qquad (135)$$

If one chooses:

$$\left| \Phi_1 = \Phi_2 = \Phi \ and \ A_2 = A_1 * tan\ \alpha \right| \Rightarrow \Phi_i = \frac{\Phi}{sin\,\alpha + cos\alpha} \qquad (136)b$$

For example.

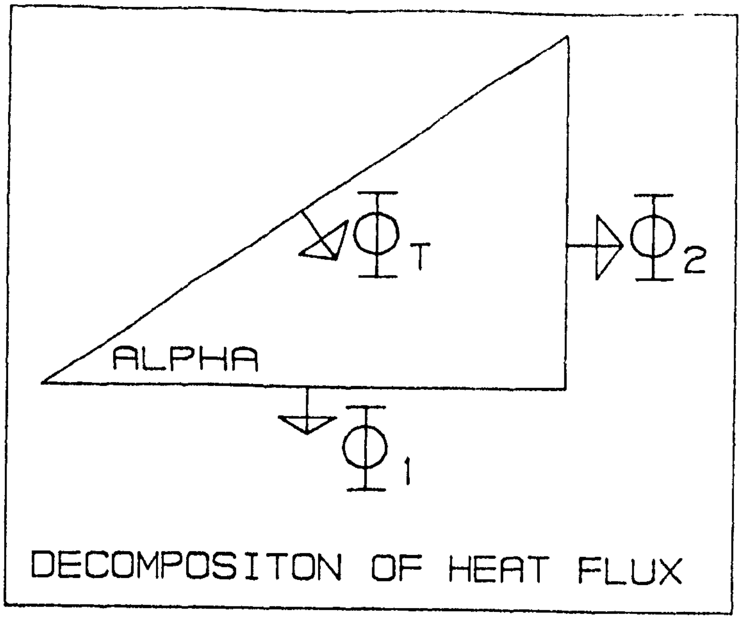

Fig 94. Decomposition of heat flux

$\alpha=45$: $\Phi i=0.707\,\Phi$

$\alpha=25$: $\Phi i=0.7545\,\Phi$

$\alpha=60$: $\Phi i=0.732\,\Phi$

And the actual heat fluxes to the computational domain boundaries have to be set up accordingly

-**For the turbulence model** the strategy was to take the wall function approach given at 2-6-3. This was done in conjunction with the GREX2 program.

-**For the concentration equation**· as the specific source of concentration at boundaries is given by a function of both the velocity and the concentration, it is not possible to set it up only in group 13 The precise definition of the concentration sinks has to be defined in GROUND For example, the statements in group 13 of the Q1 file:

```
PATCH (SS18, SOUTH, 20, 27, 1, 1, 1, NZ, 1, 1000)
COVAL(SS18, C1, 10^20, GRND)
```

allow the concentration source over the patch SS18 to be defined in the GROUND, group 13, section 12.

```
CALL ONLYIF (C1, C1, 'ALL')
IF (ISWEEP GE 2) GO TO 1301
CALL GETYX (C1, GC1, NYDIM, NXDIM)
CALL GETYX (V1, GV1, NYDIM, NXDIM)
 1301 CONTINUE
DO 1302 IX = IXF, IXL
DO 1302 IY = IYF, IYL
GVR = GVS1 + GV1 (IY, IX)
IF (GVR GE O ) GO TO 1302
GVAL (IY, IX) = 10^20 x RHO1A x GVR x GC1 (IY, IX)
 1302 CONTINUE
CALL SETYX (VAL, GVAL, NYDIM, NXDIM)
RETURN
```

So that, at the specified patch of cells, the C1 source term is:

$$S_{C1} = A \times 10^{20} \times (C1 - 10^{20} \times RHO1A \times V \times C1)$$

$$S_{C1} = A \times RHO1A \times V \times C1 \qquad (100)$$

(All boundary conditions have to be put in the form of a linear function of the variable by the way of a coefficient and a value in the COVAL statement). The mentioned approach was chosen for both the industrial and reduced scale furnacess (Figures 50-69) but the mass sinks were applied.

- At the side and bottom walls only for particles of density higher than the density of aluminum (3500 Kg/m^3)
- At the top free surface, considered as a wall for the case of particles lighter than aluminum (1800 Kg/m^3).

GROUP 14

Is inactive here since the flow is fully elliptic

GROUP 15

Is mainly used to fix the number of sweeps needed to reach convergence at each time step. At the beginning of a simulation, LSWEEP could have been as high as 250 but as the time progresses, less and less sweeps are needed This advantage comes from the fact that the solution at step i + 1 is never very far from the solution at step i if the time step remains sufficiently small In this group also reference values of residuals are specified (for termination of sweeps)

GROUP 16

Fixes the number of internal iterations needed by the solver of the linear system of equations in the tridiagonal matrix algorithm It is found that 10 internal iterations are usually sufficient for all variables except for pressure which often converges at the slowest rate (15 iterations) These numbers were not changed during the simulations

GROUP 17

Determines the under-relaxation devices For transient runs we didn't use under-relaxation except for·

- pressure· a linear under-relaxation factor of 0 3 was chosen, as recommended,

- turbulence variables, at the initial steps, "false time steps" under relaxation was provided (0 1)

GROUP 18

Was not used since the default values for the limit on variables were satisfactory

GROUP 19

Enables the user to communicate data to GROUND. This was the case for the buoyancy source term (Boussinesq approximation), for naming the output file, and for calling the GREXI program

GROUP 20 to 24

Are concerned with the control and printout of the variables at different levels of the simulation Spatial or temporal profiles of all variables can be obtained there at interesting locations of the domain

APPENDIX C

STATISTICAL DATA ON EXPERIMENTS CARRIED OUT AT ALCAN RESEARCH CENTRE

Appendix C: Computed statistics on concentrations functions.

$$N_{20}(t) = A \exp(-t/TAU)$$

```
S1  26R x 5C                                              25 AUG 89 14.00 Page 1

                        STATISTICS ON  EXPERIMENT 2006B

0 GRAPH          1 PARAMETER  2 VALUE     3 ST ERROR  4 LOWER 95%  5 UPPER 95%

-------------------------------------------------------------------------------
 1 G2006B        A             94700.00    3850.000     86700.00    103000.00
 2   < 20 MIC.   TAU               5.95       0.522         4.86         7.03
 3
 4               A             18000.00    1150.000     15600.00     20400.00
 5   20-25 MIC.  TAU              12.20       0.965        10.22        14.20
 6
 7               A              5840.00     552.000      4690.00      6990.00
 8   25-30 MIC.  TAU              15.50       1.750        11.90        19.20
 9 ----------    ----------   ----------  ----------  ----------   ----------
10 G2006B2       A              3890.00     307.000      3250.00      4530.00
11   30-35 MIC.  TAU              11.20       1.120         8.85        13.50
12
13               A              2100.00     193.000      1700 00      2500.00
14   35-40 MIC.  TAU              15.40       1.700        11.90        18.90
15
16               A              2860.00     194.000      2450.00      3260.00
17   40-45 MIC.  TAU               6 98       0.834         5.24         8.73
18 ----------    ----------   ----------  ----------  ----------   ----------
19 G2006B3       A              1736.00     120.000      1490.00      1990.00
20   45-50 MIC.  TAU               5.53       0.918         3.61         7.43
21
22               A              5546.00     400.000      4720.00      6380.00
23  50-100 MIC.  TAU               6.55       0.897         4 66         8.41
24
25               A             39800.00    2400.000     34800.00     44800.00
26  20-300 MIC.  TAU              11.40       0.865         9 60        13.20
```

```
S2  26R x 5C                                              25-AUG-89 14:02 Page 1

                        STATISTICS ON EXPERIMENT 2106B

0 GRAPH          1 PARAMETER  2 VALUE     3 ST ERROR  4 LOWER 95%  5 UPPER 95%

-------------------------------------------------------------------------------
 1 G2106B        A              8950.00    2890.000     3030.000     14900.00
 2   < 20 MIC.   TAU              16.70       7.620        1.190        32.50
 3
 4               A              4158.00     463.000     3210.000      5110.00
 5   20-25 MIC.  TAU              22.00       3.610       14.600        29.40
 6
 7               A              1685.00     148.000     1380.000      1990.00
 8   25-30 MIC.  TAU              16.80       2.020       12.700        21.00
 9 ----------    ----------   ----------  ----------  ----------   ----------
10 G2106B2       A              1370.00     123.000     1120.000      1620.00
11   30-35 MIC.  TAU               8 91       1.140        6.570        11.25
12
13               A               629.00      88.700      447.000       811.00
14   35-40 MIC.  TAU              11.00       2.090        6.670        15.30
15
16               A               469.00      39.000      389.000       550.00
17   40-45 MIC.  TAU               8.51       1.020        6.400        10.60
18 ----------    ----------   ----- - --  ----------  ----------   ----------
19 G2106B3       A               464.00      77.300      306.000       623.00
20   45-50 MIC.  TAU               1.39       0.623        0.107         2.66
21
22               A               800.00      47.200      703.000       897.00
23   > 50 MIC.   TAU               5.38       0.543        4.270         6.50
24
25               A              9200.00     638.000     7890.000     10500.00
26  20-300 MIC.  TAU              15.40       1.440       12.500        18.40
```

```
S3  26R x 5C                                          25-AUG 89 14:04 Page 1

                     STATISTICS ON EXPERIMENT 2306B

0 GRAPH           1 PARAMETER  2 VALUE     3 ST ERROR  4 LOWER 95%  5 UPPER 95%

--------------------------------------------------------------- ---- - ---
 1 G2306B         A            51800.000     6390.00     37000.00    66500 00
 2   < 20 MIC.    TAU             61.400       37.90         0.00      149.00
 3
 4                A            20600.000     3330.00     12800 00    28300.00
 5   20-25 MIC.   TAU             80.800       82.80         0 00      272.00
 6
 7                A             7000.000      687.00      5410.00     8580 00
 8   25-30 MIC.   TAU             85.900       56.70         0 00      217.00
 9 ----------     ----------   ---------  ----------    ---------   ---------
10 G2306B1        A             3750 000      502.00      2590.00     4910.00
11   30 35 MIC.   TAU             40.800       19.50         0 00       85.60
12
13                A             2500.000      244.00      1940 00     3070 00
14   35-40 MIC.   TAU             29.500        8.10        10.80       48 20
15
16                A             1620.000      192 00      1180 00     2060 00
17   40-45 MIC.   TAU             29.100        8.61         6.88       51 20
18 ----------     ----------   ----- ---  ----------   ----------   ----- ---
19 G2306B2        A              800.000      135.00       490.00     1110.00
20   45-50 MIC.   TAU             32.800       16.50         0 00       70.80
21
22                A             3460.000      467.00      2380.00     4540 00
23   > 50 MIC.    TAU              6.124        1.55         2.54        9 71
24
25                A            33700.000     2040 00     29000.00    38400 00
26   20-300 MIC.  TAU             68.000       22.50        16 20      120 00
```

```
S4  26R x 5C                                          25-AUG-89 14:06 Page 1

                     STATISTICS ON EXPERIMENT 2906B

0 GRAPH           1 PARAMETER  2 VALUE     3 ST ERROR  4 LOWER 95%  5 UPPER 95%

--------------------------------------------------------------------------
 1 G2906B1        A             40300.00     6690.00     26700.00    53900.00
 2   < 20 MIC.    TAU              33.90       11.40        10.90       57 20
 3
 4                A             31900.00     3190.00     25400.00    38400 00
 5   20-25 MIC.   TAU              42.80        8.90        24 60       61.20
 6
 7                A             18700.00     2480.00     14700.00    24800 00
 8   25-30 MIC.   TAU              25.20        6 00        13.00       37 30
 9 ----------     ----------   ----------  ----------  ----------   ---- -----
10 G2906B2        A             14100.00     2200.00      9640.00    18600.00
11   30-35 MIC.   TAU              14.00        3.93         6.06       22.10
12
13                A             17000.00     1650 00     13600 00    20300.00
14   35-40 MIC.   TAU               1.92        0.39         1.13        2 72
15
16                A              8560.00      750.00      8030.00    11100.00
17   40-45 MIC.   TAU               3.12        0.44         2 23        4.08
18 ----------     ----------   ----------  ----------  ----------   ------- --
19 G2906B3        A              7900.00      580.00      6730.00     9080.00
20   45-50 MIC.   TAU               2.04        0.29         1.49        2.75
21
22                A             21100.00     1130.00     18800 00    23400 00
23   > 50 MIC.    TAU               1.43        0 17         1.04        1 79
24
25                A             94200.00    12200.00     69300.00   119000.00
26 20-300 MIC.    TAU              20.20        4.70        10.60       30.00
```

```
~K  29R x 5C                                    25-AUG-89 14:08 Page 1

                     STATISTICS ON EXPERIMENT 1208

0 GRAPH          1 PARAMETER  2 VALUE    3 ST ERROR  4 LOWER 95%  5 UPPER 95%

-- ----------------------------------------------------------------------------
 1 G12081        A             133000.0     9300.00     114000.0     152000.0
 2   < 20 MIC.   TAU              133.0       25.00         83.0        182.0
 3 -- -------    ----------  ----------  ----------  ----------  ---------
 4 G12082        A              24300.0     1000.00      22300.0      26300.0
 5   20-25 MIC.  TAU               57.3        4.40         48.5         66.0
 6
 7               A               8790.0      488.00       7810.0       9760.0
 8   25-30 MIC.  TAU               50.0        5.00         39.8         59.7
 9
10               A               4010.0      204.00       3600.0       4420.0
11   30-35 MIC.  TAU               51.5        4.80         41.9         60.9
12
13               A               2230.0      127.00       1970.0       2480.0
14   35-40 MIC.  TAU               53.9        5.62         42.7         65.1
15 ----------    ----------  ----------  ----------  ----------  ----------
16 G12083        A               1340.0       73.00       1200.0       1490.0
17   40-45 MIC.  TAU               48.3        4.74         38.8         57.8
18
19               A               1040.0       86.70        862.0       1208.0
20   45-50 MIC   TAU               38.5        5.72         27.1         49.9
21
22               A                689.0       54.70        580.0        800.0
23   50-55 MIC.  TAU               33.9        4.77         24.4         43.4
24
25               A               2320.0      120.00       2080.0       2560.0
26   > 50 MIC.   TAU               28.3        2.61         23.1         33.5
27 ----------    ----------  ----------  ----------  ----------  ----------
28 G12084        A              43800.0     1740.00      40300.0      47200.0
29  20-300 MIC.  TAU               52.7        3.81         45.1         60.3
S6  29R x 5C                                    25-AUG-89 14:10 Page 1

                     STATISTICS ON EXPERIMENT 1508

0 GRAPH          1 PARAMETER  2 VALUE    3 ST ERROR  4 LOWER 95%  5 UPPER 95%

-------------------------------------------------------------------------------
 1 G15081        A              60400.0     1920.00      56600.0      64200.0
 2   < 20 MIC.   TAU               65.6        4.22         57.2         74.0
 3 ----------    ----------  ----------  ----------  ----------  ----------
 4 G15082        A              19100.0      502.00      18100.0      20100.0
 5   20-25 MIC.  TAU               62.3        3.25         55.8         68.8
 6
 7               A              10000.0      300.00       9440.0      10600 0
 8   25-30 MIC.  TAU               58.3        3.39         51.5         65.0
 9
10               A               6710.0      181.00       6350.0       7080.0
11   30-35 MIC.  TAU               43.4        2.14         39.1         47.7
12
13               A               3510.0      139.00       3230.0       3790.0
14   35-40 MIC.  TAU               45.4        3.31         38.8         51.9
15 ----------    ----------  ----------  ----------  ----------  ----------
16 G15083        A               2390.0       91.20       2210.0       2570.0
17   40-45 MIC.  TAU               40.4        2.82         34.8         46.1
18
19               A               1770.0      108.00       1550.0       1980.0
20   45-50 MIC.  TAU               28.8        3.16         22.5         35.1
21
22               A               1250.0      104.00       1050.0       1460.0
23   50-55 MIC.  TAU               22.7        3.45         15.9         29.6
24
25               A               4850.0      186.00       4480.0       5220.0
26   > 55 MIC.   TAU               18.0        1.27         15.5         20.5
27 ----------    ----------  ----------  ----------  ----------  ----------
28 G15084        A              47600.0      791.00      46000.0      49200.0
29   20-300 MIC. TAU               50.0        1.56         46.9         53.1
```

```
ST  29B x SC                                         25 AUG 89 14 12 Page 1

                         STATISTICS ON EXPERIMENT 1608

0 GRAPH           1 PARAMETER  2 VALUE     3 ST ERROR  4 LOWER 95%  5 UPPER 95%

- --- ----- --------- ---------- --- -       -    ----- --------- --  - ------
 1 G16081         A             61200.00    3760 000    53700 00      68800 0
 2   < 20 MIC     TAU              66 80       9.450       47 80         85.8
 3 -- -- ----     ------ ---    ------ -    ----------  ----------   - ------ -
 4 G16082         A             22120 00    1400.000    19300 00      24900 0
 5   20-25 MIC.   TAU              80 00      12.500       54.70        105.0
 6
 7                A             10600.00     890.000     8800.00      12400 0
 8   25-30 MIC.   TAU              94.80      21.500       51.70        140 0
 9
10                A              7300.00     394.000     6510.00       8090 0
11   30-35 MIC.   TAU              48.20       5.700       37.80         60 7
12
13                A              4790.00     299 000     4190.00       5390.0
14   35-40 MIC    TAU              33.30       4 280       24 70         41 8
15 ----------     ----------   - ---  ---    --------    ---- ---    -- -----
16 G16083         A              3180.00     270.000     2640 00       3720.0
17   40-45 MIC.   TAU              29 80       5.180       19.40         40 2
18
19                A              3453 00     256 000     2940.00       3970 0
20   45-50 MIC.   TAU              12 20       1.670        8 87         15 6
21
22                A              2450.00     200.000     2050.00       2850 0
23   50-55 MIC.   TAU              11.50       1.710        8.10         15.0
24
25                A             10200.00     420.000     9380.00      11100.0
26   > 55 MIC.    TAU               8 07       0.562        6.94          9.2
27 ----------     ------  --   ---------- - --- ----  ----- --     ----- ----
28 G16084         A             57300.00    3260.000    50700.00      63800 0
29  20-300 MIC.   TAU              52 60       6 460       39.60         65 58
```

TABLE OF REFERENCES

1 Doutre D, Gariepy B., Martin J P, Dube G. «Aluminum cleanliness monitoring. methods and applications in process development and quality control», Proceedings of the 114th TMS annual meeting, New-York, Feb 24-28, 1985

2 Frayce D and Martin J P.: «Etude du comportement des inclusions dans les fours: analyse des données LiMCA», Alcan International Internal Report, Jonquière, Québec, Feb 1986

3 Azbel D.S and Cheremisinoff N P.: «Fluid Mechanics and unit operations», Ann Arbor Science, Michigan, 1982.

4 Jones W.P. and Launder B.E : «The prediction of relaminarization with a two equations model of turbulence», International Journal of Heat and Mass Transfer, vol 15, pp 301-314, 1972

5 Launder B E. and Spalding D.B : «The numerical computation of turbulent flows», Computer Methods in Applied Mechanics and Engineering, vol 3, pp 269-289, 1974.

6 Chan A.M.C and Banerjee S.: «Three dimensional numerical analysis of transient natural convection in rectangular enclosures», Journal of Heat Transfer, vol 101, pp 114-119, (1979).

7 Ideriah F.J.K.: «Prediction of turbulent cavity flow driven by buoyancy and shear», J. Mechanical Engineering Science, vol 22, n°6, pp 287-295, (1980).

8 Patankar S.V.: «Numerical heat transfer and Fluid Flow» Mac Graw Hill, 1980.

9 Fraikin M.P. and Portier J.J.: «Application af a K-E turbulence model to an enclosed buoyancy driven flow», Chem. Engin Commun , vol 13, pp 289-314, (1981).

10 Markatos N.C. and Malin M.R. . «Mathematical modelling of buoyancy induced smoke flow in enclosures», Int J. Heat and Mass Transfer, vol 25 n°1, pp 63-75, (1982)

11 Bejan A. and Cunnington: «Theoritical considerations of transition to turbulence in natural convection near a vertical wall», Int J of Heat and Fluid Flow, vol 4 n°3, pp 131-139, (1983)

12 Markatos N.C. and Pericleous K A : «Laminar and turbulent natural convection in an enclosed cavity», Int. Journal of Heat and Mass Transfer, vol 27n°5, pp 755-772, (1984).

13 Vanka S.P.: «Block implicit calculation of steady turbulent recirculating flow», Int. Journal of Heat and Mass Transfer, vol 28 n°11, pp 2093 2103, (1985).

14 Ozoe H., Churchill S.W. and Lior N.: «Numerical calculation of three dimensional turbulent natural convection in a cubical enclosure using a two equations model of turbulence», Journal of Heat Transfer, vol 108,, pp 808-813, (1986).

15 Giel P.W. and Schmidt F.W.: «An experimental study of high Rayleigh number natural convection in an enclosure», Heat Transfer, pp 1459-1464, (1986).

16 Viskanta R. and Kim D.M.: «Three dimensional natural convection heat transfer of a liquid metal in a cavity», Int Journal of Heat and Mass Transfer, vol 29 n°3, pp 475-485, (1986)

17 Humphrey J A and To W M . «Numerical simulation of buoyant turbulent flow: free and mixed convection in a heated cavity», Int J of Heat and Mass Transfer, vol 29 n°4, pp 593-610, (1986)

18 Coulter J.P and Guceri S.I : «Laminar and turbulent natural convection within irregularly shaped enclosure», Numerical Heat Transfer, vol 12, pp 211-227, (1987)

19 Thompson C P , Wilkes N S and Jones I P «Numerical studies of buoyancy driven turbulent flows in a rectangular cavity», International Journal for Numerical Methods in Engineering, vol 24, 89 99, (1987)

20 Farouk B : «Turbulent thermal convection in an enclosure with internal heat generation», Journal of Heat Transfer, vol 110, pp 126-132, 1988

21 Ince N.Z. and Launder B.E.: «On the computation of buoyancy driven turbulent flows in rectangular enclosures», Int Journal of Heat and Fluid Flow, vol 10 n°2, pp 110-117, (1989)

22 Bird R B., Stewart W.E and Lightfoot E N . «Transport Phenomena», Wiley, New-York, 1960

23 Markatos N C : «The mathematical modelling of turbulent flows», Applied Mathematical Modelling, vol 10, pp 190-220, (1986)

24 Ilegbusi O.J. and Spalding D B «Prediction of fluid flow and heat transfer characteristics of turbulent shear flows with a two-fluid model of turbulence», International Journal of Heat ans Mass Transfer, vol 32 n°4, pp 767-774, 1989.

25 Thompson: «Grid generation in computational fluid dynamics», AIAA Journal, vol 22 n°11, November 1984

26 Rosten H and Spalding B : «The PHOENICS reference manual», CHAM TR/200, Wimbledon UK, October 1987

27 De Vahl Davis G «Natural convection in an enclosed rectangular cavity», International Journal of Heat and Mass Transfer, vol 11, 1968.

28 Bejan A.: «Convection heat transfer», Wiley, 1984

29 Tacke K H and Ludwig J.C.. «Steel flow and inclusion separation in continuous casting tundishes», Steel Research, vol 28 n°6, p 262-270, 1987.

30 Doutre D : «PhD Thesis», McGill University, Montreal, Canada, (1984).

31 Doutre D , Celik C , Frayce D. and Martin J.P.: «LiMCA data analysis meeting», ALCAN int Report, December 1985.

32 George W.K and Capp S.P.: «A theory for natural convection turbulent boundary layers next to heated vertical surfaces»,International Journal of Heat and Mass Transfer, vol 22,pp 813-826, 1979

33 Chiesa F. and Guthrie R.I L.: «An experimental study of natural convection and wall effect in liquid metals contained in vertical cylinders», Metallurgical Transactions, vol 2, October 1971, pp 2833-2838

34 Moretti P.M. and Kays W M. : «Heat transfer through an incompressible turbulent boundary layer with varying surface temperature», Stanford University, Thermo Sci Div ,Rep PG1, 1965

35 Hoel P G .«Introduction to mathematical statistics», John Wiley, New York, 1971.

36 Sztur C., Balestreri F , Meyer J L. and Hannart B «Settling of inclusions in holding furnaces modeling and experimental results», Proceedings of the AIME/TMS annual conference, Anaheim, 1990

LIST OF FIGURES

LIST OF TABLES

LIST OF SYMBOLS

A:	Area considered in the well mixed model
A([P]):	Function of the Peclet number P
A,B,AB,A1,B1,AB1	Monitoring points within the ALCAN furnace (experiments and simulations)
C:	Mass concentration of particles
C_μ, C_1, C_2:	Turbulent coefficients
C_D:	Drag coefficient
C_P:	Specific heat
CPU:	Computing time of simulations
D:	Equivalent diameter of particles
D:	also: Mass diffusivity of the fluid
E:	Roughness coefficient for wall friction
E(X):	Mathematical expectation of probability law n_λ
F:	Source term in the momentum equation
F(λ):	Non linear function to solve for estimation of parameter λ
Gr:	Grashoff number
G(λ):	Newton scheme function for estimation of parameter λ
H:	Difference of max. and min. particle diameters
H1:	Enthalpy variable
J:	Mass flux in the concentration equation
K:	Turbulent kinetic energy
K_P:	Turbulent energy at point P near wall
M_{XY}:	Eddy mass flux
NI,NJ:	Number of grid points in X and Y directions
Nu:	Nusselt number
NTOT:	Total number of particles considered
N_{di}:	Number of particles of a given size di
N_{20}:	Number of particles of diameter larger than 20 microns
N_{20}:	Average of N_{20} over time interval ΔT

P:	Pressure
Pe:	Peclet number
Pr:	Laminar Prandtl number
R:	Equivalent radius of inclusions
Ra:	Rayleigh number
Re:	Reynolds number
RESORΦ:	Residual sources of primary variables (Φ)
S:	Skin friction coefficient
St:	Stanton number
S_Φ:	Source term for primary variables
T:	Temperature (Kelvin)
T_0:	Reference temperature
U,V:	Velocity components of the velocity vector
V:	Velocity vector
V:	Stirred volume considered in well mixed model
V_s:	Settling velocity (Stokes, intermediate or Newton regime)
X:	Vertical position considered in the furnace from the top of the bath surface (1D model).
X,Y:	Space coordinates in two dimensional Navier-Stokes equations
Z:	Factor defined as a criterion of the flow regime
a_E,a_W,a_S,a_N:	Parameters of the discretized equation (100)
b:	Source term in the discretized equation
d:	Density of particles
d_{min},d_{max}:	Minimum and maximum diameters considered
g:	Gravitational acceleration (m/s/s)
k:	Thermal conductivity of the fluid
l:	Length scale in turbulence modeling
m''':	Mass source in convective-diffusive equation
n_D:	Number of particles per unit volume
n_D'':	Mass flux through the stagnant layer

n_i: Number of particles in class i (1D model)
n_λ: Continuous probability density of particle size distribution
q''': Heat source in convective-diffusive equation
t: Time variable in transient equations
t_0: Initial time
x^+, y^+: Dimensionless values of x,y
y: Dummy variable for integration (1D model)

α: Absorption parameter, function of turbulence level
α: also: Thermal diffusivity (eq 38)
α: also: Relaxation factor (eq 103)
β: Coefficient of thermal expansion (1/Kelvin)
δ_V: Momentum boundary layer thickness
δ_T: Thermal boundary layer thickness
ε: Dissipation rate of turbulent kinetic energy
ε_M: Momentum eddy diffusivity
ε_P: Dissipation rate of energy at point P near wall
κ: Von Karman constant
λ: Parameter of the probability density n_λ
μ: Laminar viscosity of molten aluminum
μ_t: Turbulent viscosity of fluid
ρ: Density of molten aluminum
ρ_i: Density of class i of particles of a given diameter di
ρ_P: Density of particles considered
σ_C: Turbulent Schmidt number (C1 equation)
σ_E, σ_K: Turbulent Prandtl number (KE model)
σ_T: Turbulent Prandtl number (H1 equation)
τ: Time constant (minutes) in exponential law
τ^*: Reference shear stress (wall functions)
τ_0: Shear stress
τ_{XY}: Eddy shear stress (turbulence modeling)
χ^2: Chi-square test for validation of $n\lambda$

Γ:	Diffusive coefficient in general equation (63)
ΔT:	Temperature gradient in the furnace
ΔR:	Electric resistance gradient in the ESZ device
Φ:	General primary variable (U,V,P,H1,C1,K,E)
Φ_P:	Primary variable at a given mesh point P
$\boldsymbol{\Phi}$:	Averaged value of Φ
Φ':	Correction to averaged value $\boldsymbol{\Phi}$
$\boldsymbol{\Phi}$:	Viscous dissipation term (eq.31,34)
$\Psi(y)$:	Function to integrate in the plug flow model
Ψ_{XY}:	Eddy heat flux (turbulence modeling)